Absolute gravimetry - for monitoring climate change and geodynamics in Greenland

Nielsen, Jens Emil

Publication date:
2013

Document Version
Publisher's PDF, also known as Version of record

Absolute gravimetry - for monitoring climate change and geodynamics in Greenland

J. Emil Nielsen
PhD Thesis
March 28, 2013

DTU Space
National Space Institute

Absolute gravimetry - for monitoring climate change and geodynamics in Greenland

J. Emil Nielsen
National Space Institute
PhD Thesis, Kgs. Lyngby, March 28, 2013

Supervised by Rene Forsberg, National Space Institute, Technical University of Denmark,
Gabriel Strykowksi, National Space Institute, Technical University of Denmark.

ISBN-10: 87-92477-19-4
ISBN-13: 978-87-92477-19-4

http://www.space.dtu.dk

Contents

Resume

Igennem de seneste årtier har der været en øget interesse i at studere klimaændringerne. Baggrunden for disse studier er et ønske om at opnå en forståelse af de bagvedliggende processer og om at kunne forudsige konsekvenserne, blandt andet havniveauændringer. For at kunne sige noget om disse må man vide noget om ændringerne af de globale ismasser, heriblandt Grønlands indlandsis. De globale ismasser anslås at indeholde 80% af klodens samlede ferskvand og Grønlands indlandsis alene indeholder vand nok til en havniveaustigning på cirka $7m$. Af disse årsager er der stor interesse i at studere masse ændringer af den Grønlandske indlandsis.

Flere forskellige geofysiske metoder anvendes til studiet af klimaændringerne men tolkning af disse kompliceres af tilstedeværelsen af flere forskellige signaler og ikke kun dem der relaterer til nutidige klimaændringer. De forskellige metoder har hver deres evne til at detektere de forskellige signaler og i mange geofysiske sammenhænge opnås de bedste resultater ved at sammenholde forskellige metoder.

Netop denne brug af forskellige metoder for at kunne identificere bestemte signaler har været motivationen for dette Ph.d. projekt.

Signalerne der er undersøgt stammer fra geodynamiske processer der kommer som følge af ændringer af isen. To af Jordens karakteristika giver i denne sammenhæng anledning til to forskellige geofysiske signaler, det ene skyldes asthenosfærens viskøse egenskaber, mens det andet skyldes lithosfærens elastiske egenskaber. Det viskøse signal er et "langsomt" signal. Et godt eksempel på dette er, at et signal af denne slags kan detekteres i Skandinavien i dag grundet isen fra sidste istid som forsvandt for cirka 10.000 år siden. Det måles som en langsom hævning af jordoverfladen. Det elastiske signal er et "hurtigt" signal, et eksempel herpå er, at der i Grønland kan detekteres en årlig cyklisk bevægelse af jordoverfladen som følge af, at der er mere sne om vinteren til at tynge jordoverfladen ned end om sommeren. Der vil også være et elastisk signal fra den generelle tendens af isens udvikling.

Som allerede antydet vil de to geofysiske signaler der ønskes undersøgt, give anledning til bevægelse af jordoverfladen. Til at detektere denne bevægelse anvendes GPS. I et projekt der har været i gang siden 2007, det såkaldte GNET projekt (Greenland Network), er 53 permanente GPS modtager opsat rundt om Grønlands indlandsis. De seneste resultater fra dette projekt viser at samtlige GPS modtagere måler en hævning af jordoverfladen. Problemet er at GPS modtagerne ikke kan skelne om landhævningen skyldes det viskøse signal eller det elastiske signal.

I dette projekt har målet været at indføre en ny metode til at detektere de to signal og en metode der sammenholdt med GPS dataene kan anvendes til at adskille de to signaler. Metoden anvendt i dette projekt er absolut gravimetri og til dette formål er der blevet indkøbt et absolut gravimeter af typen A10. Dette instrument kan måle tyngdeaccelerationen ned til $6\mu Gal$ $(= 60nm/s^2)$ hvilket giver nogle unikke muligheder for at studere geodynamikken i Grønland.

En del af arbejdet i dette projekt har været at vedligeholde instrument og udføre feltarbejde i Grønland og i Danmark. Dette har været med til at give en dybere forståelse for instrumentet, dets muligheder og begrænsninger. Det har ligeledes ført til en bestemmelse af instrumentets nøjagtighed der viser sig at være bedre end fabrikantens specifikationer. Tilstedeværelsen af et støjsignal i dataene har været motivationen for at teste forskellige dataprocesseringsmetoder. Støjsignalet, der kommer fra instrument selv, kaldes system responset.

Tidensrammen til Ph.d. projektet har ikke været tilstrækkelig til at indsamle nok data til en dybdegående analyse af de forskellige signaler, der kan detekteres i Grønland. I denne opgave, præsenteres de indledende målinger og de viser at der er interessante muligheder ved anvendelsen af absolut gravimetri. De geodynamiske signaler i Grønland, er forsøgt modelleret og resultaterne af disse bliver sammenholdt med de præliminære målinger. Resultaterne heraf viser at den direkte tiltrækning fra ismasserne er det størst signal der detekteres og at det skal modelleres med omhu. Et eksempel på dette er den målte tyngdeændring ved Helheim gletscheren, $54 \mu Gal/yr$, hvilket hovedsagligt skyldes en ændring i den direkte tiltrækning fra isen. Den direkte tiltrækning kan ligeledes være tilstede ved kystnære stationer hvor havet agerer som den tiltrækkende masse. Dette er undersøgt for GNET stationen THU3 og det er fundet at der er en overensstemmelse mellem den direkte tiltrækning fra havet og den målte tyngdeændring.

Det præsenteres også hvordan instrumentet er opbygget, hvordan dataene processeres og hvilke korrektioner der er nødvendige for at få de bedst mulige data. Særligt processeringen er undersøgt ved tests af forskellige processerings metoder.

Disse første resultater af vores målinger af tyngdeaccelerationen i Grønland giver interessant ny viden. Viden der giver håb om, at med tiden, når flere målinger er indsamlet, vil det være muligt at kunne adskille de forskellige geodynamiske processer og derved kunne give bedre estimater for masse balancen af den Grønlandske indlandsis. Dette vil ske i sammenspil med GPS dataene fra GNET projektet.

Abstract

Over the recent decades, there has been an increasing interest in studying climatic changes. The reason for this interest is a wish to gain an understanding of the processes behind these climatic changes, and to be able to predict the consequences of, for example, sea level change. To say something about sea level change requires a knowledge of global ice masses, in this case the Greenland Ice Sheet. Global ice masses are estimated to contain 80% of the global fresh water resources, and the Greenland Ice Sheet holds enough water for an approximated $7m$ of sea level rise. For these reasons, there is a large interest in studying the mass changes of the Greenland Ice Sheet.

There are many geophysical methods which can be used to study climatic changes. However, the interpretation of these changes is complicated due to the presence of many different signals - not all of which are related to present-day climate change. Different geophysical methods have the ability to detect different signals. In many cases, the best results are obtained through incorporating different methods.

The use of different methods for identifying certain signals has been the motivation for this PhD project.
The signals investigated come from geodynamical processes originating from ice mass changes. Two of the Earth's properties give rise to two different geophysical signals. One of these is caused by the Asthenosphere's viscoelastic properties, while the other one is due to the lithosphere's elastic properties. The viscoelastic signal is a "slow" signal. A good example of this is the uplift detectable in Scandinavia today, due to the ice which covered this area during the last ice age 10,000 years ago. The elastic signal is a "fast" signal. An example for this is an annual displacement of the Earth's surface which can be detected in Greenland, resulting from the loading and unloading of ice during winter and summer. Besides this kind of elastic signal, there will also be a more general trend due to the development of the ice.

As already indicated, the two geophysical signals under investigation give rise to a vertical displacement of the Earth's surface. GPS receivers are used for detecting this movement. In a project which has been ongoing since 2007, the GNET (Greenland Network) project, 53 permanent GPS receivers are deployed on rock at the edges of the ice sheet. The latest results from the GNET project show that all GPS receivers are detecting an uplift of the Earth's surface. The problem is that the GPS receivers do not provide any information on whether the signal is of viscoelastic or elastic origin.

The objective of this project has been to use a different method for detecting the two signals. Together with the GPS data, it is possible to separate the different signals. The method used in this study is absolute gravimetry. An absolute gravimeter of the A10 type has been purchased by DTU Space for this purpose. This instrument can measure gravity changes as small as $6\mu Gal$ $(= 60nm/s^2)$, which provides the unique possibility of geodynamical studies in Greenland.

A part of the work in this project has been to maintain the instrument and conduct field work in Greenland and Denmark. This has been beneficial in gaining a deeper understand-

ing of the instrument, its possibilities and limitations. During the studies of the instrument it is found that it performs better than the manufacture specifications. The presence of a noise signal in the data, which originates from the instrument itself, has been the motivation to investigate different processing schemes. This noise is called the system response.

The time allocated for a PhD project is not sufficient to gather enough data for an elaborated analysis of the different signals which can be detected in Greenland. However, as will be presented in this thesis, the preliminary results indicate interesting possibilities for the use of absolute gravimetry. To get an idea of the expected size of the geodynamical signals in Greenland, they are modelled and the results are compared to the preliminary measurements. These results show that the direct attraction from the ice masses is the largest signal, and care must be taken when modelling it. An example of this is the gravity change detected at Helheim, $54\mu Gal$. This is mostly a signal of direct attraction from the ice. Additionally, a signal of direct attraction from the ocean can be present at coastal sites. This is investigated for the THU3 GNET site where tide gauge data are available. The result is that the direct signal from the ocean is in accordance with the measured gravity change.

Furthermore, in the thesis it will be presented how the absolute gravimeter is constructed, how the data are processed, and which corrections are needed to obtain the best possible data. Especially is the data processing investigated with different processing methods.

These preliminary results of the gravity measurements in Greenland are interesting new data which suggest that as more measurements become available it will be possible, along with the GPS data, to separate the different geodynamical processes and thereby give a better estimate of the geodynamics occurring in Greenland. This in turn allows better mass balance of the Greenland ice sheet.

Preface

This PhD thesis, entitled; *Absolute gravimetry - for monitoring climate change and geodynamics in Greenland* is the result of my enrollment at DTU Space, which started on January 1^{st}, 2010.

Supervisors: Head of Department - Rene Forsberg at DTU Space.
Senior Scientist - Gabriel Strykowski at DTU Space.

The project is partly funded by the GNET project, KVUG and DTU.

In connection with the work of this thesis are two scientific articles enclosed,
- Nielsen et al. (2013a) and
- Nielsen et al. (2013b).
The article Nielsen et al. (2013a) is accepted and ready for print (Appendix A.1). The article Nielsen et al. (2013b) is at time of writing under the first review at Journal of Geodynamic. It was submitted on January 14^{th} (Appendix A.2).

I have participated in field work that has resulted in the article by Matzka et al. (2010).

During the PhD enrollment I have presented my work in form of posters at EGU 2010, IUGG 2011, SLALOM 2012 and AGU 2012. These are found in Appendix B.

I have participated in the GIA school in Gävle, Sweden, 2009, and in the Micro-g LaCoste's absolute gravimeter workshop in 2010.

During the PhD enrollment I have visited Prof. Giorgio Spada at University of Urbino for a week in 2010, supported by COST ACTION ES0701.

Furthermore, I have stayed five weeks in 2012 at Ohio State University visiting Prof. Micheal Bevis. This stay was funded by a scholarship received from Maersk Oil Kalaallit Nunaat A/S.

I have had a three months leave from the PhD due to extensive field work both with terrestrial and airborne gravimetry.

J. Emil Nielsen
Kgs. Lyngby, March 2013

Acknowledgment

I want to thank:
My supervisor Rene Forsberg, for letting me have this opportunity.

My supervisor Gabriel Strykowski, for many fruitful discussions.

Finn Bo Madsen for preparing, and great company during the fieldwork in Greenland. Furthermore, for providing GPS data from the Budding GPS station.

Our colleagues at Bundesamt für Kartographie und Geodäsie (BKG) for helping with our Greenland east coast campaign in 2010.

Gudfinna Adalgeirsdottir for generating the SICOPOLIS ice history used in the GIA modelling.

Louise Sandberg Sørensen for providing the ICESat mass change models for Greenland.

Giorgio Spada for providing the code used for the modelling, and for help using his code.

Micheal Bevis for fruitful discussions and letting we sit at his institute and work undisturbed for a short period.

Maersk Oil Kalallit Nunaat for funding my external stay at Ohio State University.

Derek van Westrum, Micro-g LaCoste, for help in many technical and theoretical issues regarding the A10 absolute gravimeter.

Jan Müller (Bundesamt für Kartogrphie und Geodäsie), Jeffrey R. Kennedy (U.S. Geological Survey), Ray Tracey (Geoscience Australia), Marcin Sekowski (Instytut Geodezji i Kartografii) and Ben Fuchs (National Geospatial-Intelligence Agency) for providing A10 data from their respective instruments.

All my colleagues for great support and help of all kind.

And finally without any further comments, my family.

Thank you all!

List of figures

1 Introduction

During the last couple of decades an increasing interest in the effects of the climate change has lead to an intensive research in the polar regions. The main focus is the mass balance of the ice sheets to determine their effect on the future sea level. A variety of techniques are used for monitoring the ice sheets, and of special importance is the different satellite missions. The advantage of these are, that the area of coverage is large and the measurements are repeated over a short time. A good example is the Gravity Recovery and Climate Experiment (GRACE) mission, which delivers monthly solutions of the Earth's gravity field. Many important scientific discoveries have been made with GRACE data, for the estimates of the Greenland Ice Sheets' mass balance, see for example Harig and Simons (2012).

A change in the ice masses is not the only signal GRACE detects, however it also detects geodynamical processes that are connected with movements of mass in the Earth's mantle. Since it is not possible for GRACE to separate the mass changes of the ice from the mass change in the Earth, this latter signal will deteriorate the data as described in Barletta et al. (2008) and Riva et al. (2009), when used for ice mass balance estimates.

To improve the satellite measurements, there are an increasing interest in investigating the geodynamical processes that are ongoing in glaciated areas. There are two processes that are of special interest, both are related to the Earth's response to changes of the ice masses.
The first process is related to the viscoelastic characteristics of the Earth's Asthenosphere. Whether an load, for example ice, is increasing or decreasing on the Earth's surface, this load will introduce a movement of the Asthenosphere away or towards the load, respectively. This movement is associated with mass changes within the Earth and can be detected with gravity measurements. An example of this is the signal in Scandinavia, which is still adjusting after the load from the last ice age approximately 10,000 years ago. This signal is today detected by GRACE and additionally terrestrial absolute gravimetry (Müller et al., 2010). It is not only mass changes, that are associated with GIA, a vertical displacement of the Earth's surface can also be detected. This is carried out with GPS measurements in Scandinavia (Lidberg et al., 2010) and North America (Sella et al., 2007). These examples are from regions of past glaciation, in areas with present day glaciation the other geodynamical process complicates the investigations.
The second process of interest relates to the elastic properties of the Earth's Lithosphere. This process happens on a shorter time scale. An example of the elastic signal is from the seasonal cycle of snow accumulation in Greenland, this is seen in the GPS data presented in Bevis et al. (2012). If there is a general trend of present day ice mass changes (PDIM), this will additional be seen as an elastic signal. Since this signal is related to PDIM changes it is of more interest in climate studies, whereas the first described signal is considered as a source of error.

GPS and absolute gravimetry (AG) are the preferred methods to study the geodynamics in glaciated areas. The Greenland Network (GNET) project, a network of 53 permanent GPS receivers on the bedrock, provides valuable data for the study of GIA and PDIM. The latest results from the GNET project are presented in Bevis et al. (2012). Both, the viscoelastic and the elastic signal produces a vertical displacement of the Earth's surface and the GPS

receiver can not separate the signals. As proposed in Wahr et al. (1995), the combination of vertical displacement data from GPS, and data of gravity change from AG measurements provide the tool for separating the two signals. Mémin et al. (2011a) investigated the separation of the signals in Svalbard, an area of present and past ice mass changes. Furthermore, they recognize another important signal detected by the gravimeter, the direct attraction of the ice masses. The use of absolute gravimetry in glaciated areas is recognized in Ivins et al. (2005), where it is said: *Measurement of the surface gravity change may be important for separation of solid Earth GIA signatures from current ice mass change related gravity. The future for terrestrial gravity measurements may, indeed, be a bright one....* And with more absolute gravimeters in the science community are more AG studies in glaciated areas being performed, for example in Alaska (Sato et al., 2012), Svalbard (Mémin et al., 2011b) and Antarctica (Mäkinen et al., 2007).

In this thesis, the main objective has been to initiate AG time series in Greenland at selected GNET sites. At present, 18 GNET sites have been visited by an A10 absolute gravimeter. The motivation has been the study of the geodynamical signals that with time, can be used to improve the ice sheets mass balance estimates used in climate change studies. Furthermore, I have been investigating the the performance of the A10 absolute gravimeter.

This PhD thesis is divided into two parts. The first part concentrates on the A10 absolute gravimeter purchased by DTU Space in 2008 (serial number 019). Here, the principles of the instrument will be described along with the processing of the data, and the environmental corrections, that are applied to the data. Different processing schemes are tested, and a code has been made to facilitate this. The reason for this is to investigate if the effect of the system response can be minimizing. The system response is a signal in the data that is produced by the instrument itself. There will be presented results of the measurements at our reference site in Denmark. These data are used for assessing the instrument performance, which is compared with other studies of the A10's performance by Schmerge and Francis (2006), Falk et al. (2009), Mäkinen et al. (2010) and Sekowski et al. (2012). This part has the purpose of investigating what kind of performance, that can be expected of the A10, where improvements can be made, and what kind of issues there is when measuring gravity in Greenland.
In the second part, the modelling of the viscoelastic and elastic signals are described, with the focus on the modelling of the gravity signal. Existing code has been used, however they have been modified in order to produce the gravity signal. The code used for modelling the viscoelastic signal is the freely available SELEN (Spada and Stocchi, 2007) and for modelling the elastic signal a code provided by Giorgio Spada (Spada et al., 2012) is used. Newly developed, high resolution, models of PDIM are used in the modelling of the elastic signal and estimations of the direct attraction. These models are derived from ICESat data, see Sørensen et al. (2011) for more. The preliminary results from our gravity measurements in Greenland are also presented here. In connection to this part there are two articles, Nielsen et al. (2013a) and Nielsen et al. (2013b) found in Appendix A.1 and A.2. The modelling part has the purpose of investigating what kind of magnitude the geodynamical signals can be expected to have in Greenland. This can be compared to the performance of the A10 absolute gravimeter.

The assessment of the performance of our A10 is that it perform better than the manufacture

specifications, an accuracy and repeatability down to $6\mu Gal$ for indoor measurements. When comparing the instrument performance results of this study with the results of others there are reason to believe that our instrument can perform even better. To confirm this, more intercomparison with other absolute gravimeters are needed. Furthermore, it is found, that regular calibrations of the instrument along with regular measurements at a reference site are needed for optimal results. The measurements at our reference site in Denmark has proved to be very valuable in assessing the instrument performance. Additionally, these data have proved valuable for studying geodynamics. For optimal data collection in the field, care must be taken in selecting the site and setting up the instrument. The system response signal can lead to an uncertainty in the determination of gravity. The effect of the system response, which can be up to $30\mu Gal$, is difficult to eliminate as shown with the different processing schemes, that are examined in this study.

Modelling of the gravity signal in Greenland consists of three signals, and with increasing order they will be the viscoelastic, the elastic and the direct attraction of the ice masses. The first two are due to the characteristics of the Earth, while the latter is a simple Newtonian effect of attraction. The preliminary measurements in Greenland proves, that significant changes in gravity can appear over a short time period. There are some unresolved questions regarding the nature of the gravity change detected with our measurements, although the direct attraction is a large contributer. The elastic signal can be expected to be in the range of -0.8 to -9.4 $\mu Gal/yr$. This estimate comes from a simple calculation, converting the results of the vertical displacement from the GNET project (Bevis et al., 2012) into gravity with the free air gradient. The viscoelastic signal is smaller than the elastic and will take long time to detect. The preliminary measurements in Greenland are in the range of -28 to $54\mu Gal/yr$. Comparing the measurements with the modelled gravity signal illustrates the challenges of measuring in glaciated areas.

The AG data presented in this thesis are all corrected for the laser drift. Gravity data are presented in the "gravity" coordinate system with positive z-axis downward unless stated otherwise. The AG data from Greenland and Denmark are listed in Appendix E.

Part I
Absolute gravimetry

Since the 1950's the development of the free fall absolute gravimeters have undergone major improvements. A thorough description of the development of such meters can be found in Faller (2002). The first instrument built to use a free falling corner cube, a so-called retro-reflector, in a vacuum chamber and interferometry to measure the falling distance of the corner cube was the instrument by the Joint Institute for Laboratory Astrophysics (JILAg), see Zumberge et al. (1982). This instrument allowed for a determination of g at the μGal level ($1\mu Gal = 10nm/s^2$). One of the improvements of this instrument was the so called "in-line" design. Here, the reference corner cube is located above or below the dropping corner cube. This setup is less sensitive to tilt of the interferometer. The JILAg was succeeded by the FG5 from Micro-g LaCoste, the manufacturer of most commercial gravimeters. The fact that computers, electronics and lasers have become better and more affordable has made it possible to build commercial absolute gravimeters.

This part presents an outline of the principles of the A10 absolute gravimeter and its main components. The procedure of data processing as well as the different data corrections needed for having a final gravity value will be presented. The performance of the A10 is also discussed. Following these chapters there will be an outline of the field experiences we have gained with our absolute gravimeter, the A10-019.
A Fortran code has been written to produce synthetic free fall data. This code is used to study the effect of the system response, and the uncertainty of the gradient. Furthermore, a Fortran code is made for processing the raw data that can be extracted from the Micro-g LaCoste g-software, see Microg (2008b). This code is used to study the effect of the data truncation and alternative data processing schemes. The results of processing the raw data with the aforementioned code have been cross-validated with the g-software and the difference is found to be less than one μGal.

2 The A10

The A10 is designed by Micro-g LaCoste and is build on the principles of the FG5, see Niebauer et al. (1995) for an elaborated description hereof. Small design differences exist between the A10 and the FG5. The A10 is designed to operate in the field and is therefore more sturdy and compact than the FG5. In setup, it is not as demanding as the FG5 and it is less sensitive to environmental changes, however all of these differences are on the cost of accuracy. It can be operated under different temperatures although certain precautions have to be made. Following the company specifications, the A10 has an accuracy and a repeatability of $10\mu Gal$. In studies by Schmerge and Francis (2006), Falk et al. (2009) and Mäkinen et al. (2010) it has been proven that it can preform better than this, and we have found similar results that will be presented in Chapter 5.
The A10 basically consists of three units. The controller, the two "cans" known as the Dropper- and the IB-unit (Interferometer base). The gravity is determined by measuring an object in free fall with standard units of length and time, realized with a Helium-Neon

laser and a Rubidium atomic clock, respectively. The accuracy of the measured gravity is determined by the accuracy of the measurement of these two standards. The relation between these is given by Torge (1989),

$$\frac{dg}{g} = \frac{dz}{z} - 2\frac{dt}{t} \tag{2.1}$$

where z is the length of the fall, dz is the accuracy of the length standard, t is the time of the fall, and dt is the accuracy of the time standard. For the A10, the free fall is approximately $10cm$ and lasts approximately $150ms$. In order to have an accuracy of $10\mu Gal$ or better in g, the accuracy on the position and time of the free fall needs to be on the order of $1nm$ and $1ns$. This is achieved with the laser and the atomic clock. The better accuracy of the FG5 is achieved by a longer falling length and a better accuracy of the laser.
The main parts of the A10 will be described in the following sections. Sections 2.3 and 2.2 focus on the Dropper unit, and Sections 2.4, 2.5 and 2.6 on the IB unit. Additional information can be found in the A10 manual, Microg (2008a).

2.1 The controller

This is the main electronics unit, where the initial setup of the instrument is controlled. The status of the instrument temperature and the vacuum level can be monitored during measurements. The controller is connected to the Dropper- and the IB-unit with $15m$ cables. The data are collected on a laptop connected to the controller. The main quality check of the data is made from this laptop, where the processing and visualization of the measurement is made with the g-software. Details on the processing will be given in Chapter 4.

2.2 Vacuum chamber

The vacuum is aimed to be at approximately 10^{-9} atm. The vacuum is initially established with a Turbo pump, it is an external pump used only for establishing the vacuum. When this is achieved, an Ion-pump sitting inside the Dropper unit is used to maintain the vacuum. The Ion-pump consists of an anode and a cathode plate with $4kV$ across. When an ion enters the Ion-pump it will be deflected and captured on the plates, so the Ion-pump is actually not doing any pumping. One way to check that the Ion-pump is functioning and the vacuum is at the desired level is to see if the voltage across the plates is close to $4kV$. If the Ion-pump is catching a lot of ions the voltage would go down. A poor vacuum would also show up in the residuals, this is the difference between the measured and calculated falling distance.

2.3 Dropper

The Dropper consists of the vacuum chamber and a cart that holds the free falling corner cube. The cart has two purposes; one is to bring the corner cube back to the top of the vacuum chamber after each drop; another is to move any residual molecules in front of the corner cube as it falls through the vacuum chamber. In the beginning of a drop the cart will move with a greater speed than the corner cube, making sure the corner cube is in free fall. Then it will travel with the same speed as the corner cube, keeping a fixed distance between the two until it reaches the end. There it will slow down until it catches the corner cube ready

to bring it back up.
The movement of the cart can be monitored on the controller. This is done using a servo system, where the position of the falling corner cube is determined and used to control the velocity of the cart. The servo system controls the onset of the drop, and the catch of the corner cube at the end of the drop. The servo system is tuned for optimal gravity measurements, and a bad tuning of the servo system will show up in the residuals.
The position of the Dropper will determine at which height the gravity value is measured, and this is specified by the manufacture. For an A10 the height is around $0.71m$, whereas it is $1.20 - 1.30m$ for the FG5.

2.4 Laser

The laser used in the A10 is a polarization-stabilized He-Ne laser, known as the ML-1 (Microg, 2005). It can reach a frequency stability of approximately $10nm$ on a yearly scale and down to $1nm$ on an hourly scale, Niebauer et al. (1988). The A10 laser produces two orthogonal polarized frequencies around $474THz$, approximately $633nm$. These polarizations are used to lock the frequency in two different modes separated by approximately $700MHz$. The frequency modes are denoted red and blue, and during a measurement a pre-set number of free falls, called drops, is carried out in each mode. The locking of the laser frequency is carried out by comparing the intensity of the two polarizations, and when they are equal the laser is locked in either red or blue mode. During measurements, the laser is kept locked by a feedback system that monitors fluctuations in the laser frequency and adjusts the length of the laser tube accordingly. The adjustment is made by heating or cooling the laser tube, and it is also used to switch between the two modes. This means that the laser is sensitive to temperature in the sense that it needs to be able to heat or cool the laser enough so the frequency can be locked. For this reason, it is desirable to have the laser in a steady temperature environment, by having the laser compartment at the bottom of the IB-unit heated to approximately $20 - 30^{\circ}C$ above ambient temperature. Extreme changes in this temperature can affect the performance of the laser, and this should be kept in mind when operating the instrument. In Sekowski et al. (2012), it is shown that there is a correlation between the ambient temperature change and the size of the separation between the red and blue modes. Niebauer et al. (1988) finds that the laser frequency is additionally depending on the atmospheric pressure, and they found a change in the center frequency, the mean of the two modes, of $0.2MHz/bar$. This corresponds to a gravity change of $0.42\mu Gal$ (Mäkinen et al., 2010).

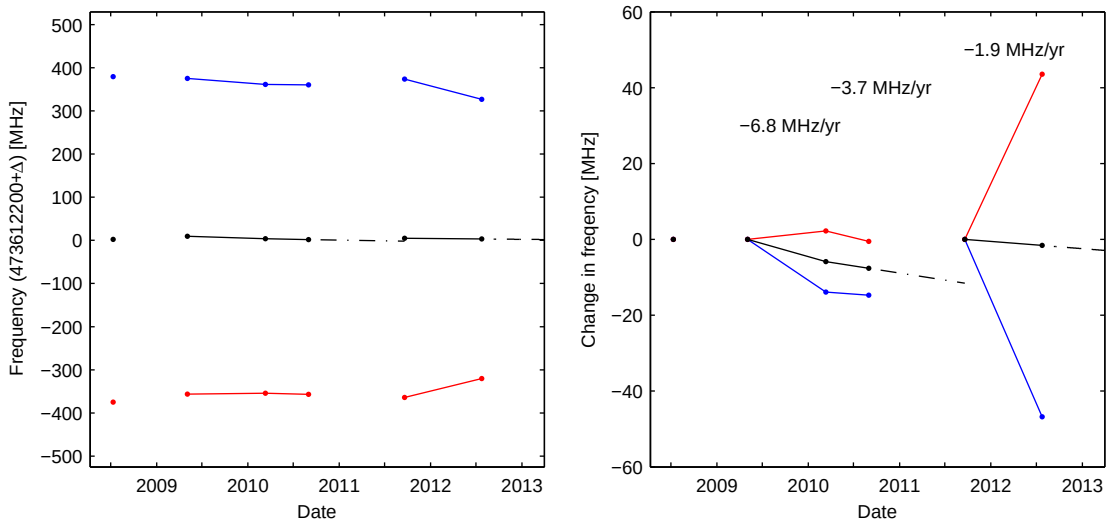

Figure 2.1: The left figure shows the frequency development of the lasers used in the A10-019. The abrupt appearance is due to different lasers installed. The right figure shows the same thing, however with the first laser calibration set as a reference, which emphasizes the drift. The two laser frequencies are presented by red and blue colors while the center frequency is presented with black. The numbers are the center frequency drift in MHz/day, and the black stippled line is the continuation.

It is well known that there is a drift in the frequency of the two modes (Mäkinen et al., 2010). This is due to pressure changes in the laser tube, e.g. due to leakage of the He-Ne gas, as well as changes in the thermal characteristics of the laser tube. When investigating the laser drift through time, it is the average of the two frequencies, the center frequency, that is of greatest interest. This is due to the fact that the two frequencies are drifting in opposite directions, which finally minimizes the effect of the drift on the g-value. In order to keep track of the frequency, the laser has to be calibrated regularly, at least once a year. The frequency history of the A10-019 laser is illustrated in Figure 2.1 with the associated laser drift rates also presented in Table 2.1. The laser frequency data is found in Appendix D, while an example of the laser drift effects on the A10-019 measurements is presented in Chapter 5.

2008 JUL 11	2009 MAY 04	2010 MAR 12	2010 AUG 31	2011 SEP 19	2012 JUL 24
-10.2[a]	-6.8	-3.7[b]	-3.7[c]	-1.9	

Table 2.1: The laser drift in the period from June 2008 to January 2013. The values are valid between the dates above. Units are MHz/yr.
[a] This is an estimated value from the AG measurements carried out at the reference site in the Rockefeller building, Copenhagen.
[b] This calibration was conducted at BKG (Bundesamt für Kartographie und Geodäsie), Germany.
[c] This value is a continuation of the drift in the period from March 12, 2010 to September 19, 2011.

2.5 Interferometer

The traveling distance of the free falling corner cube is determined by the principles of interferometry. The setup is as a Michelson interferometer where one “arm” changes length and produces fringes, a pattern of positive and negative interference of the laser beam. These fringes occur every $\lambda/2$, where λ is the laser frequency, and they are timed with an atomic

Rubidium clock. In order to determine gravity with an interferometer, only one "arm" of the laser path in the interferometer can change length. Thus, the reference corner cube, sitting in the IB-unit, needs to be kept stable while the free falling corner cube in the Dropper is moving. The reference corner cube is kept in place with a Superspring, which will be described in Section 2.6. The interferometer is located on a plate, the interferometer base, sitting on top of the Superspring in the IB-unit. This plate is leveled with two tiltmeters ensuring that the laser beam is traveling vertically and hitting the free falling corner cube. The corner cubes at the end of the two arms in the interferometer are retro-reflective corner cubes, and these ensure that even though they are tilted a little, the incoming laser beam will always be parallel to the returning beam.
Errors in the data collected during the free fall is mainly due to the motion of the reference cube or unwanted motion of the falling corner cube in connection with the onset or termination of the drop. A vibration isolating system, known as the Superspring, is used to minimize such errors, and this is the topic of the next section. Elimination of errors from the onset or termination of the free fall is made through the tuning of the Droppers servo system or by cutting away erroneous data in the data processing described in Section 3.1.

2.6 Superspring

Instruments measuring on the surface of the Earth will be subject to movement of the Earth's surface and many forces can cause these movements, for example solid Earth and ocean tides or earthquake seismicity. The tides can be corrected for through modelling, whereas data with Earthquake seismicity has to be removed. Another kind of seismicity is the background micro-seismicity which consists of Rayleigh waves with periods around $3-20s$ and amplitudes of $20\mu m$. This micro-seismicity can have a significant effect on the gravity measurements, and the Superspring was designed to minimize this effect. As stated in Rinker (1983) it was designed to 1) achieve a factor 10 isolation of the $1/6Hz$ frequency, 2) to introduce no acceleration greater than 10^{-9} of g and 3) to produce an instrument which is compact enough to permit easy transport.
A very long spring is needed to isolate frequencies of that order. The period of a spring is given by $T = 2\pi\sqrt{l/g}$, so increasing the length of the spring will increase its period. To have a spring with a period of $30s$, it needs to be approximately $1km$ long. This is not possible in practice, however it can be simulated and this is the idea behind the Superspring. Using a mass hanging at the end of a spring, as an example, the principle can be described as following: the displacement amplitude of the spring coils are highest near the oscillating mass, and it decreases with distance away from the mass. A very long spring is possible to simulate if the spring is cut, somewhere at a distance away from the mass, and this point is moved according to the oscillation of the mass.

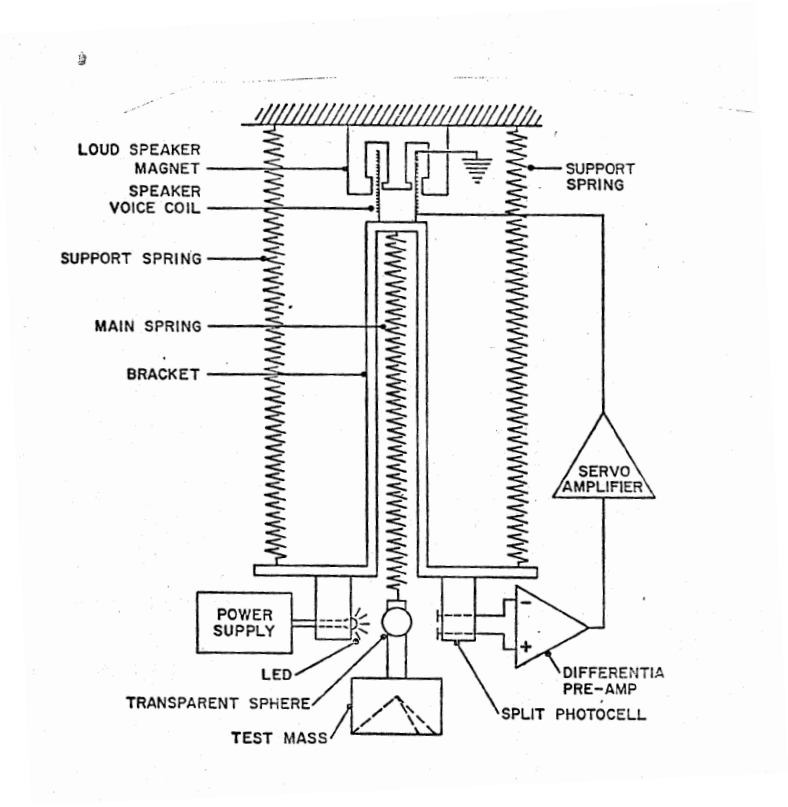

Figure 2.2: The Superspring principle. Figure 7, page 21, from the thesis of Rinker (1983).

The Superspring is build to have a period of approximately 30s. It is therefore able to dampen out frequencies higher than this, meaning that the reference corner cube is isolated from the micro-seismicity. The Superspring consists of two spring systems; the main and the supporting spring. The former is holding the reference corner cube, and the latter is holding an apparatus containing the main spring. By keeping the length of the main spring constant with a servo system, the entire system will have a period of approximately 30 seconds. Details of the Superspring can be found in the thesis by Rinker (1983) and in Faller et al. (1979), and the principle behind it is depicted in Figure 2.2 adapted from Rinker (1983).
It turns out that the system is not completely isolated form vibrations. The instrument itself introduces vibrations when initiating the drop, and this will be discussed in Section 3.3.

3 Data

The data collected with an absolute gravimeter of the free fall type are pairs of position and time. The theory behind the data processing is presented here and some additional processing schemes have been investigated. The influence of different time intervals, the truncation, is also examined. This is investigated due to the fact that the instrument is not completely isolated from vibrations despite the Superspring. As will be presented in this chapter, there is a system response, which is a signal in the data due to vibrations induced by the gravimeter itself. This signal is evident in the residual, this is the difference between the measured and modelled free fall trajectory.

3.1 The free fall

The raw data consists of time values for when a fringe is recorded. A fringe occurs with a fixed distance given by the lasers wavelength, $\lambda/2$, and as the falling corner cube accelerates the fringes will occur with shorter time intervals as seen in Figure 3.1. The total number of fringes that is produced during a fall is $n_{tot} = \Delta l/\lambda/2$, where Δl is the length of the fall. For the A10, n_{tot} is approximately 335000. Only a selection of the n_{tot} fringes are recorded and this selection is controlled electronically by the guide card Multiplex and Scale factor, M_{fac} and S_{fac}. The recorded fringes will have the following index of all fringes, $n_{tot}(i) = 1 + 4(i-1)M_{fac}S_{fac}$, where i goes from 0 to the total number of recorded fringes n, for example 700. Thus with $M_{fac} = 4$ and $S_{fac} = 30$, the fringes recorded will have index $1, 481, 961, 1921, \ldots$ of n_{tot}. In the example in Figure 3.1, the number of recorded fringes is 700.

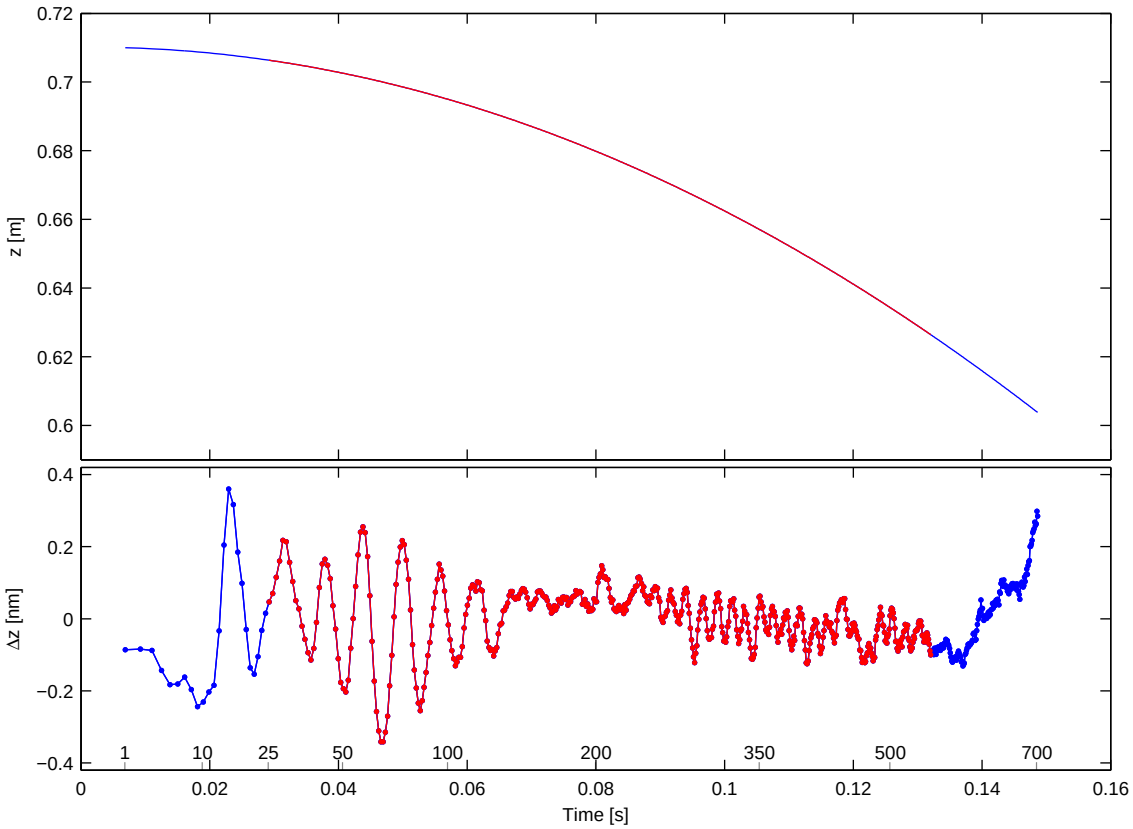

Figure 3.1: The upper figure show the position of the free falling corner cube as a function of time. The lower figure shows the residual between the theoretical and the measured drop curve. The data is the mean of 600 drops from a measurement at our reference point in the Rockefeller building on August 12^{th} 2008. The blue curves represent all the data collected, while the red part is that used for the determination of g. The time window used is from fringe #25 to #550, thus 526 fringes are processed out of 700 in total.

The example used here comes from our reference site in the Rockefeller building in Copenhagen. The data are the mean values of a total of 600 drops, which is often the minimum number of drops that is performed during a measurement.

The equation for the motion of a free falling object only influenced by the gravitational force in a constant gravity field is

$$\frac{d^2z}{dt^2} = \frac{GM}{z^2} \tag{3.1}$$

this is with the z-axis positive down. Assuming that the gravity field is described with a linear gradient, then the first order approximation of the motion becomes

$$\frac{d^2z}{dt^2} = g_0 + \gamma(z - z_0) \tag{3.2}$$

where g_0 and z_0 are the initial acceleration and position and γ is the gravity gradient. Solving this equation with respect to z it yields

$$z(t) = z_0 + v_0 t + \frac{g_0 + \gamma z_0}{2} t^2 + \frac{\gamma v_0}{6} t^3 + \frac{\gamma g_0}{24} t^4 \tag{3.3}$$

where v_0 is the initial velocity. As described earlier, the fringes occur at every $\lambda/2$ so position z_n at time t_n will be given by $n\lambda/2$. Using this and rearranging Equation (3.3) the expression becomes

$$\frac{n\lambda}{2} = z_n(t_n) = z_0 + v_0 t_n + \frac{1}{2} g_0 t_n^2 + \gamma\left(\frac{1}{2} z_0 t_n^2 + \frac{1}{6} v_0 t_n^3 + \frac{1}{24} g_0 t_n^4\right) \tag{3.4}$$

The part in the brackets is due to the linear gradient. If the free fall was carried out in a constant gravity field, $\gamma = 0$, only the first three terms applies and this would be the solution to Equation (3.1).
There is a relativistic effect on the time during the drop. This is an effect of the finite speed of light which will introduce a delay in the time from the laser beam left the falling corner cube until it is recorded. The recorded times need to be corrected for this as following

$$\tilde{t}_n = t_n - \frac{z_n - z_0}{c} \tag{3.5}$$

and therefore do the time t_n in Equation (3.4) needs to be exchanges with the time $\tilde{t}_n$. This effect is explained in Nagornyi et al. (2011) and Rothleitner and Francis (2011).

There have been studies on the determination of g without the use of γ. In this case, the concept of the effective measurement height is introduced. This is the height in the dropping chamber where the gradients influence on the determination of g is non-existing. It is studied in Niebauer (1989), Charles and Hipkin (1995) and Timmen (2003), and it is a method of interest since the determination of g is not affected by the uncertainty on the gradient and the issues of non-linearity. There will be more on the gradient in Section 4.4. If the gradient is not used in the determination of g it will be needed for example when transferring the g value to a ground fix point.

Each drop performed during a measurement is converted to a g-value and the final g-value of the measurement is the averaged value of them all. The processing of the data is presented in Section 3.2, while in Chapter 4 a description of the data corrections needed for an optimal data quality is given.

3.2 Processing

The processing of data is made with the Least Squares Method (LSQ). First rewriting Equation (3.4) and grouping the unknowns, it states

$$z_n(\tilde{t}_n) = z_0\left(1+\frac{\gamma}{2}\tilde{t}_n^2\right) + v_0\left(\tilde{t}_n+\frac{\gamma}{6}\tilde{t}_n^3\right) + g_0\left(\frac{1}{2}\tilde{t}_n^2+\frac{\gamma}{24}\tilde{t}_n^4\right) \tag{3.6}$$

which in matrix form can be written as

$$\mathbf{z} = \mathbf{T}\mathbf{a} \tag{3.7}$$

where the vector $\mathbf{a}$ contains the unknown parameters, here z_0, v_0, g_0, the vector $\mathbf{z} = [z_1, \ldots, z_n]$ contains the positions of the falling corner cube, and the matrix $\mathbf{T}$ is given by

$$\mathbf{T} = \begin{bmatrix} 1+\frac{\gamma}{2}\tilde{t}_1^2 & \tilde{t}_1+\frac{\gamma}{6}\tilde{t}_1^3 & \frac{1}{2}\tilde{t}_1^2+\frac{\gamma}{24}\tilde{t}_1^4 \\ \vdots & \vdots & \vdots \\ 1+\frac{\gamma}{2}\tilde{t}_n^2 & \tilde{t}_n+\frac{\gamma}{6}\tilde{t}_n^3 & \frac{1}{2}\tilde{t}_n^2+\frac{\gamma}{24}\tilde{t}_n^4 \end{bmatrix} \tag{3.8}$$

The LSQ method used to solve Equation (3.7) for the unknown parameters gives

$$\mathbf{a} = (\mathbf{T}^T\mathbf{T})^{-1}\mathbf{T}^T\mathbf{z} \tag{3.9}$$

One issue when determining g_0 is the choice of how many data points that should be included in the processing. One example of the data truncation is given in Figure 3.1. In the beginning and at the end of the drop there can be erroneous data points due to a bad onset or ending of the drop for reasons described in Section 2.3. In the g-software it is possible to set the start and end fringe that is to be included in the processing. It is also possible to evaluate the selected data truncation by examining a visualization of the g-values sensitivity towards the truncation at the beginning and end of the drop. This helps to determine if any post-processing is needed. This visualization is displayed during a measurement in the top and bottom drop fit sensitivity windows of the g-software. A similar result is presented in Figure 3.2 where the processing is made with the code written during this thesis.
The residual is the difference between the measured and theoretical free falls based on the parameters determined in the LSQ processing. The residual is used as a quality check of the data truncation, the health of the instrument, quality of the site, and the influence of the weather. There will be more on the residual in Section 3.3.

Data from one of our measurements at the reference site in Copenhagen, presented in Figure 3.1, is used to investigate the effect of different truncations. The results are presented in Figure 3.2 and 3.3. Originally, the data is truncated at fringe #25 and #550 in the g-software, and this is used as reference for the processing tests carried out here.

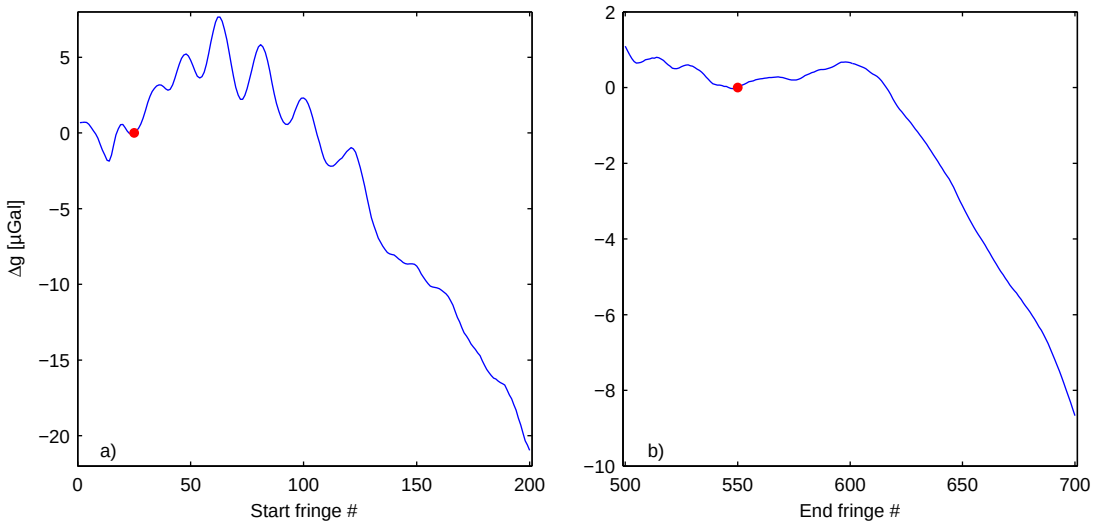

Figure 3.2: In figure a) the end fringe of the truncation is fixed at #550 while varying the start fringe, and in figure b) the start fringe is kept fixed at #25 while the end fringe is varied. The difference in μGal is relative to the truncation with start and end fringe at #25 and #550 respectively; this is marked with red dot in the two figures.

In Figure 3.2, either the start or end fringe is kept fixed, while the other is varied. In Figure 3.2 a), the end fringe is fixed at #550, while the start fringe is varied in the interval 1-200. The difference in the g-value is with respect to the reference value. In Figure 3.2 b) it is opposite, the start fringe is kept fixed at #25 while varying the end fringe in the interval 500-700.

Fringe #	1	25	200	500	550	700
Time [s]	0.007	0.028	0.079	0.124	0.131	0.147

Table 3.1: Relation between fringe number and time. These numbers are valid for the data presented in the figures 3.1, 3.2 and 3.3.

The results in the above figure show that there is a strong dependence on the data truncation. With a varying start fringe, the resulting g-value can change up to $30\mu Gal$ whereas when varying the end fringe the interval is $10\mu Gal$. Comparing this result with the residual in Figure 3.1, a connection to the residual is clear. The large harmonic signal in the beginning of the residual is seen when varying the start fringe in Figure 3.2 a). Furthermore, the last approximately 100 fringes, that in the residual continues upward, give a decrease in the g-value that results in the large variation when varying the end fringe. When those last 100 fringes have been truncated, the g-value is more stable, only varying a few μGal. There will be more on the residual in Section 3.3.

This dependence on the truncation is also examined by others. Klopping et al. (1991) examines this dependence in the processing and found changes of up to 30 μgal for different truncations. They found that removing the system response removes these changes in g with truncation. In Charles and Hipkin (1995), they found similar results; thus changing the truncation can change the determination of g up to $25\mu Gal$, and after a correction of the system response this dependence on truncation can be minimized. They also found that the residual is instrument and site dependent. In Klopping et al. (1991), the data used is from a JILAg

instrument whereas Charles and Hipkin (1995) uses data from a FG5. The system response is investigated in Section 3.3.

In the g-software there is the option of correcting the data for the system response. The author has found that using this option will reduce the effect of the system response, however the solution is not robust, there will still some dependence on the truncation selected.

Only a few fringe combinations are examined in Figure 3.2, while in Figure 3.3 all combinations using start fringes in the interval 1-200 and end fringes in the interval 500-700 are examined. The results in Figure 3.3 are relative to the reference value that is marked with a cross. The minimum and maximum differences are -40 and $12\mu Gal$.

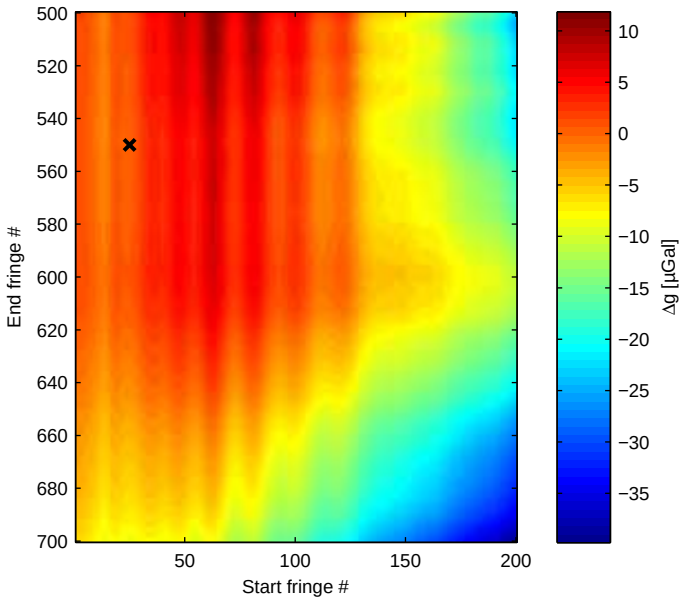

Figure 3.3: The color bar indicates the difference of a given truncation relative to the truncation with start and end fringe #25 and #550 respectively. This solution is marked with a cross.

Again, the residual signal is clear in the model space of different truncations. For example, the "blue" area in the southeast corner is due to the last 100 fringes that have an upward trend as seen in Figure 3.1. The large amplitude signal in the beginning of the residual is also seen with varying start fringe.
Besides looking at the *g*-value it is also of interest to look at the standard deviation (std) of the different combinations. In Figure 3.4 a) the std on each truncation using all drops is plotted, while in b) the std on the sets for each truncations is shown. The sets are the mean of 100 drops, and in this measurement there are six sets. The std between these sets are presented in Figure 3.4 b). The higher std in a) is due to the fact that these values also contain the drop scatter and that is larger than the signal due to the residual. It is noticed that the std is increased as the truncation is increased meaning that the drop scatter is also increased with increasing truncation. The std on the sets indicates a small influence by the truncation selected. The largest change is seen when the first 170 fringes and the last 90 fringes have been truncated.

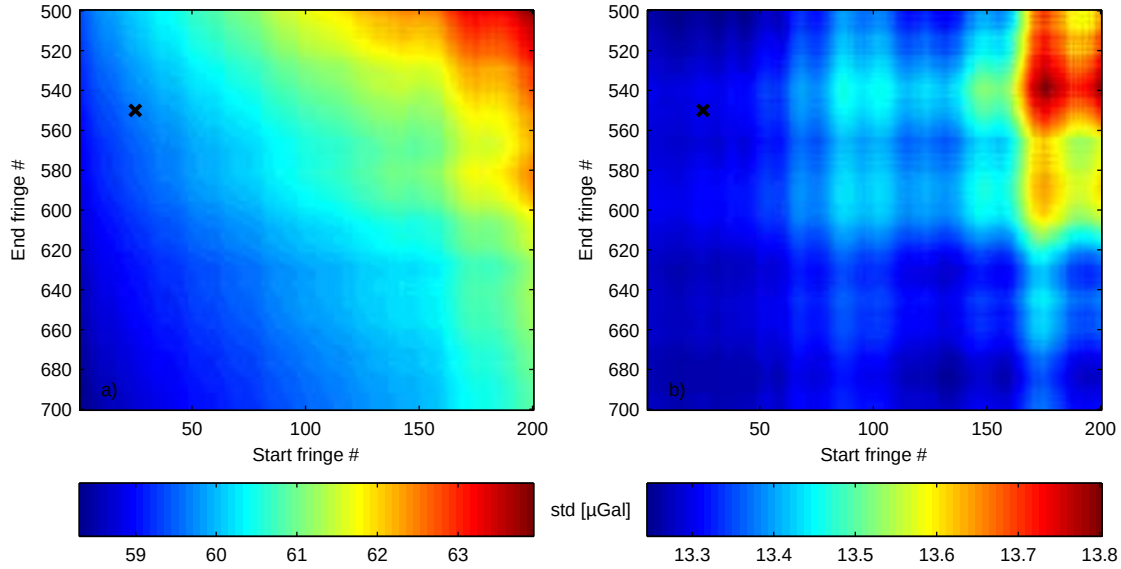

Figure 3.4: To the left, in a), is the std for all g-values in one truncation (here 600 drops). To the right is the std for the set g-values in one truncation (here 6 sets). The color bars indicate the std in μGal. The solution with start and end fringe at #25 and #550 respectively, is marked with a cross.

Different processing schemes have been examined with the intention of minimizing the effect of data truncation. The methods used are listed below with a description of the implementation and findings using both synthetic and real data.

(a) Normal LSQ:
The normal LSQ solution is described in the beginning of this section.
As shown in this section's figures, the normal LSQ solution is influenced by the data truncation. This also holds for the synthetic data where a system response is added to the data, so the residual of using the normal LSQ resembles the residual presented in Figure 3.1. The variations of the results depend on the shape of the residual.

(b) Conditioned LSQ:
In this method one extra parameter is introduced in Equations (3.7), which becomes

$$\begin{bmatrix} \mathbf{z} \\ 0 \end{bmatrix} = \begin{bmatrix} & \mathbf{T} & \\ 0 & 1 & 0 \end{bmatrix} [\mathbf{a}] \tag{3.10}$$

this version has the condition that the initial velocity is equal to zero, $v_0 = 0$. Additional conditions can be added to the solution by adding another row to Equation (3.10). It is solved in the same way as the normal LSQ by Equation (3.9).
Using this method gives the correct answer when used on the synthetic data, there is a small difference when comparing with the g-value used as input, although this difference is less than one μGal. When using this method on real data, the resulting g-value is without a doubt wrong, $960 Gal$! If a time shift is introduced in the data, the result becomes the same as in the normal LSQ, and the solution is dependent on the truncation. The size of the time shift is found through an iterative process where a search is made for the time shift that gives the smallest standard deviation on the residual.

(c) Weighted LSQ:
Assuming that some of the data points of the free fall are more erroneous than others, the weighted LSQ method can be used to minimize their influence. One example of this weighing could be that data points resulting in a large residual is weighted less in the solution. The initial equation for this method is the same as for the two previous methods, Equation (3.7). The solution is changed by the inclusion of the error covariance matrix $\mathbf{C_e}$ in Equation (3.9)

$$\mathbf{a} = (\mathbf{T}^T\mathbf{C_e^{-1}}\mathbf{T})^{-1}(\mathbf{T}^T\mathbf{C_e^{-1}}\mathbf{z}) \tag{3.11}$$

where $\mathbf{C_e}$ is given as

$$\mathbf{C_e} = \sigma_n^2 \begin{bmatrix} w_1^2 & & 0 \\ & \ddots & \\ 0 & & w_n^2 \end{bmatrix} \tag{3.12}$$

the weights, w_i, can be given by some appropriate weighing function or simply zeros and ones.
On the synthetic data, the weighted LSQ gives the correct g-value, and the solution is independent on the truncation.
Using this method on real data shows that the result is dependent on the truncation even for different weight functions.
As a test, two different weighing functions are used. One is built on the mean residual of all drops in the measurement. Here, the data points with the highest residual is given the smallest weight and vice versa. The weight is determined as a function with values between one and zero given by $ABS(MAX(residual)/residual)$.
The second weight function is a further development of the first. As an extra condition, a parabola with its apex at center of the drop is multiplied to first weight function, giving less weight to the data points at the beginning and end of the drop.
The problem with this method of weighing the data is that the residual is depends on the initial truncation and the result is highly dependent on the weight function used.
In Nagornyi (1995), different examples of weight functions are presented, however their focus is on alternative processing methods and not the truncating of data.

(d) Weighted LSQ with a priori:
This method builds on the previous equations and adds additional information to the solution. As the name indicates, it is possible to add information to the solution, for example information about the height z_0 where the drop is initiated, and it is possible to do so including an uncertainty. The equation used is (3.10), which is solved using (3.11), and the covariance matrix in Equation (3.12) gets additional information in its diagonal.
Using this method on synthetic data the result is the same as for the weighted method.
When using the method on real data the results are similar to the weighted LSQ. This solution is also dependent on the truncation, and it is very dependent on the use of the a priori information as well as the uncertainty on this information. When the uncertainty on the a priori information is high, the result resembles the normal LSQ solution. Furthermore, the two different weight functions, described under the weighted LSQ, have a significant effect on the result.

The synthetic data have been used to make different studies on what influences the determination of gravity. It shows that a 10% error on the gradient results in an approximately $1\mu Gal$ error on the g-value using the normal LSQ. For the other methods, it is found that the conditioned LSQ is least affected by errors in the gradient. Here, will a 10% error on the gradient, introduces an error of $0.5\mu Gal$, whereas in the weighted LSQ and the weighted LSQ with a priori the error is $1.8\mu Gal$.

Only the conditioned LSQ, is robust to the truncation when applied to the synthetic data. The variations are less than $1\mu Gal$. When applied to real data the picture changes. Then the methods weighted LSQ and weighted LSQ with a priori depend on the truncation, while the conditioned LSQ gives an erroneous result unless a time shift is introduced. The need for introducing a time shift comes from the fact the the initial velocity is not zero when the first fringe is recorded. In the FG5 system there is a 20-30ms delay from the corner cube is dropped till the first fringe is recorded at time $t = 0$. This means that there is an offset of approximately $5mm$ from the start of the drop to the start of the measurements (Niebauer et al., 1995).

A common feature for the synthetic and the real data is that the residual depends on the truncation of the data. Thus, if the residual is used for correcting the data, this correction will be influenced by the choice of initial truncation. The corrected data will be independent on the truncation, however the g-value will be fixed by the initial truncation. Any correction of the data thereby has to be done independently of the residual and before fitting the data.

During this study, it is also investigated if there is any value that is statistically significant in the processing of multiple truncations or a selection of truncations. The distribution of the solutions using all the truncations in Figure 3.3 is shown in Figure 3.5 a). For this distribution the mean is: $-6\mu Gal$, the median: $-4\mu Gal$ and the mode is $0\mu Gal$. Excluding the first 25 and the last 150 fringes gives the distribution in b) with the mean: $-3\mu Gal$, the median: $1\mu Gal$ and the mode: $4\mu Gal$. The distribution in c) is for the solutions using start fringes 15-35 and end fringes 500-600, which has the mean: $1\mu Gal$, the median: $1\mu Gal$ and the mode: $1\mu Gal$.

There is no clear trend, for example the mean goes from -6 to -3 to $1\mu Gal$. What is of interest is that with a selection of a few fringes, as in c) the mean, median and mode reach the same values, which holds for a normal distribution.

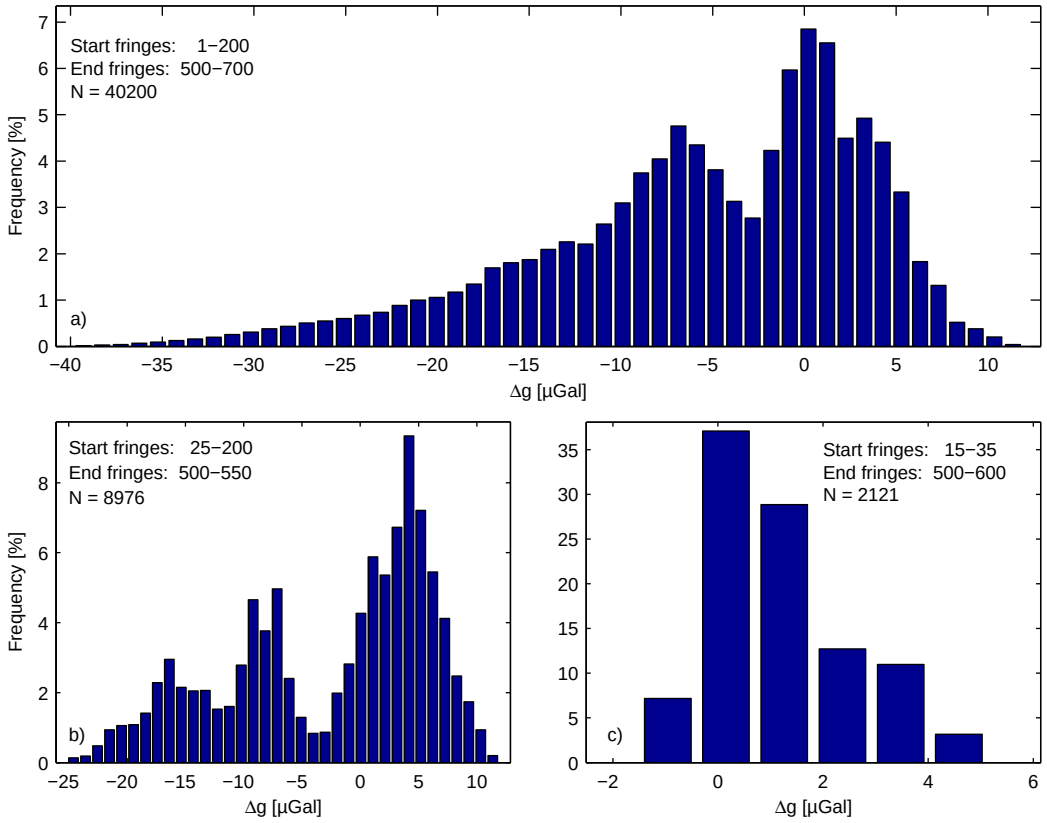

Figure 3.5: In a) all truncations are included, and it is the same data as in Figure 3.3. In b), the fringes 25-200 in the start and 500-550 in the end are included, and finally in c) the start fringes 15-35 and the fringes 500-600 are included. The difference is relative to the reference combination. The bins are $1\mu Gal$ in width.

Doing the same study on synthetic data shows that the data is slightly skewed. Investigating the difference between the processed g-value for different truncations and that the real g-value shows that the real g-value is not found as either the mean, the median or the mode. Producing another synthetic free fall, using the same harmonic signal, however flipped around the time axis, shifts the distribution, for example so the mean value of the differences becomes positive instead of negative. For these two kind of distributions, the real g-value is found to lie between 0.25 and 0.75 on the cumulative distribution function. The data can for the synthetic study is presented in Appendix G.

This has been used for a different processing approach. In this approach, every drop is processed with the 40200 different truncations that are used to produce Figure 3.5 a). The distribution of the individual drops is then investigated for different parameters.

The distribution of the solutions is presented in Figure 3.6 with a box plot of the 100 first drops. The data used is the August 12^{th}, 2008 measurement at the Rockefeller site and a box plot of all 600 drops of this measurement is presented in Appendix F.4.

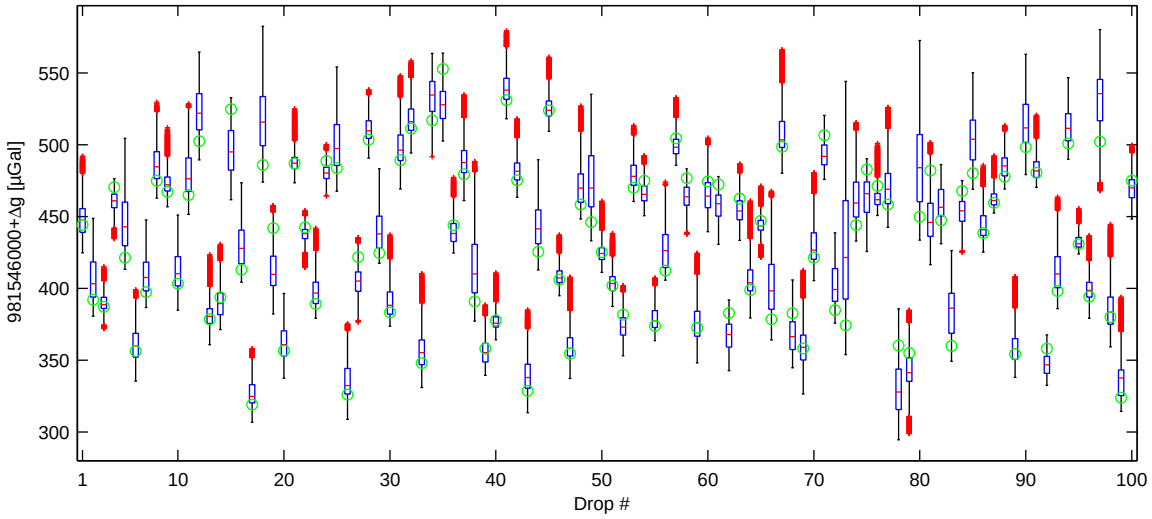

Figure 3.6: The first 100 drops of the August 12^{th}, 2008 measurement at the Rockefeller site. The green circles are the values from the normal LSQ solution. The edge of the boxes are the 25 and 75 percentiles, the red line in the box is the median. The black lines indicates the minimum and maximum value of the distribution and the red crosses are outliers.

The normal LSQ solution gives a value of: 981 546 417μGal with a std of 60μGal for this measurement. Investigating the mean, median and mode of the solutions for every drop, and calculating a mean value of all the drops gives the results presented in Table 3.2. Also presented is the mean of the g-values at the 0.25 and 0.75 probability found by calculating the cumulative distribution function. An example of this function is given in Figure G.4. These values are calculated for three different fringe combinations.

	Mean	Median	Mode	Mean($P_{0.25}$,$P_{0.75}$)
Fringe combi. 1)	423	421	416	439
Fringe combi. 2)	420	418	413	437
Fringe combi. 3)	416	417	417	419
Normal LSQ	417			

Table 3.2: The values are 981 546 000 + Δg with units μGal. The different fringe combinations included in the calculations are; 1) start 1-200, end 500-700, 2) start 25-200, end 500-550 and 3) start 15-35, end 500-600. The data are from the August 12^{th}, 2008 measurement at the Rockefeller site.

For all solutions, using the different parameters and fringe combinations, the std do not change significantly. It stays at 60μGal. This means that none of the solutions can improve the drop scatter. As presented in Table 3.2 are most value above the normal LSQ solution. It furthermore shows that as the number of different truncations used in the calculations is reduced, the smaller the difference becomes between the different parameters.

As a last study has the above investigations been made on three successive measurement at our reference site. This is to examine if the difference between the measurements are improved using this approach. The three measurements were conducted on June 10^{th}, 2010. The result is presented in Table 3.3

a)	Mean	Median	Mode	Mean($P_{0.25}$,$P_{0.75}$)
Fringe combi. 1)	419	418	418	429
Fringe combi. 2)	418	418	418	426
Fringe combi. 3)	418	418	418	426
Normal LSQ	419			

b)	Mean	Median	Mode	Mean($P_{0.25}$,$P_{0.75}$)
Fringe combi. 1)	408	407	406	416
Fringe combi. 2)	408	407	406	414
Fringe combi. 3)	407	408	408	415
Normal LSQ	407			

c)	Mean	Median	Mode	Mean($P_{0.25}$,$P_{0.75}$)
Fringe combi. 1)	410	410	408	419
Fringe combi. 2)	409	409	408	417
Fringe combi. 3)	410	410	410	418
Normal LSQ	411			

Table 3.3: The different fringe combinations included in the calculations are; 1) start 1-150, end 600-750, 2) start 35-150, end 600-705 and 3) start 25-45, end 670-730. The data are from three measurements conducted on June 10^{th}, 2010 at the Rockefeller site.

As for the measurement presented in Table 3.2, the std is not changed significantly for the different methods used on these measurements. The difference between the different methods is small. This is due to the distribution of the solutions which is less spread out and more normal distributed than the example in Table 3.2. For these three measurements the std is 35, 44 and 60μGal, respectively, and no significant change appears during the different calculations.

From the this type of processing the result can vary depending on the parameter investigated and the solutions that are included. Although, there are variations in the processing results of the three measurements conducted on June 10^{th}, they seem to be more robust towards the number of solutions used. This especially holds for the parameters, mean, median and mode. Investigating the probability function results in more diverse results than the other parameters.
The investigations that are conducted on these four measurements does not give any clear indications on the best approach to interpret the processing.

3.3 System response

When the drop is initiated, the Dropper will induce a force of more than one g into the ground, and this force will induce ground vibrations that will translate into the IB-unit and the Superspring. As mentioned in Section 2.3, the Superspring is unable to dampen all vibration and they will show up in the residual. Since the signal is due to the instrument itself it is called the system response. This response depends on the site, the instrument and the setup by the operator. An example of the effect of the site is given in Figures 6.5 and 6.6.

The presence of the system response is studied in Klopping et al. (1991). They look at the JILAg instrument and lists two reasons for the signal; micro-seismics and the Dropper itself via the air-gap modulation, see also Niebauer et al. (1995) for details. They find that the

floor-gravimeter system response not only varies from site to site, also from setup to setup and even during a measurement. In Timmen et al. (1993), it is mentioned that by having the Dropper legs of the JILAg-3 instrument outside the measurement pier, the floor recoil effect is greatly reduced. They find that a $30Hz$ signal in the residuals is produced by the instrument itself. They also see changing g-values for different truncations. In Rothleitner et al. (2009), there is a description of causes to the system response. Robertson (2001) mentions that the system response can be found in the residuals and that day to day changes in the response pattern indicates a strong dependence on the instrument setup. They conclude that is is more desirable to minimize the system response rather then introducing a post-processing scheme for its removal. It is suggested that one way of doing so is to make an instrument where the Dropper is operating with counterweights to minimize the forces involved in the drop. Micro-g LaCoste introduced the FG5X in 2010, which operates with counterweights reducing the recoil and thereby the system response. See Niebauer et al. (2012) for more on the FG5X.

The system response is described as a sum of exponentially decaying harmonics

$$R = \sum_{i=1}^{n} [a_i \sin \omega_i t + b_i \cos \omega_i t] e^{-k_i t} \tag{3.13}$$

where a and b are the amplitudes of the cosine and sine components respectively, ω is the frequency and k is the exponential decay constant. It can also be written as

$$R = \sum_{i=1}^{n} [a_i \sin(\omega_i t + \phi_i)] e^{-k_i t} \tag{3.14}$$

where ϕ is a phase shift. The effect of the system response is investigated using synthetic data. Some of the results from these investigations are presented in Figure 3.7 and 3.8. The calculations for Figure 3.7 are made for different phases in order to see the maximum effect of the harmonics.

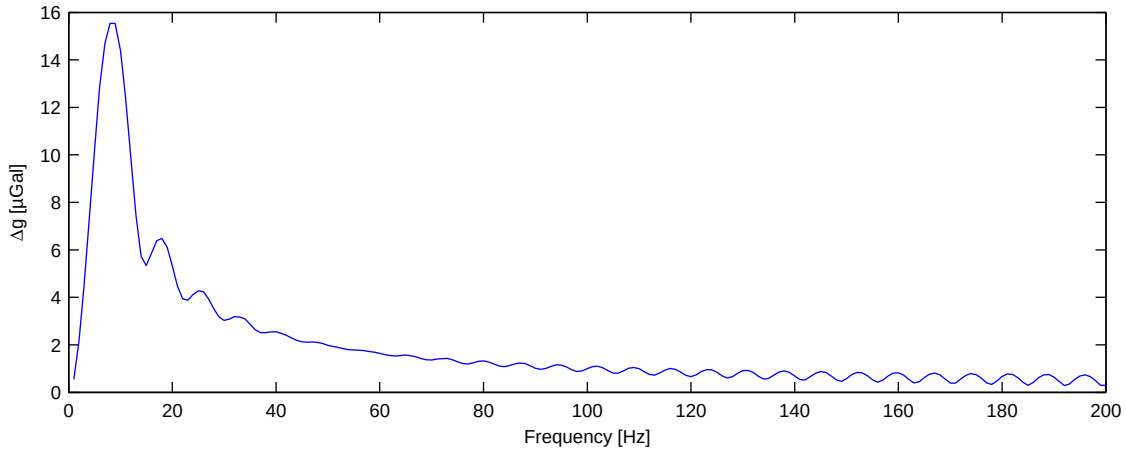

Figure 3.7: The effect of a single frequency of harmonic noise, with no exponential decay, and amplitudes of $0.1nm$, the highest effect is around $8-9Hz$ for a free fall of $0.10m$ and 750 recorded fringes.

The effect of a frequency of approximately $8Hz$ gives the largest error in the data, however as shown in Figure 3.8 it depends on the phase. The $8Hz$ corresponds approximately to one period during the full length of the free fall.

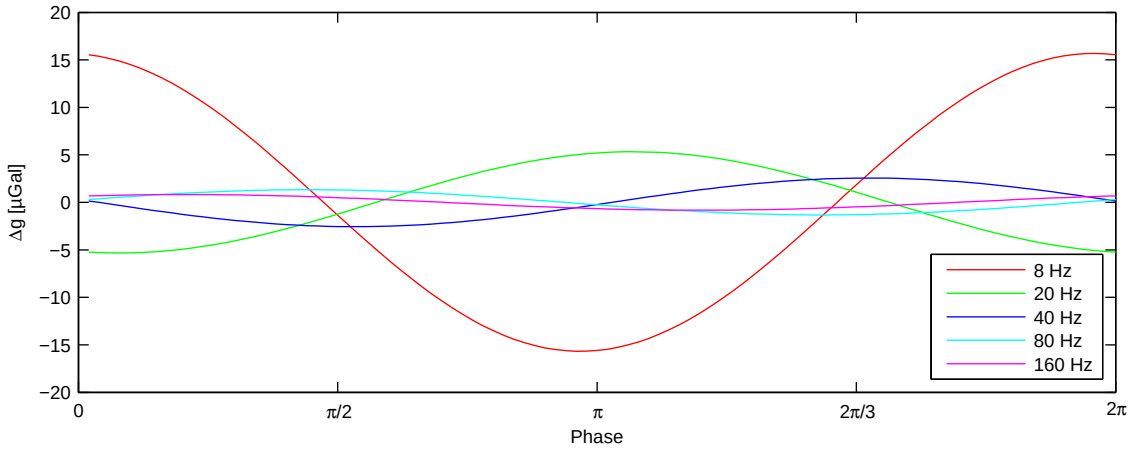

Figure 3.8: The effect of phase change of the system response with no exponential decay and amplitudes of $0.1nm$, for a free fall of $0.10m$ and 750 fringes recorded.

Studies using synthetic data show that the relation between the resulting g-value and the amplitude of the system response scales linearly, so increasing the amplitudes with a factor of ten will increase the influence on g with the same factor. An increase in the length of the free fall will minimize the effect of the system response. This is an inverse linear relationship, so increasing the travel length by a factor two will minimize the effect of the system response by a factor of $1/2$. The presence of the decay constant will minimize the effect of the residual near the ending if the drop, which is also evident when examining the different truncations. Here is can be seen that the resulting g-value is less sensitive to the truncation at the end of the drop.

The Lomb-Scargle method (Lomb, 1976) is implemented in my processing code to investigate the characteristics of the system response. This determines the frequency spectrum in the system response and estimates the associated amplitude.
Figure 3.9 shows an example of the Normalized Lomb-Scargle Periodogram for the two residuals in Figure 3.1, one for the full data set, Figure 3.9 a), and one for the truncated data set, Figure 3.9 b). The power of the frequencies in the interval $1-400Hz$ is found on the left ordinate and is given with a blue color, while the power of their amplitude is found on the right ordinate and given by a green color. The power of the amplitude can also be used as an estimate of the amplitudes order. They are merely estimates since the presence of the decaying exponential term will alter the amplitude during the fall. The three gray horizontal lines are the significance levels of 0.001, 0.01 and 0.1 from top to bottom. Any frequencies above the 0.001 line are considered to be significant.

As seen in Figure 3.9 a), a low frequency signal in the full data set exists, which becomes less significant when the data is truncated. Furthermore, with the truncation of data there are a couple of high frequencies that increase their significance and shift slightly towards lower frequencies. The minimized effect of the low frequencies is desirable since they have the

largest influence on the determination of gravity.

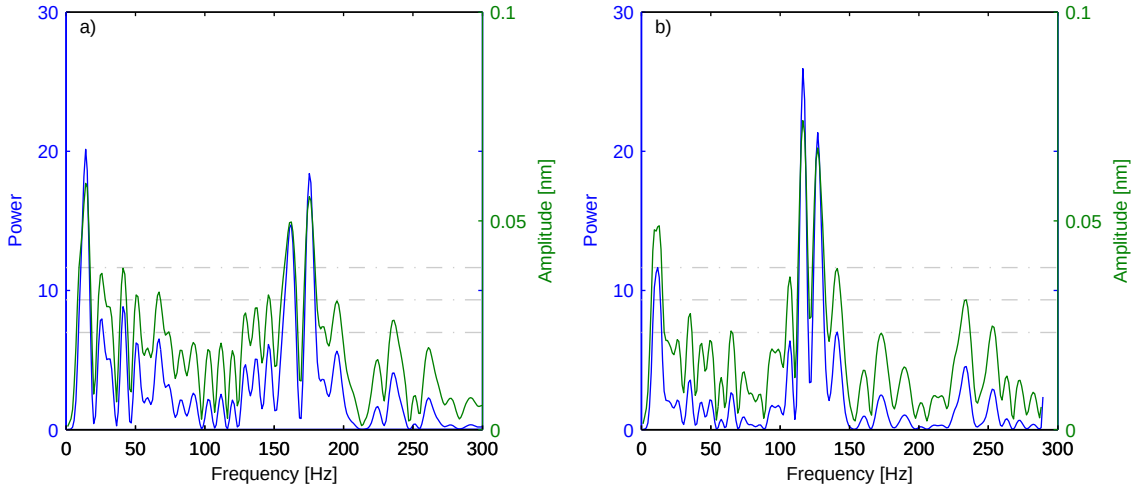

Figure 3.9: Figure a) shows the full data set, while b) shows a truncated data set using start and end fringe #25 and #550, respectively. In a), the three most significant frequencies are 14, 175 and $162Hz$, while for b) they are 116, 127 and $12Hz$, respectively.

To see the effect of different truncations on the residual, a periodogram is calculated for all fringe combinations presented in Figure 3.3, and the result is presented in Figure 3.10. The peridogram is based on the mean residual of all 600 drops.

Figure 3.10 shows that the characteristics of the residual changes according to the truncation. As the truncation is increased, the low frequency signal loses power and a shift of the higher frequencies occurs.

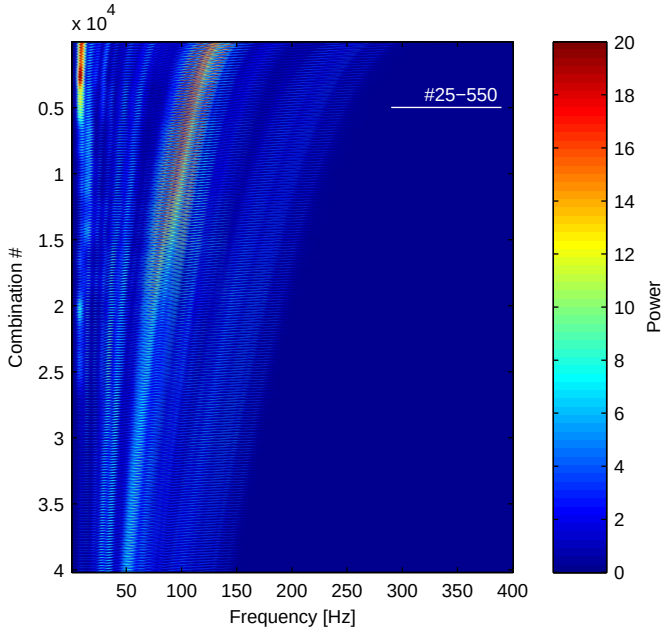

Figure 3.10: A Normalized Lomb-Scargle Periodogram is calculated for all the different truncations. Here, all the combinations are shown. The color bar indicates the power of the individual frequencies. The truncation with start fringe #25 and end fringe #550 is marked with a white line.

The system response can be expected to change from site to site and from time to time as the instrument changes it characteristics (different Dropper tuning, the state of the Superspring, etc.). Also, weather and the setup (the operator) will have an influence on the system response. Despite these factors, some common features are found to be instrument dependent. For example, there is very often a low frequency signal, approximately $15-25Hz$, present in the residual. Figure 3.11 displays the residual of 100 drops and their mean.
Besides the mentioned factors, the exponential decay is a result of the Superspring characteristics. To enhance the efficiency of the Superspring an electronic damping of the spring is implemented when excited. This damping has the appearance of an exponentially decaying harmonic (Rinker, 1983, Figure 41). Thus, the residual is a combined signal that originates from the environment and the instrument.

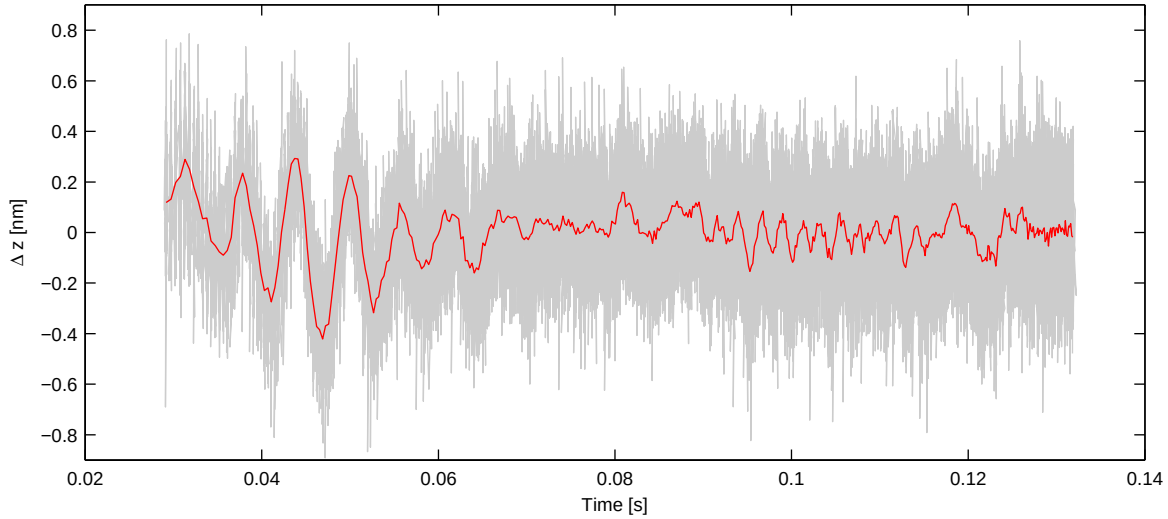

Figure 3.11: The residual of 100 drops is plotted in gray, while the mean of these is plotted in red.

Tests of a physical damping of the system response have been carried out during the PhD. Simple tests have been made in an attempt to decrease the system response. For example, the distance between the Dropper and the IB-unit has been increased from the approximately $3mm$ that the system makes itself to $3cm$. This gave a small improvement in the drop scatter, however not enough for saying anything conclusive. Furthermore, tests where the Dropper legs were fixed to make the setup more robust during the drops showed no improvements. A test has also been made where vibration absorptions pads are placed under the Dropper or the IB-unit. Placing them under the IB-unit increased the drop scatter, however the residual was damped quicker. Placing the Dropper on pads increased the drop scatter and the system response. A final test that has been made is to change the drop frequency from one per second to one per two seconds. This procedure does seem to improve the drop scatter slightly so this procedure could be used for indoor measurements. For outdoor measurements with the influence of the environment, the benefit is properly not significant.
The largest effect seems to be gained with vibration absorption pads. For these tests only one kind is tested, and more tests of different kinds would be beneficial. to test different kinds.

3.4 Uncertainties

The uncertainty associated with the final g-value is given as the sum of a system uncertainty and a statistical uncertainty

$$\delta_{set} = \sqrt{\delta_{sys}^2 + \delta_{stat}^2} \tag{3.15}$$

where $\delta_{stat} = \sigma_{set}/\sqrt{N_{set}}$. The system uncertainty of the A10 is approximately $10\mu Gal$. This value is determined from the uncertainties on instrumental parameters, modelled corrections and setup. The size of the individual uncertainties is presented in Table 3.4. Niebauer et al. (1995) describes details on the parameters that influence the system's uncertainty for the FG5, and some of these apply to the A10. In the g-software, a description of the parameters that are included in the uncertainty estimate for the A10 is given (Microg, 2008b). It is comprised by the parameters in Table 3.4.

System	Laser	0.05
	Clock	0.5
	A10	10
Modelling	Earth tides[a]	0.001
	Ocean tides[b]	0.1
	Atmospheric	1
	Polar motion	0.05
Setup	System	3
	Gradient[c]	0.03

Table 3.4: Uncertainties as given in the g-software, and they sum up to a system uncertainty of $10.50\mu Gal$. Units are in μGal except for the uncertainty on the gradient, which is in $\mu Gal/cm$.
[a,b] The uncertainty on the tidal corrections is the modelled correction multiplied by this value.
[c] This is the uncertainty on the gradient, so this only applies to the final data if the g-value needs to be transfered to another height. Thus, transferring an A10 measurement at $0.71m$ to ground level gives an uncertainty of $2.13\mu Gal$.

The A10 system accuracy is by far the parameter that controls the total uncertainty. The determination of this value is made by comparison of the instrument with another absolute gravimeter. Studies into the accuracy of the A10 have been made by others and it is proved that the A10 can perform better than the $10\mu Gal$ given by the manufacture. Schmerge and Francis (2006) finds that under laboratory conditions the accuracy can be down to $3.2\mu Gal$ when comparing with an FG5 at 15 laboratory sites. Falk et al. (2009) found an accuracy of $6\mu Gal$ in laboratory condition while the accuracy in the field is estimated to $6-8\mu Gal$. Similar result is found for our instrument. See Section 5.1 for more on this.

There are some additional parameters that can introduce an uncertainty in the g-value. These are both of instrumental and environmental character.
Regarding the instrumental there is, as mentioned in Section 2.4, the laser drift that can introduce an uncertainty if not regularly calibrated. Also there is a drift of the Rubidium clock, which is a smaller effect, however it still needs to be monitored with regular calibrations. There is also a self-gravitation of the instrument. This is the attraction the different parts of the instrument exerts on the falling corner cube. For the A10, this attraction is estimated to

be small, on the order of $\pm 0.4 \mu Gal$[1].

Of environmental character there is the positioning of the site. This is of importance for the corrections that will be presented in Chapter 4. The elevation given should be better than $10m$ and the position should be better than $10''$, approximately $30m$. When measuring outside, the weather conditions can have a large influence on the measurement. Strong winds will increase the drop scatter and can also influence the setup uncertainty since winds can make the verticality check difficult. The ambient temperature also plays an important role since it can influence the stability of the laser frequency.
There is also the uncertainty that is introduced by the system response, and which is both of instrumental and environmental character. One way to minimize this is to do more than one setup at a site, and if the setups are made with different orientations, north/south, any effects of the Coriolis force can be eliminated. This is estimated to be less than $1 \mu Gal$ for the A10 system, so the importance of this is of second order, however it is good practice.

4 Data corrections

There is a number of environmental corrections that need to be applied to the measurements before having the final g-value. These corrections are applied to every drop since they are time dependent and can change within minutes. Besides the environmental corrections, there is the correction for the laser drift mentioned in Section 2.4 as well as the optional correction for the system response described in Section 3.3. The laser correction is applied to the final result, whereas the correction for the system response is something that is applied to the individual drops. Figures 4.1 to 4.5 give an indication of the individual corrections variability and magnitude.
The different environmental corrections will be presented in the following sections conferring Timmen (2009). Section 4.4 describes the gradient, a correction which is applied if the g-value is needed at another height than the instrument height.

4.1 Tidal

The Sun and Moon (and to a lesser extend the other planets in the solar system) exert gravitational forces on the Earth. These forces give rise to two tidal phenomenons on the Earth: the solid Earth tides, or body tides, and the ocean tides. The former can easily be modelled and corrected for, whereas the ocean tides are more complex as they depend on the geographical setting of where the measurement is conducted. There can be some discrepancies from the global ocean models used in the g-software and the actual conditions at the site. This discrepancy will show up in the data as a residual periodic signal. It is possible to input a revised ocean model into the g-software (Microg, 2008b) if the information is available. A locally determined ocean tide model would improve the result of the gravity measurements at some sites.

It is recommended to conduct the gravity measurement for a duration of $24 - 48h$, as any

[1] Information is obtained from a presentation given by Derek van Westrum at the IAG meeting in Vienna, February $14^{th} - 15^{th}$, 2012.

residual tidal signal in the data will be averaged out. Measuring gravity for a short time period, $30-60min$, can introduce an offsets in the g-value if a residual tidal signal is present. If a periodic signal is present in the measurement, the first thing to check for is if the data collecting computer has an offset to UTC time.

4.1.1 The solid Earth tides

The solid Earth tides are the periodic elastic deformation of the Earth's surface. It has an amplitude range of $40cm$ at mid-latitudes and a maximum gravitational variation of $300\mu Gal$ (Timmen, 2009). The motion of the sun, the moon and the planets are well known which makes it possible to calculate the forces they exert on the Earth very accurately, so the correction becomes better than $0.1\mu Gal$.

In the g-software there are the options for using the Berger or the ETGTAB (Wenzel, 1996) tidal models, it is recommended to use the latter. The ETGTAB code is used to produce Figure 4.1, which shows the solid Earth tide correction during the period of our AG measurements in Copenhagen.

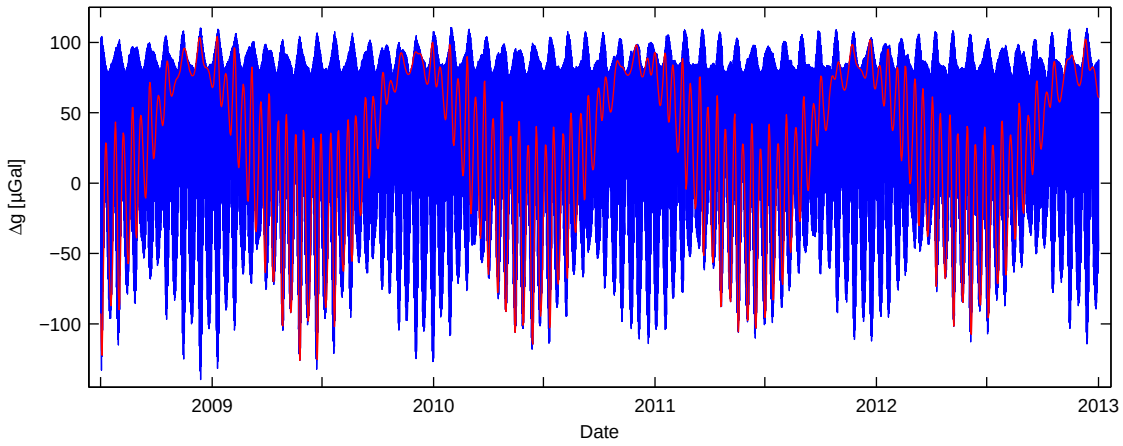

Figure 4.1: The solid Earth tide correction for the reference site at the Rockefeller building in Copenhagen in the period from June 2008 to January 2013. The data are produced from the ETGTAB code by Wenzel (1996). The blue line is hourly estimates, while the red line is daily estimates. Both show the variability of the signal.

4.1.2 The ocean tides

As the Sun and Moon exert a gravitational pull that deforms the Earth surface, their pull will also redistribute the ocean waters. This redistribution of masses will change the load on the Earth, which will deform in response. Ways of calculating the response to surface loads will be presented in the second part (Part II), with ice as the loading mass.

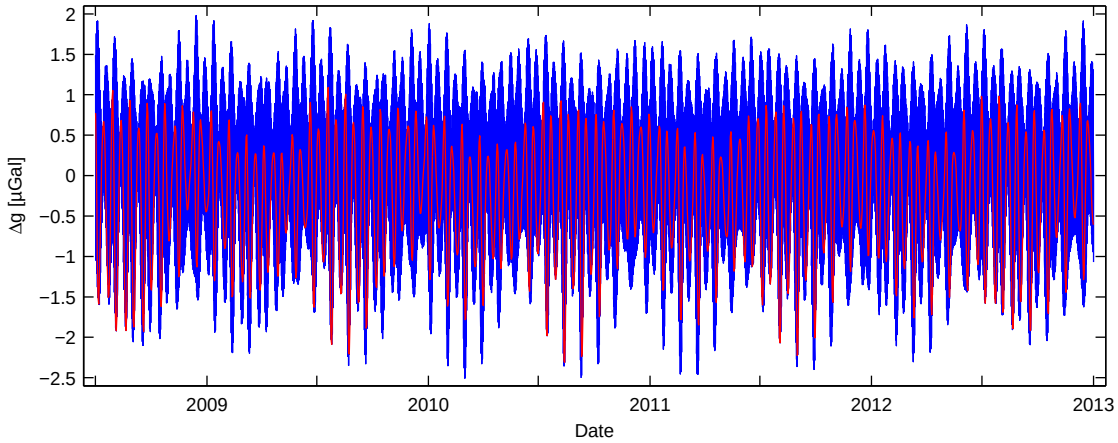

Figure 4.2: The ocean tide correction for the reference site at the Rockefeller building in Copenhagen in the period from June 2008 to January 2013. The blue line is hourly estimates, while the red line is daily estimates. Both show the variability of the signal. The ocean model used is the NAO.99b.

The ocean loading in Figure 4.2 is calculated using the NAO.99b global model (Matsumoto et al., 2000), and calculated by using the freely available code GOTIC2 (Matsumoto et al., 2001).

The ocean loading models in the g-software are the Schwiderski model (SCH) Schwiderski (1980), the CSR3.0 model (CSR) Eanes and Bettadpur (1995), and the FES2004 model (FES) Lyard et al. (2006). The SCH model is the oldest, and it is based on a fit to global tide gauge data. The CSR model, from Center of Space Research, University of Texas, has some issues with ocean grid cells over land and only covers the latitudes $66N$ - $66S$, which is the inclination of the Topex/Posidion satellites. The FES (Finite elements solution) from the University of Grenoble, is the one that is recommended to use. This model uses world wide tide gauge data and incorporates long wavelength data from the Topex/Posidion satellites. An example of the difference between the tidal corrections of the three ocean models in the g-software is presented in Figure 4.3 for two sites in Greenland.
There are other global ocean loading models, for example the GOT and the DTU10 model, which could be of interest regarding correction of the gravity measurements. The DTU10 models is an extension of the FES model to coastal regions (Cheng and Andersen, 2010) and has proved to compare well with tide gauge data in Greenland[2]. Furthermore, more regional models are available, and of interest for the Greenland region is the AOTIM-5 model (Artic Ocean tide inverse model) (Padman and Erofeeva, 2004).
Bos and Baker (2005) describes a comparison of different ocean models, while Agnew (2012) provides an overview of the different models.

The global ocean loading models have problems in shallow water where the amplitude is high and the phase is varying quickly. Some models do not cover shallow waters for this reason, and it will give problems in fjords as shown in Richter et al. (2011). They compare tide gauge measurements on the west coast of Greenland with the FES2004 model. They find a good agreement between the tide gauge data and the ocean model for station near the coast, whereas there is a discrepancy in the fjords. This discrepancy can result from a lack of

[2]Ole B. Andersen, personal communication, January 16^{th}, 2013

coastal resolution in the global models. This means that a local determination of the ocean loading, for example using local tide gauge data and a high resolution coast line, can give improvements in the gravity correction.

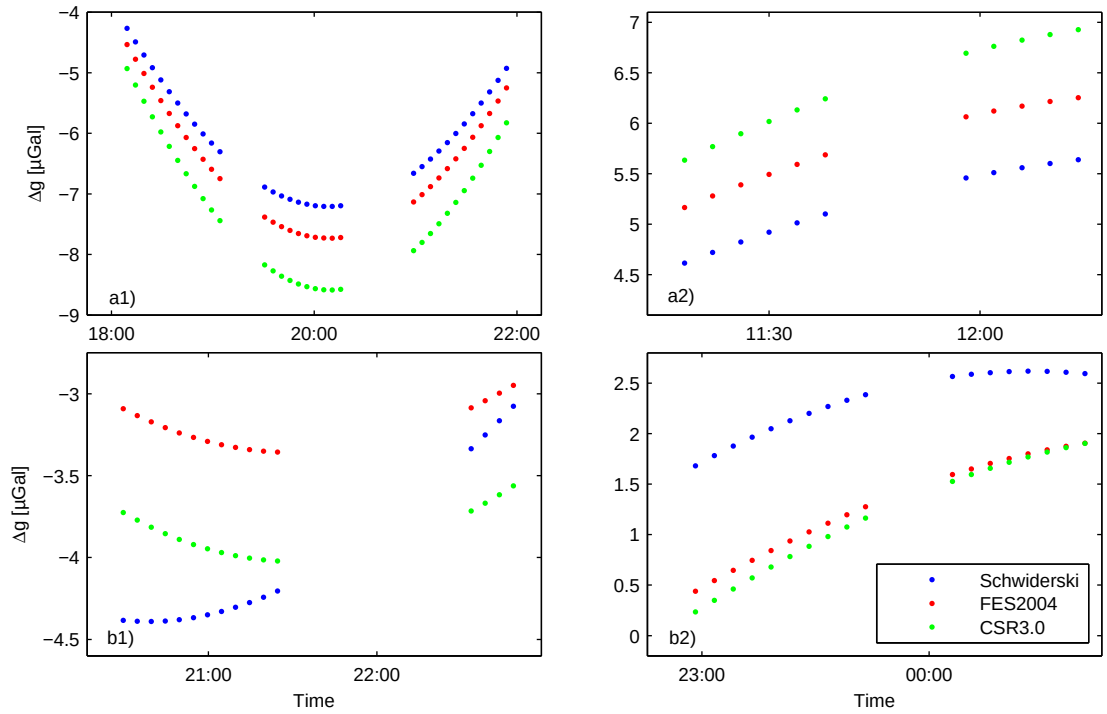

Figure 4.3: The three ocean loading models, Schwiderski, FES2004 and CSR3.0, that are included in the g-software plotted for the two sites at a) Kulusuk and b) Thule at the time of the gravity measurements in, 1) 2009 and 2) 2010.

Many studies have been made to determine the impact of the ocean loading correction on gravity data. Lysaker et al. (2008) considered different ocean loading models for four coastal gravity sites in Norway. These stations have a periodic signal up to $25\mu Gal$ in amplitude in the uncorrected measurements. They find small differences between the global models with the NAO.99b model giving the best results. Also, at some stations the global models do not completely remove the tidal effects leaving a residual signal of up to $20\mu Gal$. This is evident for the station furthest North. They show that local tidal models improve the measurements by minimizing the residual between data and the model.
In Sato et al. (2008) they discuss the impact of an insufficient ocean load correction on AG data in Alaska. They find that measuring for 48 hours or more minimizes the effect of a bad ocean model for a specific site. They also look at the possibility of using the residual signal of the ocean model in the set g-values and making a correction for this. The g-value is not improved significantly, although the standard deviation on the mean of the sets is minimized, which is desirable when looking for a trend in time series. As mentioned in Sato et al. (2012), the new ocean model used in Sato et al. (2008) improves the standard deviation of the set gravity residual by more than 50%.

There is also the non-tidal ocean loading as described in Olsson et al. (2009). These signals can be significant depending on the nature of the loading and the geography of the site. Besides the non-tidal loading there is also an effect from global sea level change. The sea

level change is estimated to rise $3mm/yr$, which would yield a gravity change of approximately $-0.12\mu Gal/yr$ (Sato et al., 2012).

4.2 Atmosphere

A correction for the atmosphere is also known as the barometric correction. It considers the direct attraction effect from the air masses above the observation point, as well as the loading effect of these masses, which can result in surface deformations of up to $1cm$ (Timmen, 2009). To calculate the atmosphere correction, the following formula is used

$$\delta g_{air} = -\alpha(p - p_n) \tag{4.1}$$

where $\alpha = -0.3\mu Gal/hPa$ is the air pressure admittance factor, which is the often used global mean, p is the actual pressure, and p_n is the normal pressure given by

$$p_n = 1013.25\Big(1 - \frac{0.0065H}{288.15}\Big)^{5.2559} \tag{4.2}$$

Here, H is the station height above sea level, which should be given with an accuracy better then $10m$ for absolute gravity measurements (Timmen, 2009). The air pressure admittance factor comes from simple calculations where an atmospheric pressure change is found to give approximately $-0.4\mu Gal/hPa$ due to the direct attraction, and approximately $0.1\mu Gal/hPa$ due to the loading of the air masses (Herring et al., 2009). Petrov and Boy (2004) finds, using very long baseline interferometry (VLBI) data, that the Earth's response to the atmospheric loading can be up to $20mm$ in vertical displacement.

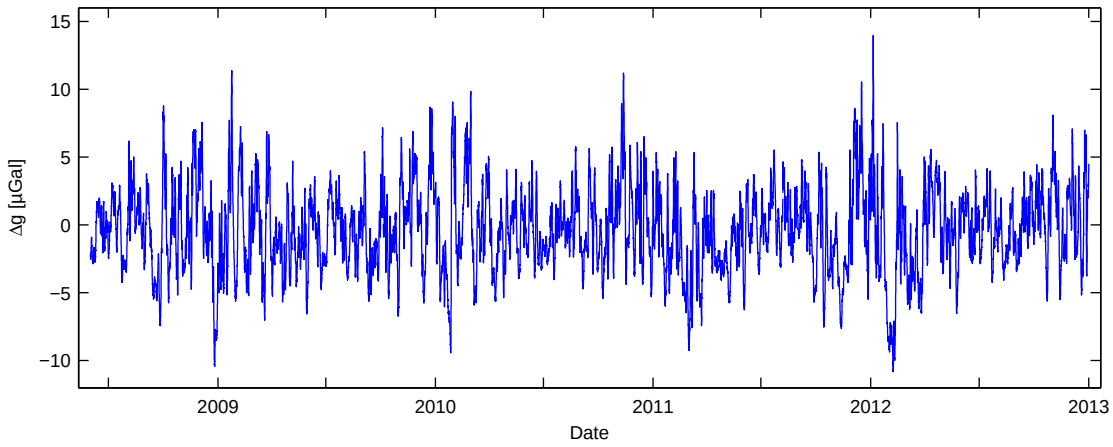

Figure 4.4: This is the correction for the atmospheric loading and attraction calculated using Equation 4.1. Data are hourly values measured at Copenhagen Airport[3].

Studies of the atmosphere's influence on the gravity measurements are described in Merriam (1992) and Boy et al. (2002). They find that the globally averaged value of the admittance factor can be improved.
Boy et al. (2002) investigated the effects of the air masses direct attraction as well as the

[3]Data is provided by the Danish Meteorological Institute (DMI), see Cappelen (2012), and www.dmi.dk. for details.

elastic deformation of the Earth due to the atmospheric load. They find that masses within $1000km$ will give rise to a direct attraction effect, while the elastic deformation is sensitive to atmospheric changes of wavelengths up to $4000km$. In Merriam (1992) they find that 90% of the direct attraction effect is found within $50km$. Since the atmosphere can be considered uniform within this distance from the site, it is concluded that a single barometer with an accuracy of $10\mu bar$ at the site is sufficient to correct the gravity data satisfactorly. Similar results are found in Niebauer (1988) and Gitlein (2009). A barometer is included in the A10 controller presented in Section 2.1.

4.3 Polar motion

Changes in the position of the rotation axis will give changes in the centrifugal force at a given point on the Earth's surface, and thereby change the gravity measurements. On the Earth's surface it looks like the pole is moving, hence the name polar motion, and the gravity correction for this motion is given by

$$\Delta g_{pol} = -\delta_{pol}\omega^2 r \sin 2\phi (x_p \cos\lambda - y_p \sin\lambda) \tag{4.3}$$

where δ_{pol} is the amplitude factor, this is the elastic response of the Earth compared to a rigid Earth. A value of 1.16 for this is often applied (Timmen, 2009). ω is the Earth's angular velocity and r its radius. Daily predictions of the pole coordinates x_p and y_p is given by IERS (International Earth Rotation and Reference System Service), who also provide real values after some days. The measurements geographical latitude and longitude are given with ϕ and λ, and for absolute gravity measurements an accuracy of a few kilometers is sufficient for this correction (Timmen, 2009). The effects of the polar motion is also studied in Wahr (1985) and Hinderer and Legros (1989).

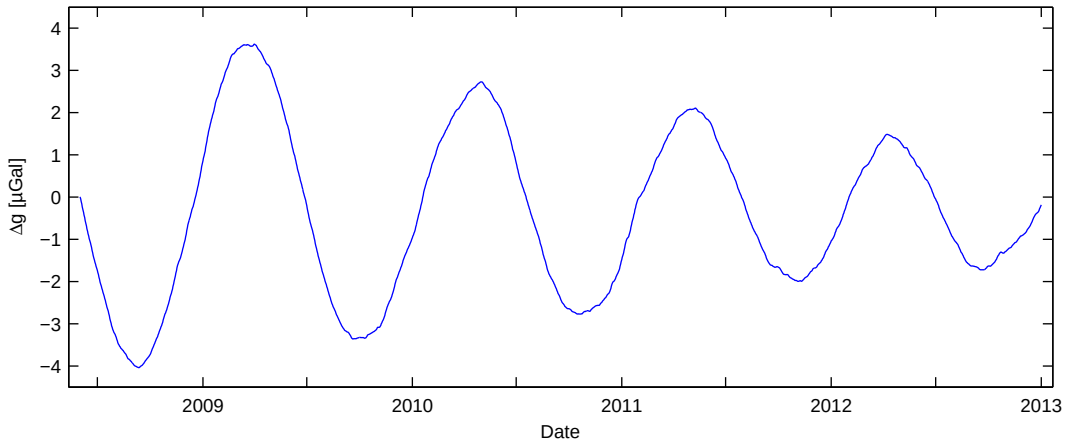

Figure 4.5: The polar motion correction for the reference site at the Rockefeller building in Copenhagen in the period from June 2008 to January 2013. The data comes from the IERS[4].

[4]Daily values can be found in the IERS bulletin A at www.iers.org.

4.4 Vertical gravity gradient

As mention in Section 2.3, the gravity value is determined at the instrument height, that is the height of where the free fall is initiated in the Dropper. For many practical reasons it is necessary to transfer the g-value to another height than the instrument height, and in order to do this, the gravity gradient is used. The gradient will vary from site to site since it depends on the surrounding masses, for example will there be a difference between an outdoor gradient and an indoor gradient where the surrounding building will exert a gravitational pull on the gravimeter. There will also be a difference between an outdoor gradient at a site in Denmark, where the underground is mainly sediments, and a gradient at a site in Greenland, where the underground is bedrock.

An often used gradient is the free air gradient, which can be determined by differentiating Newtons law of gravitation with respect to height

$$\frac{dF}{dr} = \frac{d}{dr}\frac{GMm}{r^2} = -\frac{2GMm}{r^3} = -308.6\mu Gal/m \tag{4.4}$$

where G is the gravitational constant, m is set to unity, M the mean Earth mass and r the mean radius of the Earth. This gradient is used if the local gradient is unknown. It can also be used at sites where the objective is to determine the change in gravity, as has been the case for our study in Greenland.

The gradient is normally determined using a relative gravimeter in two different heights, for example at the ground and at the instrument height of the A10, approximately $0.71m$. Since the gradient is non-linear it will depend on the height used for the determination (Charles and Hipkin, 1995). A study on the calculation of the gradient is given in Qingbin et al. (2011), who conclude that the accuracy of the gradient increases with the number of observations and the distance between the measurements. This increased accuracy with distance can be an effect from the non-linear behavior. Jiang et al. (2009) provides an example of a measuring scheme for the gradient, which includes several measurements in the respective height to improve the result.

Since the gradient is in the equation for the determination of g, Equation (3.6), there has been attempts to estimate the gradient from the free fall data. This is done in studies by Hipkin (1999), Robertson (2001) and Niebauer et al. (2011). They all find that there is a need for many drops, with very low noise level, and conclude that the uncertainty in the estimated gradient from the free fall data is properly due to low frequency noise in the data. Niebauer et al. (2011) used the newly developed FG5X that has a recoil-compensating Dropper that reduces the system response and gets an estimate of the gradient with fewer drops.

One issue with the gradient is that it is non-linear. This is especially seen at gravity sites in buildings. This means that the gradient changes during the free fall, so the error will increase with increasing free fall length. Another issue is the uncertainty in the determination of the gradient. For the A10, a free fall length of approximately $0.10m$ a 10% error in the gradient will leed to an error of approximately $1\mu Gal$ in g.

When we measure the gradient, we can determine it with better than 10% uncertainty. We

have also found, by measuring the gradient at the same site three times over a couple of months, that we can reproduce our determination of the gradient to within approximately 1%. An error on the gradient will show up in the residual, depending on the size of the error and the noise level at the site.

5 The performance of A10-019

The A10-019 was acquired by DTU Space in June 2008, and since then approximately 425 measurements have been made with the instrument. These measurements have been made during our campaigns in Denmark, Greenland, Antarctica, Bolivia, Sweden, Germany, Iceland, USA, and New Zealand. All these have helped us in gaining knowledge of the instrument's capabilities.

Many of the measurements are conducted at our reference site at the Rockefeller building. Already presented are how these data are used in the study of the laser frequency drift in Section 2.4. These measurements have helped us in assessing the condition of the instrument, and the reference site has been occupied before and after every campaign we have had, domestic and international. The reference site was established in the basement of the Rockefeller building in October 2005 with the FG5-220 owned by the Institut für Erdmessung (IfE), Leibniz Univeristät in Hannover, see Timmen et al. (2008) for details. The g-value they obtained was 981 546 595.0μGal at the mark, and 981 546 300.7 $\pm$ 3μGal at instrument height (1.20m). The measurements made with the A10-019 at the reference site are transfered to the FG5-220 instrument height with the gravity gradient of $-245\mu Gal/m$, also measured in 2005 by IfE. The gradient has been remeasured a couple of times since, and the results have agreed within the uncertainty.

Along with the successes we have had, many problems with the instrument have also occurred. The laser tube has been replaced several times, for example due to a flooding accident at our reference site. For the past year, we have been struggling with a malfunctioning laser control, and the instrument is at the time of writing at service at Micro-g LaCoste. The instrument, or parts of it, has been shipped for repair six times during the time we have had it.

5.1 Accuracy

In order to assess the accuracy of a gravimeter it needs to be compared with other gravimeters, and for this purpose are there yearly international comparison campaigns, see Vitushkin L. (2002), Francis and Van Dam (2003) and Francis (2010). Our instrument has only been compared with other absolute gravimeters a few times despite the large amount of measurements we have made.
In 2009, in connection with a repair at Micro-g LaCoste, our instrument participated in a small inter-comparison at Table Mountain Geophysical Observatory (TMGO) near Boulder, Colorado. In the comparison, the FG5-102 from the National Geodetic Survey (NGS), USA, and the A10-009 from the National Geospatial-Intelligence Agency (NGA), USA, also participated. Data from this instrument is not included since it was not functioning properly. Furthermore, it turned out that our instrument had problems with its laser lock system, so the

results from this comparison are questionable. During a campaign in Denmark and Germany we did measure at the same time on four sites, with the A10-002 from the Bundesamt für Kartographie und Geodäsie (BKG), Germany. The two sites in Denmark where in a garage and a church while the two sites Germany where outdoor. On these four sites, our instrument was able to repeat the measurements to within $8\mu Gal$. The A10-002 had some problems getting repeated measurements that where within the instrument specifications. During the campaign in Antarctica we measured at two sites that were also occupied by the FG5-206 from Ecole et Observatorie des Sciences de la Terre (EOST), France. These measurements where conducted at the gravity piers at McMurdo and Scott base.

The result of the different comparisons is given in Table 5.1. Including all data gives a mean difference of $10.3\mu Gal$. Excluding the data from the comparison at TMGO and Germany the mean is $6.7\mu Gal$. These values can be seen as the lower and upper limit of the accuracy of our A10. One value for indoor measurements and one value for outdoor field measurements.

FG5-102	2009\04\29	TMGO-AI	20.1
	2009\04\29	TMGO-AH	5.2
	2009\04\29	TMGO-AG	3.5
A10-002	2010\10\11	Højer	8.3
	2010\10\11	Døstrup	5.1
	2010\10\12	Schleswig	12.5
	2010\10\13	Oldenburg	12.9
FG5-206	2011\11\19	McMurdo	-8.9
	2011\11\25	Scott Base	-3.8

Table 5.1: The difference between the A10-019 and the other instruments. Units are in μGal. The RMS difference using all comparisons is $10.3\mu Gal$.

As mentioned, others have found that the A10 performs better than the manufacture specifications. Schmerge and Francis (2006) compared the A10-008 with a FG5-216 during a week of measurements at the Walferdange gravity station. They found an accuracy of $3.2\mu Gal$. Falk et al. (2009) found an accuracy of $6\mu Gal$ when comparing the A10-012 to FG5-101 measurements at the Bad Homburg gravity station, and they estimated an $6-8\mu Gal$ accuracy for field measurements. In Mäkinen et al. (2010) the A10-020 is compared to the FG5-221 and found an offset of $3\mu Gal$. The values found for our instrument are within the specification, although higher compared to others findings.
Thus, there is reason to believe that our instrument can perform better than the values found here, however proper, and regular, comparisons need to be made to ensure the quality of the data.

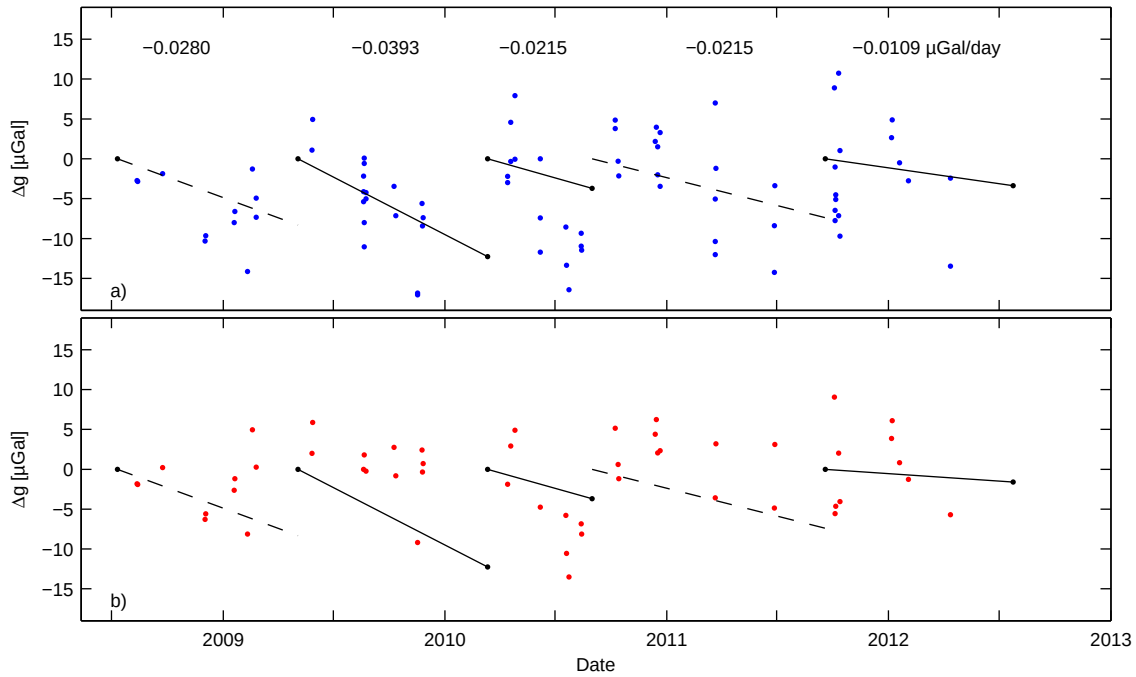

Figure 5.1: a) shows the raw measurements from the reference point in the Rockefeller building. In b), the measurements are corrected for the drift, and for measurements made on the same day, the mean is calculated. In both figures, the trend of the laser drift is plotted. The data error bars are neglected for clarity.

Also, the maintenance of the instrument is important in order to ensure a good accuracy. The laser calibrations is an example of this, and thus it should be performed regularly. In Figure 5.1 a) the g-values at our reference site relative to the 2005 FG5 measurement are plotted along with the laser drift estimates from Figure 2.1. In Figure 5.1 b) the g-values are corrected for the drift.

The standard deviation of the data before and after the correction is 7.4 and 5.5μGal, respectively. This shows the importance of the laser calibrations. The variation in Figure 5.1 can have multiple causes, one of them being the glacial isostatic adjustment (GIA) that can be expected in the Copenhagen area, see Figure 10.4 in Section 10.2, where there is more on the GIA signal. Correcting the data for a GIA trend will give a std of 5.1μGal.
Another cause can be elastic deformation of the Earth, which can be due to several causes.

5.2 Repeatability

When measuring at a site we strive to measure a least with two different setups, and usually the instrument is turned 180° between them. This is to eliminate any potential errors coming from the setup of the instrument. These measurements can be used to examine the instrument's repeatability. The repeatability is specified to be within 10μGal from the manufacture and is very dependent on the site and the setup by the operator. Figure 5.2 shows the result of the A10-019's repeatability.

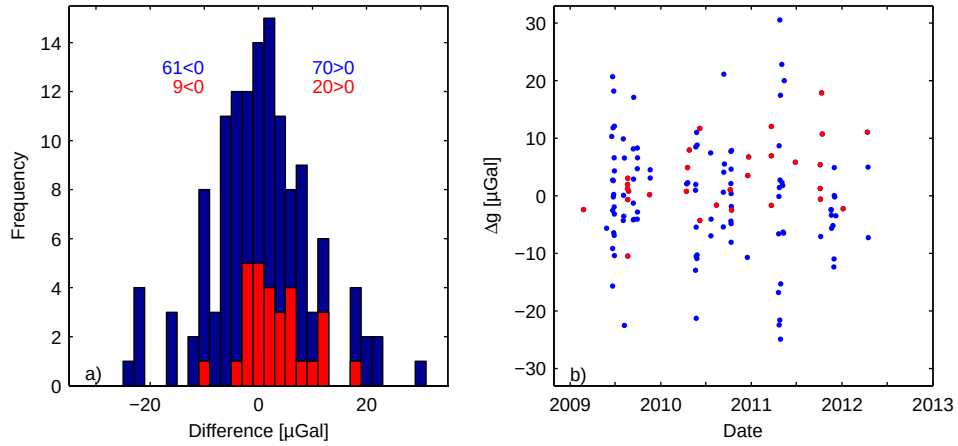

Figure 5.2: The difference $(m_1 - m_2)$ between two or more measurements made on the same site from the same day. Figure a) shows the distribution of the differences. Figure b) shows the distribution as a function of time. The red bars and dots are the data collected at the reference site in the Rockefeller building, while the blue includes all field measurements. The numbers on the histogram indicate the distribution of negative and positive differences. For all the data, $\sigma = 9.5\mu Gal$ for the reference site data, $\sigma = 6.0\mu Gal$. The bars are $2\mu Gal$ in width.

For all repeated measurements, in the field and at our reference site, the standard deviation is $9.5\mu Gal$ while for measurements at the reference site only, the standard deviation is $6.0\mu Gal$. Figure 5.2 shows a small tendency that the first measurement is larger than the second. This is especially evident for the measurements at our reference site. This can be due the fact that the point, in a cellar, is located near an outer wall. In the second of the two measurements, the instrument were often orientated towards the wall. There should not be any effect of the Coriolis force on the A10 gravimeter due to its relative short free fall, whereas this is not the case for the FG5. It is therefore standard procedure to measure in two setups with the instrument in a North and a South direction.

5.3 Measurement statistics

The number of drops, and the number of sets needed to get a measurement with a satisfactory accuracy is estimated by investigating first a measurement with many drops, and then one with many sets. Looking at the development of the cumulative mean and standard error with an increasing number of drops and sets gives an idea of this.

Figure 5.3 shows the data from a measurement of four sets, with 1024 drops in each set. The individual sets are varying up to $25\mu Gal$ during the first 30 drops. The variation of the set values stays within $10\mu Gal$ when the number of drops are increased to more than 30 drops. As seen in Figure 5.3 a), the mean of the sets, the black curve, is more stable and changes less than $5\mu Gal$ when 100 drops or more are collected. A convergence is seen in the standard error, Figure 5.3 b), when the number of collected drops are approximately 130. The error is approximately $3\mu Gal$ here. Thus, the optimal number of drops collected is between 100 and 130.

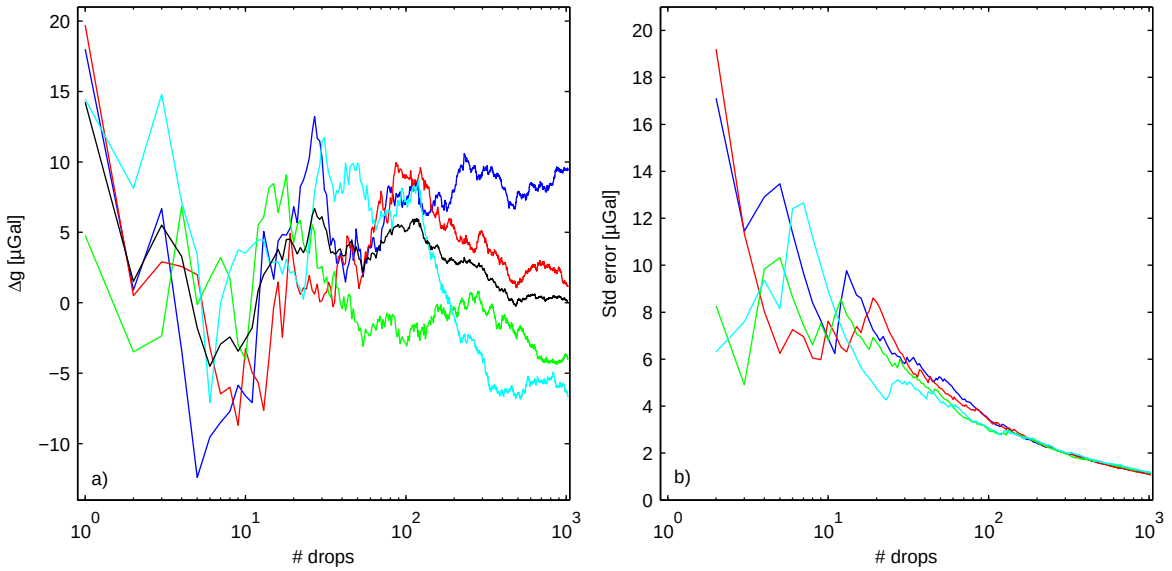

Figure 5.3: 1024 drops have been collected in four sets, with one drop per second, so the total set time is approximately $17min$. The values in a) are relative to the mean g of all the drops. The black curve in a) is the mean of the four individual sets which are collected in the following color order, blue, red, green, cyan. The measurement was carried out on June 29^{th}, 2011 at the Rockefeller site.

There might be an issue of collecting many drops in one set, although the effect is expected to be small, if present at all. The long term stability of a locked laser deteriorates the longer the laser is locked. This is discussed in Niebauer (1988) and Niebauer et al. (1995). This is illustrated in the so called Allan variance plots.

At the reference site in Copenhagen, several measurements are conducted with varying number of sets. Figure 5.4 presents a measurement containing 288 sets with 100 drops in each set. As before, the cumulative mean of the sets is presented in a) relative to the mean of all the sets while b) shows the standard error. The nature of the zig-zag curve of the cumulative mean is due to the change in laser frequency between the sets as described in Section 2.4. This shows that an equal number of sets should be collected, especially if the number of sets is small. The difference between the sets is also reflected in the standard error, which is higher with higher separation between the sets.

These data are collected over three days and therefore can be influenced by environmental changes. This could be the cause of the small bump seen in a) around 200 sets. Figure 5.5 presents the same study as in Figure 5.4, however for a different number of sets at different times.

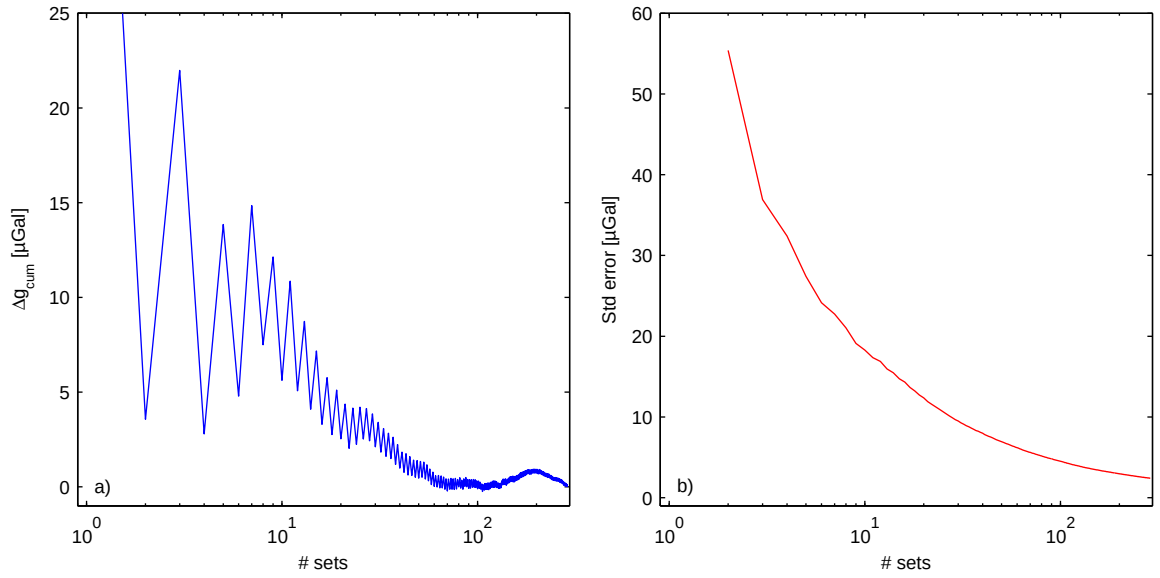

Figure 5.4: The result of a measurement with 288 sets with 100 drops in each set. The sets are collected in pairs of two with a $5min.$ interval between the sets and $30min.$ between the pair of sets. a) The gravity value is relative to the mean g of all the sets. b) is the standard error on the gravity value. Data is collected on January 6^{st}, 2012 at the Rockefeller site.

The results in Figures 5.4 and 5.5 indicate that a value that is within $10\mu Gal$ of a long term measurement can be reached during the first 4-6 sets, and within $5\mu Gal$ if ten or more sets are collected.

Now these measurements are indoor under laboratory condition. In the field it can be needed to collect more drops and more sets to reach the same results as presented here.

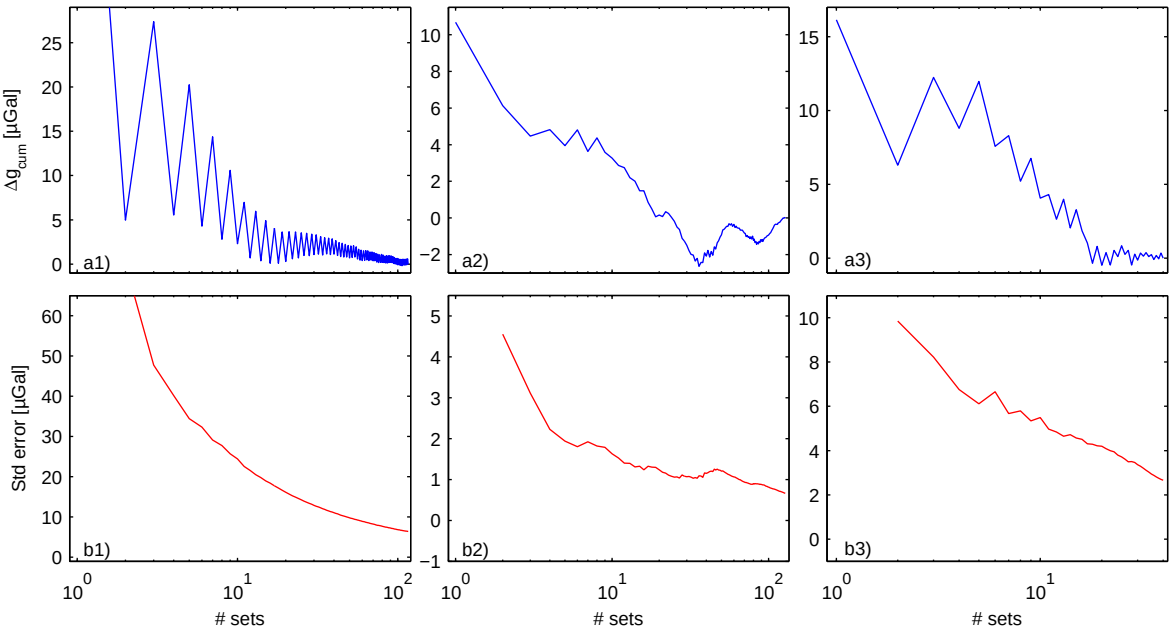

Figure 5.5: Three measurements with a) 116, b) 128 and c) 40 sets. The upper row, a) contains the cumulative mean and b) the standard error. The measurements are carried out at the reference site on 1) June 23^{rd} 2012, 2) June 28^{th} 2011 and 3) July 30^{th} 2010.

6 Field experiences

The A10-019 was acquired by DTU Space for initiating and continuing gravity time series in Greenland for studying geodynamics. Also, the purpose of the instrument is establishing and maintaining national gravity networks in Denmark and Greenland. Besides these primary objectives the instrument has participated in campaigns around the world and has measured gravity more than 275,000 times in 425 measurements.

This section, provides a short description of the major campaigns we have conducted as well as the experiences gained during these campaigns. This serves to illustrate the possibilities and the limitations when operating an A10.

When measuring at field sites we follow a standard procedure in which 6-8 sets with 100 drops in each set are conducted. The number of sets depends on the noise level at the site. For example in windy conditions, the drop scatter can be large, and more sets are made to eliminate the random noise from the wind. Two measurements with different setups are as a minimum conducted at the site. If they differ more than $10\mu Gal$, one or two more measurements are conducted. The two different setups are performed to eliminate any setup errors.

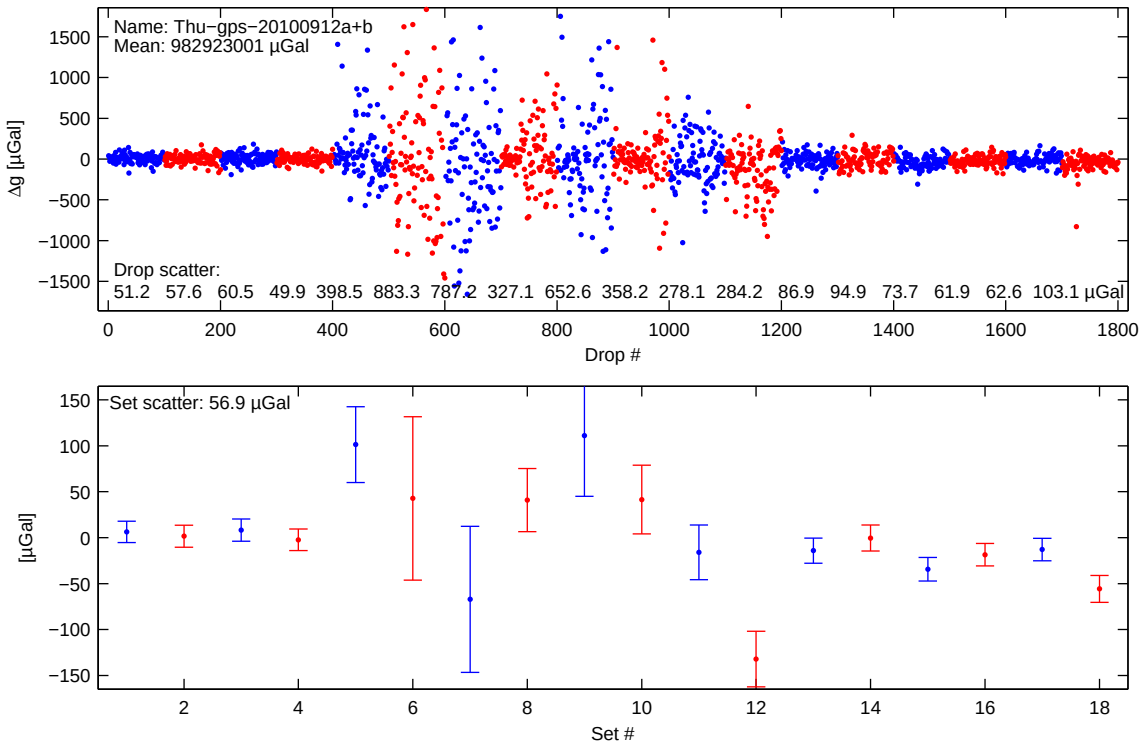

Figure 6.1: Seismic noise during the measurement at the Thule GNET site (THU3) on September 12^{th} 2010.

As an example of events that can happen while measuring, Figure 6.1 shows a seismic signal that occurred during a measurement in 2010 at the GNET station in Thule (THU3). The duration is approximately $40min$ and data from here was discarded in the post-processing. The signal is likely due to an earthquake, however a similar kind of noise originates from

the so called ice quakes. This is seismic activity that originates from the calving of ice at the glaciers, the nature of these is described in Veitch and Nettles (2012). During a measurement at the Kangia GNET site (KAGA) we suspect that such an event occurred.

The total weight of the equipment needed for a field campaign is approximately $350kg$. Traveling with a "live" instrument and the bare essentials for field measurements, the weight is approximately $150kg$. The means of transport for the field operations can be almost everything. We have tried a diversity of cars (VW Caravelle, Skoda Fabia Combi, Toyota HiLux), helicopters (Bell212, Bell222, AS350, EC130), one fix-winged aircraft (Twin Otter) and even a small boat. The limited demand for space makes it easily installed, however it is very important to ensure that the instrument does not get any hard bumps during transport. This especially applies when shipping the instrument.

Regarding power supply, different options exist. The instrument can either run with power from the local grid, or, as it is often the case in the field, from $12V$ batteries. We have also had some experience of getting power from the mean of transport. The most critical issue is to keep the Ion-pump running at all times. If it looses power for more than $5min$ it may be necessary to use the Turbo pump to re-establish the vacuum, which can take up to $24h$. After the Ion-pump, there is the laser power, and the heaters for the Dropper and the IB-unit that needs to be on power. Optimally, these should be turned on one hour before the measurement is performed as a minimum and then run continuously during the campaign. When the instrument is moved, for example from the helicopter to the gravity site, it can be necessary to switch off the instrument, and to disconnect the Dropper and IB-unit from the main controller, thereby leaving the laser and heaters without power. The time of disconnection should be minimized as much as possible. When doing this, the Ion-pump is always connected to a small battery.

We have found that a normal field day of 7-8 hours with 4-6 measurements, can be covered with two $75Ah$ batteries. The estimated power consumption[5] of the main A10 parts is listed in Table 6.1.

Laser	Ion-pump	Heaters - Full	Heaters - "Normal"
$18W$	$2W$	$100W$	$30W$

Table 6.1: Estimation of the power consumption at $12V$ for the main A10 components. Heathers - Full refers to the start up of a cold instrument, while "Normal" refers to maintaining the established temperature. These values depend on the environment, so deviations from these are to be expected.

From our experience, the average power consumption during a field campaign is approximately $120W$.

When operating the instrument outside it is good practice to setup a tent for protecting the instrument from the Sun, wind, rain, etc. The Sun may alter the temperature equilibrium. There has been evidence for that, under extreme heat conditions, the Ion-pump can have difficulties keeping the vacuum. Especially for protection from the wind, setting up the tent

[5] Mail correspondence with Derek van Westrum, Micro-g LaCoste, February 17^{th}, 2010.

is good practice. The wind does not have to be very strong to increase the drop scatter noticeably. In most cases it is necessary to setup a tent in order to collect good data.

6.1 Denmark

In Denmark, the purpose of the AG measurements is to establish and maintain a national gravity network. The measurements are located in or at buildings, and at permanent GPS receivers. For details on the gravity network in Denmark, see Andersen and Forsberg (1996) and Timmen et al. (2008).
Another purpose is the study of geodynamics in Scandinavia. This is a continuation of a project where gravity lines across Scandinavia are used to monitor GIA (Mäkinen et al., 2005). The A10 is used to re-occupying these East-West going profiles across Scandinavia, where the southern most, the 56*N* line, crosses Denmark.

Field work is fairly easy, the point are accessible and we can coordinate our field work with weather forecasts, minimizing the impact of weather on the measurements. In Denmark we gained the first experiences on the use of the A10, the power consumption and the ways to transport it, experiences we later could benefit from in other places.

The results of the Danish A10-019 measurements in the period from July 1st, 2008 to January 1st, 2013 are presented in Appendix E.1.

Figure 6.2: An overview of measurement sites throughout Denmark in the period from 2008 to 2013. The picture is adapted from Google Earth.

6.2 Greenland

As presented in this thesis, the purpose of the AG measurements in Greenland is to study geodynamics. Besides this, the instrument is used for establishing a national network. Prior to 2009 there were few AG points in Greenland, see Andersen and Forsberg (1996), Francis (2006) and Timmen et al. (2008). For an overview of the new AG sites in Greenland, see Figure 10.1 in Section 10.1.

For the study of geodynamics there is the challenge of getting to the GNET sites. Most of them are at located remote places only accessible with helicopter. It is not always possible to land at the proximity of the site meaning that the instrument has to be carried, and in order to do this, the Dropper and IB-unit have to be disconnected. This can become a problem, especially when it is cold so the laser will cool down, and this can lead to laser lock problems. To prevent this, it is important to keep the disconnection time as short as possible, and to insulate the instrument thereby minimizing its sensitivity to temperature. Getting the instrument in the tent, out of the wind, also helps stabilizing the temperature.

Figure 6.3: Gravity measurement at the Qaarsut GNET site (QAAR). This is a good and stable site.

Other challenges are the conditions of the sites. The pictures in Figure 6.3 and 6.4 are from a good and not so good site, respectively. The data from the two sites are presented in Figure 6.5 and Figure 6.6. The good site is the GNET station near Qaarsut (QAAR), while the latter site is from the GNET station at Rink glacier (RINK). The first site is a bedrock outcrop with a smooth surface making the setup easy, and keeping the system response low. At the second site (RINK) there were many loose rocks making it difficult to find a suitable spot for the AG measurement. As seen in the picture, some of the Dropper legs stand on separate rocks. These not so optimal conditions are reflected in the system response.

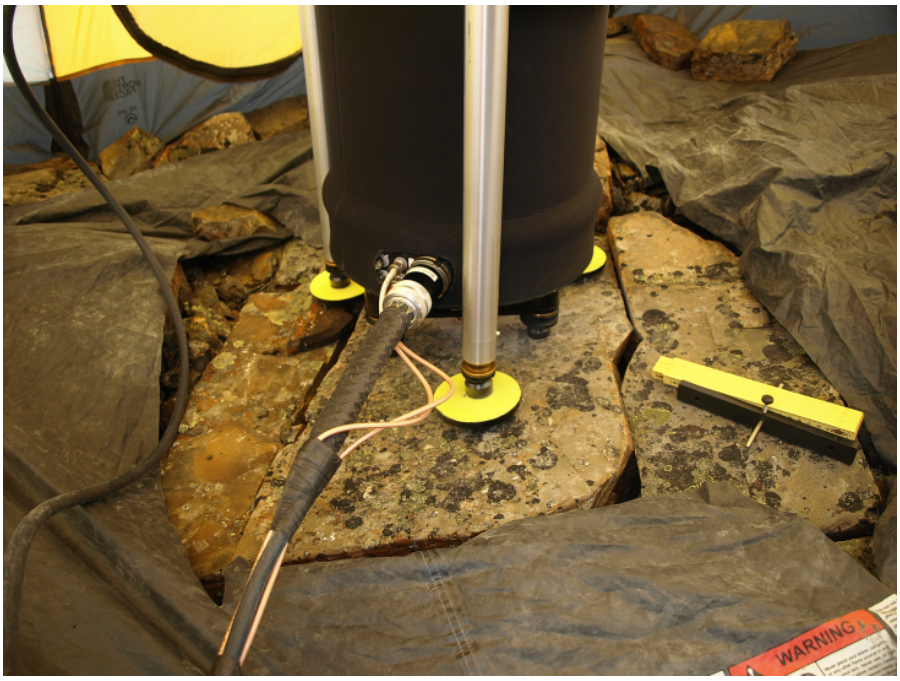

Figure 6.4: Gravity measurement at the GNET station near Rink glacier (RINK). The site is not optimal due to loose rocks.

Along with the data overview in Figure 6.5 and 6.6, additional figures of the Qaarsut and Rink measurements are presented in Appendix F.2 and F.3. The contents of these appendixes are figures similar to those presented in Figure 3.3, 3.4 and 3.5.

The results of the Greenlandic A10-019 measurements in the period from May 1st, 2009 to September 1st, 2011 are presented in Appendix E.2.

Location: Qaarsut GNET site (QAAR)
Lat.: 70.74042 **Long.:** -52.68829 **Elev.:** 20.00 m
Measured: 2010\05\24

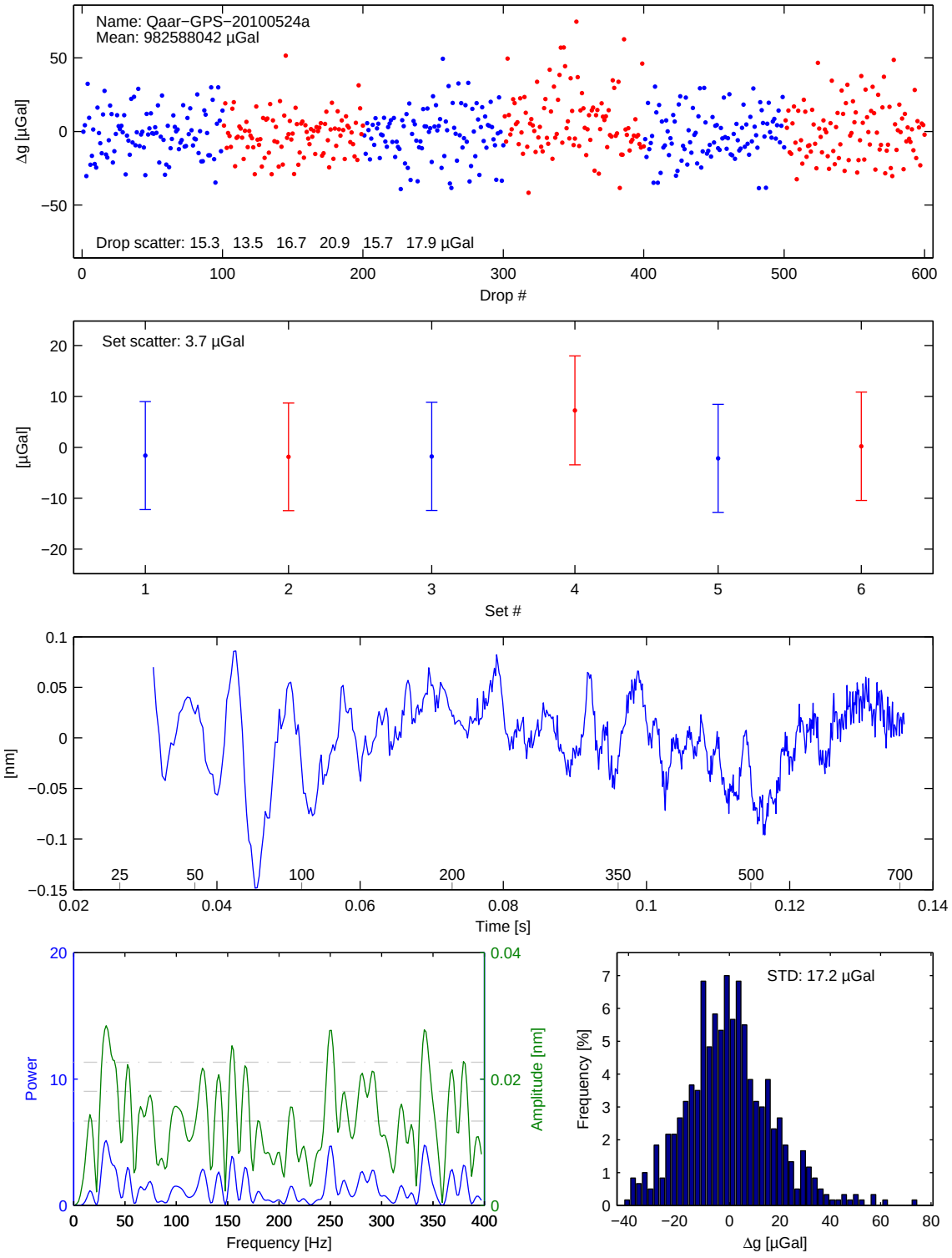

Figure 6.5: The measurement at the Qaarsut GNET station, see Figure 6.3. Code QAAR on Figure 10.1. An example of a good measurement at the GNET sites.

Location: Rink glacier GNET station (RINK)
Lat.: 71.84850 **Long.:** -50.99397 **Elev.:** 1337.82 m
Measured: 2010\05\22

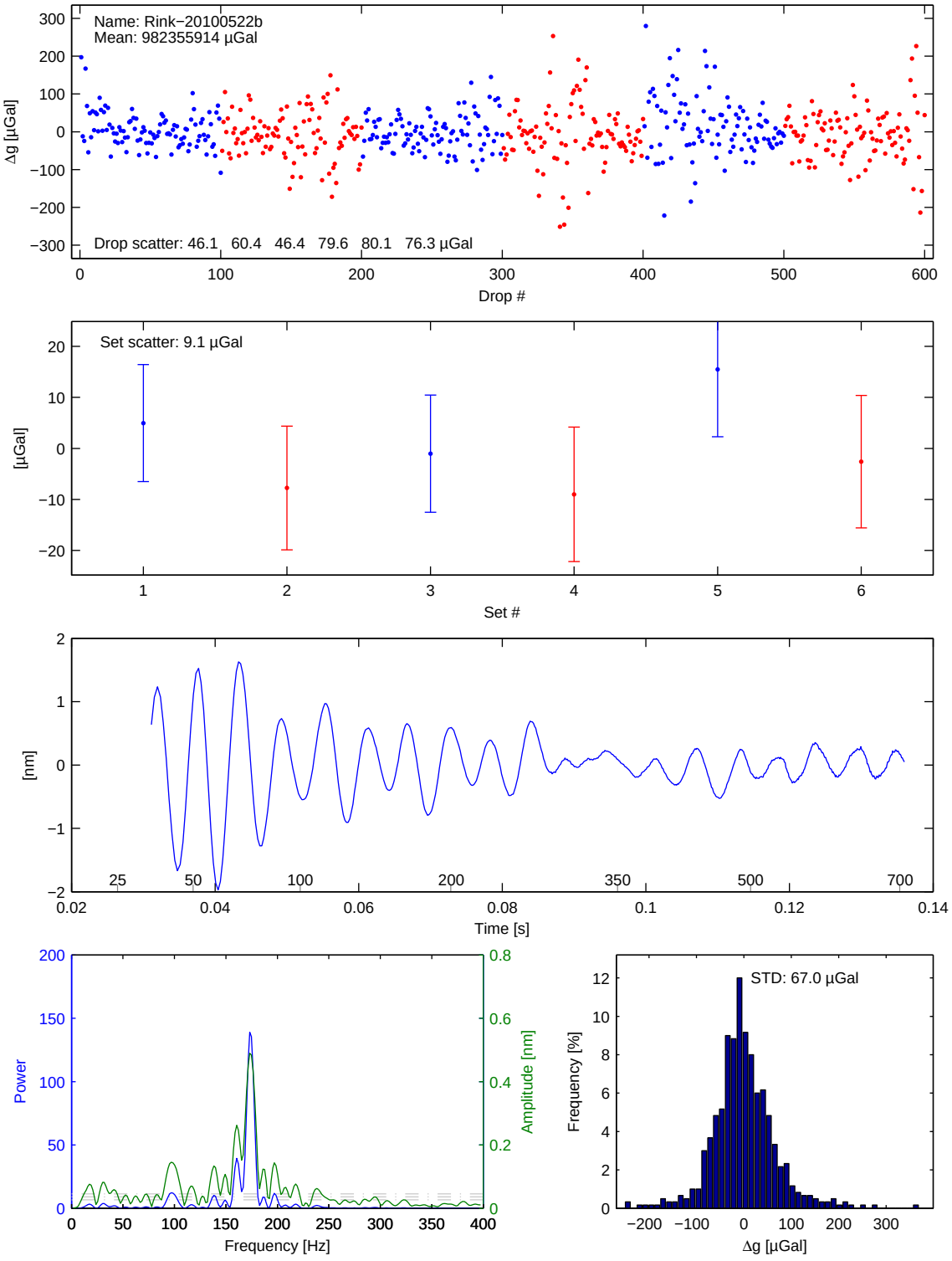

Figure 6.6: The measurement at the GNET station near Rink glacier, see Figure 6.4. Code RINK on Figure 10.1. This is an example of some of the challenges that are present at the GNET sites.

6.3 Antarctica

The purpose of the field work in Antarctica was to establish some of the first AG points at the ANET permanent GPS sites. ANET is the antipode network of GNET both a part of the Polar Earth Observing Network (POLENET) project, which main objective is geodynamical studies. At the same time, the FG5-205 from EOST was there for remeasuring sites at the Antarctic bases. Due to our experience in Greenland we were invited to participate and test how operations with an A10 could be carried out in Antarctica. The weather conditions can be more harsh, and many sites are at remote locations so fixed winged aircrafts are needed to reach them. This also means that it is not easy to land near the site, and thereby that instruments must be carried to the site. The colder weather, and the possible longer distance from aircraft to site, can be the biggest issue when during A10 measurements in Antarctica.

The presence of the FG5 gave us the possibility for comparing instruments during the campaign. There were two sites that both instruments occupied. The gravity pier, Thiel-1 at McMurdo and SGB1 at Scott Base. The difference was small at Scott Base, while it was large at McMurdo, see Table 5.1. During the campaign, the FG5 team found that the Theil-1 gravity pier was not stable; they could see it when aligning their instrument.

This campaign was running from November 12^{th} to December 13^{th} 2011, and during this period 26 measurements were conducted at six locations.

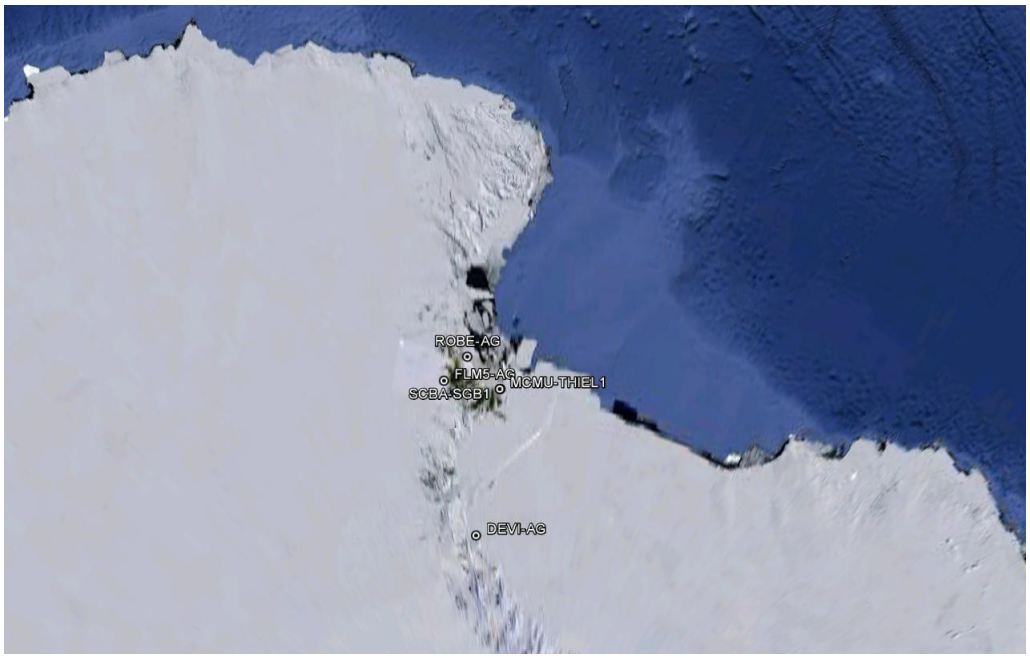

Figure 6.7: The measurement sites in Antarctica in 2011. The picture is adapted from Google Earth.

For more on absolute gravity measurements in Antarctica see Sasagawa et al. (2004), Fukuda et al. (2005), Tiwari et al. (2006), Mäkinen et al. (2007), Rogister et al. (2007) and Amalvict et al. (2007).

6.4 Bolivia

This was a campaign running from April 15^{th} to May 13^{th} 2011 with the main purpose of adding new points to the national gravity network. A total of 12 new AG points were established, and three FG5 points from 1997 were re-occupied. The re-occupation of the FG5 sites was carried out during the campaign and this helped controlling the health of the instrument. Furthermore, the first and last campaign measurement was carried out at the same FG5 site in La Paz. There was a difference of $-6\mu Gal$ between the measurements from the beginning and end of the campaign.

Figure 6.8: An overview of the 15 measurement sites in Bolivia in 2011. The picture is adapted from Google Earth.

Most of the campaign was carried out using a car, which was slightly retrofitted for transporting the A10 safely. It is always good practice to strap down the instrument when driving with it, and it was of great importance for driving on the Bolivian dirt roads. This campaign proved that with a good car set up, the instrument is very robust for transport. A couple of sites in the northern part of Bolivia were reached by commercial aircrafts.

During this campaign we measured at very different altitudes, for example $3994m$ in Potosí and $105m$ in Puerto Suárez. The change in altitude happened over a short amount of time, and a change in climate followed with it. When down in the low-land there was a change in the Ion-pumps performance, nothing critical. Whether it was due the warmer climate or the change in altitude is undetermined. Otherwise the only noticeable effect of the high altitude was the hard drive of the laptop that had problems spinning due to the low pressure ($636hPa$). This problem is fixed with a solid state disc.

7 Summary / discussion

In order to get the highest performance out of the instrument it is good practice to participate in instrument inter-comparisons, measuring regularly at a reference site, and calibrating the laser frequency and Rubidium clock at a yearly basis. The findings of others regarding the performance of the A10 is in accordance with our findings, although the latter are not as good as others, for example regarding the accuracy of 6.7 and 10.3μGal depending on the data used. These values can be interpreted as being valid for indoor and outdoor measurements, respectively. It is believed that there will be an improvement of the these estimates as more comparisons with other instruments are available. We find similar values for the instrument's repeatability, approximately 6 and 10μGal for indoor and field operations, respectively. This can only be improved by carefully instrument setup at the site. There can be situations where the site will decrease the possibility for a good repeatability. The practice of collecting a minimum of 6 sets with 100 drops in each is a good scheme, especially considering that time is often a limiting factor during field campaigns.

The largest errors when operating the instrument in the field comes from bad site quality and the setup of the instrument. The first is something that is not always in the operators control, however an effort must be made to minimize its effect. The latter is one of the most important tasks for the operator. The time spend on careful site selection and an elaborated setup procedure is well spent and will pay-off in the best possible data quality.
Even though the instrument is built for field operations it has to be treated with care. It is very rugged, however at the same time very sensitive and much of our time has gone with error finding, and fixing.

One of the challenges when measuring at the GNET sites is to get the instrument to the site. The practice of disconnecting the instrument works well. The time where the instrument is disconnected is kept short enough, keeping the instrument from loosing heat, and quickly brought back to equilibrium when connected again. The time of disconnection depends on the distance from the mean of transport to the site as well as the weather conditions; for example a cold wind will decrease the instrument's temperature quicker. The worst case scenario is when the instrument's temperature is decreased to a point where it is difficult to get back to equilibrium under the circumstances. This can lead to laser lock problems and therefore no useful data. This has been a part of our experiences.

Care must also be taken to prevent that the instrument suffers any hard bumps during transport. If safely packed, the instrument has proved to be quite robust to transport, either if it is in a car driving on dirt roads or if it is in a helicopter where everything is vibrating.

The dependence of the processing result on the data truncation has been the motivation for investigating the processing. This investigation has lead to the understanding of the importance of a good instrument setup in order to minimize the system response. The different processing schemes tested have not provided any conclusive findings on the treatment of the data truncation. This is especially valid for the processing where one truncation is selected for every drop. The method of processing every drop with a large number of truncations gives some more interesting results. However, the results are not conclusive. Data from

more measurements need to be processed for a deeper investigation of this. This has not been carried out at this point due to the extensive computation time that is needed to perform the calculations.

As in Charles and Hipkin (1995), this author find that correcting the drops for the residual, after determining the residual in a first run, eliminates the dependence on the fringe truncation, although it is also found that the g-value is still depend on the first truncation that the residual is build upon.

The fact that the residual signal is present means that something systematic is present. There are for example only small phase changes between the individual drops. There is often found either a high frequency signal around $160-180Hz$, or a low frequency signal around $15-35Hz$ in the residual. These characteristics are common for the A10. Processing data from five different A10s (the A10-002, 004, 008, 009 and 020) shows similar results.

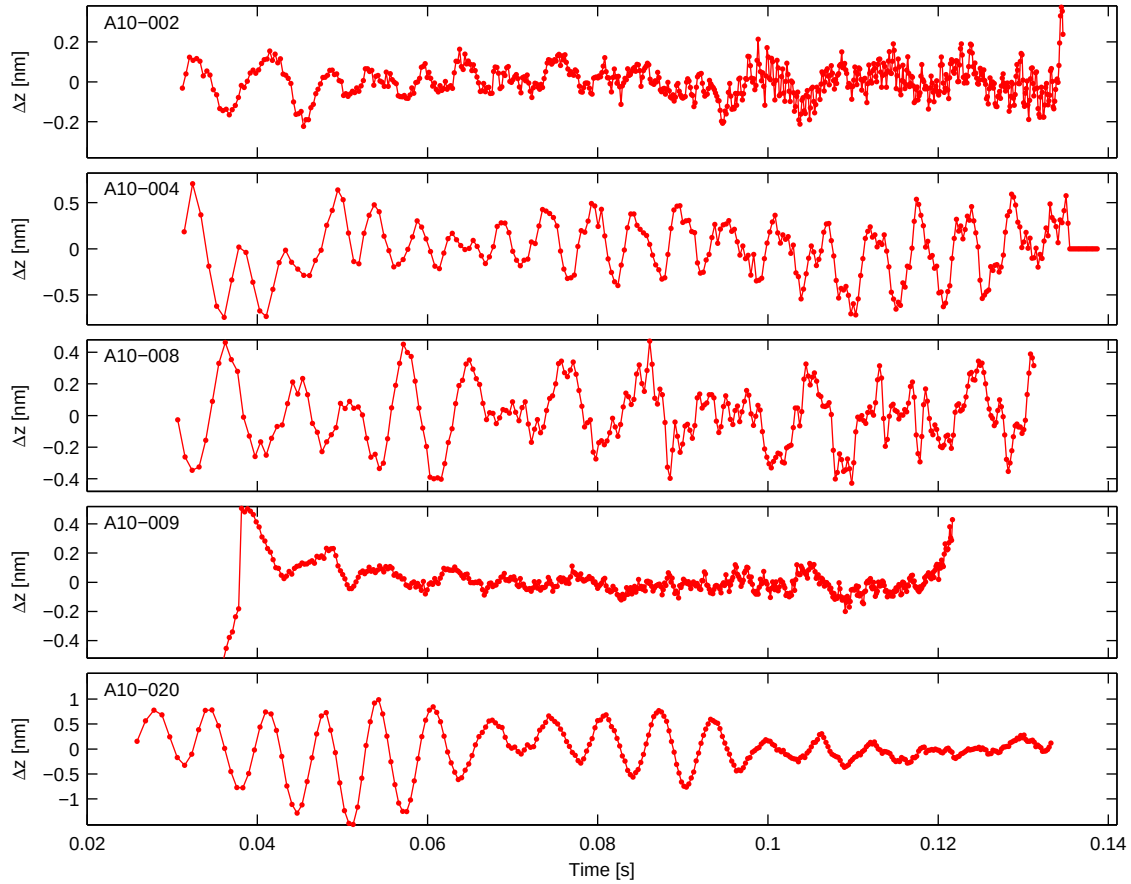

Figure 7.1: Different A10's residual at different locations. There are similarities. Pleas notice the different scales on the y-axis.

As the synthetic data show the lower frequencies have the largest influence on the processing, with $8-9Hz$ having the largest effect. The system response has the largest impact in the beginning of the drop, here the amplitude of the residual is largest. During the drop, the amplitudes decreases. This is due to the damping of the system response by the Superspring. This also shows that in order to improve the data quality, the effect of the system response

should be minimized, for example physically with vibration absorbing pads.

The processing of the data includes the correction of different environmental parameters. The effect of these parameters can be significant (see Figures 4.1 to 4.5), and therefore care must be taken to ensure that the right corrections are made. For the ocean tide correction there are many different models to choose from and the difference between them may not be large, although the model that works for one site might not be the best for another site. For some sites a more elaborated calculation of the ocean correction is needed.

Part II
Glacial isostatic adjustment

The undeformed Earth is in equilibrium, introducing a load on the surface will alter this equilibrium and the Earth will respond to the load by the principles of isostasy. If the load is allowed to sit on the Earth for sufficiently long time the Earth will reach a new state of equilibrium. The process between these states of equilibrium in glaciated areas like Greenland is called glacial isostatic adjustment (GIA). The GIA is a viscoelastic signal, resulting from the viscoelastic properties of the Earth's mantle. Present day ice mass changes (PDIM) can produce an elastic signal. A load do not need to be present for a long time to produce a signal of this kind.
The viscoelastic signal is related to mass movements in the Earth's interior whereas the elastic signal is related to the displacement of the Earth's lithosphere. A gravity change due to the surface displacement will be produced by both signals and besides this will the viscoelastic signal also produce a gravity change due to the mass movement in the mantle layers. A load needs to be present for years/decades in order to have a viscoelastic signal whereas the elastic signal is produced within hours/days. The time needed to produce one of the signals depends on the characteristics of the Earth and the load.

The last glacial maximum (LGM) was around 21,000 years ago and it ended around 11,000 years ago. In Scandinavia and North America there are still GIA remnants of the last ice age (Walcott, 1973). This has been recognized by raised shorelines and sea level changes measured by tide gauge stations (Ekman, 1991). There was also more ice in Greenland during the last ice age. This changed during the deglaciation, and therefore a viscoelastic signal is observed in Greenland today. A viscoelastic signal is also produced by more recent fluctuation in the ice volume. In a study by Sato et al. (2012) they find that a signal from the little ice age (LIA) is present in Alaska, whereas Simpson et al. (2011) using a Greenlandic surface mass balance model ranging from 1866 to 2005 predicts a small viscoelastic signal during this period.
The quick elastic response of the Earth means that other loads than ice can produce an elastic signal. Of relevances for gravity measurement there are the effects of ocean and atmospheric loading. Observations of GIA are made with time series of GPS, gravity and tide gauge measurements. It gets more complex if the ice is still present since both the viscoelastic and the elastic signal are present.

There is an increasing interest of gaining knowledge about GIA. This knowledge is important in the study of climate change where estimates of present day ice mass balance are of interest. Satellite data are often used for these estimates, however the presence of a viscoelastic GIA signal in the investigated area will give an erroneous estimate of the mass balance. This is especially a problem for GRACE which senses mass changes, and in glaciated areas the mass change detected will be a combination of the mass change of the ice and a mass change in the interior of the Earth. This has turned out to be a significant problem especially for Antarctica whereas it is not so profound in Greenland, see Barletta et al. (2008).

The essential theory behind the GIA modelling is presented in this part, the viscoelastic

signal in Section 8.4 and the elastic signal in Section 8.5. The modelling results will be presented in Chapter 9 and in the two articles, Nielsen et al. (2013a) in Appendix A.1 and Nielsen et al. (2013b) in Appendix A.2. The article Nielsen et al. (2013a) is a study regarding the Earth model and the ice history's influence on the modelled viscoelastic gravity signal. These different modelling scenarios are used to estimate the uncertainty on the viscoelastic gravity signal in Greenland. The article Nielsen et al. (2013b) is a study about the modelling of the gravity change in Greenland including the viscoelastic signal, the elastic signal and the direct attraction. The modelling gravity is compared absolute gravity (AG) measurements in Greenland.
Results from AG measurements conducted in Greenland, and in Denmark during the time of this PhD project, will be presented. The measurements in Denmark are used for a short study on GIA in Denmark, Section 10.2. This part of the thesis ends with a summary and discussion.

8 GIA theory

To estimate the GIA signal, an Earth model and an ice history are needed. The Earth model is build on assumptions that will simplify the modelling. The ice history describes the spatial and temporal evolution of the load. A short description of the Earth model and the ice history will follow in Sections 8.1 and 8.2.

For an overview of ways to calculate the GIA signals the reader is referred to Whitehouse (2009). Additionally, see Meur and Hindmarsh (2000) for different approaches on the viscoelastic signal and Spada et al. (2012) for two ways of calculating the elastic signal.

8.1 The Earth model

The Earth is often assumed being spherical symmetric, non-rotating and having an isotropic Maxwell rheology. These are also the assumptions used for the modelling carried out here. The combination of an elastic lithosphere and a viscoelastic mantle is known as the Maxwell rheology model. It can be depicted as a spring and a dashpot in series connection, representing the lithosphere and mantle, respectively.
The assumption of spherical symmetry allows for the use of a spherical harmonic representation of the Earth and it simplifies the calculations. Milne and Mitrovica (1996) and Mitrovica et al. (2001) study the effect of a rotating Earth and find that it affects the sea level predictions. A model with isotropic rheology also simplifies the calculations. The effect of a 3D viscosity are presented in Latychev et al. (2005) and Davis et al. (2008). The major effect is on the prediction of the lateral displacements.
The Earth model parameters comes from the preliminary reference Earth model (PREM) (Dziewonski and Anderson, 1981). This model contains 93 layers, for the GIA modelling are used more simple models, with fewer layers. These will have average values of the PREM parameters.

8.2 The ice history

There are a number of different ice histories that can be used for calculating the GIA signal and global or regional histories are used depending on the focus of the study. For studies of the viscoelastic GIA signal the histories are often dated back to the LGM. In the article Nielsen et al. (2013a) some of them are presented. One of the most used is the ICE-5G (Peltier, 2004). This ice history is build on many different geological and geophysical data, for example sea level records form around the world are used to constrain the ice volume at a specific time. A global ice history is needed when solving the sea level equation which will be presented in Section 8.3.
For the elastic calculations more recent, short time spanned, models of mass balance are used. One example is the ICESat derived model presented by Sørensen et al. (2011). Models of this kind are used for calculating the elastic gravity signal as presented in Nielsen et al. (2013b) and Section 9.2.

8.3 Sea level equation

The sea level equation describes the relation between the water stored in the ice sheets and the sea level in a gravitational consistent manner and insuring mass conservation. If ice is melted, the water will be distributed over the ocean and change the sea level and the load on the Earth, this will change the surface which again will change the sea level. For these reasons the sea level equation is solved in an iterative process and for every time step of the ice history. Making the sea level equation gravitational consistent means that the melting ice will decrease the direct attraction it exerts on the sea. This is also known as the self-gravitational model. A detailed description on the sea level equation can be found in Mitrovica and Peltier (1991) and Milne et al. (1999).
Following Spada et al. (2012), the sea level change S with respect to the solid Earth is equal to

$$S = N - U \tag{8.1}$$

where N is the geoid and U is the vertical displacement of the solid Earth. The sea level equation states that the sea level change at coordinate (θ, λ) and at time t is given by

$$S(\theta,\lambda,t) = \left(\frac{V}{g_0} - U\right) + S^E - \overline{\left(\frac{V}{g_0} - U\right)} \tag{8.2}$$

where V is the potential and S^E is the eustatic sea level. The first term in the brackets is the sea level change due to changes in the ice volume and the bar over the last term in the brackets denotes that the signal is averaged over the oceans. The determination of V, N and U is the topic of the following sections.

SELEN solves the sea level equation for a given ice history and Earth model. Things that are not taken into account in the modelling, using SELEN, are migrating shorelines, rotational feedback and horizontal varying viscosities in the Earth model. These assumptions will have different impact on the modelling results.

8.4 The viscoelastic signal

The viscoelastic signal is produced when a load is applied to a Maxwell Earth that has both viscoelastic and elastic properties. For simplicity, the procedure to calculate the elastic part will be described here, and at the end it is outlined how it can be used for the full viscoelastic solution.
For the calculation of the viscoelastic signal load Love numbers and a Green's function are needed, where the Green's function is a combination of scaled load Love numbers (see Farrell and Clark (1976) and Mitrovica and Peltier (1989)). The use of Love numbers comes from Love and Sedleian (1909) who found that there is a linear relation between the perturbed and unperturbed Earth. This relation is given by the Love numbers, in this case the load Love numbers since they are associated with a load on the surface on the Earth. The load Love numbers, *h'*, *l'* and *k'* are connected to the radial displacement, the horizontal displacement and the potential perturbation, U_n^r, U_n^θ and V_n respectively, as follows

$$\begin{bmatrix} U_n^r \\ U_n^\theta \\ V_n \end{bmatrix} = W_n \begin{bmatrix} h'_n/g_0 \\ l'_n/g_0 \\ k'_n \end{bmatrix} \tag{8.3}$$

where V_n is the potential perturbation due to internal mass redistribution at the undeformed surface and W_n is the potential perturbation due to the load. The load Love numbers depends on the radius and the rheology of the Earth. A point-like load on the surface of the Earth deforms the Earth (Farrell, 1972). The load changes the potential field of the Earth and for an observer standing on the perturbed surface the potential becomes

$$V_p = V_0 + W_n + U_n^r \frac{dV_0}{dr} + V_n \tag{8.4}$$

where V_0 is the normal potential. The third term is the potential change due to the vertical movement of the observer. Using the expression for U_n^r in Equation (8.3) we get

$$V_p = V_0 + W_n + W_n \frac{h'_n}{g_0} \frac{dV_0}{dr} + V_n \tag{8.5}$$

To derive an expression for gravity, Equation (8.5) is differentiated with respect to r. It is used that $dV/dr = -g$, $d^2V/dr^2 = -dg/dr = 2g/r$, also the differentiation of the spherical harmonic expansion of the potentials as described in Torge (2001) is used.

$$-g_p = -g_0 + \frac{nW_n}{r} + h'_n \frac{W_n}{g_0} \frac{2g_0}{r} - (n+1)\frac{W_n}{r} k'_n \tag{8.6}$$

Here $r = a$, the Earth's radius. The quantity of interest is the gravity change $\Delta g = g_p - g_0$, then Equation (8.6) becomes

$$\Delta g = -[n + 2h'_n - (n+1)k'_n]\frac{W_n}{a} \tag{8.7}$$

This is the Green's function related to the gravity change as seen by an observer on the surface of the Earth. The first term is the direct attraction, the second is the contribution from the vertical movement of the observer and the last term is due to the mass changes within the Earth.

The expansion of the radial displacement, the horizontal displacement and the potential perturbation into spherical harmonic is

$$u_r(\vartheta) = \sum_{n=0}^{\infty} U_n^r P_n(\cos\vartheta) \tag{8.8}$$

$$u_\theta(\vartheta) = \sum_{n=0}^{\infty} U_n^\theta \frac{\partial P_n(\cos\vartheta)}{\partial\vartheta} \tag{8.9}$$

$$v(\vartheta) = \sum_{n=0}^{\infty} V_n P_n(\cos\vartheta) \tag{8.10}$$

where ϑ is the angular distance between the point load and the observation point. Using the spherical harmonic expansion and that $W_n = ag_0/M_e$ the Green's function for the gravity change becomes

$$\Delta g(\vartheta) = -\frac{g_0}{M_e} \sum_{n=0}^{\infty} [n + 2h_n' - (n+1)k_n'] P_n(\cos\vartheta) \tag{8.11}$$

This is the same Green's function as presented in Longman (1963), Farrell (1972) and Peltier (1974). Equation (8.11) is valid for observations made below the loading masses.
Other geophysical quantities can be expressed in a similar manner

$$u_r(\vartheta) = \frac{a}{M_e} \sum_{n=0}^{\infty} h_n' P_n(\cos\vartheta) \tag{8.12}$$

$$u_\theta(\vartheta) = \frac{a}{M_e} \sum_{n=0}^{\infty} l_n' \frac{\partial P_n(\cos\vartheta)}{\partial\vartheta} \tag{8.13}$$

$$\phi(\vartheta) = \frac{ag_0}{M_e} \sum_{n=0}^{\infty} [1 + k_n' - h_n'] P_n(\cos\vartheta) \tag{8.14}$$

$$N(\vartheta) = \frac{a}{M_e} \sum_{n=0}^{\infty} (1 + k_n') P_n(\cos\vartheta) \tag{8.15}$$

$$g_{FA}(\vartheta) = -2\frac{g_0}{M_e} \sum_{n=0}^{\infty} [n + 2 - (n-1)k_n'] P_n(\cos\vartheta) \tag{8.16}$$

Here u_r is the vertical displacement, u_θ is the horizontal displacement, ϕ is the gravitational perturbation, N is the geoid anomaly and g_{FA} is the free air anomaly.

The term for the direct attraction n is excluded in the calculation of the viscoelastic signal in the articles Nielsen et al. (2013a) and Nielsen et al. (2013b). One of the reasons for this is the study made by Merriam (1980) where the focus is on the ocean load however it is applicable for all loads. Merriam (1980) finds that the spherical representation of the load can give a spurious signal in the interior of continents. The problem arises with the truncation of the spherical harmonic representation of the load which gives a Gibbs like phenomenon. Increasing the number of harmonic degrees will decrease Gibbs phenomenon away from the load although it will still be present near the edge of the load. Figure 9.1 displays the result of the viscoelastic signal calculated with and without the direct attraction in Equation (8.11). In Olsson et al. (2012) they find that the best way to calculate the viscoelastic signal is to use a solution where the direct attraction is calculated with a different approach. They find

that it is even better to use the $\dot{g}/\dot{z}$ relation (see Section 8.7) rather than the solution with the direct attraction included in the Green's function. Examining this relation also gave reason for excluding the n-term. See Section 9.5 for further details.

The final Green's function for gravity change at the surface of the Earth due to a surface load then becomes

$$\Delta g_{vis}(\vartheta) = -\frac{g_0}{M_e}\sum_{n=0}^{\infty}[2h'_n - (n+1)k'_n]P_n(\cos\vartheta) \tag{8.17}$$

This is the equation used to calculate the modelled signals in Section 9.1 and it has been implemented in SELEN by the author.

The viscoelastic load Love numbers can be expressed as

$$\begin{bmatrix} h'_n \\ l'_n \\ k'_n \end{bmatrix}(t) = \begin{bmatrix} h^e_n \\ l^e_n \\ k^e_n \end{bmatrix}\delta(t) + \sum_i^M H(t)\begin{bmatrix} h^v_{n_i} \\ l^v_{n_i} \\ k^v_{n_i} \end{bmatrix} e^{-s_{n_i}t} \tag{8.18}$$

where the δ function and the Heaviside step function H represents the load at time t. s is the relaxation time given by the inverse of the Maxwell relaxation time $s = 1/\tau$ with $\tau = \mu/\nu$ being the viscosity divided by the rigidity. The sum runs over the number of modes that depends on the Earth model (number of boundary layers and rheology). These load Love numbers are used in the Green's functions presented in Equations (8.12) to (8.17).
The transformation of the elastic solution into the viscoelastic case comes about by a Laplace transform of the elastic case in time domain into the viscoelastic case in the s domain. This procedure is known as the correspondence principle, see Peltier (1974).

8.5 The elastic signal

The elastic signal is calculated analytically as a convolution of an ice model, representing the load, with the Green's function of gravity. The procedure is the same as presented in Spada et al. (2012) and the main reason for choosing this method is to save computation time when working with the high detailed ice models. It allows for calculations to higher degrees and increased resolution. The theory behind the calculation of the elastic signal is presented in for example Merriam (1980) and Spada (2003).

The gravity signal is derived from the potential of a layer with infinitesimal thickness

$$V(\theta,\lambda) = G\iint_s \frac{\sigma(\theta'\lambda')a^2 sin\theta' d\theta' d\lambda'}{R(\theta,\lambda,\theta',\lambda')} \tag{8.19}$$

Differentiating the potential with respect to r gives

$$\frac{\partial V}{\partial r} = -2\pi G\sigma(\theta,\lambda) + G\iint_s \sigma(\theta',\lambda')\frac{\partial}{\partial r}\left(\frac{1}{R}\right)a^2 sin\theta' d\theta' d\lambda \tag{8.20}$$

where $R(\theta',\lambda',\theta,\lambda)$ is the distance between the loading point (θ',λ') and the observation point (θ,λ) and $\sigma(\theta',\lambda')$ is the surface density. G is the gravitational constant and a is the

Earth's radius. The first term is related to the direct attraction of the load. It will be calculated separately in Section 8.6. The integral part of Equation (8.20) expanded in spherical harmonics gives

$$\frac{\partial V}{\partial r} = -\frac{3g_0}{a\rho_e}\sum_{n=0}^{\infty}\Big[\frac{2h_n-(n+1)k_n}{2n+1}\Big]\sigma(\vartheta) \tag{8.21}$$

where ρ_e is the mean density of the Earth. The load $\sigma(\vartheta)$ is represented as an axis symmetric disc load in a load reference frame system where the load axis of symmetry coincide with the pole of the reference system. The load described in spherical harmonics becomes

$$\sigma(\vartheta) = \sum_{n=0}^{\infty}\sigma_n P_n(\cos\vartheta) \tag{8.22}$$

where ϑ is the colatitude of the observer with respect to the center of the load. The disc load σ_n is given by

$$\sigma_n = \frac{\rho_i \Delta h_n}{2}\begin{cases} 1-\cos\vartheta & \text{if } n=0 \\ P_{n-1}(\cos\vartheta) - P_{n+1}(\cos\vartheta) & \text{if } n\geq 0 \end{cases} \tag{8.23}$$

where Δh_n is the height change of the n'th ice elements and ρ_i is the density of ice. The equation that is used to calculate the elastic signal becomes

$$\Delta g_{ela} = \frac{3g_0}{a\rho_e}\sum_{n=0}^{\infty}\Big[\frac{2h_n-(n+1)k_n}{2n+1}\Big]\sigma_n P_n(\cos\vartheta) \tag{8.24}$$

The author has implemented Equation (8.24) in the code provided by Spada that is used here.

In Spada et al. (2012) they compare two methods of calculating the elastic signal, one is as described in this section and the second is by solving the sea level equation following the procedure outlined in Section 8.3 and 8.4. For both methods they do the calculations up to degree $n_{max} = 128$ for comparison. The largest differences are located around the shoreline of Greenland, which is expected due to the gravitational consistent sea level equation. This is something to keep in mind since many of the GNET stations are located near the coastline. When modelling the elastic signal the optimal approach is to have the Earth model tuned to what is expected in Greenland instead of using global models. This will give more reliable results.

8.6 Direct attraction

Another signal detected by a gravimeter is the pull from the surrounding masses. This pull is known as the direct or Newtonian attraction.
The equation for calculating the direct attraction is derived from Newton's law

$$\overline{F} = -G\frac{Mm}{d^2}\frac{\hat{d}}{d} \tag{8.25}$$

which describes the force between two objects that are separated with distance d. Using the equation for the gravitational force, $\overline{F} = m\overline{g}$, where $\overline{g} = -g\overline{n}$ and using that it is the change

in gravity due to a change of the attracting mass that is of interest, Equation (8.25) becomes

$$\Delta\overline{g} = -G\frac{\Delta m}{d_m^2}\frac{\hat{d}}{d} \tag{8.26}$$

It is used that $\hat{d} = \hat{r_o} - \hat{r_m}$, that the distance between observer and mass is given by the difference in the the radius vectors from the center of Earth to the observer and the mass. Using that the gravimeter measures along the plumb-line so that $\hat{r} = r\cos(\vartheta)$ the final expression for the direct attraction, with positive z-axis down, is

$$\Delta g_{DA} = G\frac{\Delta m}{d_m^3}(h_o - h_m)\cos(\vartheta) \tag{8.27}$$

where $d = \sqrt{r_m^2 + r_o^2 - 2r_m r_o\cos(\vartheta)}$, ϑ being the angle between the two points, $r_m = r_e + h_m$ is the radial distance of the mass and $r_o = r_e + h_o$ is the radial distance of the observer. Equation (8.27) is visualized in Figure 8.1 for different scenarios.

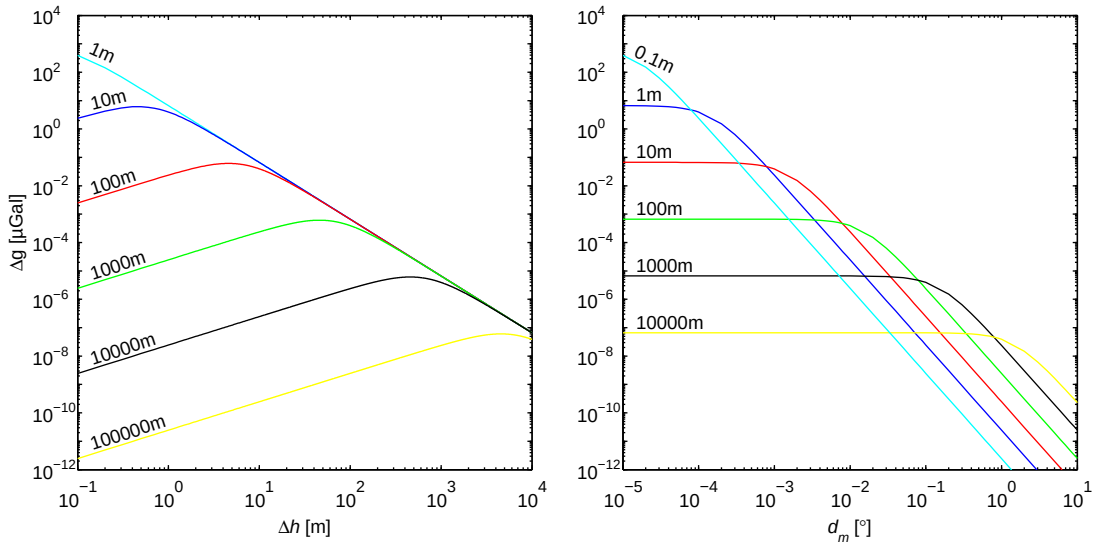

Figure 8.1: The effect of one ton mass gain, approximately one cubic meter of ice, as a function of the observers height above the mass for different distances (left) and as a function of distance for different heights (right). Increasing the mass by one order will increase the signal by one order.

If the observer and the mass interchange position the signal in Figure 8.1 will change sign. Also, a negative mass change, a mass loss, will change the sign of the signal.

All masses will give a signal of direct attraction, however only the signal from the ice is presented here. In gravimetry the masses of water (groundwater or the oceans) or the atmosphere are often investigated as a source of gravity change.

8.7 The $\dot{g}/\dot{z}$ relation

A relation that is useful in GIA studies is the $\dot{g}/\dot{z}$-relation. In Ekman and Mäkinen (1996) it is mentioned that this relation can be used to indicate which process is dominating in an area

with GIA. For a purely elastic signal the $\dot{g}/\dot{z}$-relation is given by $2g/R = -0.31\mu Gal/mm$. This is also known as the free air gradient and no mass movement is related to this signal. For a purely viscoelastic signal the $\dot{g}/\dot{z}$-relation is given by $2g/R + 2\pi G\rho = -0.17\mu Gal/mm$. This can be regarded as a Bouguer signal, where the signal is related to mass movement in the mantle. In Ekman and Mäkinen (1996) they also introduce a ratio of these two signals

$$c = \frac{\dot{g}/\dot{z} - (\dot{g}/\dot{z})_{FA}}{(\dot{g}/\dot{z})_B - (\dot{g}/\dot{z})_{FA}} \tag{8.28}$$

Hence, if the signal is purely viscoelastic $c = 1$ and in the case of a pure elastic signal $c = 0$.

Another use of this relation is that it can indicate how well the reference system, that the GPS solutions are calculated in, aligns with the Earths center of mass. This is carried out by fitting a line to the $\dot{g}$ and $\dot{z}$ values in a cross plot. The closer this line goes through the origin, the better is the reference frame. This is used in a study the by Mazzotti et al. (2011) where they conclude on the basis of AG and GPS measurements in North America that GPS velocities aligned to the ITRF2005 and ITRF2008 (International terrestrial reference frame) can be directly compared to modelled GIA signals whereas velocities aligned to ITRF2000 contains a bias of approximately $1.5mm/yr$. In Linage et al. (2007) and Linage et al. (2009) the ratio is examined for different loading scenarios.

8.8 AG and GPS

Combining AG and GPS data is a powerful tool for studying GIA and besides the relation presented in Section 8.7 these two data sets can also be used to separate the viscoelastic and the elastic signals in AG and GPS data from glaciated areas.
A study on the separation of the GIA signals is conducted by Wahr et al. (1995). Their idea is to remove the viscoelastic signal from the data in order to constrain the signal from present day ice mass changes. The first step is to remove the elastic effect from the gravity data (dg) using the free air gradient, $dg_v/dt = dg/dt - dz/dt \times dg_{FA}/dz$. Then the viscoelastic effect can be removed from the GPS measurement (dz) and what remains is the vertical displacement due to present-day ice mass changes

$$\frac{dz_e}{dt} = \frac{dz}{dt} - 6.5\frac{dg_v}{dt} \tag{8.29}$$

The number 6.5 $[mm/\mu Gal]$ is the inverse of the Bouguer approximation mentioned in Section 8.7. Wahr et al. (1995) found that Equation (8.29) is valid for a number of Earth models and ice histories. An example where Equation (8.29) is used is given in James and Ivins (1998) where they study the GIA signals in Antarctica.

The separation of the GIA signals is dependent on the factors mentioned in Section 8.7 where, connected to the elastic signal, is the free air gradient and for the viscoelastic signal it is the Bouguer approximation. Sato et al. (2012) investigates the Bouguer approximation, which they call the viscoelastic ratio, using AG and GPS data from southeast Alaska. They correct the measurements for modelled present-day ice mass changes and find that the relation between $\dot{g}$ and $\dot{z}$ depends on the melting history of the glaciers near the measurements, and the distance between the AG site and the GPS station used for the calculations.

For six stations they find a mean value of the Bouguer approximation between -0.18 to $-0.21\mu Gal/mm$ which is a little larger compared to the $-0.15\mu Gal/mm$ found by Wahr et al. (1995). Linage et al. (2007) study the Bouguer approximation using a spectral approach, by expanding the equation of gravity change and vertical displacement into spherical harmonics for different Earth models. They estimate a value of $-0.21\mu Gal/mm$. In Linage et al. (2009) they study the relation for different type of loads. Another study using AG and GPS data is made by Mémin et al. (2011a). They make a more refined Bouguer approximation where they take the topography and the relative position of the load and the observation into consideration.

A successful separation of the GIA signals can turn out to be a powerful tool to gain knowledge about the processes in glaciated areas and can be used to improve the mass balance estimates of the major ice sheets based on gravity change from GRACE.

9 GIA modelling

The theory outlined in Chapter 8 is used to produce the results presented in Nielsen et al. (2013a), Nielsen et al. (2013b) and the following sections.

The viscoelastic signal is calculated by solving the sea level equation using the freely available code SELEN (Spada and Stocchi, 2007). This is carried out in Section 9.1. The elastic signal is calculated by convolving the elements of an ice model with the gravity Green's function. The code for modelling this is provided by Giorgio Spada and is the same used in Spada et al. (2012). This is done in Section 9.2.

The author has implemented the equations for calculating the gravity change for both the viscoelastic (Equation 8.17) and the elastic (Equation 8.24) case.

9.1 Viscoelastic signal

The main modelling results of the viscoelastic gravity signal are presented in Nielsen et al. (2013a). Here are presented some additional modelling results using the ICE-5G ice history and an Earth model consisting of a $90km$ lithosphere, an upper and lower mantle with viscosities of 0.5 and $1.6\times10^{21}Pas$. The results are modelled up to maximum degree $n_{max}=64$. There is a pronounced difference in the viscoelastic gravity signal depending on if the direct attraction is included in the Green's function (Equation 8.17), see Figure 9.1.

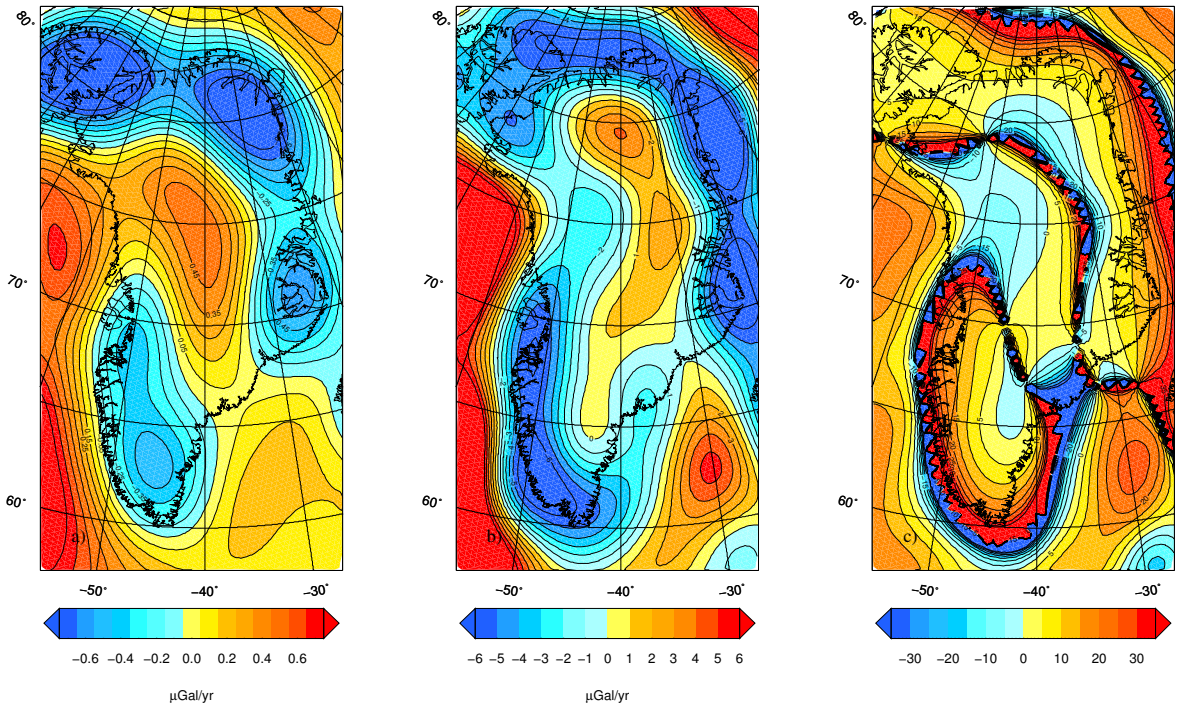

Figure 9.1: a) The modelled viscoelastic signal excluding the n-term, and b) including the term. c) The relative difference, $\dot{g}'/\dot{g}$. $\dot{g}'$ denotes the gravity with the direct attraction included in the calculations.

Not only is there a large difference in the magnitude of the signal, furthermore in the spatial distribution of the signal. The main variation is around the edge of the load as expected since the n-term relates to the load described in the sea level equation. The features in Figure 9.1 c) delineates the zero contours in 9.1 a) and 9.1 b).

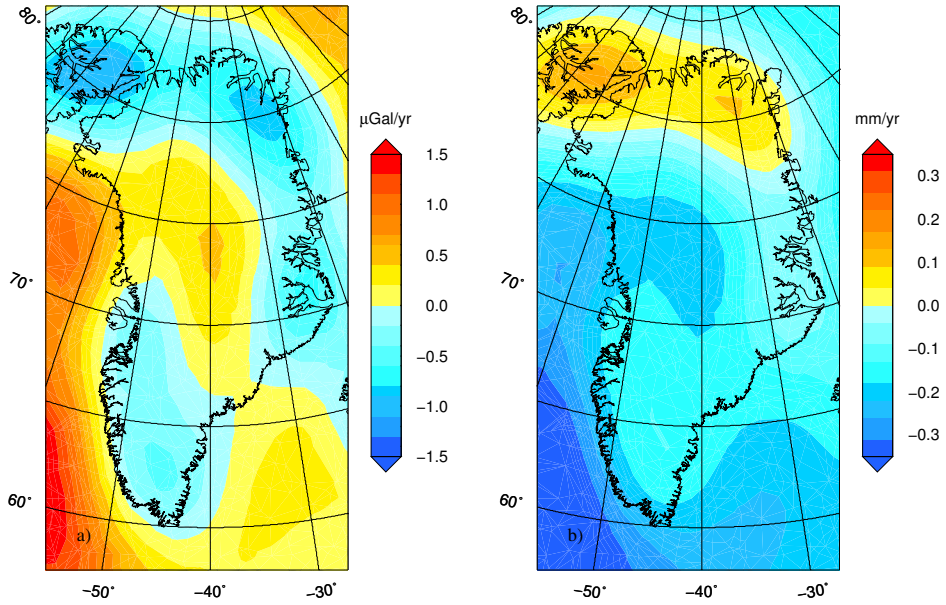

Figure 9.2: a) The change in the free air anomaly and, b) the geoid for Greenland using the ICE-5G ice history and a simple Earth model containing a 90km lithosphere and two mantle layers with the viscosities 0.5 and $1.6 \times 10^{21} Pa\,s$.

Other outputs from SELEN are the changes of the free air gravity anomaly g_{FA}, calculated using Equation (8.15) and of the geoid N, calculated using Equation (8.14). The modelling results are presented in Figure 9.2 a) and b) respectively. The free air gravity anomaly can be used to predict how close the Earth is to be in isostatic equilibrium. An example of this is found in Scandinavia and North America, where the free air gravity anomaly indicates a mass deficit. This deficit is a result of the displacement of mass in the mantle due to the LGM ice load. The signature of the free air anomaly change in Figure 9.2 a) resembles the map of the free air anomaly found in Braun et al. (2007).

9.2 Elastic signal

The main results from modelling the elastic gravity signal are presented in Nielsen et al. (2013b) and the reader is referred there. Some additional results are presented in this section. To calculate the elastic signal, an ice mass model of present day mass changes is needed. Here, ICESat derived mass change models similar to the M3 model presented in Sørensen et al. (2011) are used. They derive mass change models from ICESat height changes of the Greenlandic ice sheet and investigate different processing methods. The only difference is that the models used here are divided in time periods covering the years, 2004-2007, 2005-2008, 2006-2009. The grid size of the models is $5 \times 5km$. In the code used for calculating the elastic signal, the loads are presented as discs. To use the ICESat models with the code the area of the grid cells must be converted into equal area discs.

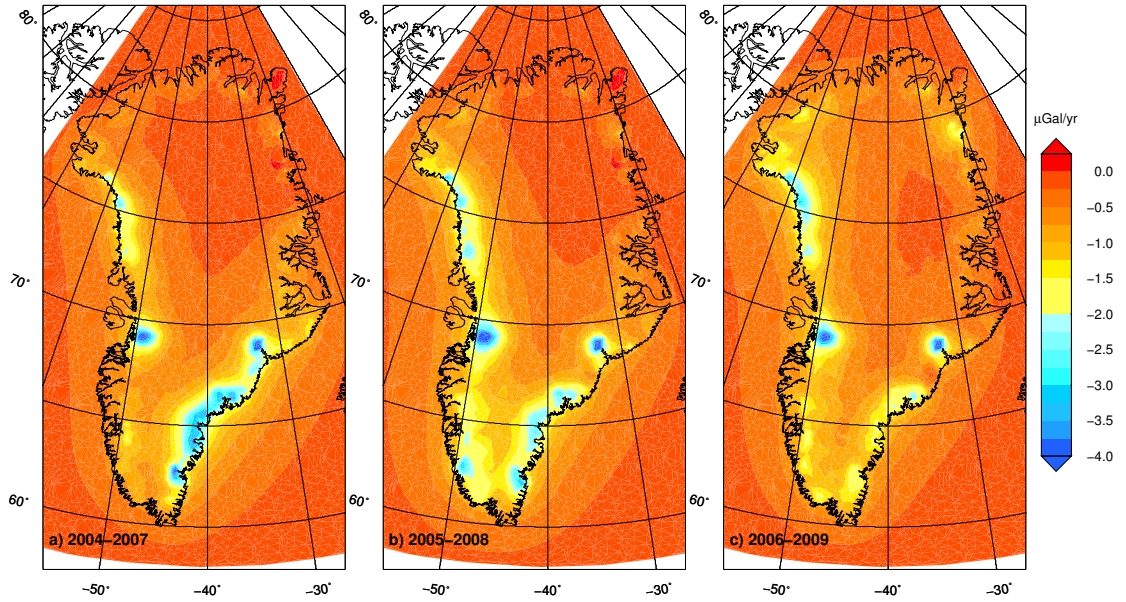

Figure 9.3: The elastic gravity signal in Greenland using the ICESat ice mass models. For a) the value range from 0.72 to $-7.53\mu Gal$, for b) 0.63 to $-7.50\mu Gal$ and for c) 0.18 to $-6.45\mu Gal$.

The elastic signal for all Greenland using all three ICESat models are presented in Figure 9.3. During the entire time span 2004-2009, there is a change in the signature of the signal. The spatial distribution of the largest signal is moving from the southeast to the northwest. The ice mass loss of the major outlet glaciers are seen clearly. Kangerdlugssuaq on the east coast and the Jacobshavn Isbræ on the west coast. At these two glaciers GNET is also recording

the largest vertical displacement, 30.5 and 18.8mm/yr respectively (Bevis et al., 2012). The modelled elastic gravity signal at six selected GNET stations are displayed in Table 9.1.

9.3 Direct attraction

A gravimeter on the surface of the Earth is also affected by the masses surrounding it. A change in the surrounding masses will change the pull that these masses exert on the gravimeter. Simplified, the effect is given by the distance between the gravimeter and the mass, and by the angle of which the mass is compared to the plump line at the gravimeter, $\Delta g = \Delta m \cos\theta / r$. The effect increases with increasing mass changes, while it decreases with distance and the angle to the mass. Theoretically this means that a mass juxtaposed to the gravimeter will not affect the gravity measurement. The exact equation to calculate the direct attraction is given as Equation (8.27) in Section 8.6.

	Elastic			Direct		
	2004-2007	2005-2008	2006-2009	2004-2007	2005-2008	2006-2009
HEL2	3.9±0.4	3.0±0.3	1.8±0.2	228.0±22.8	165.0±16.5	52.0±5.0
KBUG	3.9±0.4	2.9±0.3	1.7±0.2	-83.0±8.0	-55.0±6.0	-28.0±3.0
LYNS	2.2±0.2	1.6±0.2	1.1±0.1	-0.6±0.1	-0.5±0.1	-0.4±0.0
ISOR	2.6±0.3	1.9±0.2	1.9±0.2	-6.9±0.7	-4.1±0.4	-6.0±1.0
KULU	1.4±0.1	1.1±0.2	0.9±0.1	-0.2±0.0	-0.1±0.0	-0.1±0.0
THU3	0.6±0.1	0.8±0.2	0.9±0.1	-0.2±0.0	-0.2±0.0	-0.2±0.1

Table 9.1: The modelling results for the elastic signal and the direct attraction for all three ICESat ice models at six selected GNET sites. Units are $\mu Gal/yr$.

As presented in Figure 8.1 is the direct attraction very sensitive to masses near the observer, so accurate data on the position and the mass is crucial for reliable estimation of the direct attraction. A digital elevation models (DEM) is used to calculate the height difference between the observer and the masses, and increasing the resolution of the DEM will resolve in a more accurate result. Due to this the mass change models are re-sampled from a $5km$ grid to a $1km$ grid, meaning that the mass change in the $5km$ grid is evenly distributed to 25 equally sized $1km$ grids ensuring that the mass is conserved. The effect of a high resolution DEM is seen from the results presented in Table 9.1 compared to the numbers in the caption of Figure 9.4 where a low resolution DEM is used.
The results of the calculations of the direct attraction at the six selected GNET sites for the three ICESat models are presented in Table 9.1. The result for all of Greenland is presented in Figure 9.4.

Gravity measurements in glaciated areas can also be used to estimate the ice mass changes. For example at the Helheim glacier, the GNET data can be used to remove the elastic signal from the gravity change, assuming a neglible viscoelastic signal, then the remaining signal is related to changes in the direct attraction from the ice. The gravity change at the Helheim glacier from 2009 to 2010 is found to be $-54.0 \pm 6.0 \mu Gal/yr$ (in the GPS reference frame), the vertical displacement is $15.3 \pm 0.3 mm/yr$ (Bevis et al., 2012). Using the relation, $-0.31 \mu Gal/mm$ (see Section 8.7), and correcting the gravity measurement for the vertical displacement, the gravity change becomes $-49 \mu Gal/yr$.

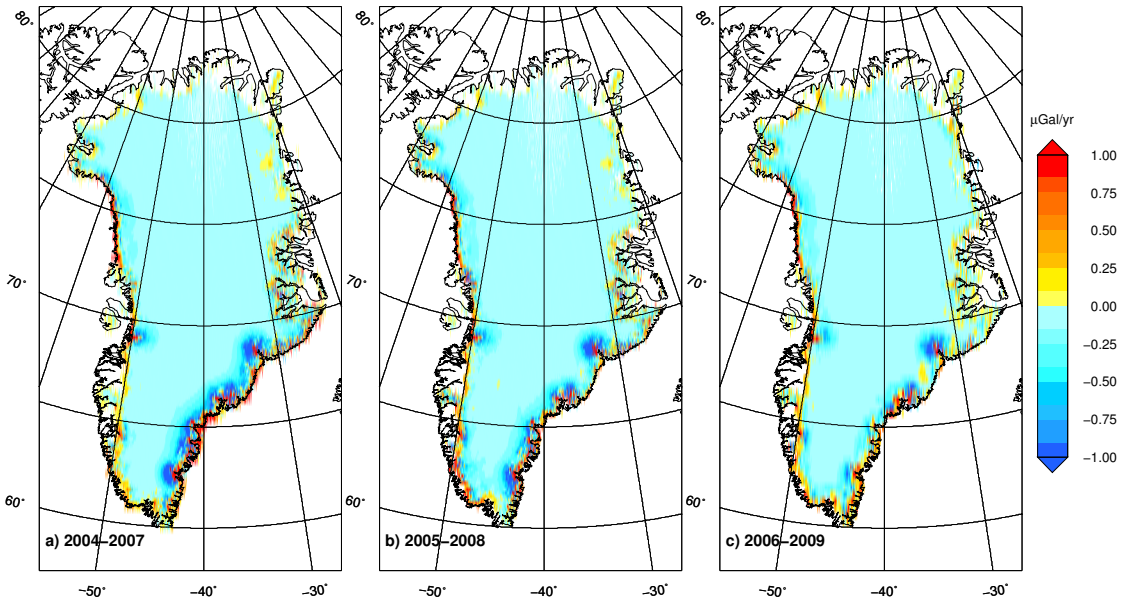

Figure 9.4: The direct attraction in Greenland using the ICESat ice mass models. The value range from a) 22.2 to $-20.2\mu Gal$, b) 15.8 to $-20.0\mu Gal$ and, c) 14.5 to $-16.8\mu Gal$.

Modelling the direct signal at the Helheim GNET site indicates that ice within a radius of 0.5° contributes to the direct attraction (see Figure 4 in Nielsen et al. (2013b)). The ice mass change, from the ICESat 2006-2009 model, within this radius is $-2.28 Gt/yr$ and this gives rise to a modelled direct attraction of $-52.0 \pm 5.0 \mu Gal/yr$ (Table 9.1). The measured gravity change at the Helheim glacier is approximately 6% smaller than the modelled result for 2006-2009. Using this, the mass loss of the area surrounding the Helheim site, in the period from June 2009 to June 2010, should also be 6% smaller, around $-2.14 Gt/yr$. These fast calculations demonstrates another potential use of the gravity measurements.

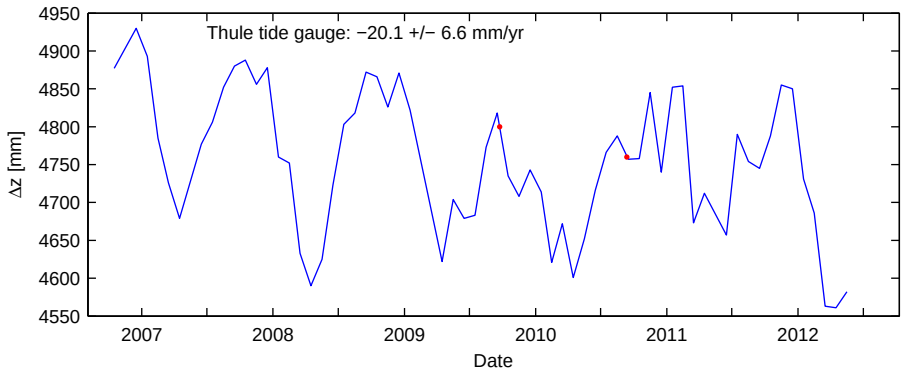

Figure 9.5: Tide gauge data from Thule shows a relative sea level fall of approximately $-20 mm/yr$. This will give a gravity change due to the less amount water mass near the station. The two red dots shows when the AG measurements were conducted.

Olsson et al. (2009) show that non-tidal sea level changes influence the gravity time series because of the change in the surrounding water masses and thereby the direct attraction from these. This is an issue for coastal stations.

Tide gauge data[6] from Thule presented in Figure 9.5, shows a sea level fall of approximately $-20mm/yr$ during the a period from 2007 to 2013, this corresponds to a gravity change of approximately $0.8\mu Gal$.

Investigating the tide gauge data shows that there is a difference in the sea level at the time of the two measurements conducted at THU3. There is a low stand of approximately $30cm$ when the measurement was conducted in 2010 compared to 2009. Modelling the direct attraction from this change in sea level gives approximately a change of $-12\mu Gal$. This corresponds very well with the measured gravity change.

9.4 Bouguer signal

This signal is not relevant for the study we are doing in Greenland. It is only relevant in the case where gravity measurements are conducted on the ice. It is a signal that arises from the change in mass under the gravimeter approximated as a Bouguer plate. Following Meur and Huybrechts (2001) it can be calculated with the following expression

$$\Delta g_B = 2\pi G[\Delta m - \sqrt{\rho_i r_c^2 + \Delta m^2} + \rho_i r_c] \tag{9.1}$$

where Δm is the mass elements and r_c is the disc radius of mass elements. The Bouguer signal, using the ICESat ice models described in Section 9.2, is presented in Figure 9.6.

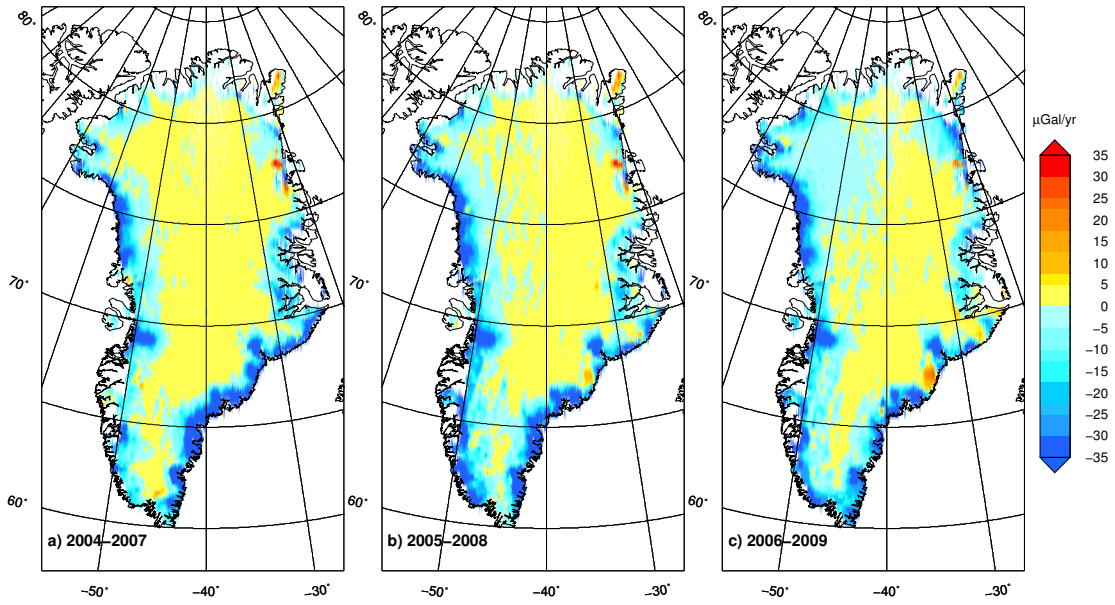

Figure 9.6: The Bouguer gravity signal in Greenland due to ice mass changes described in the ICESat ice mass models. The value range for a) from 60.5 to $-346.7\mu Gal$, for b) 76.2 to $-358.3\mu Gal$, and for c) 51.0 to $-289.7\mu Gal$.

This signal can be significant when measuring directly on the ice. Since non of the measurements in this study are conducted on the ice this signal will not be considered further in this study.

[6]Data are from the global sea level observing system (GLOSS): http://www.gloss.sealevel.org

9.5 The $\dot{g}/\dot{z}$ relation

This signal (see Section 8.7) can give an idea of the dominating process in an area with GIA. Here the relation is studied when excluding or including the direct attraction in the modelled viscoelastic signal. Also presented are calculations of the relation using the preliminary results of our AG measurements with GPS data from the GNET.
Whether or not the *n*-term is included in the modelling gives significant differences as seen in Figure 9.7 and it is a result of the higher gravity values from modelling with the *n*-term as shown in Figure 9.1.

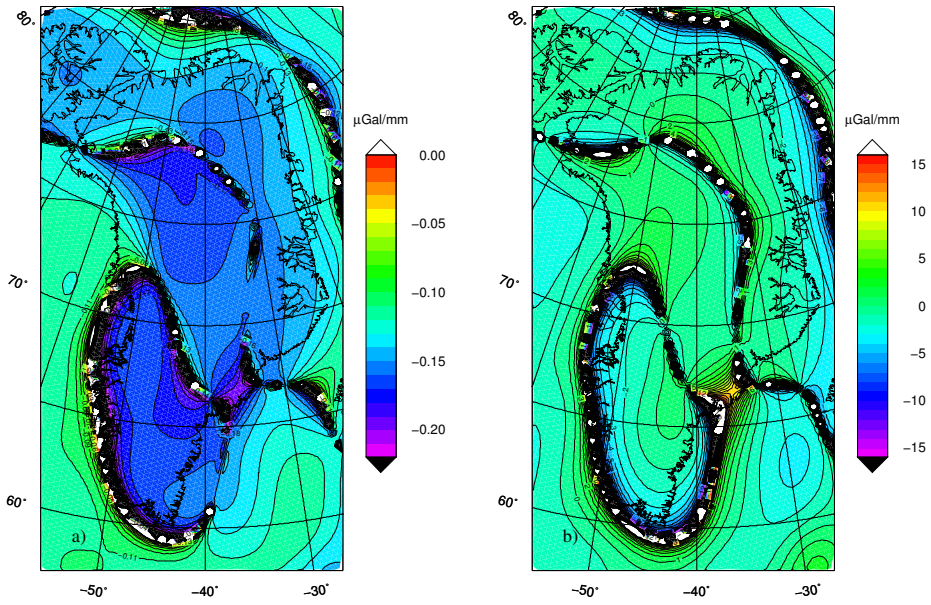

Figure 9.7: The ratio of $\dot{g}/\dot{z}$ for the case where the direct attraction is not included a) in the Green's function and where it is b). The equation for the gravity calculations is Equation (8.17).

The relation between the two ratios $\dot{g}'/\dot{g}$, where $\dot{g}'$ denotes the gravity change including the direct attraction, has the same appearance as in Figure 9.1 c).
If looking at the ratio from modelling without the direct attraction the result is closer to the empirical found values found in Scandinavia, Ekman and Mäkinen (1996) and in North America, Lambert et al. (2006). In Scandinavia Ekman and Mäkinen (1996) finds a value of $c = 0.79$ (see Equation (8.28)) having $\dot{g}/\dot{z} = -0.20\mu Gal/mm$, while Lambert et al. (2006) find the ratio to be $-0.18\mu Gal/mm$ using 4 sites in Canada and USA. This gives a value of $c = 0.93$ close to a pure viscoelastic signal.

	Measured gravity	Measured displacement	$\dot{g}/\dot{z}$	Free air dg/dt	Bouguer dg/dt
HEL2	-2.4±8.0	15.3±0.3	-0.16±0.5	-4.7±0.9	-2.6±0.1
KBUG	-0.4±9.0	18.2±0.3	-0.02±0.5	-5.6±0.9	-3.1±0.1
LYNS	13.6±10.0	9.2±0.3	1.52±1.2	-2.9±0.9	-1.6±0.1
ISOR	-1.0±2.0	7.4±0.4	-0.16±0.3	-2.3±1.2	-1.3±0.1
KULU	16.9±11.0	6.3±0.1	2.70±1.8	-2.0±0.3	-1.1±0.0
THU3	12.4±8.0	5.1±0.1	2.53±1.6	-1.6±0.3	-0.9±0.0

Table 9.2: Data of gravity (measured gravity minus the modelled direct attraction) and vertical displacement for six GNET sites. Also, estimates of gravity change from GPS data are presented here. Units are [$\mu Gal/yr$ - mm/yr - $\mu Gal/mm$ - $\mu Gal/yr$ - $\mu Gal/yr$]. The data is presented in a coordinate system with positive z-axis upward.

In Table 9.2 is presented the estimates of $\dot{g}/\dot{z}$ for the six GNET sites that have been occupied twice. The results of the measurements and the modelling are presented in Nielsen et al. (2013b). The first column is the measured gravity with the modelled direct attraction subtracted. The second column is the GPS vertical displacement published in Bevis et al. (2012) and the third column is the $\dot{g}/\dot{z}$ estimate. In the two last columns, the GPS data are converted to gravity change using the free air gradient and the Bouguer approximation, as mentioned in Ekman and Mäkinen (1996) these values can be seen as the upper and lower value of the expected gravity change. The values used for the conversion are $-0.31\mu Gal/mm$ and $-0.17\mu Gal/mm$ for the free air and Bouguer approximation, respectively. These values may differ from what is most suited for Greenland as discussed in Section 8.7.

10 Gravity measurements

Here, the measurements we have made in Greenland and in Denmark since 2009 and 2008 respectively are presented. Some of the measurements in Greenland are presented in the article Nielsen et al. (2013b). The main purpose of the gravity measurements are to study GIA, to build and maintain gravity networks.

10.1 Greenland

A total of 18 GNET site have been visited with an A10 gravimeter. We have also established 11 new AG sites in e.g. airports and three old sites have been re-occupied. This gives a total of 32 AG sites spread around Greenland. Ten of these sites have been visited twice, where six of these are GNET sites. Their locations are presented in Figure 10.1.

The general tendency for the measurements at the sites visited in 2009 and 2010 is, that the difference between the measurements are larger than the accuracy of the instrument. This holds for most cases, and for some sites, those close to the ice margin, the difference can be many times the accuracy. The trend varies, nevertheless for most GNET sites the trend is negative.

The results of the measurements at the six GNET sites are presented in Nielsen et al. (2013b), while the results of the remaining four are presented in Figure 10.2. It is of cause too opti-

mistic to make reliable trends based on the few data points we have, however the trends give an idea of the possibilities of doing AG measurements in Greenland.

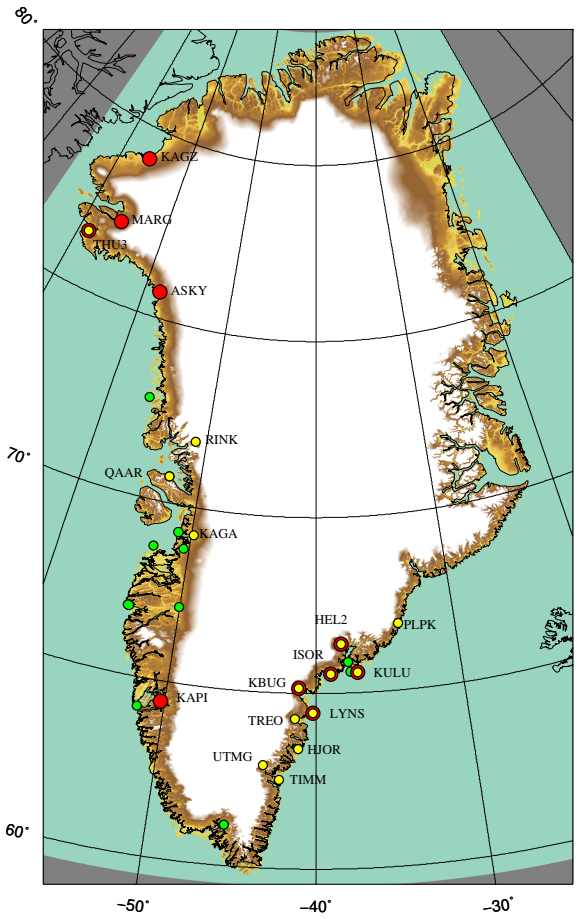

Figure 10.1: The GNET sites with AG measurements conducted in 2009 are plotted as red dots, while measurements conducted in 2010 are the yellow dots. The name code for the GNET stations are collocated with their respective dots. The green dots are other AG measurements we have conducted in Greenland. The DEM used is from Bamber et al. (2001)

The measurements reveal the large influence of the direct attraction and its significance near the ice margin. As presented in Section 8.6 a mass loss below the observations leads to a negative change in gravity. Now, considering the change at Helheim glacier and only taking the direct attraction into consideration, then for a gravimeter to detect a positive trend there must either has been a mass increase below or a mass decrease above the station. Since the station is located near the glacier front and above it, the most likely event is that there has been a mass increase below the station. This does not agree with the ICESat data, which is used to calculate the direct attraction, or the GPS measurements from GNET. However, in Howat et al. (2011) it is stated that Helheim has gained mass, $7Gt$, during the period from 2006-2010. Whether the positive trend at Helheim is due to a mass increased below the site or mass decrease above the site is unresolved. To resolve this, detailed models of the ice mass balance and the topography of an area up to 1° around the site are needed. Information about the GNET stations presented in Nielsen et al. (2013b) is listed in Table 10.1.

	Lat	Long	Elev [m]	Sea [km]	Ice [km]
HEL2	66.401	-38.216	425	20-30	0.2-0.3
KBUG	65.144	-41.158	291	10	0.3-0.5
LYNS	64.430	-40.198	174	0.4-0.6	1.5-2.0
ISOR	65.547	-38.975	83	0.1-0.2	8-10
KULU	65.579	-37.148	68	0.1-0.2	40-60
THU3	76.537	-68.825	36	0.1	15-20

Table 10.1: Information regarding the location of the six GNET sites presented in the article Nielsen et al. (2013b). The distance to the sea and the ice margin are rough estimations. Position of the sites are illustrated in Figure 10.1.

As mentioned earlier there are four sites, not GNET sites, that have been visited twice or more. Two of these are newly established sites at the Illulisat airport and at Camp Tuto near Thule airbase close to the ice margin. The two other sites were first occupied with an absolute gravimeter of the JILAg type in 1988. These are the sites at Thule airbase and in the Nuuk town hall. The site in Nuuk has, besides the measurement in 1988, been occupied with a FG5 absolute gravimeter in 2009.

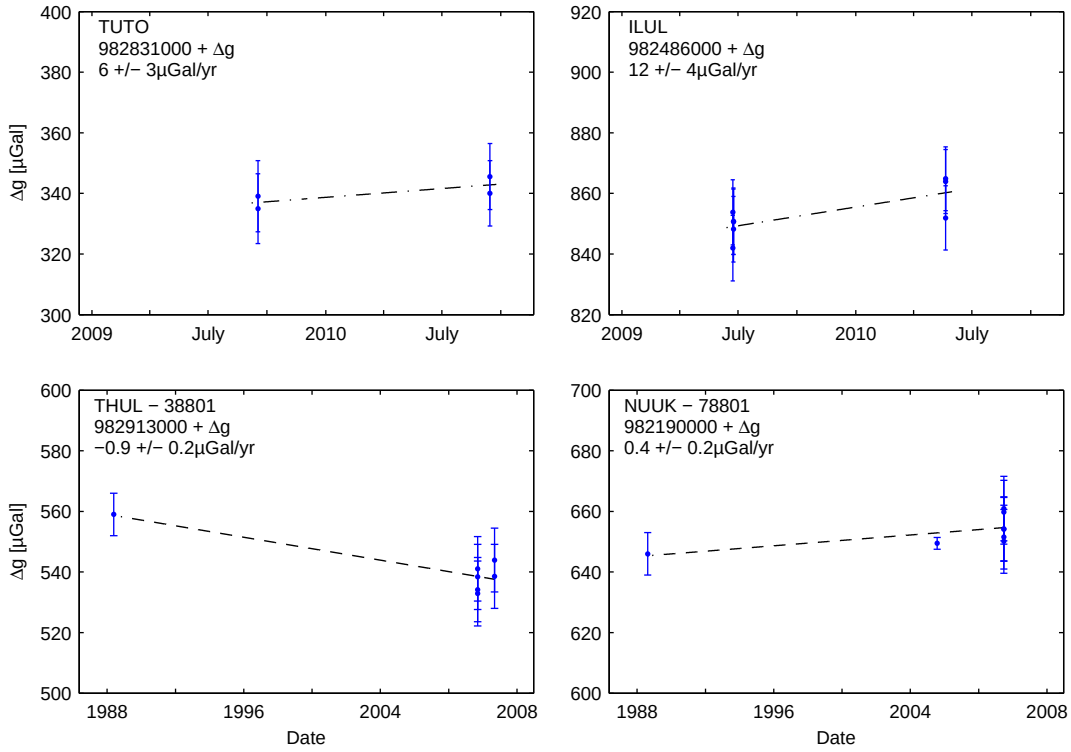

Figure 10.2: Data from four sites in Greenland that have repeated gravity measurements. A trend and its uncertainty is calculated using linear regression. Some of the early measurements are conducted with a JILAg gravimeter, while one measurement at Nuuk is made with a FG5. These values are presented with the $z-$axis running positive towards nadir

The modelled viscoelastic signal can be compared with the long term measurements in Thule and Nuuk, assuming that at the time of the measurements the viscoelastic signal is detectable. For the site Thule-38801 the trend is found to be $0.9 \pm 0.2 \mu Gal/yr$, while the modelled trend, as presented in Nielsen et al. (2013a), is $0.1 \pm 0.2 \mu Gal/yr$. For Nuuk the trend is found to

be $-0.4 \pm 0.2 \mu Gal/yr$ while the modelled trend is $-0.2 \pm 0.2 \mu Gal/yr$. The modelled trend for Nuuk is not presented in Nielsen et al. (2013a) although it is determined on the same data. The data from the Thule and the Nuuk sites are from Timmen et al. (2008) and Francis (2006). The location of the four sites (see Figure 10.2) is listed in Table 10.2

	Lat	Long	Elev [m]	Sea [km]	Ice [km]
TUTO	76.421	-68.453	480	15-25	0.5-0.6
ILUL	69.241	-51.066	14	0.2-0.3	35-45
THUL	76.538	-68.801	27	0.6-0.8	15-20
NUUK	64.178	-51.740	23	0.3-0.4	100-120

Table 10.2: Information regarding the location of the four other AG sites in Greenland. The data from these sites are presented in Figure 10.2. The distance to the sea and ice margin are estimations.

The Thule-38801 site, has also been occupied by our instrument twice (Figure 10.2). Looking only at the data we have collected at this site the trend changes from the one found when including the 1988 measurement. It goes from a trend of $-0.9 \pm 0.2 \mu Gal/yr$ to a trend of $4.6 \pm 3.3 \mu Gal/yr$. Our measurements are presented in Figure 10.3.

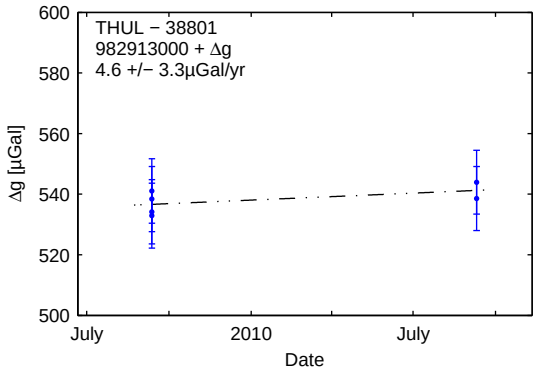

Figure 10.3: Data from our measurements at site Thule - 38801. This site was measured with a JILAg instrument in 1988, see Figure 10.2.

The positive trend is similar to the trend at Camp Tuto. These two stations are separated by approximately $17km$ with Camp Tuto closer to the ice margin. The trends the sites, Thule - 38801 and Camp Tuto, has an opposite trend compared to the trend at the GNET site, THU3 (Nielsen et al., 2013b). At the GNET site the trend is found to be $-13 \pm 8 \mu Gal/yr$, and this change is likely due to direct attraction of the sea. The distance between site THU-38801 and the THU3 GNET site is approximately $650m$. The results from the three AG sites in the Thule area illustrates the challenges of interpreting the data.

Wahr et al. (2001) presents gravity data from Kellyville and Kulusuk covering the years from 1995 to 2000. No rates are presented. A gravity change of $-1.6 \pm 1.2 \mu Gal/yr$ is found for Kellyville in van Dam et al. (2000), they also present data from Kulusuk, no rate however. The variation in the Kellyville data indicates that an elastic signal could be present. The data varies $10 \mu Gal$ in the period presented. In the Kulusuk data there is introduced a jump due to the construction of a hotel nearby the site.

Gravity changes in other glaciated areas are presented in Mäkinen et al. (2007) (Antarctica), Sun et al. (2010) and Sato et al. (2012) (Alaska), Mémin et al. (2011a) (Svalbard). The highest rates are found in Alaska, in the Glacier Bay area, ranging from -3.5 to $-5.6\mu Gal/yr$.

10.2 Denmark

The viscoelastic signal is present in former glaciated areas like Scandinavia. Figure 10.4 shows a time series of AG measurements at our reference site in the Rockefeller building, Copenhagen. A near-zero trend is estimated (Figure 10.4).

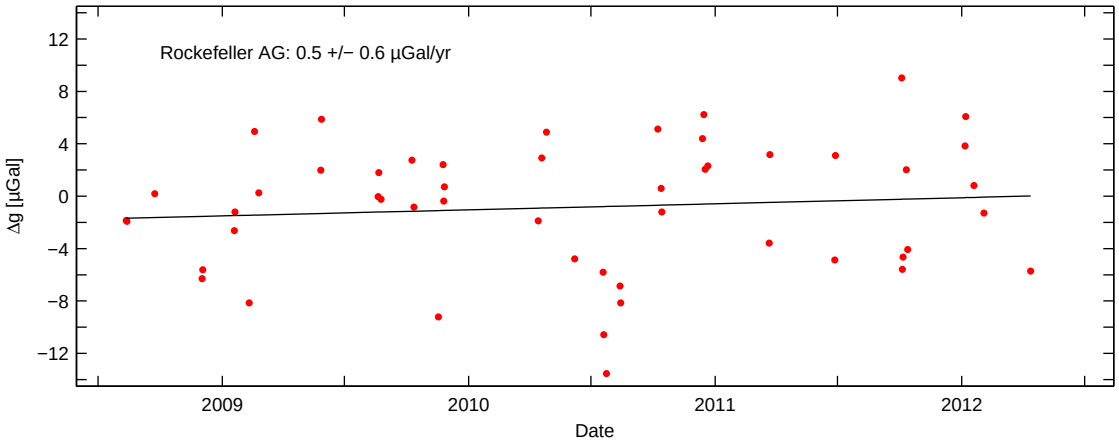

Figure 10.4: The measurements at the Rockefeller reference site, Copenhagen. It is the same data as in Figure 5.1. A line is fitted to the data and the trend is $0.5 \pm 0.6\mu Gal/yr$. The data error bars are neglected for clarity. Including the 2005 FG5 measurement results in a trend of $0.3 \pm 0.6\mu Gal/yr$

The result shows a small positive trend, although with a high uncertainty. The product-moment correlation coefficient (Equation C.5) for this regression is $r = 0.10$ indicating a weak fit. Including the FG5 measurement made in 2005 (Timmen et al., 2008), the trend becomes $0.3 \pm 0.6\mu Gal/yr$. For the Vestvolden site in the Copenhagen area, $8km$ from the Rockefeller building, Timmen (2009) finds a rate of $0.2 \pm 0.6\mu Gal/yr$.

Gravity rates from former glaciated areas are presented in Gitlein (2009) and Steffen et al. (2009) for Scandinavia and in Lambert et al. (2001) and Mazzotti et al. (2011) for North America. For both regions the maximum change in gravity is approximately $-2.0\mu Gal/yr$ and is found near the center of the uplift pattern.

Data from the nearest permanent GPS station is used to determine the $\dot{g}/\dot{z}$-relation. The GPS station, Budding, is located approximately $6km$ from the AG reference site and the trend of the data is estimated to $0.7 \pm 6.0mm/yr$. The high variability in the GPS data leads to the high uncertainty on the vertical displacement (Figure 10.5).

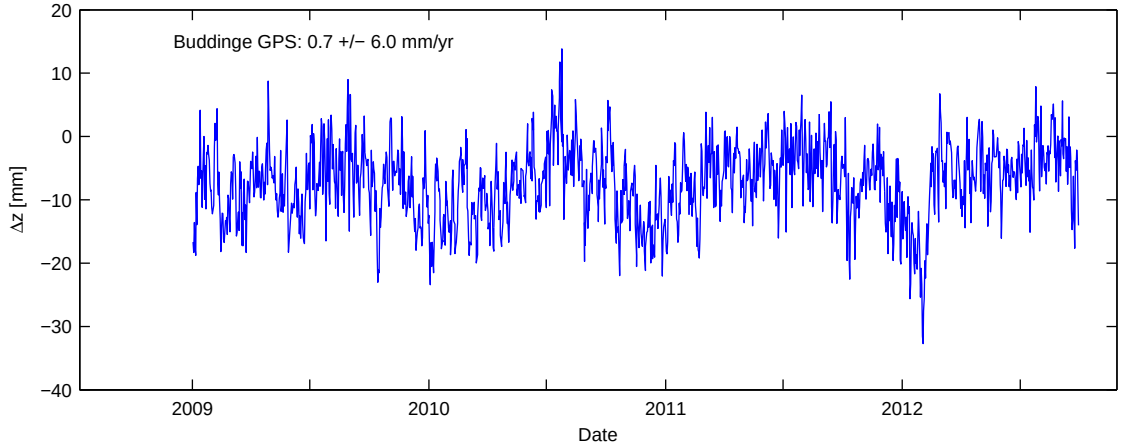

Figure 10.5: Data from the permanent GPS station at Buddinge, Copenhagen. We only present data from the period where AG data is collected at the reference site in the Rockefeller building.

By combining the data from Budding GPS with the AG data from the Rockefeller site, the $\dot{g}/\dot{z}$ relation for the Copenhagen area is estimated. The gravity trend in Figure 10.4 is given with the z axis running positive downwards. Hence, the $\dot{g}/\dot{z}$ relation becomes

$$\dot{g}/\dot{z} = \frac{-0.5 \pm 0.6 \mu Gal/yr}{0.7 \pm 6.0 mm/yr} = -0.6 \pm 6.0 \mu Gal/mm \tag{10.1}$$

This value is quite larger than what is expected for an area with a viscoelastic GIA signal, however the uncertainty of the data is large. The uncertainty is calculated using Equation (C.4). The relation is estimated to be $-0.4 \mu Gal/mm$ when the 2005 FG5 measurement is included in the trend calculation. Using the gravity change at Vestvolden estimated by Timmen (2009), the relation is $-0.3 \mu Gal/mm$ which is close to what is expected for an elastic signal and not what is expected for an area with a GIA signal. With time more measurements will be available and an improvement of this value is expected. Also, when more sites gets gravity time series these data will aid the estimation of the $\dot{g}/\dot{z}$ relation.

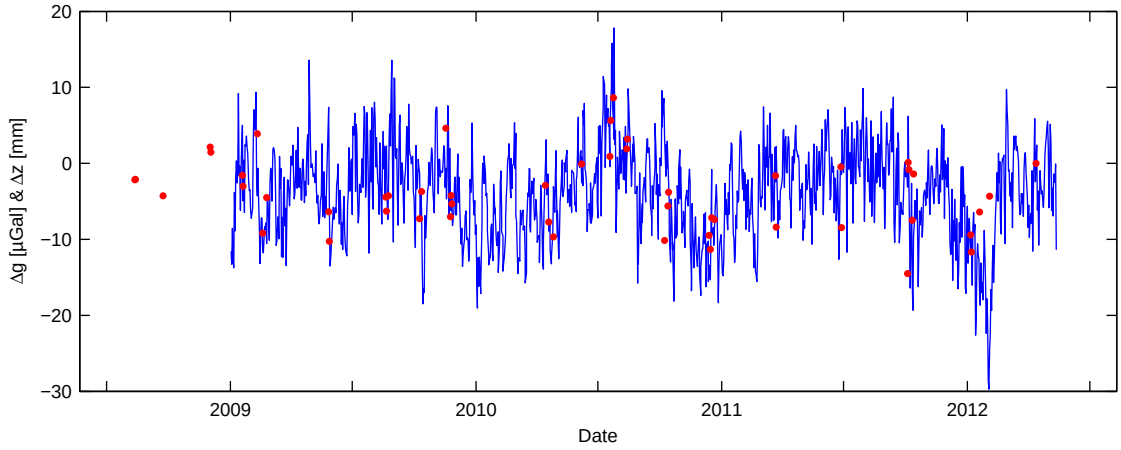

Figure 10.6: The AG data from the Rockefeller building is here plotted with GPS data from the permanent GPS station at Buddinge, both in Copenhagen, distanced by approximately $6km$. Both data sets are de-trended and there is a gap in the GPS data in the beginning of the gravity time series.

Plotting the de-trended AG and GPS data in the same coordinate system (Figure 10.6), there are indications of a correlation between the two data sets.

Figure 10.7 a) displays time series of the AG and GPS data only where there are AG data, this is to clarify the relation between the two data sets. The two data sets are plotted as the difference relative to the last measurement in the time series, hence the last data point for both AG and GPS is at 0 Δg and Δz, respectively. There is some degree of correlation between the two data sets and in the cross plot, (Figure 10.7 b) the correlation is found to be $r = -0.54$ which indicates a moderate correlation. The slope of the regression line is $\alpha = -0.85$ which indicates the presence of a linear relation.

Taking a step back, to the data that are not de-trended, and performing the same calculations, the correlation and regression coefficient are found to change a little. Since this data is not de-trended it contains a viscoelastic signal and the $\dot{g}/\dot{z}$ relation presented in Section 8.7 should hold.

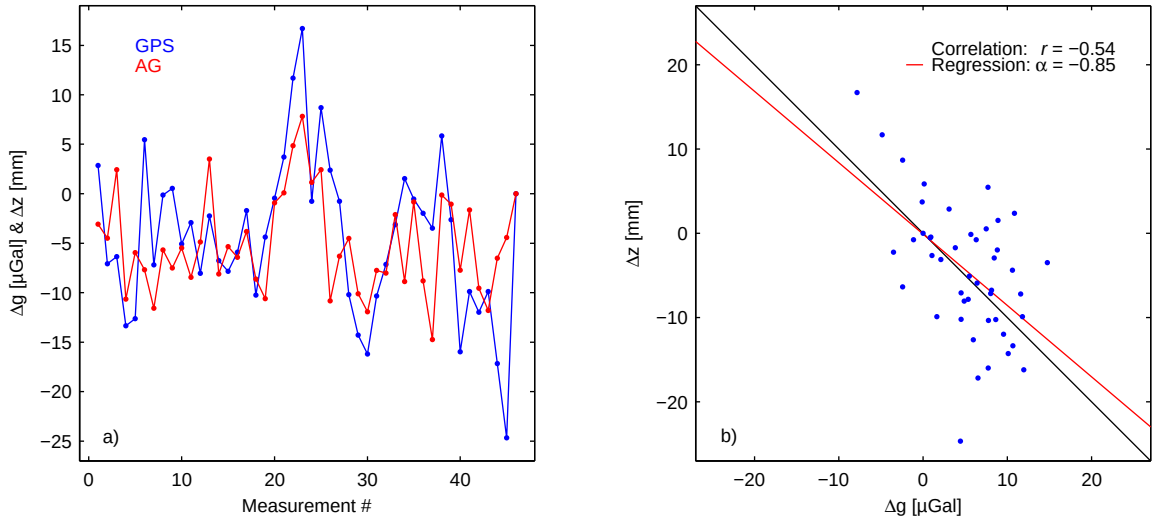

Figure 10.7: In Figure a) the AG and GPS measurements are plotted according to the order of when the measurements are conducted it is basically the same as Figure 10.6. In Figure b) is the cross plot of the AG and GPS measurements with the correlation factor of $r = -0.54$ and regression coefficient $\alpha = -0.85$.

This $\dot{g}/\dot{z}$ relation between the AG and the GPS measurements has been investigated as follows: Different values of the relation are multiplied to the GPS data, which convert them into gravity data. The original AG data are then corrected by these converted GPS data. Finally the correlation coefficient and the linear regression coefficient are calculated for the cross plot of the corrected AG data and the GPS data. These coefficient for the different relations are used to evaluate the result (Figure 10.8 a).

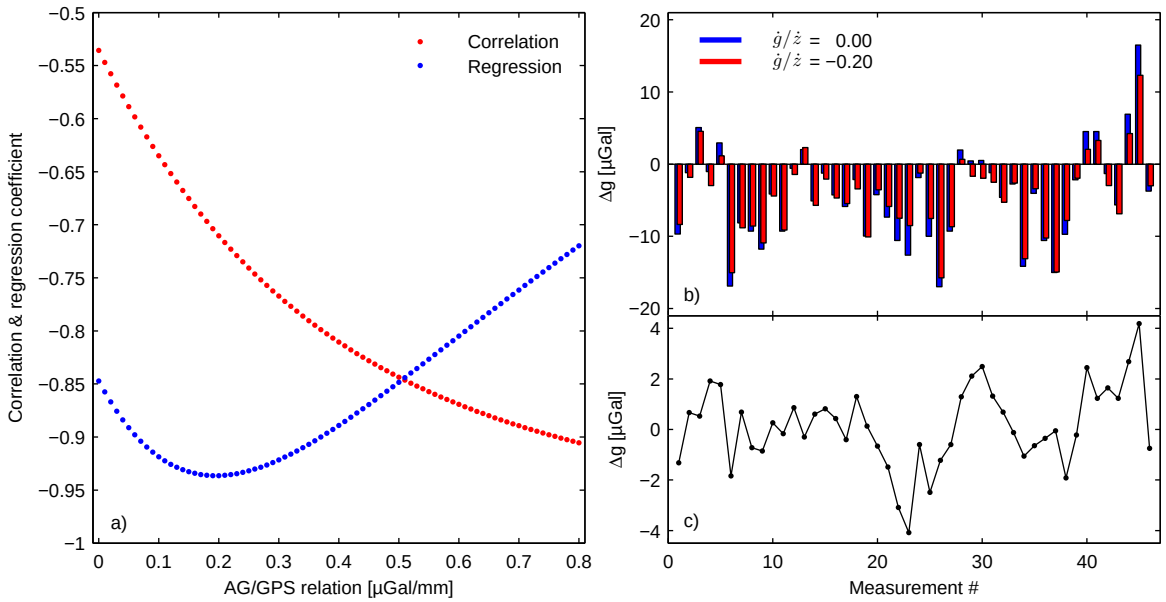

Figure 10.8: In a) is the correlation and regression coefficients for different $\dot{g}/\dot{z}$ factors, in b) is the difference between the AG and GPS data for two values of $\dot{g}/\dot{z}$ and in c) is the difference between the two data sets in figure b).

The first values of the correlation and regression coefficients in Figure 10.8 a) are the same as in Figure 10.7 b). The correlation coefficient is increasing with an increasing $\dot{g}/\dot{z}$ relation, however at the same time is the regression coefficient decreasing. Hence, increasing the $\dot{g}/\dot{z}$-relation will elongate the spread of the AG points in Figure 10.7 b) and thereby increase the correlation. The best regression coefficient, assuming a linear relation, is found at $-0.195\mu Gal/mm$ (Figure 10.8 a), rounded to $-0.20\mu Gal/mm$. This is the same as Ekman and Mäkinen (1996) found for Scandinavia and close to the value Lambert et al. (2006) found for North America. Also, considering the theoretical value for a former glaciated area in Section 8.7, this value is in good agreement.

The moderate correlation at $-0.20\mu Gal/mm$ (Figure 10.8 a) can be due to noise or abnormal instrument behavior for some of the measurements, although assuming that the data is corrected for the viscoelastic signal only an elastic signal should be present and more fluctuations can be expected. Figure 10.8 b) shows the difference between the AG and GPS measurement of the uncorrected AG data and the corrected AG data by the $-0.20\mu Gal/mm$ relation. Figure 10.8 c) displays the difference between the two data sets (Figure 10.8 b). These differences can be used to pinpoint abnormalities in the data or in the processing of the data. These should also be the size of the viscoelastic signal. If the data is corrected for the signal in Figure 10.8 c) the remaining signal should be of elastic character.

If the fluctuations in Figure 10.6 are elastic then the source of the signal must be related to some forcing acting over a larger area since the distance between the two stations is approximately $6km$. Hence, local groundwater levels are likely not the reason. A more likely reason would be uncorrected atmospheric loading and the ocean loading from the Øresund region. Virtanen (2004) finds that atmospheric loading and loading of the Baltic sea is responsible for 40% of the daily GPS height variation. Hence, this would also influence the gravity signal.

11 Summary / discussion

The main results are presented in the articles Nielsen et al. (2013a) and Nielsen et al. (2013b). In this part, additional results from the modelling and our measurements are presented. All of which, enables an investigation of different GIA aspects. Comparison between our measurements in Greenland and the modelling results is carried out in Nielsen et al. (2013b). Below I summarize the findings from the modelling and the comparison of measurements with the modelling results and the main conclusions.

The preliminary measurements exhibit some similarities with the modelling results. For example, converting the latest data from the GNET project into gravity data using the free air gradient, results in gravity changes in the range of -0.8 to $-9.4 \mu Gal/yr$. The modelled elastic gravity signal using newly developed ice mass change models results in gravity changes in the range of 0.2 to $-6.5 \mu Gal/yr$ (Figure 9.3 c). Also, the long term gravity trends measured in Thule and Nuuk gives rates of 0.9 and $-0.4 \mu Gal/yr$, respectively. The modelling results of the viscoelastic signal for these sites are 0.1 and $-0.2 \mu Gal/yr$, respectively. There is also a resemblance of the measurements and the estimated direct attraction for some GNET sites.

The modelling shows that the gravity change related to the GIA processes is small compared to our preliminary measurements at the GNET sites. The modelling also shows that a large signal is expected due to the direct attraction from the changing ice, and modelling this signal depends on the resolution of the mass change model and the DEM. Care must be taken since the direct attraction is highly sensitive to the location of the mass and observer.

The assumptions regarding the Earth model and the ice history that are made in connection with the modelling leave room improvements. More realistic Earth models and detailed ice histories are where improvements can be made. Different ice histories or different steps in the ice histories are desirable since a viscoelastic signal not only from the LGM, however also the LIA can be present todays. The implementation of the mathematics also leaves room for improvements, for example, the implementation of evolving shorelines as the sea level changes would make the modelling more realistic. This was not an option in the version of SELEN used in this study. The modelling of the elastic signal would be improved by considering the sea level equation. In Spada et al. (2012) they find that the difference between solving the full sea level equation and convolving the mass elements with the Green's function is up to 10% of the signal. Solving the sea level equation would produce a more realistic result for the coastal GNET stations.

There are other geodynamical processes that produce mass movement in the Earth's mantle. For example will convection in the mantle produce a signal of long wavelength that could be interpreted as GIA. James (1992) mention the possible presence of a mantle convection signal in North America. However, this signal is expected to be small.

The $\dot{g}/\dot{z}$ relation can give an idea of the dominating GIA process in an area when comparing the theoretical expected values with the empirical estimates. When comparing the modelled $\dot{g}/\dot{z}$ relations with the empirical relations for Scandinavia and North America, it is found

that excluding the direct attraction in the Green's function will produce results that are closer to what is empirical found value. This is valid for both the viscoelastic and the elastic signals.

In Table 9.2 it is seen that the relations determined on our gravity measurements are not near the expected values for the $\dot{g}/\dot{z}$ relation, although the uncertainty on the estimates are very high. This is due to the large uncertainty on the gravity trends, which will be improved with more measurements. The stations LYNS, KULU and THU3 have large, positive $\dot{g}/\dot{z}$ relations, which could be due to a signal of direct attraction. Mémin et al. (2011a) states that the $\dot{g}/\dot{z}$ relation for the elastic signal can become positive when a direct attraction signal is present and it can become lower than $-0.26\mu Gal/mm$ if the load is below the observer. Our results might confirm this, however the uncertainties on the results are high due to the limited number of measurements. For the sites HEL2, KBUG and ISOR the relations determined from our data are of the expected order, however they resemble more the relation expected for a viscoelastic signal. Again, the large uncertainties make it difficult to say anything conclusive.

When more reliable estimates of the $\dot{g}/\dot{z}$ relation are made, they can be used to tune the modelling of the signals due GIA and PDIM, since the relation contains information on the Earth's properties. The study presented in Section 10.2 gives an example of the use of AG data with GPS and that these two kind of data sets are complementary and an important tool in the study of GIA.

In gravity time series, it can be expected that the viscoelastic signal is a nearly constant linear trend, while the elastic signal is more complex. One issue with the elastic signal is the seasonal signal which is seen in the GNET data (Bevis et al., 2012). This signal is due to the seasonal loading variations of the ice and air masses, which not necessarily are in phase. The averaged seasonal change in atmospheric loading leads to a vertical displacement of $8mm$ peak-to-peak (Bevis et al., 2012), approximated to $2.5\mu Gal$ with the free air gradient. The averaged total seasonal vertical displacement is $1cm$ peak-to-peak, approximated to $3.1\mu Gal$ using the free air gradient. The seasonal loading change will also affect the gravity measurements, however with the GPS data it is possible to asses if the gravity change, or a part of it, is related to the seasonal variability. The effect of this can be minimized by planning the campaigns so that sites are re-visited at the same time of the year. This has been the case for our campaigns.

With time, when more AG measurements are available in Greenland, they will improve the GIA modelling. Gravity measurements can be used not only in the determination of the GIA signals them self, furthermore for improving the Earth model and ice history used in the modelling. Another study that gravity data could be used for, is local mass balance estimates. In areas where the gravity signal is dominated by the direct attraction, the mass changes needed to produce the observed gravity change is an estimate of the local mass balance. However, all of this relies on accurate AG measurements.

Part III
Future work & conclusion

12 Future work

During the process of finishing this thesis, several ideas for further exploration have emerged. The more reasonable once will be outlined here as suggestions for future work.

Study 1:
At our reference site in Copenhagen we have four years of measurements. As seen in Figure 10.4, there is some correlation with nearby GPS measurements presented in Figure 10.6. It could be interesting to investigate how these fluctuations in the AG and GPS data correlate with changes of the atmospheric pressure and the sea level in the Øresund region, especially non-tidal sea level changes. If there is loading of the Copenhagen area by the waters in Øresund, the AG and GPS data can be used to investigate the elastic properties of the area.

A similar study is made by Virtanen and Mäkinen (2003) where they compare Superconducting gravimeter (SG) data from Metsähovi, Finland, with tide gauge data from Helsinki. Also, satellite data from GRACE or GOCE could be included and compared to the AG variations as done in Steffen et al. (2009).

To investigate the non-tidal sea level changes, tide gauge data can be used, and preferredly data from stations surrounding Copenhagen. These could also be held against data of atmospheric pressure and wind direction. All of this should give information about non-tidal sea level changes and their nature.

The know-how gained from a study like this could be used in Greenland when the data for it becomes available. Extracting knowledge about the elastic properties of the Earth's Lithosphere could be used for improved modelling of the elastic signal due to PDIM or inversely to make mass balance estimates from GPS and AG data.

Study 2:
Further investigations of the correction for atmospheric pressure and ocean loading in Greenland are of interest. As shown in for example Boy et al. (2002) and Lysaker et al. (2008), these corrections can be improved by more detailed modelling of the signal.

Regarding the calculation of the atmospheric correction, models[7] or data[8] can be used to improve the result. There is a seasonal signal of the atmospheric loading in Greenland, which is detected by the GNET (Bevis et al., 2012), and it is found to be a significant signal being of the same order as the seasonal ice mass changes. Regarding the gravity measurements will this signal introduce a signal from the loading effect and the direct attraction effect.

[7] Atmospheric model, Polar MM5, www.polarmet.osu.edu
[8] The Greenland Climate Network (GC-NET), www.cires.colorado.edu

For the ocean loading modelling, the optimal procedure would be to measure the constituents of the ocean loading signal. This can be done with relative gravimeters like the LCR or CG5 measuring for up to a year at the site. An example of this is found in Bos et al. (2002). If this is not possible, present ocean loading models can be used, however the loading should then be calculated for a local area and with a detailed coastline of the region. Furthermore, the use of different ocean models should be investigated.

At sites near the coast, and where no tide gauge data is available, the ocean models could also be used to estimate the direct attraction from the sea. This attraction can introduce a gravity change if there is a change in sea level between the measurements. This seems to be the case for the gravity change detected at the THU3 site, and there is reason to believe that a similar effect is present at other sites.

And, on the topic of the direct attraction. To estimate the direct attraction from the ice more accurately, a more detailed model of the mass balance is needed. This would be most interesting to do for Helheim since this is the place where the largest gravity change is detected. Helheim is also interesting since many studies have been made on this glacier and its mass balance. Therefore, many different data types of the mass balance are available to estimate the direct attraction.

Study 3:
Investigating the improvement of the A10 setup with focus on minimizing the vibrations from the instrument. This can be achieved through more tests with different kinds of absorption materials placed under the Dropper and/or the IB-unit. Reducing the vibrations will minimize the drop scatter and the system response, which will further improve the measurement.

Furthermore, more investigations on the nature of the system response and its influence on the gravity determination are of interest. These investigations should be conducted on synthetic data. The question is how the system response is reflected in the distribution of solutions using different truncations. It should then be investigated if these distribution can be used for a statistical approach in the determination of g, and possibly develop a processing scheme that is more robust towards the influence of the system response and data truncation.

Any scheme that is reliable on synthetic data should be tested on real data that is collected within a short time period and even data from different instruments. This is to ensure that the influence of any environmental variables is minimized.

13 Conclusion

In this thesis it is found that the absolute gravimeter A10-019 owned by DTU Space performs better than the manufacture specifications. For indoor measurements, the accuracy and repeatability is found to be $6\mu Gal$, while for outdoor measurements these numbers increase to $10\mu Gal$. The performance of the instrument for outdoor measurements is in accordance with the instrument's specifications. There is reason to believe that the instrument can perform even better than these values, however more inter-comparisons with other absolute gravimeters are needed to estimate this.
To be able to make inter-comparisons, the instrument needs to be calibrated on a yearly basis. This will keep track on the laser frequency drift, which can be up to $-14\mu Gal/yr$.

We have proved that we can operate the instrument under different environments using transportations as car, helicopter and fix winged aircrafts in order access remote sites. The biggest challenges when measuring in the field, especially in Greenland, is to prevent the instrument from cooling. During the time of ownership the instrument has proved useful for many different tasks in many different environments.
Through fieldwork we have gained valuable experience regarding operating the instrument. From these experiences we know that a good setup of the instrument is crucial for optimal data quality. This will minimize the system response. Also, minimizing the environmental impact on the measurement is crucial. Winds will increase the drop scatter, and large temperature fluctuations will deteriorate the performance of the laser. All of this should be kept in mind when operating the instrument.

The collection of data should be carried out for as long as it is possible at the site. The number of drops per set should be 100-130, while the number of sets should be as many as possible. The precision is not improved significantly when collecting over 8-10 sets, however a continuation of measurements would eliminate any residual ocean loading signal. Ideally, a measurement should be conducted over 48 hours.

In the data processing, care must also be taken to obtain optimal data quality. The choice of ocean loading model is important and especially if measuring over a short time period. The presence of the system response can not be eliminated completely and it is difficult to remove during the processing as it is shown here. More investigations into the reduction of the system response effect in the processing is needed.

During the time we have had our instrument it has proved to operate well in the field. It is quick to setup and can run under many different conditions as we have tried. When this is said, it should also be mentioned that we have had a lot of problems with our instrument, which has lead to many long emails with the manufacture, and overseas shipments for repairment.

The main reason for acquiring the instrument was to initiate gravity time series in Greenland for studies of geodynamics. Of special interest is the gravity change at the GNET sites.

Our preliminary measurements in Greenland shows that we are detecting a gravity change.

With a one year interval, the smallest and largest detected gravity changes of -5 and $54\mu Gal$, are obtained for the sites at Isortoq and Helheim, respectively. The gravity changes are well above, or just at the limit of the gravimeters accuracy, so there is reason to believe that the detected gravity change is of natural origin and not instrumental.

The nature of these gravity changes is investigated through modelling. The modelled elements are the viscoelastic GIA signal, the elastic PDIM signal and the direct attraction of PDIM. Of these, the direct attraction can be the most significant especially when the observation is made close to the ice margin.

There are sites located far away from the ice margin and thereby away from the direct attraction effect of the ice that exhibits a large gravity change, which cannot be explained with the signals modelled in this thesis. These stations are located near the shore so further studies into the ocean loading at these sites is of interest. This will furthermore be used to estimate the direct attraction from the ocean.

The objective is to be able to separate the viscoelastic and elastic signal in Greenland. In order to do this, the gravity time series are used with GPS time series from the GNET project. For this, the gravity time series are too short however with time, this separation of the different signals should be possible. This will in the end improve the constraining of the GIA signal and thereby the mass balance estimates of the Greenland Ice Sheet.

This study has underlined that absolute gravity data are collectible, even in remote places, and that possibilities with this kind of data are manyfold especially when used in connection with GPS time series.

References

Agnew, D. C. (2012). SPOTL: Some programs for ocean-tide loading. Program version 3.3.0.

Amalvict, M., Rogister, Y., Hinderer, J., Luck, B., McQueen, H., and G., L. (2007). Absolute gravity measurements in Terre Adélie (Antarctica) and at Canberra (Australia). Institut de Physique du Globe de Strasbourg.

Andersen, O. B. and Forsberg, R. (1996). Danish precision gravity reference network. Skrifter 4, National Survey and Cadastre - Denmark.

Bamber, J., Ekholm, S., and Krabill, W. (2001). A new, high-resolution digital elevation model of Greenland fully validated with airborne laser altimeter data. *J. Geophys. Res.*, 106:6733–6745.

Barletta, V. R., Sabadini, R., and Bordoni, A. (2008). Isolating the PGR signal in the GRACE data: impact on mass balance estimates in Antarctica and Greenland. *Geophys. J. Int.*, 172:18–30.

Bevis, M., Wahr, J., Khan, S. A., Madsen, F. B., Brown, A., Willis, M., Kendrick, E., Knudsen, P., Box, J. E., van Dam, T., Caccamise, D. J., Johns, B., Nylen, T., Abbott, R., White, S., Miner, J., Forsberg, R., Zhou, H., Wang, J., Wilson, T., Bromwich, D., and Francis, O. (2012). Bedrock displacements in Greenland manifest ice mass variations climate cycles and climate change. *PNAS*, 109:1–14.

Bos, M. and Baker, T. (2005). An estimate of the errors in gravity ocean tide loading computations. *J. Geod.*, 79:50–63.

Bos, M. S., Baker, T. F., Røthing, K., and Plag, H.-P. (2002). Testing ocean tide models in the nordic seas with tidal gravity observations. *Geophys. J. Int*, 150:687–694.

Boy, J.-P., Gegout, P., and Hinderer, J. (2002). Reduction of surface gravity data from global atmospheric pressure loading. *Geophys. J. Int*, 149:534–545.

Braun, A., Kim, H. R., Csatho, B., and von Frese, R. R. (2007). Gravity-inferred crustal thickness of Greenland. *Earth Planet. Sci. Lett.*, 262:138–158.

Cappelen, J. (2012). Denmark - DMI historical climate data collection 1768-2011. Technical Report TR12-02, DMI - Ministry of Climate and Energy.

Charles, K. and Hipkin, R. (1995). Vertical gradient and datum height corrections to absolute gravimeter data and the effect of structered fringe residuals. *Metrologia*, 32:193–200.

Cheng, Y. and Andersen, O. B. (2010). Improvement in global ocean tide model in shallow water regions. In *Poster, SV.1-68 45 pp., OST-ST Meeting on Altimetry for Oceans and Hydrology, Lisbon.*

Davis, J. E., Latychev, K., Mitrovica, J. X., Kendall, R., and Tamisiea, M. E. (2008). Glacial isostatic adjustment in 3-D earth models: Implications for the analysis of tide gauge records along the U.S. east coast. *J. Geodyn.*, 46:90–94.

Dziewonski, A. M. and Anderson, D. L. (1981). Preliminary reference earth model. *Phys. Earth Planet. In.*, 25:297–356.

Eanes, R. J. and Bettadpur, S. (1995). The CSR 3.0 global ocean tide model: Diurnal and semi-diurnal ocean tides from TOPEX/POSEIDON altimetry. Technical report, Center for Space research - The university of Texas, Austin.

Ekman, M. (1991). A concise history of postglacial land uplift research (from its beginning to 1950). *Terra Nova*, 3:358–365.

Ekman, M. and Mäkinen, J. (1996). Recent postglacial rebound gravity change and mantle flow in Fennoscandia. *Geophys. J. Int.*, 126:229–234.

Falk, R., Müller, J., Lux, H., Wilmes, H., and Wziontek, H. (2009). Precise gravimetric surveys with the field absolute gravimeter A10. In *Geodesy for planet Earth*.

Faller, J. E. (2002). Thirty years of progress in absolute gravimetry: a scientific capability implemented by technological advances. *Metrologia*, 39:425–428.

Faller, J. E., Rinker, R. L., and Zumberge, M. A. (1979). Plans for the development of a portable absolute gravimeter with a few parts in a 10^9 accuracy. *Tectonophysics*, 52:107–116.

Farrell, W. E. (1972). Deformation of the Earth by surface loads. *Rev. Geophys. Space Phys.*, 10:761–797.

Farrell, W. E. and Clark, J. A. (1976). On postglacial sea level. *Geophys. J. R. astr. Soc.*, 46:647–667.

Francis, O. (2006). Absolute and relative gravity measurements in Nuuk (Greenland) in July 2005. Technical report, University of Luxembourg and ECGS.

Francis, O. (2010). *Results of the European Comparison of Absolute Gravimeters in Walferdange (Luxembourg) of November 2007*, volume 135 of *Gravity, Geoid and Earth Observation - International Association of Geodesy Symposia*, chapter 5, pages 31–35. Springer.

Francis, O. and Van Dam, T. (2003). Results of the international comparison of absolute grvimeters in Walferdange (Luxembourg) of November 2003. In *Gravity, Geoid and Space Missions*.

Fukuda, Y., Higashi, T., Takemoto, S., Iwano, S., Doi, K., Shibuya, K., Hiraoka, Y., Kimura, I., McQueen, H., and Govind, R. (2005). *Absolute Gravity Measurements in Australia and Syowa Station - Antarctica*, volume 129 of *Gravity, Geoid and Space Missions - International Association of Geodesy Symposia*, pages 280–285. Spring.

Gitlein, O. (2009). *Absolutgravimetrische bestimmung der Fennoskandischen landhebung mit dem FG5-220*. PhD thesis, Geodäsie und Geoinformatik der Leibniz Universität Hannover.

Harig, C. and Simons, F. J. (2012). Mapping Greenlands mass loss in space and time. *PNAS*, 109:19934–19937.

Herring, T. A., Jekeli, C., Niebauer, T., Hinderer, J., Crossley, D., Warburton, R. J., Agnew, D. C., X., M. J., Tamisiea, M. E., Wahr, J., Gross, R. S., Dehant, V., Mathews, P. M., Blewitt, G., Simons, M., and Rosen, P. A. (2009). *Treatise on geophysics - Geodesy*, volume 3. Elsevier.

Hinderer, J. and Legros, H. (1989). Elasto-gravitational deformation - relative gravity change and earth dynamics. *Geophys. J. Int*, 97:481–495.

Hipkin, R. G. (1999). Absolute determination of the vertical gradient of gravity. *Metrologia*, 36:47–52.

Hocke, K. (1998). Phase estimation with the Lomb-Scargle periodogram method. *Ann. Geophysicae*, 16:356–358.

Howat, I. M., Ahn, Y., Joughin, I., van den Broeke, M. R., Lenaerts, J. T. M., and Smith, B. (2011). Mass balance of Greenland's three largest outlet glaciers, 2000–2010. *Geophys. Res. Lett.*, 38:1–5.

Ivins, E., Rignot, E., Wu, X., S., J. T., and Casassa, G. (2005). *Ice Mass Balance and Antarctic Gravity Change - Satellite and Terrestrial Perspectives*, chapter 1, pages 3–12. Springer.

James, T. S. (1992). The Hudson Bay free-air gravity anomaly and glacial rebound. *Geophys. Res. Lett.*, 19:861–864.

James, T. S. and Ivins, E. R. (1998). Predictions of Antarctic crustal motions driven by present-day ice sheet evolution and by isostatic memory of the Last Glacial Maximum. *J. Geophys. Res.*, 103:4993–5017.

Jiang, Z., Becker, M., Francis, O., Germak, A., Palinkas, V., Jousset, P., Kostelecky, J., Dupont, F., Lee, C. W., Tsai, C. L., Falk, R., Wilmes, H., Kopaev, A., Ruess, D., Ullrich, M. C., B Meurers and, J. M., Deroussi, S., Métivier, L., Pajot, G., Santos, F. P. D., van Ruymbeke, M., Naslin, S., and Ferry, M. (2009). Relative gravity measurement campaign during the 7th international comparison of absolute gravimeters (2005). *Metrologia*, 46:214–226.

Klopping, F., Peter, G., Robertson, D. S., Berstis, K. A., Moose, R. E., and Carter, W. E. (1991). Improvements in absolute gravity observations. *J. Geophys. Res.*, 96:8295–8303.

Lambert, A., Courtier, N., and James, T. (2006). Long-term monitoring by absolute gravimetry - Tides to postglacial rebound. *J. Geodyn.*, 41:307–317.

Lambert, A., Courtier, N., Sasagawa, G. S., Klopping, F., Winester, D., James, T. S., and Liard, J. O. (2001). New constraints on Laurentide postglacial rebound from absolute gravity measurements. *Geophys. Res. Lett.*, 28:2109–2112.

Latychev, K., Mitrovica, J. X., Tromp, J., Tamisiea, M. E., Komatitsch, D., and Christara, C. C. (2005). Glacial isostatic adjustment on 3-d earth models: a finite-volume formulation. *Geophys. J. Int.*, 161:421–444.

Lidberg, M., Johansson, J. M., Scherneck, H.-G., and Milne, G. A. (2010). Recent results based on continuous GPS observations of the GIA process in Fennoscandia from BIFROST. *J. Geodyn.*, 50:8–18.

Linage, C. D., Hinderer, J., and Boy, J.-P. (2009). Variability of the gravity-to-height ratio due to surface loads. *Pure Appl. Geophys.*, 166:1217–1245.

Linage, C. D., Hinderer, J., and Rogister, Y. (2007). A search for the ratio between gravity variation and vertical displacement due to a surface load. *Geophys. J. Int.*, 171:986–994.

Lomb, N. R. (1976). Least-squares frequency analysis of unequally spaced data. *Astrophysics and Space Science*, 39:447–462.

Longman, I. M. (1963). A Greens function for determining the deformation of the Earth under surface mass loads. 2 - Computation and numerical results. *J. Geophys. Res.*, 68:485–496.

Love, A. E. H. and Sedleian, F. R. S. (1909). The yielding of the Earth to disturbing forces. *Proc. R. Soc. Lond. A*, 82:73–88.

Lyard, F., Lefevre, F., Letellier, T., and Francis, O. (2006). Modelling the global ocean tides: modern insights from FES2004. *Ocean Dynam*, 56:394–415.

Lysaker, D. I., Breili, K., and Pettersen, B. R. (2008). The gravitational effect of ocean tide loading at high latitude coastal stations in Norway. *J. Geod.*, 82:569–583.

Matsumoto, K., Sato, T., Takanezawa, T., and Ooe, M. (2001). GOTIC2: A program for computation of Oceanic tidal loading effect. *J. Geod. Soc. Japan.*, 47:243–248.

Matsumoto, K., Takanezawa, T., and Ooe, M. (2000). Ocean tide models developed by assimilating TOPEX/POSEIDON altimeter data into hydrodynamical model: A global model and a regional model around Japan. *J. Oceanog.*, 56:567–581.

Matzka, J., Rasmussen, T. M., Olesen, A. V., Nielsen, J. E., Forsberg, R., Olsen, N., Halpenny, J., and Verhoef, J. (2010). A new aeromagnetic survey of the North Pole and the Arctic Ocean north of Greenland and Ellesmere Island. *Earth Planets Space*, 62:829–832.

Mazzotti, S., Lambert, A., Henton, J., James, T. S., and Courtier, N. (2011). Absolute gravity calibration of GPS velocities and glacial isostatic in mid-continent North America. *Geophys. Res. Lett.*, 38:1–5.

Merriam, J. B. (1980). The series computation of the gravitational perturbation due to an ocean tide. *Phys. Earth Planet. In.*, 23:81–86.

Merriam, J. B. (1992). Atmospheric pressure and gravity. *Geophys. J. Int*, 109:488–500.

Meur, E. L. and Hindmarsh, R. C. A. (2000). A comparison of two spectral approaches for computing the Earth response to surface loads. *Geophys. J. Int.*, 141:282–298.

Meur, E. L. and Huybrechts, P. (2001). A model computation of the temporal changes of surface gravity and geoid signal induced by the evolving Greenland ice sheet. *Geophys. J. Int.*, 145:835–849.

Microg (2005). Ml-1 polarization stabilized laser. Technical report, Micro-g LaCoste.

Microg (2008a). *A10 Portable gravimeter user's manual*. Micro-g LaCoste.

Microg (2008b). *g8 user's manual*. Micro-g LaCoste.

Milne, G. A. and Mitrovica, J. X. (1996). Postglacial sea-level change on a rotating Earth: first results from a gravitationally self-consistent sea-level equation. *Geophys. J. Int*, 126:F13–F20.

Milne, G. A., Mitrovica, J. X., and Davis, J. L. (1999). Near-field hydro-isostasy: the implementation of a revised sea-level equation. *Geophys. J. Int.*, 139:464–482.

Mitrovica, J. and Peltier, W. (1991). On postglacial geoid subsidence over the equatorial oceans. *J. Geophys. Res.*, 96:53–71.

Mitrovica, J. X., Milne, G. A., and Davis, J. L. (2001). Glacial isostatic adjustment on a rotating earth. *Geophys. J. Int*, 147:562–578.

Mitrovica, J. X. and Peltier, W. R. (1989). Pleistocene deglaciation and the global gravity field. *J. Geophys. Res.*, 94:651–671.

Mäkinen, J., Amalvict, M., Shibuya, K., and Fukuda, Y. (2007). Absolute gravimetry in Antarctica: Status and prospects. *J. Geodyn.*, 43:339–357.

Mäkinen, J., Engfeldt, A., Harsson, B., Ruotsalainen, H., Strykowski, G., Oja, T., and Wolf, D. (2005). The fennoscandian land uplift gravity lines 1966–2003. In *Gravity, Geoid and Space Missions. International Association of Geodesy Symposia*, volume 129, pages 328–332.

Mäkinen, J., Sekowski, M., and Krynski, J. (2010). The use of the A10-020 gravimeter for the modernization of the Finnish first order gravity network. *Geoinformation issues*, 2:5–16.

Müller, J., Naeimi, M., Gitlein, O., Timmen, L., and Denker, H. (2010). A land uplift model in Fennoscandia combining GRACE and absolute gravimetry data. *Physics and Chemistry of the Earth*, 12:1–7.

Mémin, A., Hinderer, J., and Rogister, Y. (2011a). Separation of the geodetic consequences of past and present ice-mass change: Influence of topography with application to Svalbard (Norway). *Pure Appl. Geophys.*, Online:1–16.

Mémin, A., Rogister, Y., Hinderer, J., Omang, O. C., and Luck, B. (2011b). Secular gravity variation at Svalbard (Norway) from ground observations and GRACE satellite data. *Geophys. J. Int*, 184:1119–1130.

Nagornyi, V. D. (1995). A new approach to absolute gravimeter analysis. *Metrologia*, 32:201–208.

Nagornyi, V. D., Zanimonskiy, Y. M., and Zanimonskiy, Y. Y. (2011). Correction due to the finite speed of light in absolute gravimeters. *Metrologia*, 48:101–113.

Niebauer, T. M. (1988). Correcting gravity measurements for the effects of local air pressure. *J. Geophys. Res.*, 93:7989–7991.

Niebauer, T. M. (1989). The effective measurement height of free-fall absolute gravimeters. *Metrologia*, 26:115–118.

Niebauer, T. M., Billson, R., Ellis, B., Mason, B., van Westrum, D., and Klopping, F. (2011). Simultaneous gravity and gradient measurement from a recoil-compensated absolute gravimeter. *Metrologia*, 48:154–163.

Niebauer, T. M., Billson, R., Schiel, A., van Westrum, D., and Klopping, F. (2012). The self-attraction correction for the FG5X absolute gravity meter. *Metrologia*, 50:1–8.

Niebauer, T. M., Faller, J. E., Godwin, H. M., Hall, J. L., and Barger, R. L. (1988). Frequency stability measurements on polarization-stabilized He-Ne lasers. *Applied Optics*, 27:1285–1289.

Niebauer, T. M., Sasagawa, G. S., Faller, J. E., Hilt, R., and F., K. (1995). A new generation of absolute gravimeters. *Metrologia*, 32:159–180.

Nielsen, J., Forsberg, R., and Strykowski, G. (2013a). Estimation of PGR induced absolute gravity changes at Greenland GNET stations. *IAG International Symposium, Melbourne, Australia, 28 June - 7 July.*, 139:1–6.

Nielsen, J., Forsberg, R., and Strykowski, G. (2013b). The measured and modelled absolute gravity change in Greenland. *J. Geodyn.*, X:X.

Olsson, P.-A., Ågren, J., and Scherneck, H.-G. (2012). Modelling of the GIA-induced surface gravity change over Fennoscandia. *J. Geodyn.*, 61:12–22.

Olsson, P.-A., Scherneck, H.-G., and Ågren, J. (2009). Effects on gravity from non-tidal sea level variations in the Baltic sea. *J. Geodyn.*, 48:151–156.

Padman, L. and Erofeeva, S. (2004). A barotropic inverse tidal model for the Arctic Ocean. *Geophys. Res. Lett.*, 31:1–4.

Peltier, W. R. (1974). The impulse response of a Maxwell Earth. *Rev. Geophys. Space Phys.*, 12:651–669.

Peltier, W. R. (2004). Global glacial isostasy and the surfacce of the ice-age Earth: The ICE-5G (VM2) model and GRACE. *Annu. Rev. Earth Planet. Sci.*, 32:111–149.

Petrov, L. and Boy, J. P. (2004). Study of the atmospheric pressure loading signal in VLBI observations. *J. Geophys. Res.*, 109:1–14.

Qingbin, W., Rui, Z., and Wen, S. (2011). Precision analysis of gravity vertical gradient measurement based on CG - 5 relative gravimeter. *Adv. Mater. Res.*, 301-303:1036–1041.

Richter, A., Rysgaard, S., Dietrich, R., Mortensen, J., and Petersen, D. (2011). Coastal tides in west Greenland derived from tide gauge records. *Ocean Dynam*, 61:39–49.

Rinker, R. L. (1983). *Super spring - A new type eof low-frequency vibration isolator*. PhD thesis, University of Colorado.

Riva, R. E., Gunter, B. C., Urban, T. J., Vermeersen, B. L., Lindenbergh, R. C., Helsen, M. M., Bamber, J. L., van de Wal, R. S., van den Broeke, M. R., and Schutz, B. E. (2009). Glacial Isostatic Adjustment over Antarctica from combined ICESat and GRACE satellite data. *Earth Planet. Sci. Lett.*, 288:516–523.

Robertson, D. S. (2001). Using absolute gravimeter data to determine vertical gravity gradients. *Metrologia*, 38:147–153.

Rogister, Y., Amalvict, M., Hinderer, J., Luck, B., and Memin, A. (2007). Absolute gravity measurements in Antarctica during the International Polar Year. Technical report, U.S. Geological Survey and The National Academies.

Rothleitner, C. and Francis, O. (2011). Second-order Doppler-shift corrections in free-fall absolute gravimeters. *Metrologia*, 48:187–195.

Rothleitner, C., Svitlov, S., Mérimèche, H., Hu, H., and Wang, L. J. (2009). Development of new free-fall absolute gravimeters. *Metrologia*, 46:283–297.

Sasagawa, G., Meunier, T. K., Mullins, J. L., McAdoo, D., and Klopping, F. (2004). Absolute gravimetry in Antarctica - 1995 obeservations at McMurdo station and Terra Nova bay station. Technical report, U.S. Department of the interior - U.S. Geological Survey.

Sato, T., Miura, S., Ohta, Y., Fujimoto, H., Sun, W., Larsen, C., Heavner, M., Kaufman, A., and Freymueller, J. (2008). Earth tides observed by gravity and GPS in southeastern Alaska. *J. Geodyn.*, 46:78–89.

Sato, T., Miura, S., Sun, W., Sugano, T., Freymueller, J. T., Larsen, C. F., Ohta, Y., Fujimoto, H., Inazu, D., and Motyka, R. J. (2012). Gravity and uplift rates observed in southeast Alaska and their comaprison with GIA model predictions. *J. Geophys. Res.*, 117:1–13.

Schmerge, D. and Francis, O. (2006). Set standard deviation, repeatability and offset of absolute gravimeter A10-008. *Metrologia*, 43:414–418.

Schwiderski, E. W. (1980). On charting global ocean tides. *Rev. Geophys. Space Phys.*, 13:243–268.

Sekowski, M., Krynski, J., Dykowski, P., and Mäkinen, J. (2012). Effect of laser and clock stability and meteorological conditions on gravity surveyed with the A10 free-fall gravimeter first results. Under review.

Sella, G. F., Stein, S., Dixon, T. H., Craymer, M., James, T. S., Mazzotti, S., and Dokka, R. K. (2007). Observation of glacial isostatic adjustment in stable North America with GPS. *Geophys. Res. Lett.*, 34:1–6.

Simpson, M. J. R., Wake, L., Milne, G. A., and Huybrechts, P. (2011). The influence of decadal- to millennial-scale ice mass changes on present-day vertical land motion in Greenland - Implications for the interpretation of GPS observations. *J. Geophys. Res.*, 116:1–19.

Spada, G. (2003). The theory behind TABOO. Samizdat Press, 2003, Release 1.0.

Spada, G., Ruggieri, G., Sørensen, L. S., Nielsen, K., Melini, D., and Colleoni, F. (2012). Greenland uplift and regional sea level changes from ICESat observations and GIA modelling. *Geophys. J. Int*, 189:1457–1474.

Spada, G. and Stocchi, P. (2007). Selen - A Fortran 90 program for solving the Sea-level-equation. *Comput. Geosci.*, 33:538–562.

Sørensen, L. S., Simonsen, S. B., Nielsen, K., Lucas-Picher, P., Spada, G., Adalgeirsdottir, G., Forsberg, R., and Hvidberg., C. S. (2011). Mass balance of the Greenland ice sheet (2003-2008) from ICESat data - the impact of interpolation, sampling and firn density. *The Cryosphere*, 5:173–186.

Steffen, H., Gitlein, O., Denker, H., Müller, J., and Timmen, L. (2009). Present rate of uplift in Fennoscandia from GRACE and absolute gravimetry. *Tectonophysics*, 474:69–77.

Sun, W., Miura, S., Sato, T., Sugano, T., Freymueller, J., Kaufman, M., Larsen, C. F., Cross, R., and Inazu, D. (2010). Gravity measurements in southeastern Alaska reveal negative gravity rate of change caused by Glacial Isostatic Adjustment. *J. Geophys. Res.*, 115:1–40.

Taylor, J. R. (1997). *An Introduction to Error Analysis: The Study of Uncertainties in Physical Measurements*. University Science Books.

Timmen, L. (2003). Precise definition of the effective measurement height of free-fall absolute gravimeters. *Metrologia*, 40:62–65.

Timmen, L. (2009). *Sciences of Geodesy - I, Advanvances and Future Directions*, chapter 1, pages 1–48. Springer.

Timmen, L., Gitlein, O., Müller, J., Strykowski, G., and Forsberg, R. (2008). Absolute gravimetry with the Hannover meters JILAg-3 and FG5-220, and their deployment in a Danish-German cooperation. *Fachbeitrag*, 133:1–15.

Timmen, L., Röder, R., and Schnüll, M. (1993). Absolute gravity determination with JILAg-3- improved data evaluation and instrumental technics. *Bull. Geodesique*, 67:71–80.

Tiwari, V. M., Singh, B., Rao, M. B. S. V., and Mishra, D. C. (2006). Absolute gravity measurements in India and Antarctica. *Current Science*, 91:686–689.

Torge, W. (1989). *Gravimetry*. Walter de Gruyter.

Torge, W. (2001). *Geodesy*. Walter de Gruyter.

van Dam, T., Larson, K., Wahr, J., and Francis, O. (2000). Using GPS and gravity to infer ice mass changes in Greenland. *EOST. Am. Geophys. Un.*, 81:421–427.

Veitch, S. A. and Nettles, M. (2012). Spatial and temporal variations in Greenland glacial-earthquake activity - 1993-2010. *J. Geophys. Res.*, 117:1–20.

Virtanen, H. (2004). Loading effects in Metsähovi from the atmosphere. *Geodynamics*, 38:407–422.

Virtanen, H. and Mäkinen, J. (2003). The effect of the Baltic Sea level on gravity at the Metsähovi station. *J. Geodyn.*, 35:553–565.

Vitushkin L., e. a. (2002). Results of the sixth international comparison of absolute gravimeters, ICAG-2001. *Metrologia*, 39:407–424.

Wahr, J. (1985). Deformation induced by polar motion. *J. Geophys. Res.*, 90:9363–9368.

Wahr, J., H., D., and A., T. (1995). Predictions of vertical uplift caused by changing polar ice volumes on a viscoelastic earth. *Geophys. Res. Lett.*, 22:977–980.

Wahr, J., van Dam, T., Larson, K., and Francis, O. (2001). Geodetic measurements in Greenland and their implications. *J. Geophys. Res.*, 106:567–581.

Walcott, R. I. (1973). Structure of the Earth from Glacio-Isostatic rebound. *Annu. Rev. Earth Planet. Sci.*, 1:15–37.

Wenzel, H.-G. (1996). The nanogal software: Earth tide data processing package ETERNA 3.30. *Bulletin d'Informations Marees Terrestres*, 124:9425–9439.

Whitehouse, P. (2009). Glacial isostatic adjustment and sea-level change - state of the art report. Technical report, Durham University / Svensk Kärnbränslehantering AB.

Zumberge, M. A., Rinker, R. L., and Faller, J. E. (1982). A portable apparatus for absolute measurements of the Earths gravity. *Metrologia*, 18:145–152.

A Articles

A.1 Estimation of PGR induced absolute gravity changes at Greenland GNET stations.

The motivation for this study was to investigate the GIA signal in Greenland using a range of Earth models and ice histories. A total of 9 different model combinations were tested. These were used to give an uncertainty estimate on the modelling results.

A comparison of the different model combinations with relative sea level curves from two sites in Greenland, shows that the ICE-5G ice history is the history that fits the data best. The Earth model should have a Lithosphere of 90-100km and consists of five layers or more. The viscosities of the layers needs to be investigated further.

It is found that the GIA signal in Greenland is significant smaller than the instrument's accuracy. For six different site the GIA signal is found to be less than $1\mu Gal$. The detection of this signal calls for long time series.

The different modelling scenarios indicates that the uncertainty on the GIA signal can be as large as the signal itself.

myjournal manuscript No.
(will be inserted by the editor)

Estimation of PGR induced absolute gravity changes at Greenland GNET stations

Emil Nielsen · Gabriel Strykowski · Rene Forsberg · Finn Bo Madsen

Received: date / Accepted: date

Abstract An important subject in the climate debate is the study of the major ice sheets mass balance. Knowledge of the mass balance provides understanding of changes in the relative sea-level (RSL). Several methods are used for mass balance studies but they are associated with large uncertainties. One reason for the uncertainty is the presence of the postglacial rebound (PGR) signal in the geodetic data used for mass balance estimates. Estimates of the PGR signal can be obtained by modelling and then being subtracted from the data to eliminate its influence. In this study, the PGR gravity signal will be investigated through modelling. The modelling of seven different scenarios shows that the PGR gravity signal in Greenland is less then $1\mu Gal$ ($= 10nm/s^2$). Repeated absolute gravity (AG) measurements at selected Greenland network (GNET) GPS sites were initiated in 2009. These data will in the future help constrain PGR and present-day ice mass changes. The data is collected with an A10 absolute gravimeter, which has an accuracy of $10\mu Gal$ (manufacturer specification). Here we will evaluate the modelled PGR gravity signal at selected GNET sites and conclude that the signal is significantly smaller then the gravity instruments accuracy and a long time is needed to detect it. Also, it can be expected that the elastic signal will be larger and other data like GPS is needed to separate the viscous and elastic signal.

Keywords Greenland · postglacial rebound · absolute gravity

Emil Nielsen
DTU Space - Geodynamics
Juliane Maries Vej 30
Tel.: +45-35325750
Fax: +45-35362475
E-mail: jemni@space.dtu.dk

Gabriel Strykowski
DTU Space - Geodynamics

Rene Forsberg
DTU Space - Geodynamics

Finn Bo Madsen
DTU Space - Geodesy

1 Introduction

In glaciated areas like Greenland and Antarctica the changing ice mass is affecting the load on the Earth. The Earth will give an instantaneous response to these changes because of the elastic properties of the crust and a long term delayed response because of the viscous properties of the mantle. The latter is known as the PGR signal and evidence of this is that the response to the deglaciation of the Pleistocene glacial maximum is still measurable today. It is evident in former glaciated areas like Scandinavia (Lidberg et al., 2010) and North America (Sella et al., 2007) but it will also be present in glaciated areas like Greenland. Knowledge of the viscous response is important when geodetic data (GPS, AG, satellite altimetry and satellite gravimetry) are used for studies of present-day ice mass changes. Since both the elastic and the viscous response are measured, the viscous response will give rise to less accurate mass balance estimates (Barletta et al., 2008). One procedure to remove the influence of the viscous response is to use modelled values and subtract these from the observed values. This procedure was used by Bevis et al. (2009) and Khan et al. (2010) for the vertical displacement (dU/dt) measured by GPS.
Studies on the separation of the viscous and the elastic response in GPS and AG data are presented by Wahr and Dazhong (1997) and Mémin et al. (2011). In order to obtain reliable estimates of the two responses, data

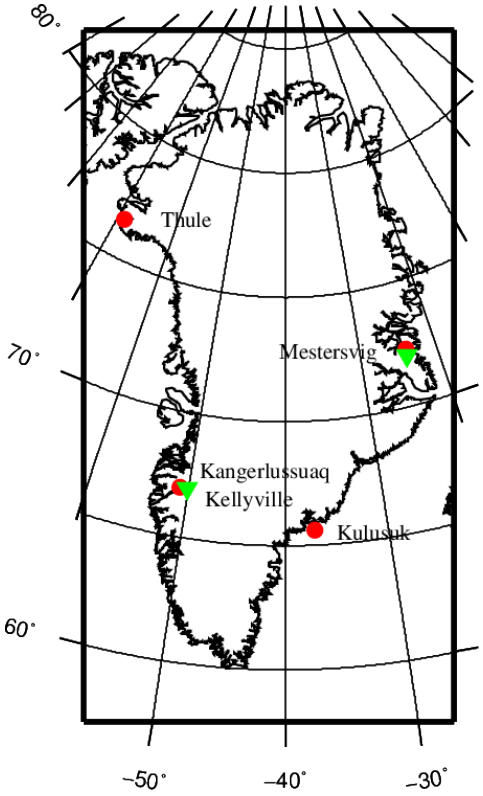

Fig. 1 Location of the four selected GNET sites (red dots) and the two selected sites with RSL data (green triangles).

must be collected over a long time period. Measurements of the absolute gravity at selected GNET sites started in 2009 with an A10. To date, six GNET sites have been occupied twice, in 2009 and 2010, and a total of 18 GNET sites have a gravity measurement.
The modelling of the PGR signal will be the focus of this study. The *SELEN* code by Spada and Stocchi (2007) is used for the modelling. Seven modelling results will be presented, all done with different Earth models and ice histories. The modelling results will be compared to relative sea-level (RSL) data at two sites, the location of which is presented in figure 1. The size of the PGR signal with associated root-mean-square (rms) error estimates will be calculated for four different GNET sites. Their locations are also presented in figure 1.

2 Theory

The sea level equation (SLE) describes how changes in the ice volume will change the load on the Earth, and how these changes will influence the sea-level globally. The input parameters for the SLE are an ice history and an Earth model. The theory behind it is explained in Farrell and Clark (1976) and Wu and Peltier (1983). The *SELEN* code solves the SLE and calculates the sea-level change, the geoid change and the vertical displacement (dS/dt, dN/dt, dU/dt). There are different ways to solve the SLE but the *SELEN* code uses the pseudo-spectral method introduced by Mitrovica and Peltier (1991). To simplify the calculations, the following assumptions are made about the Earth: it is self-gravitating, non-rotating and incompressible, with a spherical symmetry, radial stratified layers, and a linear viscoelastic Maxwell rheology in the mantle layers. Also, the ocean function in the SLE is assumed constant, meaning that the shorelines are not evolving. Version 2.7 of *SELEN* is used with the implementation of the Green's function for calculating the solid surface gravity anomaly. The latter was done in cooperation with Giorgio Spada. The Green's function used here is adapted from Mitrovica and Peltier (1989)

$$G_{sg} = \frac{a}{m_e} \sum_{n=0}^{\infty} [2h_n^v - (n+1)k_n^v] P_n(cos\alpha) \quad (1)$$

where a is the Earth's radius, m_e is the mass of the Earth, k_n^v and h_n^v are the viscous load Love numbers, P_n is the Legendre polynomial of degree n and α is the angular distance from the observation point to the loading point. In the kernel, the first term is the vertical displacement of the surface of the Earth and the second term is the disturbance from the redistribution of mass in the mantle layers.

3 Modelling

3.1 Model setup

The PGR signal is calculated for different Earth models and ice histories. Seven different results are presented here, all calculated to harmonic degree 128. The data for the Earth models comes from the Preliminary reference Earth model (PREM) described in Dziewonski and Anderson (1981) and is used in the VM2 model described in Peltier (1998) and Argus and Peltier (2010). The ice histories used are the ICE-5G model by W. R. Peltier, (Peltier, 2004), ICE-3G, (Tushingham and Peltier, 1991), the ice history by K. Lambeck, here named ANU (after the Australian National University, see Whitehouse (2009) for details), and the SICOPOLIS ice history by R. Greve, (Greve, 1997). The SICOPOLIS ice history is a stand-alone ice history for Greenland. To make a global ice history, SICOPOLIS is incorporated into the ICE-5G ice history. All ice histories start at $21ka$ before present except ANU that starts at $18ka$ BP. The model combinations are:

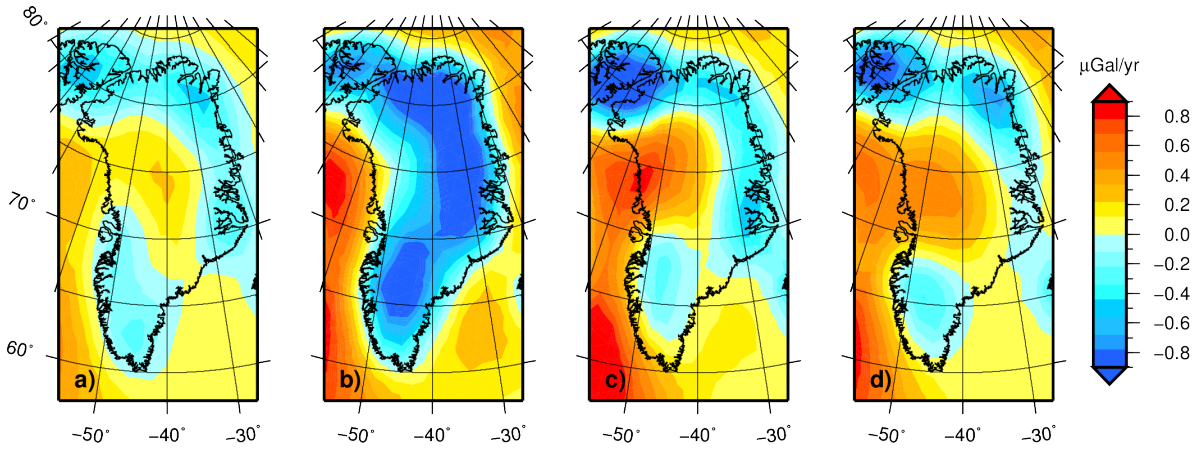

Fig. 2 Modelled PGR gravity change for different ice histories with the same Earth model, VM2. a) ICE-5G, b) ICE-3G, c) ANU and d) SICOPOLIS/ICE-5G. Units are in $\mu Gal/yr$.

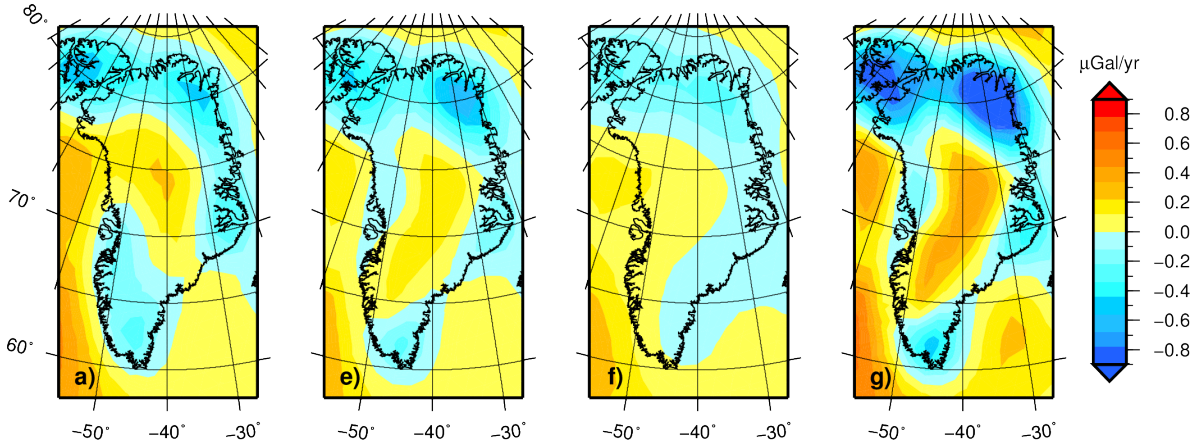

Fig. 3 Modelled PGR gravity change for different Earth models with the same ice history, ICE-5G. a) VM2, e) VMml, f) VM2lt and g) VMb. Units are in $\mu Gal/yr$.

a) The ICE-5G ice history used with a simplified 4 layer version of the VM2 Earth model, having averaged PREM parameters. It consists of a 90km lithosphere, upper and lower mantle layers having viscosities of 0.5 and $1.6 \times 10^{21} Pa \cdot s$ and an inviscid core with a radius of 3480km. The upper and lower mantle boundary is at 670km depth. This Earth model is hereafter named VM2.

b) The ICE-3G ice history used with the VM2 Earth model.

c) The ANU ice history used with the VM2 Earth model.

d) The SICOPOLIS/ICE-5G ice history used with the VM2 Earth model.

e) The ICE-5G ice history used with a multi-layered PREM averaged Earth model. The lithosphere is 90km. The upper mantle, transition zone and lower mantle consists of 14, 8 and 64 layers having mean viscosities of 0.5, 0.5 and $2.8 \times 10^{21} Pa \cdot s$ respectively. The mantle boundaries are at 420 and 671km depth and radius of the core is 3485.5km. This Earth model is hereafter named VMml.

f) The ICE-5G ice history used with the VM2 Earth model with a 180km lithosphere. This model is named VM2lt.

g) The ICE-5G ice history used with a 5 layered Earth model, with a 90km lithosphere, a 3 layered mantle with viscosities of 1.0, 1.0 and $2.0 \times 10^{21} Pa \cdot s$. The mantle boundaries are at 400 and 670km depth and a core radius of 3480km. This model is named VMb.

Information about the Greenlandic lithosphere thickness can be obtained by using teleseismics as in Derbyshire et al. (2004), who found that the lithosphere varies from approximately 100km in the southeast re-

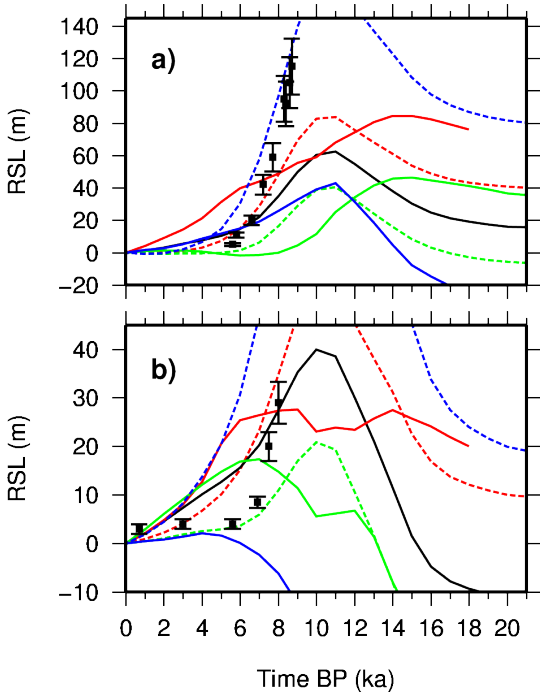

Fig. 4 RSL data and modelled RSL data at a) Kangerlussuaq and b) Mestersvig, Greenland. The solid lines are different ice histories with same Earth model (VM2) and the dashed lines are different Earth models with same ice history. Black is ICE-5G(VM2), red is ICE-3G(VM2), green is ANU(VM2), blue is SICOPOLIS(VM2), dashed red is ICE-5G(VMml), dashed green is ICE-5G(VM2lt) and dashed blue is ICE-5G(VMb). Site locations are presented in figure 1.

gion to approximately $180km$ in the central southern region of Greenland. Based on their study the VMlt Earth model was set up. The setup of the VMb Earth model is the same as the one used in the benchmark study by Spada et al. (2011).
In table 1 are PGR values at four GNET sites presented for the different models used in this study. This is of interest for the AG measurements conducted at these sites.

3.2 RMS error

Using the ICE-5G(VM2) model as reference, x_{ref}, the rms error can be calculated at the GNET sites on the basis of the other models. The ICE-5G(VM2) combination is chosen as reference because of its relative good fit to the RSL curves. The results are presented in table 1. The rms error is calculated with the following expression

$$rms_{error} = \sqrt{\frac{\sum_{i=1}^{n}(x_i - x_{ref})^2}{n-1}} \qquad (2)$$

Table 1 The PGR gravity change at four GNET sites in Greenland. Last row gives the change in gravity with the rms error calculated with ICE-5G(VM2), model a, as reference. In parenthesis after each model is the difference to the reference model. Values are in $\mu Gal/yr$. Site locations are presented in figure 1.

	Kulusuk	Mestersvig	Thule	Kellyville
Model a	0.0 (-)	-0.3 (-)	0.1 (-)	-0.2 (-)
Model b	-0.1 (-0.1)	-0.4 (-0.1)	0.3 (0.2)	-0.5 (-0.3)
Model c	0.1 (0.1)	-0.4 (-0.1)	0.0 (-0.1)	-0.1 (0.1)
Model d	0.0 (0.0)	-0.1 (0.2)	0.3 (0.2)	-0.2 (0.0)
Model e	0.0 (0.0)	-0.1 (0.2)	-0.1 (-0.2)	0.0 (0.2)
Model f	0.0 (0.0)	-0.1 (0.2)	0.0 (-0.1)	0.1 (0.3)
Model g	0.0 (0.0)	-0.3 (0.0)	-0.1 (-0.2)	0.1 (0.3)
	0.0±0.1	-0.3±0.2	0.1±0.2	-0.2±0.2

where x_i is the result of the i'th model and n is the number of models. The variation in the rms error stems from the differences in the Earth models and the ice histories. Evaluating each individual site provides an idea of the influences that affect the result. The Kellyville site is more influenced by changing the ice history than the Earth model, whereas the Kulusuk site is not significantly influenced by changing the Earth model or ice history.

4 Discussion

The modelled gravity change is presented in figure 2 and 3, which display the results from the different combinations listed in section 3.1. The choice of ice history has most influence on the signal. This influence comes from the uncertainty in the ice thickness and its distribution. Significant information about the Greenland ice sheets history is gained since the ICE-3G history which explains the large differences between the ICE-3G and the others. One difference is that the ICE-3G history does not contain a re-advancing of the ice sheet near Kellyville (Wahr et al., 2001) which could help to explain the relatively larger value at this site (see table 1). Changes to the lithosphere do not impose as large an effect as changing the ice history. In model f, figure 3, it is noticed that a thicker lithosphere will dampen the signal, with the biggest effect at the west coast of Greenland. Here, the presence of the North American ice sheet can also affect the result. A change of the viscosity alters the size of the signal more than its shape which is more controlled by the ice history. Higher viscosities will give quicker relaxation times of the signal and the effect will be most prominent in the interior of the ice sheet as in model f, figure 3. The effect of a higher viscosity is most evident when the changes are made to the upper mantle layer.

The *SELEN* code contains a database of global RSL curves from Tushingham and Peltier (1991) and Peltier and Tushingham (1993). A way to asses the output from *SELEN* is to evaluate how the modelled RSL curves fit the data. RSL curves from Kangerlussuaq and Mestersvig are presented in figure 4 with the modelled RSL curves from *SELEN*. Evaluating the results indicates that Earth models with more than two layers and the ICE-5G history give a better fit. Also, the ICE-3G model does not fit the RSL curve for Kangerlussuaq, near Kellyville, very well, which could be caused by the missing re-advance in the ice history. At Kangerlussuaq the best fitting model would be a model between model f and g, whereas at Mestersvig the model would be between model e and f. The difference between model e and f is the thickness of the lithosphere, so as indicated by teleseismics this study could support a lithosphere thickness of approximately $100km$. The lithosphere thickness of approximately $180km$ mentioned in Derbyshire et al. (2004) refers to the central parts of Greenland, therefore, the effect is not as evident along the coast where the RSL data is collected. Also, there are indications that higher viscosities in the mantle layers (model d and g) will give a better fit.
The fit to the RSL curves could be improved but the result would not change the magnitude of the PGR signal significantly so no further investigation is done regarding this.

5 Conclusion

It is found that the modelled PGR signal at the GNET sites in Greenland is small when compared with accuracy of modern absolute gravimeters. The FG5's measurement accuracy is $2\mu Gal$ (Okubo et al., 1997) while the A10's is $10\mu Gal$ (manufacturers specification). The A10 was proven to perform better (Falk et al., 2009). The PGR signal in former glaciated areas like Scandinavia and North America is detected with AG measurements, see Steffen et al. (2009) and Mazzotti et al. (2011). Results from these studies indicate that AG rates in the periphery of the former glaciated areas are of the same order as the results found in this study. There are not many repeated gravity measurements in Greenland. Gravity data from Kulusuk is described by Wahr et al. (2001), but no rate of change is presented. Van Dam et al. (2000) found a rate of change of $-1.6 \pm 1.2\mu Gal/yr$ at Kellyville. Considering the results of this study the rate of change in Kellyville is dominated by the elastic response. Repeated gravity measurements in glaciated areas like Alaska and Svalbard are presented in Sun et al. (2010) and Mémin et al. (2011). The gravity rates found in these places are one order of magnitude larger than the PGR signal found in this study.
When comparing the solid surface gravity signal with other signals we notice that the viscous gravity signal is negative correlated with the vertical movement (dU/dt) of the Earth as pointed out in Mitrovica and Peltier (1989) and Okuno and Nakada (2001). This correlation is understandable in the sense that changes in the height will move the point of observation relative to the center of mass and thereby change the gravity value.
Here the ICE-5G ice history is used to test how sensitive the PGR signal is to different Earth parameters, but it is important to remember that the correct approach when using the ICE-5G model is to use it with the VM2 Earth model since it is with this Earth model that the ice history is generated.
Modelling of the gravity signal is of interest for the ongoing AG measurements in Greenland. This and other studies on AG measurements in glaciated areas indicate that the elastic signal will be significantly larger than the viscous signal. Investigation of the elastic signal will be the aim for future studies and experiences gained in this study will be of use.

Acknowledgements Thanks go to Gudfinna Adalgeirsdottier (Danish Metrological Institute) for generating the SICOPOLIS ice model for Greenland and Giorgio Spada (Urbino University "Carlo Bo") for assistance in working with his program.

References

Argus DF, Peltier WR (2010) Constraining models of postglacial rebound using space geodesy: a detailed assessment of model ICE-5G (VM2) and its relatives. Geophys J Int 181:697–723

Barletta VR, Sabadini R, Bordoni A (2008) Isolating the PGR signal in the GRACE data: impact on mass balance estimates in Antarctica and Greenland. Geophys J Int 172:18–30

Bevis M, Kendrick E, Jr RS, Dalziel I, Caccamise D, Sasgen I, Helsen M, Taylor FW, Zhou H, Brown A, Raleigh D, Willis M, Wilson T, Konfal S (2009) Geodetic measurements of vertical crustal velocity in West Antarctica and the implications for ice mass balance. Geochem Geophy Geosy 10:1–11

Van Dam T, Larson K, Wahr J, Francis O (2000) Using GPS and gravity to infer ice mass changes in Greenland. EOS T Am Geophys Un 81:421–427

Derbyshire FA, Larsen TB, Mosegaard K, Dahl-Jensen T, Gudmundsson O, Bach T, Gregersen S, Pedersen HA, Hanka W (2004) A first look at the Greenland

lithosphere and upper mantle using Rayleigh wave tomography. Geophys J Int 158:267–286

Dziewonski AM, Anderson DL (1981) Preliminary reference Earth model. Phys Earth Planet In 25:297–356

Falk R, Müller J, Lux H, Wilmes H, Wziontek H (2009) Precise gravimetric surveys with the field absolute gravimeter A10. Geodesy for planet Earth. IAG conference 2009.

Farrell WE, Clark JA (1976) On postglacial sea level. Geophys J R astr Soc 46:647–667

Greve R (1997) Application of a polythermal three-dimensional ice sheet model to the Greenland ice sheet - response to steady-state and transient climate scenarios. J Climate 10:901–918

Khan SA, Liu L, Wahr J, Howat I, Joughin I, van Dam T, Fleming K (2010) GPS measurements of crustal uplift near Jakobshavn Isbræ due to glacial ice mass loss. J Geophys Res 115:1–13

Lidberg M, Johansson JM, Scherneck HG, Milne GA (2010) Recent results based on continuous GPS observations of the GIA process in Fennoscandia from BIFROST. J Geodyn 50:8–18

Mazzotti S, Lambert A, Henton J, James TS, Courtier N (2011) Absolute gravity calibration of GPS velocities and glacial isostatic in mid-continent North America. Geophys. Res. Lett. 38:1–5

Mémin A, Hinderer J, Rogister Y (2011) Separation of the geodetic consequences of past and present ice-mass change: Influence of topography with application to Svalbard (Norway). Pure Appl Geophys DOI 10.1007/s00024-011-0399-7

Mémin A, Rogister Y, Hinderer J, Omang OC, Luck B (2011) Secular gravity variation at Svalbard (Norway) from ground observations and GRACE satellite data. Geophys. J. Int 184:1119–1130

Mitrovica J, Peltier W (1991) On postglacial geoid subsidence over the equatorial oceans. J Geophys Res 96:53–71

Mitrovica JX, Peltier WR (1989) Pleistocene deglaciation and the global gravity field. J Geophys Res 94:651–671

Okubo S, Yoshida S, Sato T, Tamura Y, Imanishi Y (1997) Verifying the precision of a new generation absolute gravimeter FG5 - comparison with superconducting gravimeters and detection of oceanic loading tide. Geophys Res Lett 24:489–492

Okuno J, Nakada M (2001) Effects of water load on geophysical signals due to glacial rebound and implications for mantle viscosity. Earth Planets Space 53:1121–1135

Peltier WR, Tushingham AM (1993) Relative Sea Level Database. IGBP PAGES/World Data Center for Paleoclimatology Data Contribution. NOAA/NCDC Paleoclimatology Program. 93–016

Peltier WR (1998) Postglacial variations in the level of the sea: implications for climate dynamics and solid earth geodynamics. Rev. Geophys. 36:603–689

Peltier WR (2004) Global glacial isostasy and the surface of the ice-age Earth: The ICE-5G (VM2) model and GRACE. Annu Rev Earth Planet Sci 32:111–149

Sella GF, Stein S, Dixon TH, Craymer M, James TS, Mazzotti S, Dokka RK (2007) Observation of glacial isostatic adjustment in stable North America with GPS. Geophys Res Lett 34:1–6, DOI 10.1029/2006GL027081

Spada G, Stocchi P (2007) SELEN - A Fortran 90 program for solving the sea-level-equation. Comput Geosci 33:538–562

Spada G, Barletta VR, Klemann V, Riva REM, Martinec Z, Gasperini P, Lund B, Wolf D, Vermeersen LLA, King MA (2011) A benchmark study for glacial isostatic adjustment codes. Geophys J Int 185:106–132

Steffen H, Gitlein O, Denker H, Müller J, Timmen L (2009) Present rate of uplift in Fennoscandia from GRACE and absolute gravimetry. Tectonophysics 474:69–77

Sun W, Miura S, Sato T, Sugano T, Freymueller J, Kaufman M, Larsen CF, Cross R, Inazu D (2010) Gravity measurements in southeastern Alaska reveal negative gravity rate of change caused by Glacial Isostatic Adjustment. J Geophys Res 115:1–40

Tushingham AM, Peltier WR (1991) Ice-3G - a new global model of late Pleistocene deglaciation based upon geophysical predictions of post-glacial relative sea level change. J Geophys Res 96:4497–4523

Wahr J, Dazhong H (1997) Prediction of crustal deformations caused by changing polar ice on a viscoelastic Earth. Surv Geophys 18:303–312

Wahr J, van Dam T, Larson K, Francis O (2001) Geodetic measurements in Greenland and their implications. J Geophys Res 106:567–581

Whitehouse P (2009) Glacial isostatic adjustment and sea-level change - State of the art report. Durham University / Svensk Kärnbränslehantering AB

Wu P, Peltier WR (1983) Glacial isostatic adjustment and the free air gravity anomaly as a constraint on the deep mantle viscosity. Geophys J R astr Soc 74:377–449

A.2 The measured and modelled absolute gravity change in Greenland.

The motivation for this study was to use the latest PDIM models to estimate the elastic gravity change and the effect of the direct attraction. These modelling results are then compared with the preliminary estimates of gravity change found in our measurements at the GNET sites.

The gravity change presented here is determined on only a few data points and this should be kept in mind when evaluating the results.

The measurements shows that at some sites the gravity change is significant larger than the accuracy of the instrument.

When comparing the measured gravity change with the modelled, it is clear that the direct attraction has a significant effect on the results. This is especially valid for sites located close to the ice margin.

For some sites there is measured a gravity change that does not seem to originate from the direct attraction from the ice. The origin of this signal is unresolved, however investigations of either the ocean loading correction or the direct attraction from the ocean are considered.

It is overall concluded that it is possible to make gravity measurements in Greenland for geodynamical studies, and that care must be taken when interpreting the data due to the different signals that are present.

The measured and modelled absolute gravity change in Greenland

J.Emil Nielsen*, Rene Forsberg, Gabriel Strykowski

DTU Space. Elektrovej, Build.328, 2800 Kgs. Lyngby, Denmark

Abstract

In glaciated areas the Earth is responding to the ongoing changes of the ice sheets. This Earth response is known as the glacial isostatic adjustment (GIA). This can be investigated by observations of gravity change. The study of GIA is important in the ongoing assessments of the ice sheets mass balance where satellite data are used. Here the GIA signal will act as an error source. The GIA consists mainly of three signals as seen by a gravimeter on the surface of the Earth. These signals are the subject of this study. The ICE-5G ice history and recent developed ice models of present day change are used to model an estimate of the gravity change in Greenland. The result is compared with the initial measurements of absolute gravity (AG) change at selected Greenland Network (GNET) sites.

We find that observations close to the ice is highly influenced by the direct attraction from the ice masses. This is evident in the measurements done at the GNET station near the Helheim Glacier. The effect of the direct attraction diminishes at sites that are distanced with more than one degree from the ice. Here the effect of the elastic signal from present day ice mass changes is the dominant signal. We find an agreement between the measured and the modelled gravity change at sites that are close to the ice whereas the agreement disappears for sites that are close to the ocean. This indicates that some improvements to the modelling results or the processing of the gravity data are needed. The AG measurements presented here are the very preliminary results, more AG measurements are needed to strengthen the time series of gravity change.

Keywords: Greenland, absolute gravimetry, gravity change, modelled gravity

1. Introduction

The Earths response to changes in the ice volume known as the GIA, can be one or a sum of an elastic signal and/or a viscous signal. A gravimeter also detects the change in mass as a change in the direct attraction. In present day glaciated areas all signals can be present, whereas in former glaciated areas, e.g. Scandinavia or North America, only the viscous signal can be present. Other forces can produce an elastic signal e.g. the atmosphere or the ocean tides but in this study the focus will be on the signals produced by changes in the ice masses.

There is an interest in knowing the GIA signal since it can lead to erroneous mass balance estimates when using satellite data. The satellite data are biased by the presence of the GIA signal

*Corresponding author

Email address: jemni@space.dtu.dk (J.Emil Nielsen)

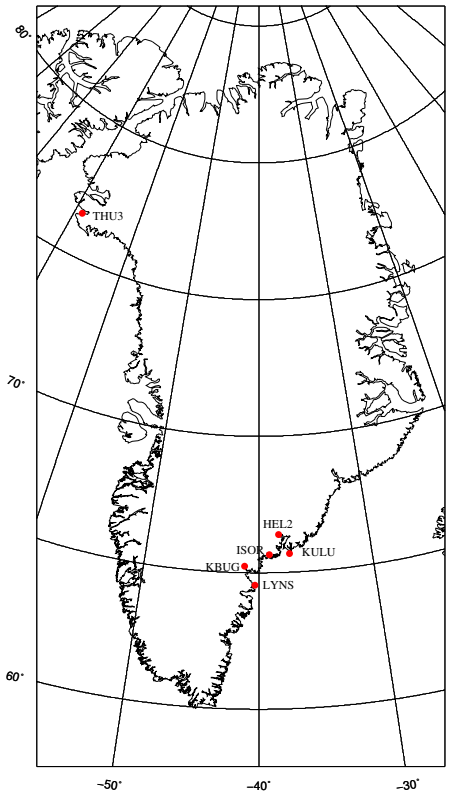

Figure 1: Location of the studied sites. THU3 - Thule, HEL2 - Helheim Glacier, KULU - Kulusuk, ISOR - Isortoq, LYNS - Lynæs, KBUG - Køge Bugt.

since they can not distinguish between the signal form presents day mass changes and the signal due to mass changes from e.g. the last glacial maximum (LGM), see Barletta et al. (2008) and Shepherd et al. (2012). The signals are not only of interest for studies of mass balance, studies of geodynamics and the Earths rheology can also benefit from knowledge of the GIA signals.
To study the GIA global positioning system (GPS), tide gauge and AG are the methods used. In the GNET project, a part of POLENET (The Polar Earth Observing Network), a number of permanent GPS stations are deployed on the Greenlandic bedrock surrounding the ice sheet. This project started in 2007 and at present a total of 57 stations are deployed. Some results from the GNET project are presented in Khan et al. (2010) and Bevis et al. (2012).

In 2009 DTU Space started to make AG measurements at selected GNET stations with the purpose of initiating future time series of gravity change. Precise measurements of gravity change in remote places is a novel research area that has become possible with the advent of portable precise absolute gravimeters.
Studies by De Linage et al. (2007) and Mémin et al. (2011) have shown attempts to separate the viscous and the elastic signal using data from GPS and AG. Since we do not have sufficient AG

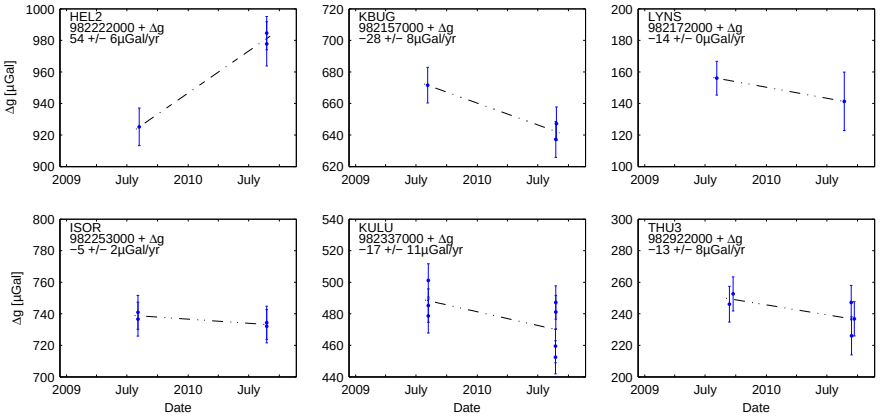

Figure 2: AG measurements at the six selected GNET sites presented in figure 1. The gravity change with associated uncertainty is written in the figure window. The zero uncertainty on the LYNS estimate is due to the few measurement. It will be attributed a $\pm 10 \mu Gal$ uncertainty.

data to initiate a study like this we will look into modelling the gravity signal and compare the results with our preliminary AG measurements.

Modelling of the gravity signal is a complex matter since it consists of many parameters and some assumptions about the Earth are needed in order to make the computations feasible.
Different ice histories with different temporal resolution are used. The ice history going back to LGM are often modelled since there is very limited data available to constrain the ice history 21.000 years back in time. Satellite mission like ICESat and CryoSat has delivered valuable data about changes in the ice volume during the last decade. These satellite data give new possibilities for making present day ice mass models.
Uncertainties in the GIA signal originates from the uncertainties in the Earth model and the ice sheets thickness and extent through time. Uncertainty estimates of the different signal will be calculated.

2. Measurements

DTU has since 2009 made gravity measurements in Greenland with an A10 (serial number 019) absolute gravimeter from Micro-g LaCoste. The manufactures specifications for this instrument is an accuracy and a repeatability of $10 \mu Gal$ ($1 \mu Gal = 10 nm/s^2$). We have found that under laboratory conditions our instrument performs better then this, down to $6 \mu Gal$ in accuracy and repeatability. Others have made similar observations, see Falk et al. (2009) and Mäkinen et al. (2010). In the field we expect our instrument to perform better then the manufactures specifications but it can be worse then under laboratory conditions. Here is presented six sites that has been visited in 2009 and 2010, the locations are depicted in figure 1 while the measurements are presented in figure 2.

The data are corrected for Earth and ocean tides, polar motion, barometric pressure and instrument laser drift. Before and after every campaign observations are made at our reference

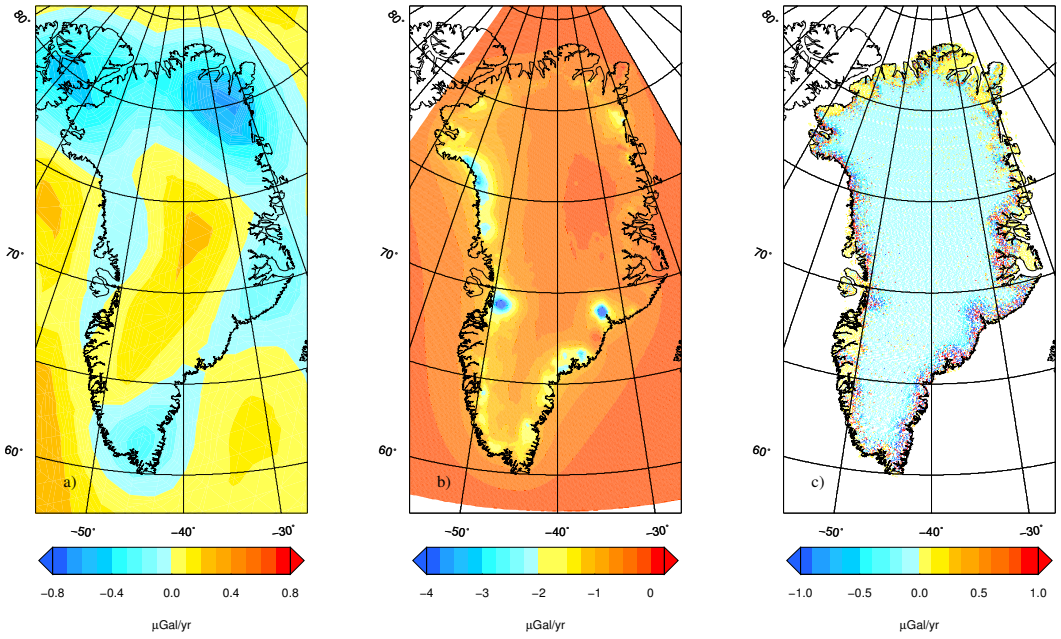

Figure 3: The modelling results. a) the viscous signal, b) the elastic signal, c) the direct attraction. Note the difference in the color scales. Units are in $\mu Gal/yr$.

site in Copenhagen to detect any suspicious behaviour of the gravimeter.

3. Modelling

For a gravimeter standing on the Earths surface the measurement will consist of several signals, three of these will be considered here, the viscous, the elastic and the direct attraction. The last two signals relates to present-day ice mass changes while the first is due to changes occurring over time scales of several thousand years, here since the LGM. The viscous and the elastic signal is due to the rheology of the mantle and the elasticity of the lithosphere respectively. The direct attraction is a result of changes in the volume of the surrounding ice masses as seen by an observer.

The modelling results for Greenland are presented in figure 3 whereas the results for the selected GNET sites are presented in figure 5 and table 1.

3.1. The viscous signal

The viscous gravity signal is computed by solving the sea-level equation using the free code SELEN (Spada and Stocchi, 2007). The input for SELEN is an Earth model and an ice history. For SELEN to calculate the gravity signal a small modification is made to the code. This modification is the implementation of the gravity Green's function adapted from Farrell (1972) but

without the direct attraction term n

$$\Delta g_{vis} = -\frac{G}{a^2}\sum_{n=1}^{\infty} \mathbf{GS}\, P_n(cos\theta) \tag{1}$$

where G is the Gravitational constant, a the Earths radius, n the harmonic degree, h and k are the load Love numbers, P_n is the Legendre polynomial of degree n and θ is the angle between the loading point and the observation point. In $\mathbf{GS} = 2h_n - (n+1)k_n$ the first term is the vertical movement of the observation point and the second term is the redistribution of masses in the mantle layers. The direct attraction term is not included since the spherical harmonic representation of this can give rise to an erroneous signal near the load. This is mentioned in Merriam (1980). In Olsson et al. (2012) they conclude that it is better to exclude the direct attraction term and calculate it in another way.
The modelling of the viscous signal is done with the ICE-5G ice history (Peltier, 2004) and a simplified version of the VM2 Earth model (Peltier, 1998) it consists of a $90km$ lithosphere, with upper and lower mantle layers viscosities of 0.5 and $1.6 \times 10^{21} Pa\ s$. See Nielsen et al. (2013) (in press) for details on the modelling and estimates of the uncertainty on the viscous signal.

3.2. The elastic signal

Modelling of the elastic signal is done in a similar way to that presented in Spada et al. (2012) where the procedure is named RER. It is a convolution of the gravity Green's function with the elements of an ice model. The ice model used for the calculations are similar to the models presented in Sørensen et al. (2011). They are derived from ICESat data and gives an estimate of the ice mass changes in the periods 2004-2007, 2005-2008 and 2006-2009. To model the elastic gravity signal it is of interest to let the harmonic degree go to as high a degree as possible $n \to \infty$ since it will increase the spatial resolution. The load Love numbers have an asymptotic behaviour as $n \to \infty$. The formula given in Farrell (1972) state that

$$\begin{bmatrix} h_\infty \\ nl_\infty \\ nk_\infty \end{bmatrix} = \frac{gm_e}{4\pi a^2 \eta} \begin{bmatrix} -\frac{\sigma}{\mu} \\ 1 \\ -\frac{3\rho\eta}{2\rho_e\mu} \end{bmatrix} \tag{2}$$

where g is the gravitational acceleration, m_e is the mass of the Earth, a is the Earth radius, $\sigma = \lambda + 2\mu$ and $\eta = \lambda + \mu$ are given by the Lamé parameters μ and $\lambda = 2\mu\nu/(1-2\nu)$ where ν is Poission's ratio. Using the information about the PREM[1] model in Dziewonski and Anderson (1981) the following asymptotic values can be found for the load Love numbers, $h_\infty \approx -6.22$, $l_\infty \approx 1.89$ and $k_\infty \approx -3.06$. The equation for calculating the elastic signal is

$$\Delta g_{ela} = 3\Delta H \frac{\rho_i}{\rho_e} \sum_{n=0}^{n_{max}} \Big[\frac{\sigma_n}{2n+1}\mathbf{GS}\Big] P_n(cos\theta) \tag{3}$$

with ρ_i and ρ_e being the density of ice and the mean density of the Earth respectively, ΔH is the height of the mass elements represented as discs, n the harmonic degree, P_n the Legendre polynomial of degree n, θ the angle between the load point and observation point, $\sigma_n = (1 -$

[1] Informations can be found on `http://geophysics.ou.edu/solid_earth/prem.html`.

$\cos\theta)/2$ for $n = 0$ and $\sigma_n = (P_{n-1}(\cos\theta) - P_{n+1}(\cos\theta))/2$ for $n > 0$. $\mathbf{GS} = 2h_n - (n+1)k_n$ is the Green's function kernel where the individual terms has the same physical meaning as described under the viscous case in section 3.1. The direct attraction due to present day ice mass changes is not included in the Green's function for the elastic signal, this is calculated separately in section 3.3.
The load Love numbers used for the calculation of the elastic signal are from the Atmospheric Pressure Loading Service (APLO) and goes up to degree 1024, see Petrov and Boy (2004). The asymptotic behaviour mentioned earlier is used to go to higher degrees.
The uncertainty on the elastic signal is determined from only considering the uncertainty in the ice model, meaning that the elastic signal is calculated with a ±10% uncertainty on the ice mass model. This results in a ±10% uncertainty on the gravity signal.

3.3. The direct attraction

The direct attraction for an observer due to mass changes of the i surrounding elements can be calculated with the following expression

$$\Delta g_{da} = \sum_{i \in \Omega} \frac{G\dot{L}_i \Delta x^2}{D^3}[S - S_i] \tag{4}$$

where $\dot{L}_i$ is the mass change per year of element i, Δx^2 is the area of the mass change elements, D is the distance from the observer to the point of the mass element, S is the elevation of the observer and S_i is the elevation of element i.
Mass elements with a distance more then one degree from the observer do not contribute significantly to the signal. This is illustrated in figure 4 where the direct attraction is calculated for an increasing area surrounding the six sites.

When calculating the direct attraction for all of Greenland, see figure 3 c), the DEM by Bamber et al. (2001) is used to save computation time. It has a resolution of $1km$. When calculating the direct attraction for the individual sites a higher resolution is preferred. The grid with mass change elements is densified giving it an $100m$ resolution while ensuring the total mass balance is conserved. The elevation of the mass elements comes from the ASTER GDEM[2] which has a $30m$ resolution. On average the ASTER GDEM accuracy is within $0.2m$ (Tachikawa et al., 2011). The uncertainty on the ASTER GDEM will give a variation of up to ±0.04% in the estimate gravity value. It will vary for the different sites. The uncertainty in the position of the observer is small since the sites are collocated with permanent GPS receivers and the uncertainty on the estimated gravity signal will therefore also be small. The total uncertainty in gravity due to the uncertainties in position of the mass elements and the observer will be ignored in the calculations. The uncertainty of the ice mass models is approximately 10% and this gives an uncertainty of ±10% on the estimated gravity value.

4. Discussion

For the sites HEL2, KBUG and ISOR there is an agreement between the measured and the modelled gravity change. For HEL2 and KBUG the modelling results show that there is a decrease in the ice melt with the majority of the melt happening below and above the observer

[2]ASTER GDEM is a product of METI and NASA

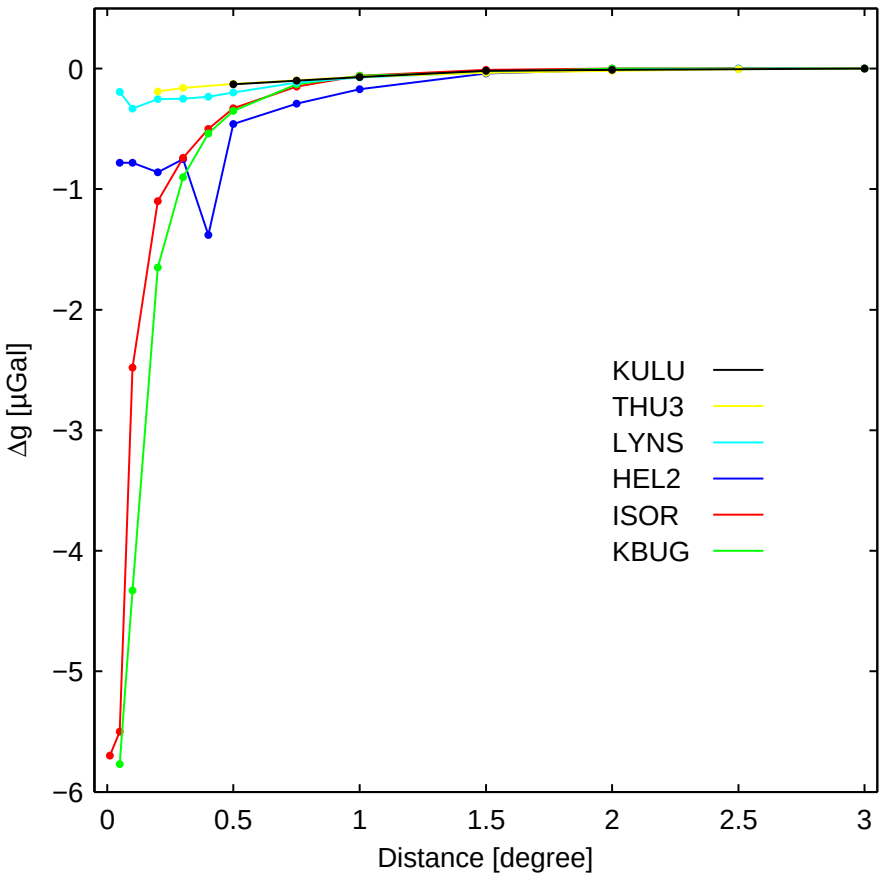

Figure 4: The direct attraction calculated with increasing distance from the each of the six GNET sites. The effect falls of quickly and is gone when the mass elements are further away then one degrees.

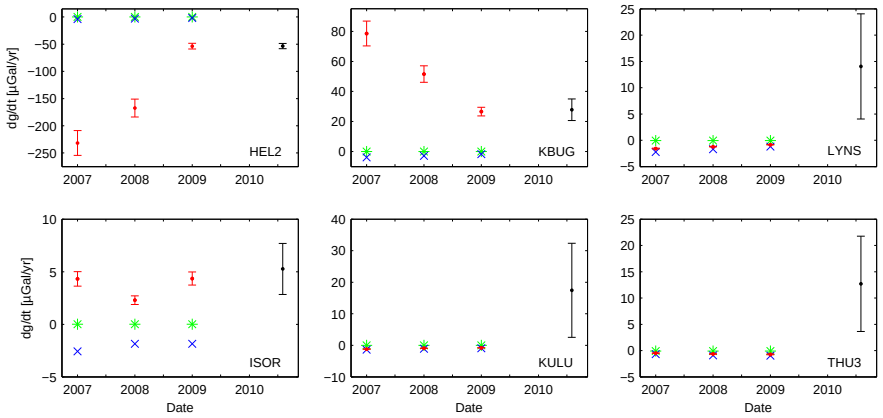

Figure 5: The modelled and the measured results at the six GNET sites. The green stars are the viscous signal, the blue crosses are the viscous + the elastic signal, the red dots with uncertainty are the viscous + the elastic + the direct attraction. The black dots with uncertainty are the measured results presented in figure 2. Only the uncertainty on the summed modelled signals and the measured signals are displayed for clarity.

respectively. For the sites LYNS, KULU and THU3 there is a difference between the measured and modelled gravity change and it is nearly of the same size for the three sites, approximately $15\mu Gal$. The reason for this difference can either be found in the measurements a) or in the modelling b).

a) The measurements done at the southern stations (HEL2, KULU, ISOR, KBUG, LYNS) are done with different instruments (A10-019 and A10-002), while the measurements at the northern station (THU3) are done with the same instrument (A10-019). This would indicate that the differences at LYNS, KULU and THU3 are not instrument depended. Also, the procedure of measuring at a known reference site before and after a campaign would reveal any instrument errors. In the processing of the data the correction due to the ocean loading could maybe be improved. The ocean loading is investigated in Lambert et al. (1998) for North America where they find that using a high-detailed coastline they can alter the tide signal from the global models by $10-20\%$. In Richter et al. (2011) they find that there is a difference between the global ocean tide models and what tide gauge stations measure in the fjords on the West coast. To avoid errors due to the a residual tidal signal, the standard procedure is to measure up to $24-48h$. This is not possible when occupying remote sites where the helicopter ground time is only $3h$.

b) The difference could also be due to a missing signal in the modelled result. In the calculation of the viscous signal the term for the direct attraction, n, is excluded. Looking at the measured $(dg/dt)/(dz/dt)$ or $\dot{g}/\dot{z}$ for Scandinavia, see Ekman and Mäkinen (1996), we find that the modelling without the n-term is in better agreement with the observations then the modelling results including the n-term. Also, the modelling confirms the erroneous signals mentioned in section 3.1. In the calculation of the elastic signal the sea-level equation is not solved excluding the attraction of the sea in the modelling. In Spada et al. (2012) it is shown that the difference between the results calculated as in this study and the results of solving the sea-level equation is no more then 10% in the case of vertical displacement. Solving the sea-level equation is very time consuming for the high resolution ice models used for calculating the elastic signal and for these

Table 1: Measured and modelled gravity results for the six GNET site investigated in this study. The modelled signal are the results of using the ice model spanning the years 2006-2009. The gravity measurements are done in 2009 and 2010. Units are in $\mu Gal/yr$.

	Measured gravity	Modelled gravity	Viscous	Elastic	Direct
HEL2	54.0±6.0	50.2±5.4	0.0±0.2	-1.8±0.2	52.0±5.0
KBUG	-28.0±8.0	-26.3±3.4	0.0±0.2	1.7±0.2	-28.0±3.0
LYNS	-14.0±0.0	0.8±0.3	0.1±0.2	1.1±0.1	-0.4±0.0
ISOR	-5.0±2.0	-4.1±1.4	0.0±0.2	1.9±0.2	-6.0±1.0
KULU	-17.0±11.0	0.8±0.2	0.0±0.1	0.9±0.1	-0.1±0.0
THU3	-13.0±8.0	0.4±0.4	0.1±0.2	0.9±0.1	-0.6±0.1

reasons is the sea-level equation not solved for the elastic signal.
There is also other signals that could be included in the modelling. There is a direct attraction effect from the non-tidal changes of the sea-level, it is investigated in Olsson et al. (2009) for the Baltic. Tide gauge data[3] from Thule shows a relative sea-level fall of approximately $3.8cm/yr$. The direct attraction from this non-tidal sea-level change is $1.5\mu Gal/yr$. Modelling the effect of the atmospheric pressure could also be included. This effect is detected by the GNET as pointed out by Bevis et al. (2012) and the barometric admittance correction due to the atmospheric pressure that is applied to the data can be improved as studied by Merriam (1992). The atmosphere will give rise to two signals, a direct attraction of the atmospheric masses and an elastic signal due to the atmospheres load on the Earth. Also, modelling of the signal due to ice changes over different time scales could be of interest. In Sato et al. (2012) they study the viscous effect from the little ice age (LIA) in Alaska. They find that the signal from the LIA is larger then the viscous signal from the LGM and the elastic signal from present day mass changes.

5. Summery & conclusion

We have used satellite derived ice mass models to estimate the present day elastic signal and the direct attraction as seen by a gravimeter on the surface of the Earth. We present the preliminary results of our AG measurements in Greenland and have proved that we can operate the instrument in remote places and collect useful data but more data are needed to improve the study of GIA.
We have a good agreement between the modelled and the measured gravity change at three of the stations. This is the stations where the direct attraction has the biggest influence. The agreement is less obvious for the sites away from the ice, close to the ocean. Since the difference is of the same size both in the northwest and the southeast the reason for this error could be common for all data and a more elaborated processing and/or the inclusion of more signals in the modelling is needed.
Ice models covering other time scales like the LIA should also be considered when modelling the viscous signal.
It is expected that the viscous signal is very close to linear in time whereas the elastic signal will

[3]Data is The global sea level observing system, GLOSS, `http://www.gloss.sealevel.org`

vary from year to year. For this reason long time series are needed to investigate the viscous signal and short intervals between the observations to investigate the elastic signal. In the proximity of the changing ice other kinds of data, e.g. satellite data, are needed to investigate the direct attraction. The change in the direct attraction from the ice can be a significant contributor to the gravity changes, and should be kept in mind for future site selection.
When looking at the AG data one needs to keep in mind the seasonal signal as a result of the yearly thinning and accumulation of snow. The seasonality is seen in the GPS data from the GNET stations and therefore provides an important tool when evaluating the AG data.

Acknowledgment

The authors would like to thank Giorgio Spada for providing the code to model the viscous and elastic signal and for assistance with any questions regarding his code. Thanks to Louise Sandberg Sørensen and Karina Nielsen for providing the ICESat ice models. We would also like to thanks our colleagues at Bundesamt für Kartographie und Geodäsie (BKG) for their help in the 2010 season. The APLO service is provided by the Goddard VLBI group, data which are available on the web at `http://gemini.gsfc.nasa.gov/aplo` (Petrov and Boy, 2004).

References

Bamber, J.L., Ekholm, S., Krabill, W.B., 2001. A new, high-resolution digital elevation model of Greenland fully validated with airborne laser altimeter data. Journal of Geophysical Research - Solid Earth 106, 6733–6745

Barletta, V.R., Sabadini R., Bordoni A., 2008. Isolating the PGR signal in the GRACE data: impact on mass balance estimates in Antarctica and Greenland. Geophysical Journal International 172, 18–30

Bevis M., Wahr J., Shfaqat A.K., Madsen F.B., Brown A., Willis M., Kendrick E., Knudsen P., Box J.E., van Dam T., Caccamise D.J., Johns B., Nylen T., Abbott R., White S., Miner J., Forsberg R., Zhou H., Wang J., Wilson T., Bromwich D., Francis O., 2012. Bedrock displacements in Greenland manifest ice mass variations climate cycles and climate change. Proceedings of the National Academy of Sciences 109, 1–14

Dziewonski A.M., Anderson D.L., 1981. Preliminary reference Earth model. Physics of the Earth and Planetary Interiors 25, 297–356

Ekman M., Mäkinen J., 1996. Recent postglacial rebound gravity change and mantle flow in Fennoscandia. Geophysical Journal International 126, 229–234

Falk R., Müller J., Lux H., Wilmes H., Wziontek H., 2009. Precise gravimetric surveys with the field absolute gravimeter A10. IAG Scientific Assembly "Geodesy for planet Earth", Buenos Aires, Argentina 31 August – 4 September 2009. Springer.

Farrell W.E., 1972. Deformation of the Earth by surface loads. Reviews of Geophysics and Space Physics 10, 761–797

Khan S.A., Wahr J., Bevis M., Velicogna I., Kendrick E., 2010. Spread of ice mass loss into northwest Greenland observed by GRACE and GPS. Geophysical Research Letters 37, 1–5

Lambert A., Pagiatakis, S.D., Billyard, A.P., Dragert H., 1998. Improved ocean tide loading corrections for gravity and displacement: Canada and northern United States. Journal of Geophysical Research. 103, 30,231–30,244

De Linage C., Hinderer J., Rogister Y., 2007. A search for the ratio between gravity variation and vertical displacement due to a surface load. Geophysical Journal International 171, 986–994

Mäkinen J., Sekowski M., Krynski J., 2010. The use of the A10-020 gravimeter for the modernization of the Finnish first order gravity network. Geoinformation issues 2, 5–16

Mémin A., Hinderer J., Rogister Y., 2011. Separation of the Geodetic Consequences of Past and Present Ice-Mass Change: Influence of Topography with Application to Svalbard (Norway). Pure Applied Geophysics doi:10.1007/s00024-011-0399-7

Merriam J.B., 1980. The series computation of the gravitational perturbation due to an ocean tide. Physics of Earth and Planetary Interiors 23, 81–86

Merriam J.B., 1992. Atmospheric pressure and gravity. Geophysical Journal International 109, 488–500

Nielsen E., Forsberg R., Strykowski G., 2013. Estimation of PGR induced absolute gravity changes at Greenland GNET stations. IAG International Symposium, Melbourne, Australia, 28 June - 7 July. IAG Symposia volume 139 - IN PRESS - Springer-Verlag.

Olsson P-A., Scherneck H-G., Ågren J., 2009. Effects on gravity from non-tidal sea level variations in the Baltic Sea. Journal of Geodynamics 48, 151–156

Olsson P.-A., Ågren J., Scherneck H.-G., 2012. Modelling of the GIA-induced surface gravity change over Fennoscandia. Journal of Geodynamics 61, 12–22

Peltier W.R., 1998. Postglacial variations in the level of the sea: implications for climate dynamics and solid earth geodynamics. Reviews of Geophysics 36, 603–689

Peltier W.R., 2004. Global glacial isostasy and the surfacce of the ice-age Earth: The ICE-5G (VM2) model and GRACE. Annual Review of Earth and Planetary Sciences 32, 111–149

Petrov L., Boy J.-P., 2004. Study of the atmospheric pressure loading signal in VLBI observations. Journal of Geophysical Research 109. DOI:10.1029/2003JB002500

Richter A., Rysgaard S., Dietrich R., Mortensen J., Petersen D., 2011. Coastal tides in West Greenland derived from tide gauge records. Ocean Dynamics 61, 39–49

Sato T., Miura S., Sun W., Sugano T., Freymueller J.T., Larsen C.F., Ohta Y., Fujimoto H., Inazu D., Motyka R.J., 2012. Gravity and uplift rates observed in southeast Alaska and their comaprison with GIA model predictions. Journal of Geophysical Research 117, DOI:10.1029/2011JB008485

Shepherd A., Ivins E.R., Geruo A., Barletta V.R., Bentley M.J., Bettadpur S., Briggs K.H., Bromwich D.H., Forsberg R., Galin N., Horwath M., Jacobs S., Joughin I., King M.A., Lenaerts J.T.M., Li J., Ligtenberg S.R.M., Luckman A., Luthcke S.B., McMillan M., Meister R., Milne G., Mouginot J., Muir A., Nicolas J.P., Paden J., Payne A.J., Pritchard H., Rignot E., Rott H., Srensen L.S., Scambos T.A., Scheuchl B., Schrama E.J.O., Smith B., Sundal A.V., van Angelen J.H., van de Berg W.J., van den Broeke M.R., Vaughan D.G., Velicogna I., Wahr J., Whitehouse P.L., Wingham D.J.,Yi D., Young D., Zwally H.J., 2012. A reconciled estimate of ice-sheet mass balance. Science 2012 338, 1183–1189

Spada G., Stocchi P., 2007. SELEN - A Fortran 90 program for solving the Sea-level-equation. Computers & Geosciences 33, 538–562

Spada G., Ruggieri G., Sørensen L.S., Nielsen K., Melini D., Colleoni F., 2012. Greenland uplift and regional sea level changes from ICESat observations and GIA modelling. Geophysical Journal International 189, 1457–1474

Sørensen L.S., Simonsen S.B., Nielsen K., Lucas-Picher P., Spada G., Adalgeirsdottir G., Forsberg R., Hvidberg, C.S., 2011. Mass balance of the Greenland ice sheet (2003-2008) from ICESat data - the impact of interpolation, sampling and firn density. The Cryosphere 5, 173–186

Tachikawa T., Kaku M., Iwasaki A., Gesch D., Oimoen M., Zhang Z., Danielson J., Krieger T., Curtis B., Haase J., Abrams M., Crippen R., Carabajal C., 2011. ASTER Global Digital Elevation Model Version 2 Summary of Validation Results. METI and NASA.

B Posters

B.1 First measurements with the Danish absolute gravimeter A10-019 in Greenland.

Presented at EGU conference, Vienna, 2010.
This is a presentation of the idea and motivation for the AG activities in Greenland.

B.2 A Study of Glacial Isostatic Adjustment in Greenland.

Presented at EGU conference, Vienna, 2010.
The material presented in this poster was a result of my participation in the GIA summer school in Gävle in 2009.
The objective was to compare the ice histories ICE-5G and SICOPOLIS and the modelled vertical displacement using these models. The displacement is compared to GPS measurements of vertical displacement.
It is found that the models have difficulties predicting the observed vertical displacement and that the large differences between the ice histories calls for more investigations in order to produce improvement on these.

B.3 Absolute gravity changes from GIA models and measurements at Greenland GNET stations.

Presented at IUGG conference in Melbourne, 2011. The presentation was carried out by Gabriel Strykowski.
This poster lead to the paper Nielsen et al. (2013a).
The work presented here were the first results of modelling the GIA signal in Greenland.
The results are used as an indicator on the time interval for repeated measurements.

B.4 Modelled gravity change caused by GIA in Greenland.

Presented at the SLALOM Conference in Athens, 2012.
COST ACTION ES0701 meeting on Sea Level and Adjustment of the Land Observations and Models.
Using the PDIM from Sørensen et al. (2011) was the first estimate on the elastic signal modelled. This was made with the $\dot{g}/\dot{z}$ relation of $-0.26\mu Gal/mm$.
The relative size of the different gravity signal is recognized and that care must be taken when modelling them.

B.5 Measured and modelled absolute gravity in Greenland.

Presented at AGU 2012
The work presented here is the preliminary results that resulted in the article Nielsen et al. (2013b).

First measurements with the Danish absolute gravimeter A10-019 in Greenland.

DTU Space
National Space Institute

J. E. Nielsen, F. B. Madsen, R. Forsberg, G. Strykowski and S. A. Khan.
DTU Space, National Space Institute.
Juliane Maries Vej 30, 2100-DK

Introduction

Changes of the ice mass in Greenland causes the Earth to respond due to its elastic and viscoelastic properties. Depending on whether it is an increase or decrease in mass will there be subsidence or uplifting of the Earth. This vertical movement can be detected with GPS or absolute gravity (AG) time series.

This vertical movement consists of two superimposed signals; one related to the present-day changes of ice mass and another related to mass changes in the past, also known as GIA (Glacial Isostatic Adjustment). One way to separate these two signals is to measure independently both with GPS and a gravimeter.

The magnitude of the two signals gives information on present day ice mass changes as well as on the rheological properties of the Earth. To get a reasonable data set are long time series needed.

In 2008 DTU Space acquired a portable A10 absolute gravimeter - a free-fall instrument produced by Micro-g LaCoste. The main purpose is to measure the change in gravity with time at the GNET GPS stations.

One of the challenges is to measure at the remote places of the GNET stations. It requires careful preparation of equipment and logistics. Because of the expensive helicopter charters, time is an import issue when in operating the field.

These first measurements in Greenland have given us a lot of experience and knowledge of the gravimeter and with time these measurements will give interesting new research opportunities.

A10 measurement at Thule GNET station.

GPS & AG

Wahr et al., 1997 shows one way to separate the elastic and the viscoelastic component of the vertical movement. For a range of common Earth and Ice models they find the following relation:

$$\Delta = u - A\delta g_m$$

Where Δ is the elastic component, u is dh/dt from GPS measurements, A is a constant (6.5mm/μGals) and δg_m is the gravity anomaly, the perturbation minus the free-air contribution.

A10

The A10 absolute gravimeter determines the gravity with an accuracy of 10μGals (100nm/s²). This is achieved by doing a number of free falls in a vacuum chamber. We do 600 free-falls as a minimum. The time and distance of the free falling object is recorded and the gravity can be determined.

With the accuracy of the instrument are we able to resolve what corresponds to a vertical movement of three centimetres.

The instrument is sensitive to the wind so a tent is needed for giving shelter and we run it with 12V batteries.

The quality of the measurement is very depended on the site conditions and weather at the time of measurement.

GNET

Since 2007, in collaboration between the Ohio State University, the Luxembourg University and DTU Space (Technical University of Denmark), have a number of permanent, autonomous GPS stations been deployed in Greenland in the GNET project (Greenland Network). These autonomous stations are placed all around the Greenland Ice Sheet, on the ice-free bedrock. At the present are 56 stations deployed.

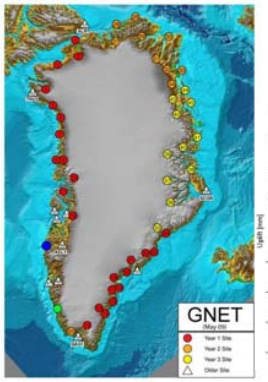

Here is shown the result from the Ilulissat GNET station. An uplift trend of 17 mm/y is seen. Also seen is the annual variation.

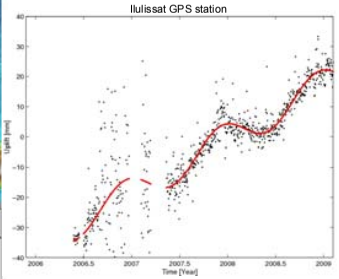

A10 measurements 2009

In 2009 have 25 absolute gravity stations in Greenland been measured, out of these are 11 GNET stations *(blue stars)*, 9 new point where made as a part of a new 1.order net *(green stars)*, 5 old established points where re-measured *(red stars)*.

Before and after every campaign has the instrument been measuring at our AG point in Copenhagen. Here the changes are small and it can be checked if the instrument has experienced some damage during transport.

When measuring at the GNET station we do not measure the gradient, the reason is that it is time consuming. But at the GNET stations it is the gravity change that is of interest and therefore we use the free-air gradient if we need to transpose the measurement.

IfE Hannover visited in 1988 Nuuk, Ilulissat and Thule with their JILAg-3, *Timmen et al., 2008.*

There is also done some measurements in Nuuk and Kulusuk starting 1996, v*an Dam et al., 2000.*

Nuuk, Thule and Kulusuk were revisited in 2009 with the A10-019 but no comparison has been made between these measurements yet.

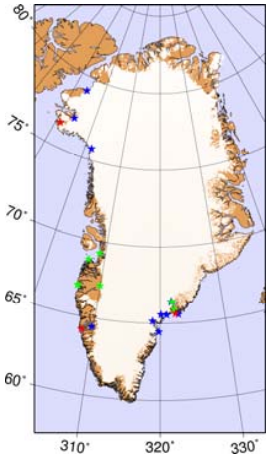

Future work

The first measurements where done in 2009 initiating the future time series of the gravity change. It is planned that some of these stations will be revisited in the future; roughly with 2-3 years interval.

With time when we have more repeated measurements of gravity we can start to look into the different components of the signal. The GPS stations will also have long time series and the data sets will be unique.

The campaigns for this year are planned and this time will the A10 be accompanied with a ScinTrex CG5 relative meter. This can help assess if instrument problems occur during the field campaigns.

References

Timmen et al., 2008. Absolute Gravimetry with the Hannover meters JILAg-3 and FG5-220, and their Deployment in a Danish-German Cooperation. *Fachbeitrag, 133, 1-15.*

van Dam et al., 2000. Using GPS and Gravity to Infer Ica Mass Changes in Greenland. *EOS Trans. AGU 81(37), 421-427.*

Wahr et al., 1997. Predictions of crustal deformation caused by changing polar ice on a viscoelastic earth. *Surveys in Geophysics, 18, 303-312.*

J. E. Nielsen (jemni@space.dtu.dk), F. B. Madsen (bm@space.dtu.dk), R. Forsberg (rf@space.dtu.dk)
G. Strykowski (gs@space.dtu.dk), S. A. Khan (abbas@space.dtu.dk)

A Study of Glacial Isostatic Adjustment in Greenland.

J. E. Nielsen[1)], L. S. Sørensen,[1)] G. Aðalgeirsdóttir, [2)] and G. Spada.[3)]

1) DTU Space, National Space Institute, Geodynamics. Denmark.
2) Danish Climate Centre, Danish Meteorological Institute, Copenhagen, Denmark
3) Department of Mathematics, Physics and Computer Science, Urbino University "Carlo Bo", Italy.

Introduction

Glacial isostatic adjustment (GIA) is the viscoelastic response of the Earth caused by changes in ice loads during glaciations and deglaciations. Knowledge of the GIA signal is particularly important in cryospheric applications of satellite gravimetry and altimetry, where the origin of the observed changes must be separated into past and present response.

Modeling the present-day GIA signal must include knowledge of both the ice loading history and the Earth's rheology. Neither of these models are well constrained in Greenland, and hence the GIA estimates here are uncertain.

We have implemented a loading history of the Greenland Ice Sheet derived from the ice sheet model SICOPOLIS and we have studied the present-day vertical crustal motion derived from using this ice history. The results are compared with those derived from the widely used ICE-5G ice history.

For calculation of the present day GIA signal, we assume the Earth's rheology to be a simplified version of the VM2 Earth model. The calculated GIA signal in Greenland, derived from the two ice loading histories are compared with geodetic measurements of vertical crustal motion from GPS time series corrected for present-day ice mass changes.

The freely available code SELEN is used to calculate the effects of the Earth model and the different ice loading histories. This study is performed within the Working Group 4 of the ESF COST Action ES0701 "Improved constraints on models of Glacial Isostatic Adjustment".

Data

To validate the ice model we use available GPS data (*Khan et al. 2008).* The uplift rate for Nuuk is derived from tide gauge data.

The uplift rate from present day ice mass changes has been removed. The data spans 96-08 (Kellyville, Thule, Kulusuk), 98-08 (Scoresbysund), 02-08 (Qaqortoq) and 94-04 (Nuuk).

GPS station	Vert. uplift rate
Kellyville	-1.2 ± 1.1 mm/a
Thule	3.6 ± 1.1 mm/a
Scoresbysund	0.0 ± 1.1 mm/a
Kulusuk	-0.4 ± 1.1 mm/a
Qaqortoq	-0.3 ± 1.1 mm/a
Nuuk	-2.2 ± 1.3 mm/a

***Table 1**. Rate of vertical uplift from 6 permanent GPS stations.*

Ice models

The ice loading histories used for this study are derived from the ICE-5G model (Peltier, 2004) and the thermomechanical ice flow model SICOPOLIS (Greve, 1997). The ICE-5G is a global ice sheet reconstruction consistent with isostatic rebound of the earth and sea level records. The SICOPOLIS model simulates ice volume of the Greenland Ice Sheet over two glacial-interglacial cycles by forcing the model with climate that is based on surface temperature records from the GRIP and Vostok ice cores and interpolation between the present climatic conditions and the Last Glacial Maximum climate anomalies (Greve, 2005). The two ice loading histories from 20 ky BP until present are used to compute present day uplift rates for Greenland with the code SELEN (Spada and Stocchi, 2007). The figures below show the difference in ice thickness between the two ice loading histories, ICE-5G and SICOPOLIS, at a few time steps. Starting from 9 ky BP the two models show different trends in ice thickness variation, mostly at the ice margin.

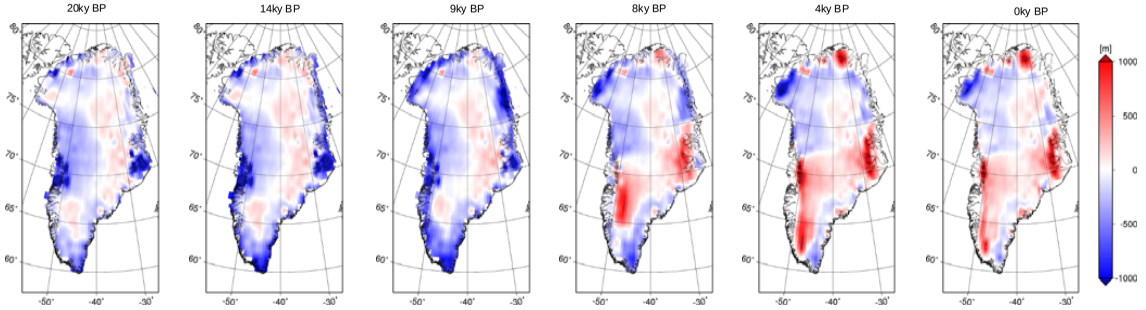

***Figure 1**. Snap shots of the thickness difference between the SICOPOLIS and ICE-5G ($\Delta H = H_{SICOPOLIS} - H_{ICE\text{-}5G}$) resulting from the two ice loading histories. It is clearly seen that starting from 9ky BP the two ice histories show very different ice thickness variation.*

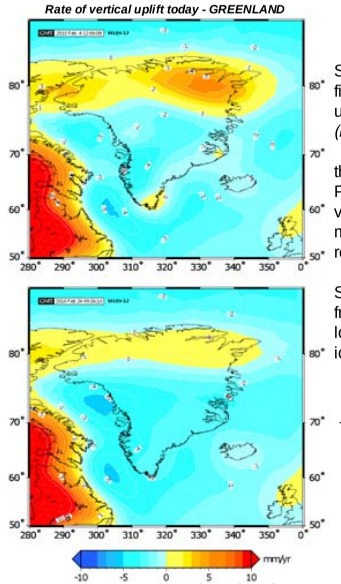

***Figure 2**. Vertical uplift rate from ICE-5G (top) and SICOPOLIS (bottom) ice loading histories*

Results

The present the uplift rate is obtained using the SELEN code (Spada and Stocchi, 2007). The figures show the rate of the vertical movement using the ICE-5G *(top)* and the SICOPOLIS *(bottom)* ice loading histories for Greenland.

The Earth model used for the calculations is the VM2 model, a three layered averaged PREM model with a lithosphere of 90km. The viscosities of the lithosphere, upper and lower mantle are 0.4, 0.4 and 4.0 x 10^{21} Pa·s, respectively.

The largest difference is in the North and Southeast Greenland. The uplift rate derived from the SICOPOLIS ice loading history is lower, which is a result of the slower changing ice volume.

GPS station	SICOPOLIS	ICE-5G
Kellyville	-4.4 mm/a	-3.9 mm/a
Thule	-0.9 mm/a	2.3 mm/a
Scoresbysund	-2.5 mm/a	-0.2 mm/a
Kulusuk	-2.9 mm/a	-0.9 mm/a
Qaqortoq	-2.7 mm/a	0.9 mm/a
Nuuk	-4.1 mm/a	-3.7 mm/a

***Table 2**. Vertical uplift rate from the ICE-5G and SICOPOLIS ice histories at 6 locations*

Conclusions

Due to the fact that Greenland is still covered with ice, the number of uplift measurements is very limited. This means that the ice loading history of the Greenland Ice Sheet is poorly constrained. We show that present day uplift rate based on the two different ice histories (ICE-5G and SICOPOLIS) give different patterns of present-day uplift rate. The difference in the ice thickness (Figure 1) shows significantly different ice volume evolution starting from 9 ky BP. SICOPOLIS has thicker ice in some areas compared to ICE-5G from 8 ky BP until present, this results in a larger present day rate of subsidence (see Table 2).

We find that the GIA signal from neither of the ice loading histories agrees with the GPS derived uplift rate, which highlights the need for further studies in this region in order to better constrain the ice loading histories as well as present and future sea level change is this region.

References

Greve, R. 1997. Application of a polythermal three-dimensional ice sheet model to the Greenland ice sheet: response to steady-state and transient climate scenarios. J. Climate, 10(5), 901-918

Greve, R. 2005. Relation of measured basal temperatures and the spatial distribution of the geothermal heat flux for the Greenland Ice Sheet. Annals of Glaciology, 42, 424-432

Khan et al., *Geodetic measurements of postglacial adjustment in Greenland*, J. of Geo .Rev., Vol.113, 2008.

Peltier, W.R., 2004, *Global glacial isostasy and the surface of the Ice-Age Earth:the ICE5G(VM2) model and GRACE*. Ann. Rev. Earth Pl.

Spada, G. and Stocchi P., 2007, *SELEN: A Fortran 90 program for solving the "sea-level equation"*, Comp. & Geo.Sci., Vol 33.

EGU 2010-4309, May 3-7, Vienna.

COST ACTION ES0701
improved constraints on models of GIA

J.Emil Nielsen (jemni@space.dtu.dk)
Louise Sandberg Sørensen (slss@space.dtu.dk)
Guðfinna Aðalgeirsdóttir (gua@dmi.dk)
Giorgio Spada (giorgio.spada@gmail.com)

#5108 IAG – JG02/46

DTU Space
National Space Institute

Absolute gravity changes from GIA models and measurements at Greenland GNET stations

J. E. Nielsen, **G. Strykowski**, F. B. Madsen, R. Forsberg
DTU Space, National Space Institute
Juliane Maries Vej 30, 2100-DK

Introduction

Changes of the ice mass in Greenland causes the Earth to respond due to its elastic and viscoelastic properties. Depending on whether it is an increase or decrease in mass will there be upward or downward movement of the Earth which can be detected with GPS or absolute gravity.

This vertical movement consists of two superimposed signals; one related to the present-day changes of ice mass and another related to mass changes in the past, also known as GIA (Glacial Isostatic Adjustment). One way to separate these two signals is to combine GPS and gravity time series as shown by *Whar et al., 1997*.

In 2008 DTU Space acquired a portable A10 absolute gravimeter - a free-fall instrument produced by Micro-g LaCoste. The main purpose is to measure the change in gravity with time at the GNET stations in Greenland.

The first measurements where done in 2009 initiating the future time series of the gravity change. It is planned that some of these stations will be revisited roughly with 2-4 years interval. This estimate is purely based on GPS data.

Estimation of the gravity changes caused by GIA can be obtained by solving the sea level equation with a specific ice history and Earth model. Here are shown three modeling results.

The results from the modeling gives an idea of where to expect the largest gravity GIA signals.

A10 measurement at Thule GNET station.

A10

The A10 absolute gravimeter determines the gravity with an accuracy of 10μGals (100nm/s^2). This is achieved by doing free falls in a vacuum chamber. We do 600 free-falls in 2 setups as minimum.

With the instruments accuracy can a vertical movement of 3 cm be resolved.

Up to now we have measured gravity at 18 GNET sites where the instrument has performed within the specifications however, the quality of the measurement is very depended on the site conditions and weather at the time of measurement.

GIA modeling

For modeling GIA is the free code *SELEN* used. It is a sea level equation solver that uses tide gauge data as constraints (*Spada et al., 2007*). To get gravity changes is the code modified in cooperation with G. Spada.

The Earth is assumed to be incompressible with layers having Maxwell viscoelastic properties, self-gravitating, spherical symmetric and non-rotating. In this study the GIA response is calculated for different Earth models and Ice histories. Presented here are three different results calculated to maximum degree 128.

The models are:

1) The ICE-5G ice history used with a 28 layered PREM averaged Earth model.

2) The ICE-5G ice history used with a simplified version of the VM2 Earth model, also with averaged PREM parameters. It consists of the incompressible lithosphere, upper and lower mantle layers having viscosities of 0.4 and 4.0 x 10^{21} Pa·s and an inviscid core. The lithosphere has a thickness of 90 km.

3) The ANU05 ice model used with a simple Earth model. A 80 km. lithosphere and two mantle layers with viscosities of 0.4 and 10.0 x 10^{21} Pa·s.

The modeled rate and the shape of the solid surface gravity change varies a little for different Earth models. Adding more layers gives stronger signal and some changes in the shape while changing the ice history changes the shape. Calculating to a lower degree gives a weaker signal but do not change the shape noticeably.

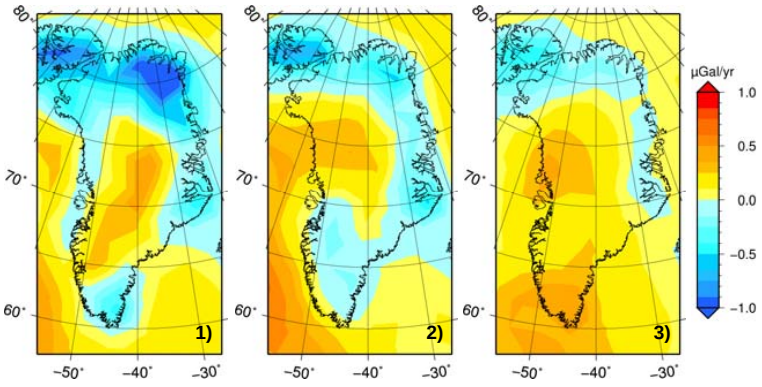

GNET

Since 2007, in collaboration between the Ohio State University, the Luxembourg University and DTU Space (Technical University of Denmark), number of permanent, autonomous GPS stations have been deployed in Greenland in the GNET project (Greenland Network). These autonomous stations are placed all around the Greenland Ice Sheet, on the ice-free bedrock. At present are 56 stations deployed.

Here is shown the result from the Kangia station (KAGA) near Ilulissat. An uplift trend of ~17 mm/yr is seen. Also seen is the annual variation.

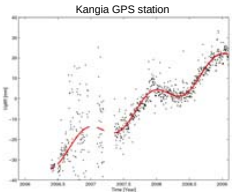

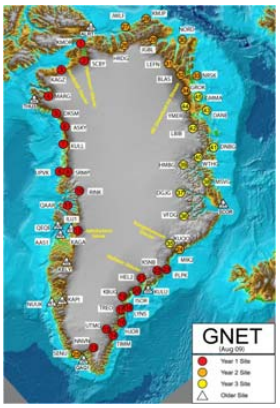

Conclusion

Regarding the AG time series are we only started, so it is too early to make any conclusions based on these data. Not many are revisted.

The solid surface gravity change do not exceed 1.5μGal/yr in the different model runs. This means that the GIA signal is very small and therefore are long time series of absolute gravity change needed before the GIA signal can be detected. All models tested for this study shows a negative signal in North Greenland while it is more complex in the southern part where the signal is very sensitive to the model parameters used.

Next step would be to estimate the size of the elastic signal caused by the present day ice mass changes. One ice model for this could be the one published by *Sørensen et al., 2011*. This would help giving an idea of how offen the sites should be revisted and where to expect the largest signals.

With time, when we have more repeated measurements of gravity, we can start to look into the different components of the signal. The GPS stations will also have long time series and the two data sets will be unique.

References

Spada et al., 2007. SELEN – A Fortran 90 program for solving the Sea-level-equation. *Computers & Geoscience, 33, 538-562.*

Sørensen et al., 2011. Mass balance of the Greenland ice sheet (2003-2008) from ICESat data – the impact of interpolation, sampling and firn density. *The Cryosphere 5, 173-186*

Wahr et al., 1997. Predictions of crustal deformation caused by changing polar ice on a viscoelastic earth. *Surveys in Geophysics, 18, 303-312.*

J. E. Nielsen (jemni@space.dtu.dk) , G. Strykowski (gs@space.dtu.dk),
F. B. Madsen (bm@space.dtu.dk), R. Forsberg (rf@space.dtu.dk)

Modelled gravity change caused by GIA in Greenland.

DTU Space
National Space Institute

J. E. Nielsen, R. Forsberg, G. Strykowski
DTU Space, National Space Institute
Juliane Maries Vej 30, 2100-DK

Introduction

Absolute gravimetry (AG) is an important tool in GIA studies, especially when used with GPS. With sufficient long time series of both kind of data it is possible to separate the viscous and elastic signal. The separation has several purposes. The elastic signal can be used in present day ice mass balance estimations, while the viscous signal can be used in studies of the Earths structure.

The present day gravity signal as seen by a gravimeter on the ground is a sum of 4 different signals: the viscous, the elastic, a Bouguer and a terrain type signal.

The main purpose of this study is to get an estimation of the gravity changes in Greenland as seen by a gravimeter on the ground. This is of interest to the newly established gravity sites in Greenland at the permanent GPS stations in the Greenland Network (GNET). Knowing the size of the signal is of interest for planning AG campaigns, having in mind the measurement precision of today's absolute gravimeters. The FG5 has a precision of 20 nm/s², while the A10 has a precision of 80 nm/s² (10 nm/s² = 1 µGal).

Presented here are the preliminary results of the modelled gravity change in Greenland.

A10 measurement at Thule GNET station.

Results

The ice mass model used has changes ranging from -226 to 29 Gkg/yr in the period 2003-2008, the mean is -3 Gkg/yr. The viscous signal has minimum and maximum values of -22 to 12 nm/s² and, the mean is 0 nm/s². For the elastic signal are the values -81 to 2 nm/s² and, the mean is -9 nm/s². The terrain signal is in the range of -116 to 144 nm/s² with a mean of -0.3 nm/s², while the Bouguer signal is in the range of -3804 to 488 nm/s² with a mean of -46 nm/s².

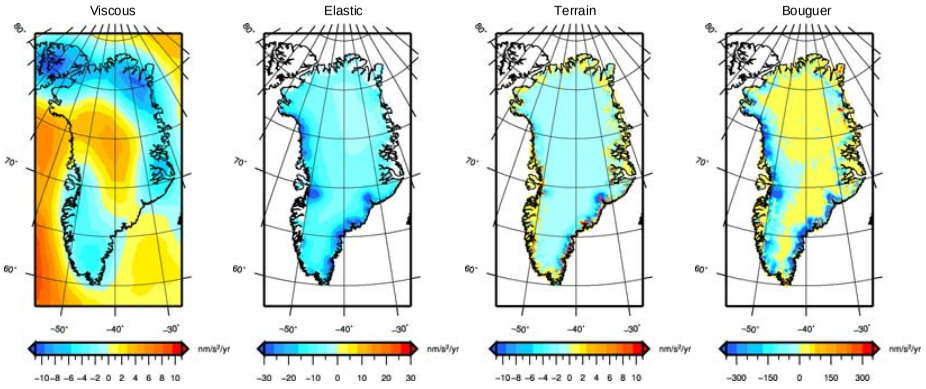

Modelling

The viscous signal is modelled using SELEN *(Spada, 2007)* with the ICE-5G ice history and a simplified version of the VM2 Earth model (90 km lith., 2 mantle layers with viscosities 0.5 and 1.6 x 10^{21} Pa·s).

Calculation of the elastic signal is done with the relation between the vertical displacement and the gravity change investigated in *de Linage 2007*. They look at different relations but find a value of -2.6 nm/s²/mm in the case of being outside the loaded area and omitting the Newtonian attraction. The vertical displacement used to calculate the elastic gravity change is the same as published in *Sørensen 2011.*

Calculation of the Bouguer and terrain signal is done using the ice mass model also published in *Sørensen 2011*. This ice mass model is derived from ICESat data in the interval 2003-2008. The procedure for the calculation is the same as presented in *Le Meur and Huybrechts 2001.* The Bouguer signal is a consequence of the changes in ice mass to the observer standing on the ice. This will only have influence if measuring on the ice. The terrain signal is due to mass changes surrounding the observer. This will influence the observer standing near the ice margin.

Gravity Green's function: $$G_{sg} = -\frac{G}{a^2}\sum_{n=1}^{\infty}\left[2h_n - (n+1)k_n\right]P_n(\cos\gamma)$$

Gravity – height relation: $$\dot{g} = -2.6\,\dot{u}$$

Bouguer type anomaly: $$\Delta\dot{g}_b(i,j) = 2\pi G\left[\dot{L}(i,j) - \sqrt{\rho^2 R_c^2 + \dot{L}(i,j)^2} + \rho R_c\right]$$

Terrain type anomaly: $$\Delta\dot{g}_t(i,j) = \sum_{i_1,j_1}\frac{G\,\dot{L}(i_1,j_1)\Delta x^2}{D^3}\left[S(i,j) - S(i_1,j_1)\right]$$

Conclusion & future work

The Bouguer signal is the largest signal but this is only relevant when measuring on the ice and this is not the case for the established gravity sites in Greenland. Thereafter is the terrain and the elastic signal the largest. Summing the signal would give an idea of the time span needed to have good time series of gravity change, which is also depended on the instrument used.

Next step is to implement the elastic Green's function and try different model scenarios to investigate the impact of different parameters. This can be used to estimate the uncertainty on the gravity signal. It also makes sense to do local studies at areas of special interest.

References

Le Meur, E. & Huybrechts P., 2001. A model computation of the temporal changes of the surface gravity and geoid signal induced by the evolving Greenland ice sheet. Geophys. J. Int. 145:835-849

de Linage, C., Hinderer, J. & Rogister, Y., 2007. A search for a ratio between gravity variation and vertical displacement due to a surface load. Geophys. J. Int. 171:986-994

Spada, G. & Stocchi, P., 2007. SELEN: A Fortran 90 program for solving the "Sea-level equation". Comput. Geosci. 33:538-56

Sørensen, L. S. et. al., 2011. Mass balance of the Greenland ice sheet (2003-2008) from ICESat data – the impact of interpolation, density and firn density. The Cryosphere 5:173-186

J. E. Nielsen (jemni@space.dtu.dk), R. Forsberg (rf@space.dtu.dk), G. Strykowski (gs@space.dtu.dk)

G21A-0870

Measured and modelled absolute gravity in Greenland.

DTU Space
National Space Institute

Nielsen, J.E., Forsberg, R. and Strykowski, G.
DTU Space, Danish National Space Institute
jemni@space.dtu.dk

Introduction

In this study we will look into changes of the absolute gravity (AG) in Greenland. These changes are due to variations of the ice masses and the Earths response to these changes. We will present some preliminary results from our measurements done at selected GNET (Greenland GPS Network) sites. The present day gravity signal as seen by a gravimeter on the ground is a sum of mainly three signals: the viscous, the elastic and the direct attraction of the ice masses. The interest of knowing the gravity change is that this information, with GPS data, can be used to separat the different signals and knowlegde of the different signals can give a better understanding of present day ice mass changes and the properties of the Earth. The gravity measurements are done with a Micro-g LaCoste A10 that has a accuracy of 5-8µGal (1µGal = 10nm/s^2).

Presented here are the preliminary results of the gravity measurements in Greenland along with a modelled estimate of the gravity change.

Measured & modelled gravity

The first gravity measurement in Greenland with the A10-019 gravimeter (owned by DTU) was done in 2009. In 2010 some of the measurements were redone. In the figure below we present these measurements for six GNET sites and make an estimate of the gravity change. This is the preliminary results and more data is needed to make more solid conclusions.

Here we compare the measurements with the modelled gravity change. At the sites where we are close to the ice (HEL2, KBUG, ISOR) our modelled signal are in the range of the measurements, whereas at the sites that are further from the ice (LYNS, KULU, THU3) there is a discrepency of approximately the same size. For the direct attraction calculation at the GNET sites the ASTER DEM[1)] is used.

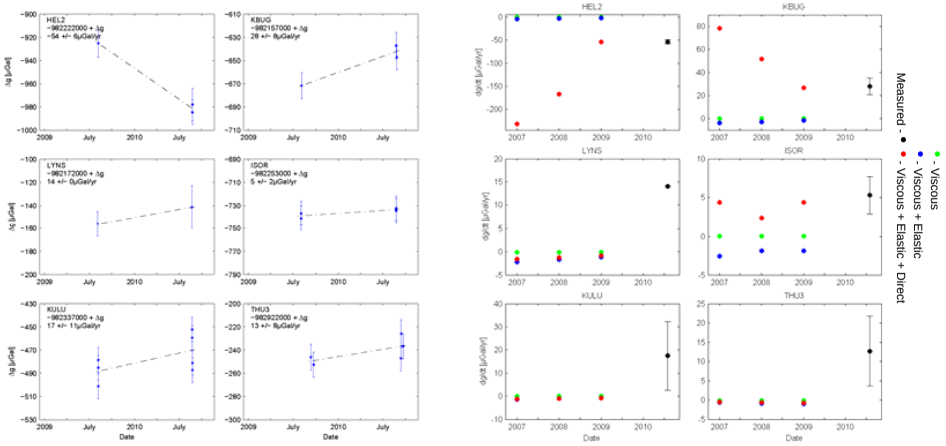

Modelled gravity in Greenland

The viscous signal is modelled using SELEN *(Spada, 2007)* with the ICE-5G ice history and a simplified version of the VM2 Earth model (90 km lith., 2 mantle layers with viscosities 0.5 and 1.6 x 10^{21} Pa·s). SELEN calculates different geophysical signal by solving the sea-level equation.

Calculation of the elastic signal is done analytically by convolving the gravity Greens function with ice mass models similar to that presented in *Sørensen et. al. 2011*. Here three different models, spanning the years 2004-2007, 2005-2008 and 2006-2009, are used.

Calculation of the direct attraction is done using the same ice models.

The min and max values for the three signals are – Viscous: -1.4 to 0.3µGal. Elastic: -6.5 to 0.2µGal. Direct attraction: -16.8 to 14.5µGal. The DEM used for calculating the direct attraction for Greenland is more coarse then the ASTER DEM used for the specific site calculations.

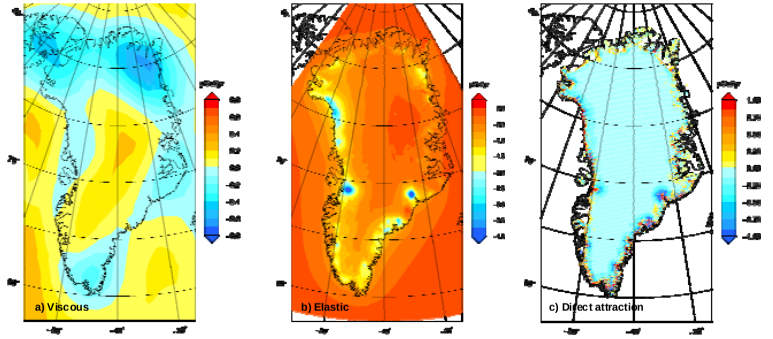

Conclusion & future work

The direct attraction from the changing ice masses is very dependent on the location and can be the largest signal measured by the gravimeter. This should be kept in mind when measuring gravity in glaciated areas.

As pointed out in *Bevis et. al. 2012* the atmospheric loading gives rise to a significant signal in the GNET GPS data. We need to look into this effect on the gravity measurements and try to improve this correction.

This study shows the preliminary results of our AG measurements in Greenland and that there are many challenges in interpretating the results. The time series needs to be continued for many years in order to make more in-depth investigations into the nature of the gravity change.

With time, with longer time series, this study will help to address different issues like mass balance estimates, studies of GIA and the Earths rheology.

References

Bevis et. al., 2012. Bedrock displacements in Greenland manifest ice mass variations, climate cycles and climate change. PNAS

Spada & Stocchi, 2007. SELEN: A Fortran 90 program for solving the "Sea-level equation". Comput. Geosci. 33:538-56

Sørensen et. al., 2011. Mass balance of the Greenland ice sheet (2003-2008) from ICESat data – the impact of interpolation, density and firn density. The Cryosphere 5:173-186

[1)] ASTER DEM is a product of METI and NASA

AGU 2012, December 3-7, San Francisco

Acknowledgement: Thanks to Louise Sandberg Sørensen and Karina Nielsen (DTU) for providing ICESat models. To Giorgio Spada (Urbino University) for help in using his programs. To Micheal Bevis (OSU) for letting me visit him and his group. To Maersk Oil Kalaallit Nunaat A/S for funding this trip.

C Formulas

Unless stated differently the formula presented here are from Taylor (1997).

C.1 Linear regression

The expressions for the slope when implementing least squares linear regression

$$B = \frac{\sum x^2 \sum y - \sum x \sum xy}{N\sum x^2 - (\sum x)^2} \tag{C.1}$$

and for the $y-$axis interception

$$A = \frac{N\sum xy - \sum x \sum y}{N\sum x^2 - (\sum x)^2} \tag{C.2}$$

where N is the number of observations. The linear relation is given by $y = A + Bx$.
The uncertainty in the slope is found with

$$\sigma_B = \sqrt{\frac{N\sum (y - A - Bx)^2}{(N-2)(N\sum x^2 - (\sum x)^2)}} \tag{C.3}$$

Linear regression will be used on several data sets in this thesis and in the way it is used it is assumed that there is non or very little uncertainty on the data along the abscissa. Also it is assumed that the data are normal distributed.

C.2 Uncertainty

The uncertainty on a relations $z = x/y$, with uncertainty on the individual elements, δx and δy, is calculated with the following expression

$$\delta z = \frac{x}{y}\sqrt{\left(\frac{\delta x}{x}\right)^2 + \left(\frac{\delta y}{y}\right)^2} \tag{C.4}$$

This applies to data where the uncertainties are independent and random.

C.3 Correlation

The correlation coefficient is calculated as

$$r = \frac{\sum (x_i - \bar{x})(y_i - \bar{y})}{\sqrt{\sum (x_i - \bar{x})^2 \sum (y_i - \bar{y})^2}} \tag{C.5}$$

This is also known as the Pearson product-moment correlation coefficient.

C.4 Lomb-Scargle Periodogram

This method is a least squares fit of a number of harmonics to a data set and investigates the frequency spectrum in a signal. It calculates the power of the individual frequencies and it can be used on unevenly sampled data. See Lomb (1976) and Numerical Recipes Section 13.5.

The periodogram, using the Normalized Lomb-Scargle method, is given by

$$P_x(\omega) = \frac{1}{2\sigma^2}\left(\frac{[\sum_j X_j \cos(\omega(t_j-\tau))]^2}{\sum_j \cos^2(\omega(t_j-\tau))} + \frac{[\sum_j X_j \sin(\omega(t_j-\tau))]^2}{\sum_j \sin^2(\omega(t_j-\tau))}\right) \tag{C.6}$$

where τ is the time delay given by

$$\tau = \frac{1}{2\omega}\tan^{-1}\left(\frac{\sum_j \sin 2\omega t_j}{\sum_j \cos 2\omega t_j}\right) \tag{C.7}$$

Following Hocke (1998), estimating the amplitudes and the power of the amplitudes is carried out with

$$a = \frac{\sqrt{2/n}\sum_{i=1}^{n} y_n \cos\omega(t_i-\tau)}{\left(\sum_{i=1}^{n}\cos^2\omega(t_i-\tau)\right)^{1/2}} \tag{C.8}$$

$$b = \frac{\sqrt{2/n}\sum_{i=1}^{n} y_n \sin\omega(t_i-\tau)}{\left(\sum_{i=1}^{n}\sin^2\omega(t_i-\tau)\right)^{1/2}} \tag{C.9}$$

$$\tag{C.10}$$

and the amplitude power spectrum is calculated with

$$A(\omega) = \sqrt{a^2+b^2} \tag{C.11}$$

D A10-019 Laser frequencies

Date	Mode	Frequency [MHz]		Wavelength [nm]		Rubidium clock frequency [Hz]	Instrument height [m]	Comment
2008 JUL 11	Red	473 611 824.919	± 0.029	632.9919192	±0.0	10 000 000	0.700	
	Blue	473 612 579.544	± 0.113	632.9909106	$\pm 2.0e^{-7}$			
	Center	473 612 202.232						
2009 MAY 04	Red	473 611 843.738	± 0.115	632.9918940	$\pm 2.0e^{-7}$	10 000 000	0.718	New laser tube
	Blue	473 612 575.095	± 0.085	632.9909166	$\pm 1.0e^{-7}$			
	Center	473 612 209.417						
2010 MAR 12	Red	473 611 845.967	± 0.168	632.9918910	$\pm 2.0e^{-7}$	10 000 000	0.718	New laser tube
	Blue	473 612 561.181	± 0.346	632.9909351	$\pm 5.0e^{-7}$			
	Center	473 612 203.574						
2010 AUG 31	Red	473 611 843.232		632.9918947			0.718	Calibration at BKG
	Blue	473 612 560.394		632.9909362				
	Center	473 612 201.813						
2011 SEP 19	Red	473 611 836.052	± 0.395	632.9919043	$\pm 2.0e^{-7}$	10 000 000	0.718	New laser tube
	Blue	473 612 573.495	± 0.343	632.9909187	$\pm 2.0e^{-7}$			
	Center	473 612 204.774						
2012 JUL 24	Red	473 611 879.609	± 0.117	632.9918461	$\pm 2.0e^{-7}$	10 000 000	0.718	
	Blue	473 612 526.724	± 0.092	632.9909812	$\pm 1.0e^{-7}$			
	Center	473 612 203.167						

Table D.1: The history of the A10-019 laser frequency in the period from June 2008 to January 2013.

E Measurements 2008-2012

E.1 Denmark

Location	Code	Lat. [°]	Long. [°]	Elev. [m]	dg/dz [$\mu Gal/m$]					
	Date	g @ $0m$ [μGal]	g @ h [μGal]	h [m]	SS [μGal]	R/B [μGal]	#sets	#drops	#fringes	g8sf-g8ef
Døestrup (ABS)	DSKR(ABS)	55.11492	8.79925	3.00	-288.9					
	20101011	981532994 ± 11	981532787 ± 11	0.718	3.67	2.29	6	100	750	35-635
	20101011	981532999 ± 11	981532791 ± 11	0.718	3.86	7.78	6	100	750	35-635
Døestrup (ECC)	DSKR(ECC)	55.11492	8.79925	3.00	-302.1					
	20101011	981533000 ± 11	981532756 ± 11	0.808	3.11	12.08	6	100	750	35-635
	20101011	981532999 ± 11	981532754 ± 11	0.815	2.86	11.76	6	100	750	35-635
DTU Space	DTUS	55.78320	12.516258	20.00	-286.1					
	20120802	981545983 ± 11	981545777 ± 11	0.718	4.10	35.39	12	100	750	16-565
	20120802	981545969 ± 11	981545764 ± 11	0.718	5.09	38.82	10	100	750	16-565
	20120802	981545979 ± 11	981545773 ± 11	0.718	2.64	43.60	6	100	750	16-565
Esbjerg (GPS)	ESBG(GPS)	55.49355	8.45675	14.89	-310.0					
	20091119	981556018 ± 11	981555795 ± 11	0.718	10.57	56.07	6	100	750	35-635
	20091119	981556019 ± 15	981555796 ± 15	0.718	29.28	7.75	6	100	750	35-606
Esbjerg Airport	ESBG(AIR)	55.52216	8.54788	69.44	-305.9					
	20091119	981555483 ± 13	981555263 ± 13	0.718	17.66	30.03	6	100	750	35-534
	20091119	981556480 ± 17	981555261 ± 17	0.718	31.34	32.09	6	100	750	35-534
Ferring (GPS)	FERG(GPS)	56.52302	8.11823	23.07	-322.0					
	20100721	981637694 ± 11	981637463 ± 11	0.718	6.49	18.10	10	100	750	35-635
	20100721	981556687 ± 11	981637456 ± 11	0.718	14.13	3.73	10	100	750	35-635
Fredericia (ABS)	FRDK(ABS)	55.56488	9.75352	11.00	-307.5					
	20101216	981564262 ± 11	981564041 ± 11	0.718	11.47	4.00	8	100	750	35-635
	20101216	981564272 ± 11	981564051 ± 11	0.718	6.54	5.74	6	100	750	35-635
Fredericia (ECC)	FRDK(ECC)	55.56488	9.75352	11.00	-293.0					
	20101010	981564545 ± 11	981564335 ± 11	0.718	1.68	4.28	6	100	750	35-635
	20101010	981564543 ± 11	981564332 ± 11	0.718	3.67	6.47	6	100	750	35-635
Fynshav (ABS)	FYNH(ABS)	54.98618	9.97642	11.00	-295.4					
	20101010	981516989 ± 11	981516777 ± 11	0.718	1.85	10.79	6	100	750	35-635
	20101010	981516994 ± 11	981516781 ± 11	0.718	3.04	9.58	6	100	750	35-635

Denmark

Location	Code	Lat. [°]	Long. [°]	Elev. [m]	dg/dz [$\mu Gal/m$]					
	Date	g @ 0m [μGal]	g @ h [μGal]	h [m]	SS [μGal]	R/B [μGal]	#sets	#drops	#fringes	g8sf-g8ef
Fynshav (ECC)	FYNH(ECC)	54.98618	9.97642	11.00	-319.5					
	20101010	981516790 ± 11	981516560 ± 11	0.718	5.21	2.51	6	100	750	35-635
	20101010	981516797 ± 11	981516568 ± 11	0.718	2.27	1.43	6	100	750	35-635
Gedser (GPS)	GEDS	54.57443	11.92289	2.20	-310.7					
	20090528	981471692 ± 15	981471469 ± 15	0.718	27.50	62.56	6	100	700	25-456
	20090528	981471697 ± 11	981471474 ± 11	0.718	15.57	47.76	12	100	700	25-456
Helsingør (ABS)	HLSR(ABS)	56.04528	12.57972	32.00	-265.0					
	20080808	981580397 ± 11	981580209 ± 11	0.710	4.20	18.78	6	100	700	25-540
Højer (ABS)	HJKR(ABS)	54.96460	8.69902	2.00	-293.9					
	20101011	981509161 ± 11	981508950 ± 11	0.718	5.61	0.06	6	100	750	35-635
	20101011	981509156 ± 11	981508945 ± 11	0.718	2.96	4.60	6	100	750	35-635
Højer (ECC)	HJKR(ECC)	54.96460	8.69902	2.00	-306.3					
	20101011	981509114 ± 11	981508894 ± 11	0.718	5.58	2.30	8	100	750	35-635
	20101011	981509122 ± 11	981508903 ± 11	0.718	6.60	4.68	6	100	750	35-635
Rønne (ABS)	RONN(ABS)	55.09880	14.69970	12.00	-302.1					
	20101011	981517207 ± 14	981516992 ± 14	0.710	20.58	9.25	6	100	700	25-550
	20101011	981517222 ± 14	981517007 ± 14	0.710	19.56	2.99	12	100	700	25-550
Havneby (GPS)	HVBY	55.97188	11.35535	21.35	-300.1					
	20100415	981577412 ± 11	981577196 ± 11	0.718	4.89	13.66	8	100	750	35-635
	20100415	981577410 ± 11	981577194 ± 11	0.718	2.64	18.39	6	100	750	35-635
	20111007	981577408 ± 12	981577193 ± 12	0.718	15.33	29.02	8	100	750	16-565
	20111007	981577415 ± 11	981577200 ± 11	0.718	3.42	53.82	8	100	750	16-565
	20120415	981577408 ± 11	981577193 ± 11	0.718	6.15	138.38	8	100	750	16-565
	20120415	981577411 ± 11	981577195 ± 11	0.718	12.63	126.83	6	100	750	16-565
Smidstrup (GPS)	SMID	56.64060	9.55930	79.11	-322.0					
	20100722	981557239 ± 11	981557008 ± 11	0.718	5.83	2.91	10	100	750	35-635
	20100722	981517246 ± 11	981557015 ± 11	0.718	7.77	33.39	10	100	700	35-635

Denmark

Location	Code	Lat. [°]	Long. [°]	Elev. [m]	dg/dz [$\mu Gal/m$]					
	Date	g @ $0m$ [μGal]	g @ h [μGal]	h [m]	SS [μGal]	R/B [μGal]	#sets	#drops	#fringes	g8sf-g8ef
Suldrup (GPS)	SULD	56.84166	9.74214	76.82	-319.4					
	20100723	981638679 ± 11	981638450 ± 11	0.718	11.80	6.32	10	100	750	35-635
	20100723	981638683 ± 11	981638454 ± 11	0.718	12.89	15.33	10	100	750	35-635
Tejn	TEJN	55.24380	14.84730	15.00	-266.0					
	20080710	981550024 ± 11	981549833 ± 11	0.710	4.63	4.82	12	100	700	25-540
Vestvolden	VEST	55.68690	12.43500	24.00	-283.0					
	20080808	981547618 ± 11	981547418 ± 11	0.710	3.48	23.98	6	100	700	25-540
	20100419	981547607 ± 11	981547404 ± 11	0.718	5.01	8.50	32	100	750	35-635
	20100420	981547616 ± 11	981547413 ± 11	0.718	11.37	13.52	30	100	750	35-635
	20100420	981547614 ± 11	981547411 ± 11	0.718	2.58	24.57	8	100	750	35-635

E.2 Greenland

Location	Code	Lat. [°]	Long. [°]	Elev. $[m]$	dg/dz $[\mu Gal/m]$					
	Date	g @ $0m$ $[\mu Gal]$	g @ h $[\mu Gal]$	h $[m]$	SS $[\mu Gal]$	R/B $[\mu Gal]$	#sets	#drops	#fringes	g8sf-g8ef
Aasiaat Airport	AASA	68.72000	-52.79200	19.0	-260.0					
	20090625	982475521 ± 11	982475334 ± 11	0.718	3.23	32.64	12	100	750	35-525
	20090625	982475521 ± 11	982475334 ± 11	0.718	5.22	13.07	6	100	750	35-525
	20090625	982475539 ± 11	982475352 ± 11	0.718	5.07	12.51	12	100	750	35-525
	20090625	982475527 ± 11	982475340 ± 11	0.718	5.24	22.84	12	100	750	35-525
	20090626	982475530 ± 11	982475343 ± 11	0.718	3.64	19.15	10	100	750	35-525
Astrup Kystland (GNET)	ASKY	75.72613	-58.25735	687.3	-308.6					
	20090924	982725385 ± 14	982725142 ± 14	0.788	22.70	31.74	6	100	750	35-635
Helheim Glacier (GNET)	HEL2	66.401170	-38.215670	424.00	-308.6					
	20090807	982222923 ± 12	982222677 ± 12	0.798	13.65	18.95	6	100	750	35-525
Ilulissat Airport	ILUA	66.401170	-51.066050	14.00	-292.0					
	20090623	982486842 ± 11	982486632 ± 11	0.718	3.10	7.53	8	100	750	35-534
	20090623	982486854 ± 11	982486644 ± 11	0.718	1.84	24.94	6	100	750	35-534
	20090624	982486849 ± 11	982486639 ± 11	0.718	5.16	19.28	12	100	750	35-534
	20090624	982486851 ± 11	982486641 ± 11	0.718	3.07	11.09	8	100	750	35-534
	20090624	982486851 ± 11	982486641 ± 11	0.718	6.22	0.44	8	100	750	35-534
	20100521	982486852 ± 11	982486642 ± 11	0.718	3.22	10.89	8	100	750	35-635
	20100521	982486840 ± 11	982486630 ± 11	0.718	3.17	9.82	6	100	750	35-635
	20100521	982486853 ± 11	982486643 ± 11	0.718	2.05	9.39	6	100	750	35-635
Isortoq (GNET)	ISOR	65.546620	-38.974630	83.00	-308.6					
	20090803	982253749 ± 11	982253527 ± 11	0.718	2.96	22.19	6	100	750	48-493
	20090803	982253738 ± 11	982253516 ± 11	0.718	2.66	12.74	6	100	750	48-493
Kangerlussuaq	SFJ1	67.153470	-50.061060	502.00	-333.0					
	20090617	982300084 ± 13	982299818 ± 13	0.798	23.98	36.44	12	100	750	35-534
	20090617	982300094 ± 12	982299855 ± 12	0.718	15.65	22.60	10	100	750	35-534
Kangia (GNET)	KAGA	69.222220	-49.816110	149.00	-308.6					
	20100522	982469857 ± 11	982469613 ± 11	0.790	0.84	3.39	6	100	750	35-635
	20100522	982469856 ± 11	982469611 ± 11	0.793	1.64	4.85	6	100	750	35-635

Greenland

Location	Code	Lat. [°]	Long. [°]	Elev. $[m]$	dg/dz $[\mu Gal/m]$					
	Date	g @ $0m$ $[\mu Gal]$	g @ h $[\mu Gal]$	h $[m]$	SS $[\mu Gal]$	R/B $[\mu Gal]$	#sets	#drops	#fringes	g8sf-g8ef
Kap Agassiz (GNET)	KAGZ	79.131960	-65.852950	86.54	-308.6					
	20090914	982968440 ± 11	982968197 ± 11	0.789	4.04	35.98	6	100	750	35-534
	20090914	982968422 ± 18	982968179 ± 18	0.789	48.64	59.65	12	100	750	35-534
Kapisilit (GNET)	KAPI	64.432310	-50.271640	70.00	-378.5					
	20090619	982158103 ± 11	982157831 ± 11	0.718	3.49	17.24	8	100	750	35-635
Køge Bugt (GNET)	KBUG	65.143670	-41.157500	291.00	-308.6					
	20090805	982157671 ± 11	982157430 ± 11	0.782	11.83	2.95	8	100	750	35-525
Kulusuk (GNET)	KULU	65.577590	-37.156320	14.00	-308.6					
	20090807	982337501 ± 11	982337252 ± 11	0.807	3.81	27.73	12	100	750	35-615
	20090807	982337485 ± 11	982337237 ± 11	0.805	3.13	14.96	12	100	750	35-615
	20090807	982337478 ± 11	982337230 ± 11	0.804	8.14	24.53	10	100	750	35-615
Lynæs (GNET)	LYNS	64.430500	-40.198170	174.00	-308.6					
	20090805	982173159 ± 11	982172899 ± 11	0.841	5.29	16.30	8	100	750	35-525
Marie Gletscher (GNET)	MARG	77.187040	-65.694620	670.57	-308.6					
	20090926	982784239 ± 11	982783997 ± 11	0.783	2.91	30.31	5	100	750	35-635
Nuuk (Town hall)	78801	64.177830	-51.740330	23.10	-284.4					
	20090621	982190654 ± 11	982190450 ± 11	0.718	3.04	1.29	6	100	750	35-635
	20090621	982190654 ± 11	982190450 ± 11	0.718	1.16	27.34	6	100	750	35-635
	20090621	982190650 ± 11	982190446 ± 11	0.718	1.88	17.42	6	100	750	35-635
	20090621	982190651 ± 11	982190447 ± 11	0.718	1.90	18.68	6	100	750	35-635
	20090621	982190659 ± 11	982190455 ± 11	0.718	0.00	21.63	6	100	750	35-635
Qasigiannguit	QASI	68.801170	-50.462970	502.40	-308.6					
	20100527	982374506 ± 11	982374262 ± 11	0.791	4.04	7.75	6	100	750	35-635
	20100527	982374515 ± 11	982374271 ± 11	0.791	3.95	14.54	6	100	750	35-635
	20100527	982374505 ± 11	982374261 ± 11	0.791	1.69	0.06	6	100	750	35-635

Greenland

Location	Code	Lat. [°]	Long. [°]	Elev. [m]	dg/dz [$\mu Gal/m$]					
	Date	g @ $0m$ [μGal]	g @ h [μGal]	h [m]	SS [μGal]	R/B [μGal]	#sets	#drops	#fringes	g8sf-g8ef
Qaarsut Airport	QARA	70.732200	-52.696720	60.00	-308.6					
	20100524	982576145 ± 11	982575898 ± 11	0.800	10.11	6.48	8	100	750	35-635
	20100524	982576156 ± 11	982575934 ± 11	0.718	12.86	1.12	8	100	750	35-635
Qaarsut (GNET)	QAAR	70.740420	-52.688290	20.00	-308.6					
	20100524	982588288 ± 11	982588042 ± 11	0.796	1.95	2.07	6	100	750	35-635
	20100524	982588309 ± 11	982588064 ± 11	0.795	1.23	1.76	6	100	750	35-635
	20100525	982588314 ± 11	982588069 ± 11	0.795	3.68	5.62	6	100	750	35-635
Rink Isbræ(GNET)	RINK	71.848500	-50.993970	1337.82	-308.6					
	20100522	982356161 ± 11	982355914 ± 11	0.802	3.29	10.17	6	100	750	35-635
	20100522	982356170 ± 11	982355922 ± 11	0.805	4.44	1.57	6	100	750	35-635
Sisimiut ARTEK	SIAR	66.934140	-53.660460	38.00	-272.8					
	20090628	982402352 ± 11	982402156 ± 11	0.718	3.11	5.04	12	100	750	35-635
	20090628	982402364 ± 11	982402168 ± 11	0.718	2.93	2.28	10	100	750	35-635
	20090628	982402361 ± 11	982402165 ± 11	0.718	3.51	7.53	12	100	750	35-635
	20090628	982402365 ± 11	982402169 ± 11	0.718	1.81	18.61	10	100	750	35-635
	20090628	982402362 ± 11	982402166 ± 11	0.718	4.23	2.60	10	100	750	35-635
	20090628	982402356 ± 11	982402160 ± 11	0.718	5.26	13.55	12	100	750	35-635
Sisimiut Airport	SISA	66.952030	-53.722110	17.00	-292.0					
	20090627	982415324 ± 11	982415114 ± 11	0.718	2.70	18.69	6	100	750	35-635
	20090627	982415317 ± 11	982415107 ± 11	0.718	3.70	13.59	24	100	750	35-635
	20090627	982415322 ± 11	982415112 ± 11	0.718	3.02	21.65	10	100	750	35-635
	20090627	982415332 ± 11	982415122 ± 11	0.718	3.34	14.37	12	100	750	35-635
	20090628	982415325 ± 11	982415115 ± 11	0.718	5.62	8.88	16	100	750	35-635
	20090627	982415315 ± 11	982415105 ± 11	0.718	2.20	17.38	10	100	750	35-635
Tasiilaq	78172	65.612170	-37.619500	9.00	-308.6					
	20090804	982322968 ± 11	982322710 ± 11	0.835	7.37	38.60	12	100	750	35-525
	20090804	982322923 ± 12	982322684 ± 12	0.776	20.36	23.36	12	100	750	35-525
Tasiilaq	78211	65.612170	-37.619500	9.00	-308.6					
	20090804	982322676 ± 11	982322454 ± 11	0.718	4.69	24.89	12	100	750	35-594
	20090804	982322676 ± 11	982322454 ± 11	0.718	1.06	14.11	6	100	750	35-594

Greenland

Location	Code	Lat. [°]	Long. [°]	Elev. [m]	dg/dz [$\mu Gal/m$]					
	Date	g @ $0m$ [μGal]	g @ h [μGal]	h [m]	SS [μGal]	R/B [μGal]	#sets	#drops	#fringes	g8sf-g8ef
Thule	38801	76.538330	-68.801670	26.85	-308.6					
	20090912	982921533 ± 11	982921311 ± 11	0.718	7.37	5.31	12	100	750	35-635
	20090912	982921541 ± 11	982921319 ± 11	0.718	5.36	12.32	12	100	750	35-635
	20090912	982921539 ± 11	982921317 ± 11	0.718	7.94	7.35	12	100	750	35-635
	20090912	982921535 ± 11	982921313 ± 11	0.718	4.25	11.75	12	100	750	35-635
	20100910	982921544 ± 11	982921322 ± 11	0.718	1.78	6.22	8	100	750	35-635
	20100910	982921539 ± 11	982921317 ± 11	0.718	2.51	7.14	6	100	750	35-635
Thule	38802	76.537920	-68.796720	26.91	-308.6					
	20090928	982921678 ± 11	982921456 ± 11	0.718	4.96	13.42	6	100	750	35-635
	20090928	982921674 ± 11	982921452 ± 11	0.718	1.53	46.68	6	100	750	35-635
Thule (GNET)	THU3	76.537040	-68.824950	21.00	-308.6					
	20090912	982923246 ± 11	982922999 ± 11	0.800	14.08	40.33	12	100	750	35-534
	20090923	982964301 ± 11	982964055 ± 11	0.796	3.04	0.43	5	100	750	35-534
	20090923	982923253 ± 11	982923007 ± 11	0.796	6.82	22.12	8	100	750	35-534
	20090923	982923263 ± 11	982923017 ± 11	0.796	6.28	31.91	4	100	750	35-534
	20100912	982923247 ± 11	982923003 ± 11	0.790	5.38	9.53	10	100	750	35-635
	20100913	982923227 ± 12	982922982 ± 12	0.793	15.45	9.43	8	100	750	35-635
	20100921	982923237 ± 11	982922993 ± 11	0.790	3.15	0.80	8	100	750	35-635
Thule - Camp Tuto	TUTO	76.430767	-68.339567	490	-308.6					
	20090917	982831335 ± 11	982831113 ± 11	0.718	13.14	42.64	8	100	750	35-534
	20090917	982831339 ± 12	982831117 ± 12	0.718	14.93	33.09	8	100	750	35-534
	20100914	982831346 ± 11	982831102 ± 11	0.790	3.91	1.41	6	100	750	35-635
	20100914	982831340 ± 11	982831096 ± 11	0.790	1.74	1.34	6	100	750	35-635
Upernavik Airport	UPAI	72.786890	-56.129220	95.00	-308.6					
	20100525	982711031 ± 11	982710809 ± 11	0.718	2.55	19.82	6	100	750	35-635
	20100525	982711042 ± 11	982710820 ± 11	0.718	2.59	22.38	6	100	750	35-635
	20100526	982711043 ± 11	982710821 ± 11	0.718	2.56	15.60	6	100	750	35-635
	20100526	982711054 ± 11	982710832 ± 11	0.718	1.29	15.95	6	100	750	35-635

F Measurement examples

F.1 Measurements at Døstrup church, A10-019 and A10-002

Example of data from Døstrup church in Denmark. The example is of measurements conducted by the A10-019 and the A10-002 with approximately two hours between the measurements. Below is presented for the A10-019 measurement. The result of using multiple truncations, and the distribution of different selections of truncations. See Section 3.2

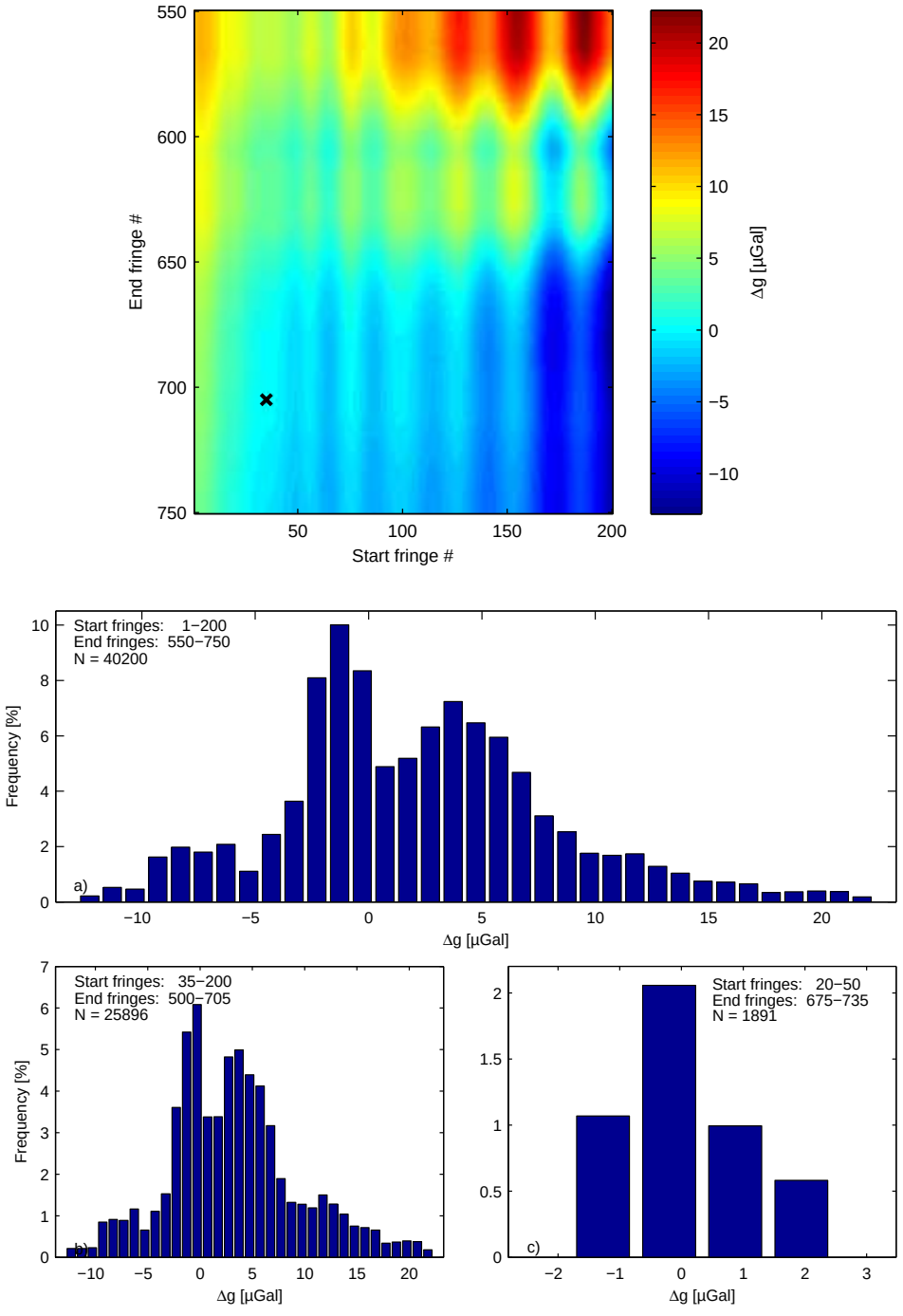

Location: Døstrup church, Denmark
Lat.: 55.11492 **Long.:** 8.79925 **Elev.:** 3.00 m
Measured: 2010\10\11

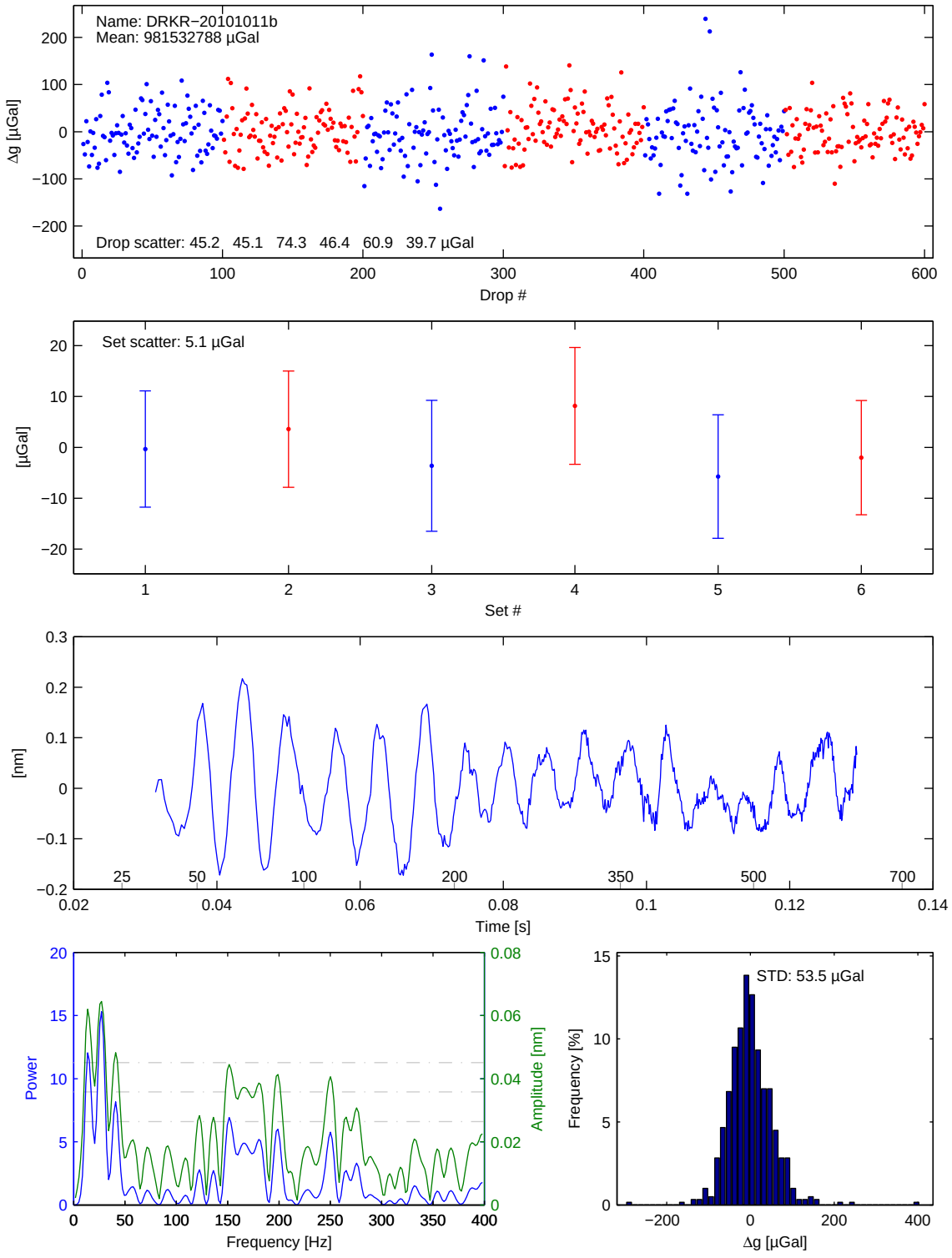

Figure F.1: .

Location: Døstrup church, Denmark
Lat.: 55.11492 **Long.:** 8.79925 **Elev.:** 3.00 m
Measured: 2010\10\11

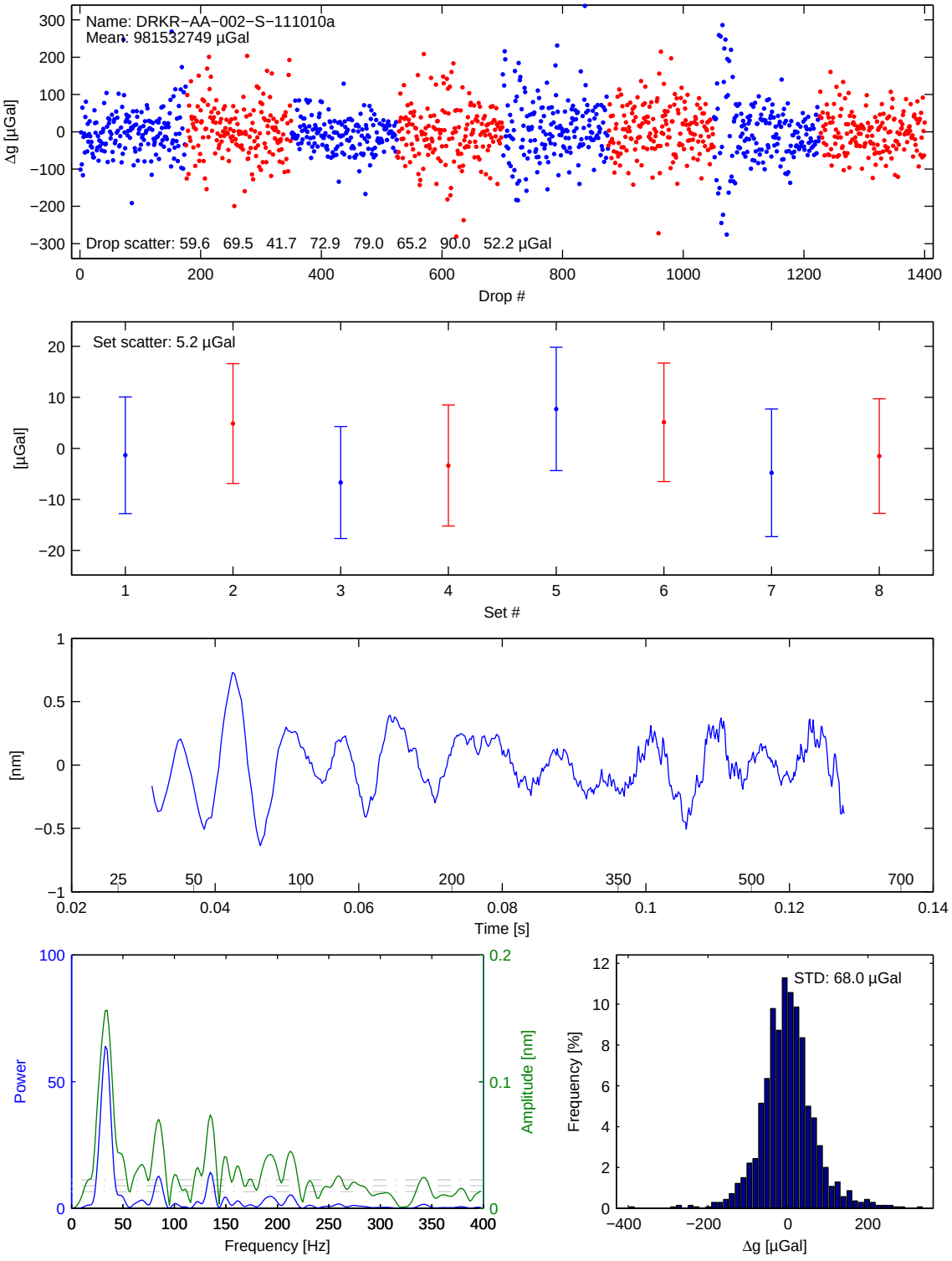

Figure F.2: .

F.2 Additional figures of the QAAR data

Presented here are figures of the solution of the full truncation investigation, the std on the drops and sets. Furthermore, a plot with three different distributions of selected truncations is presented here. The principles behind these are the same as described in the text for Figure 3.3, 3.4 and 3.5, respectively.

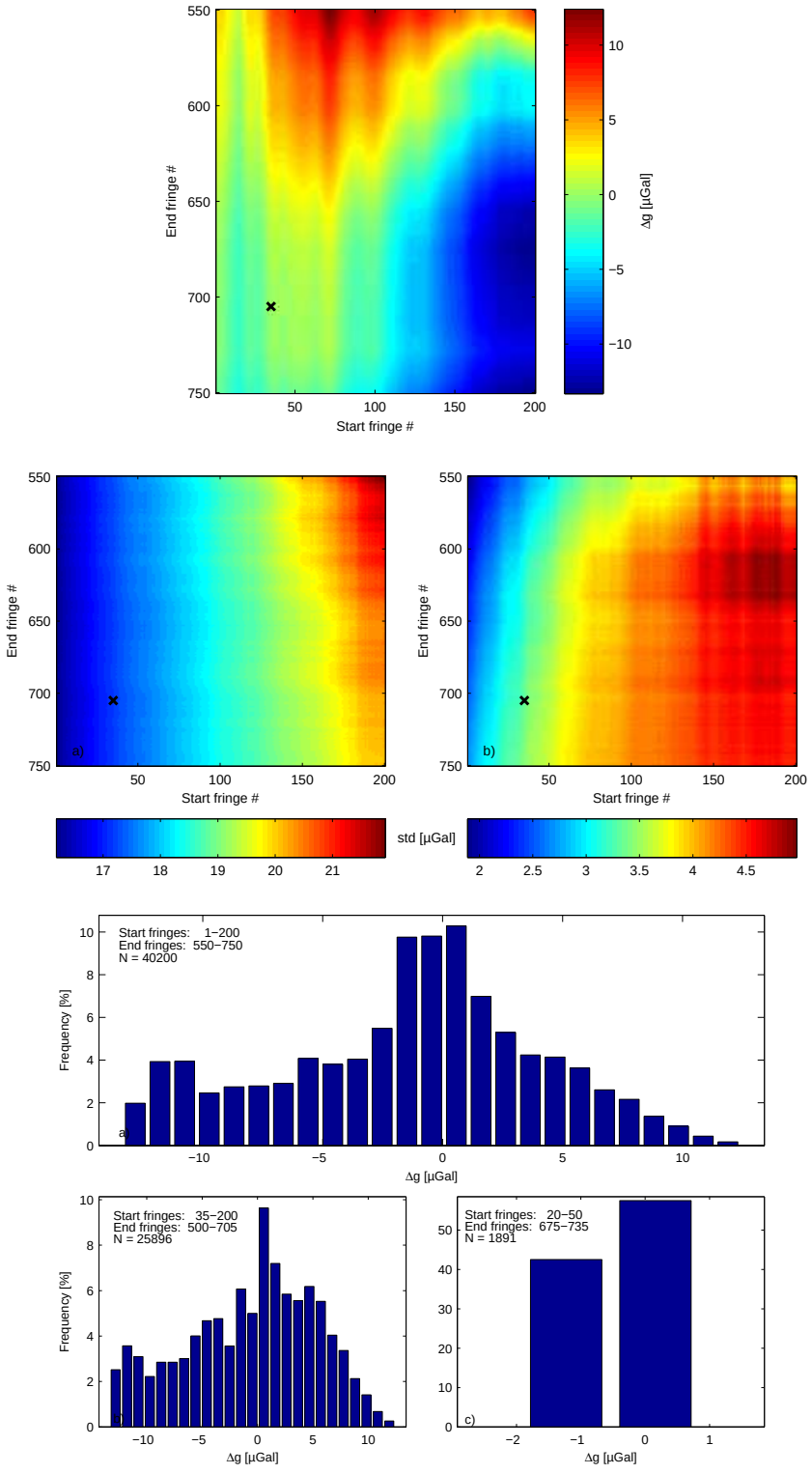

F.3 Additional figures of the RINK data

As for the Qaarsut site here is presented figures of the solution of the full truncation investigation, the std on the drops and sets. Furthermore, a plot with three different distributions of selected truncations is presented here. The principles behind these are the same as described in the text for Figure 3.3, 3.4 and 3.5, respectively.

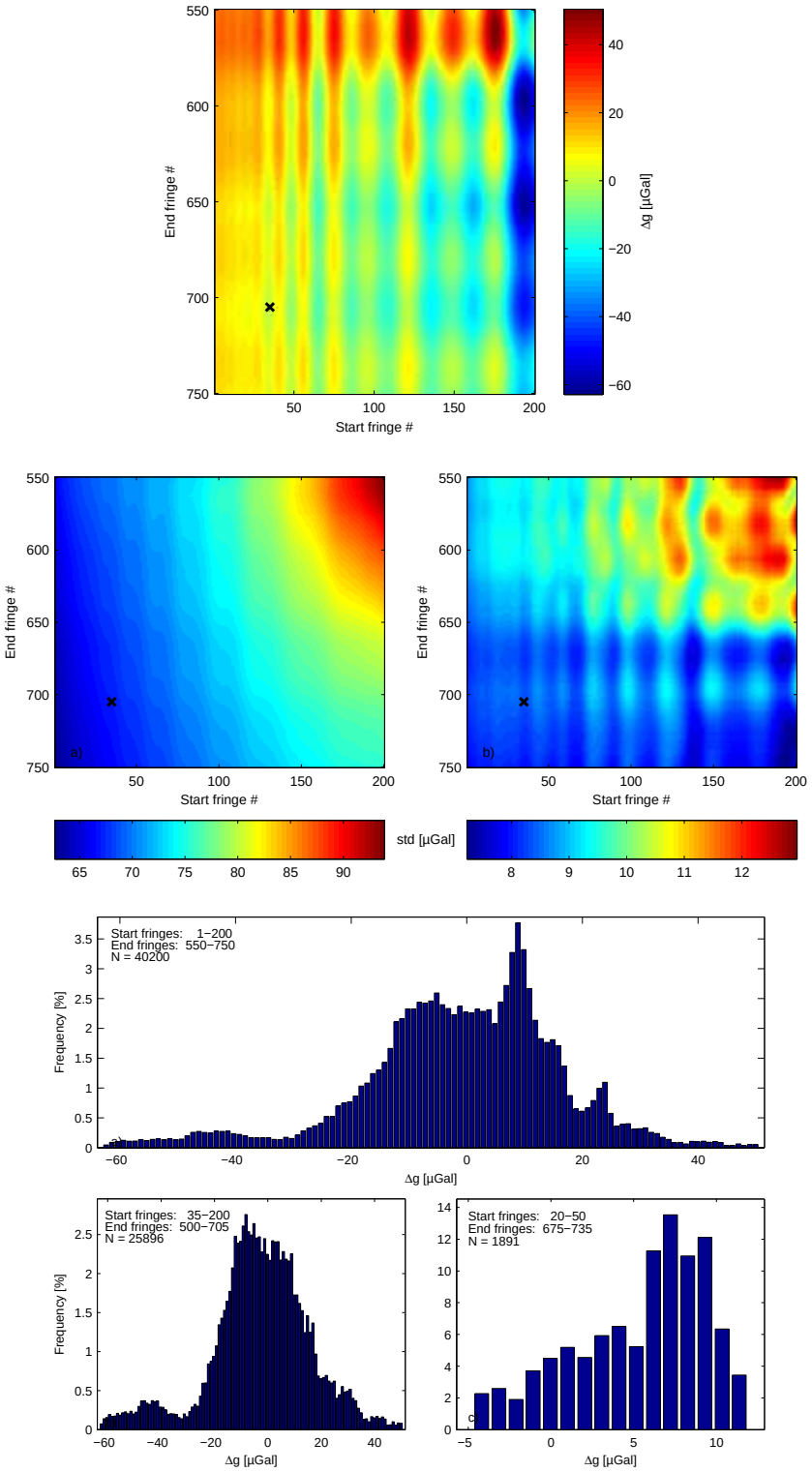

F.4 Box plot of full measurement on August 12^{th}, 2008

Box plot of all 600 drop of the August 12^{th} 2008 measurement. See Section 3.2 for details.

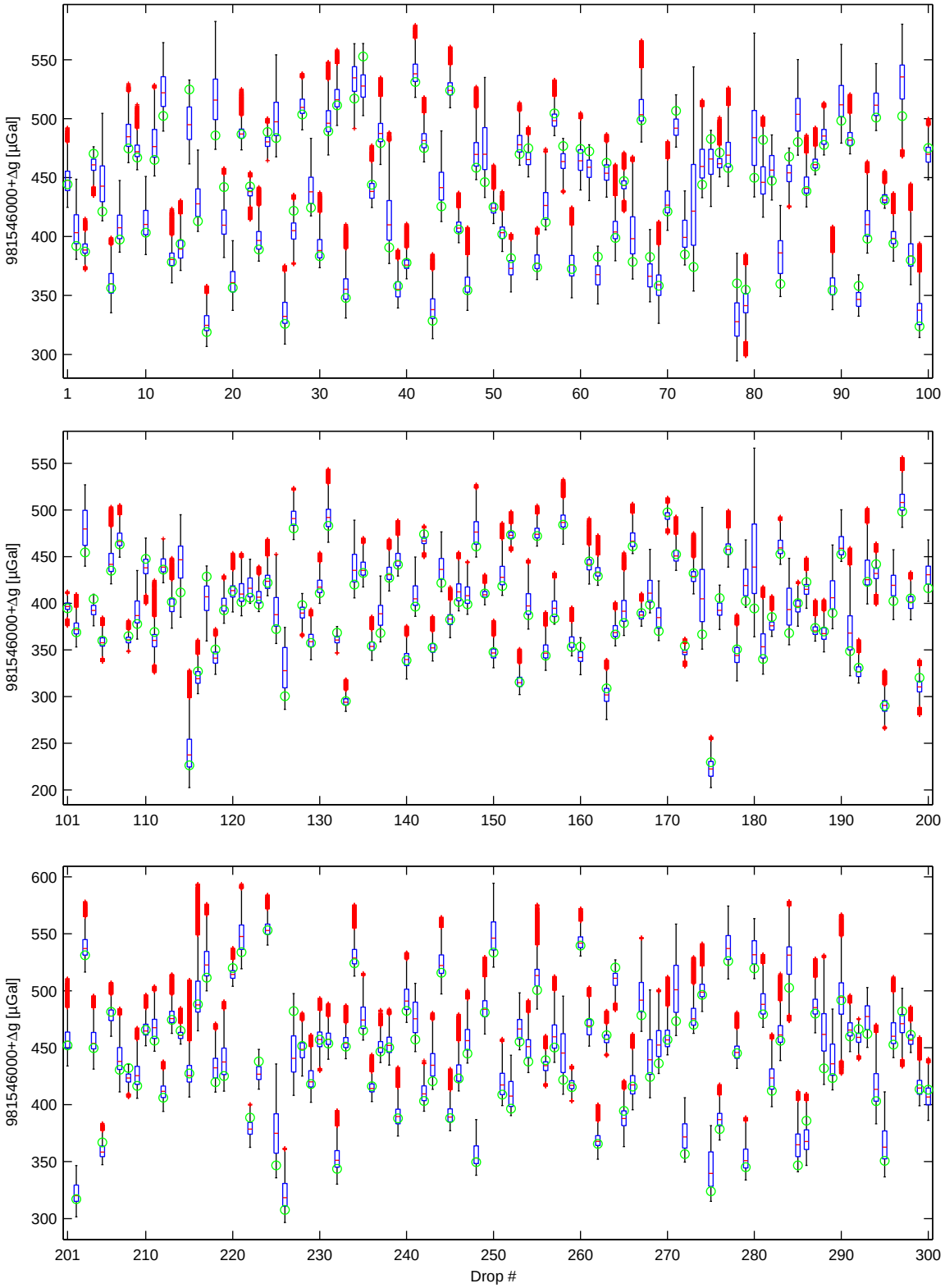

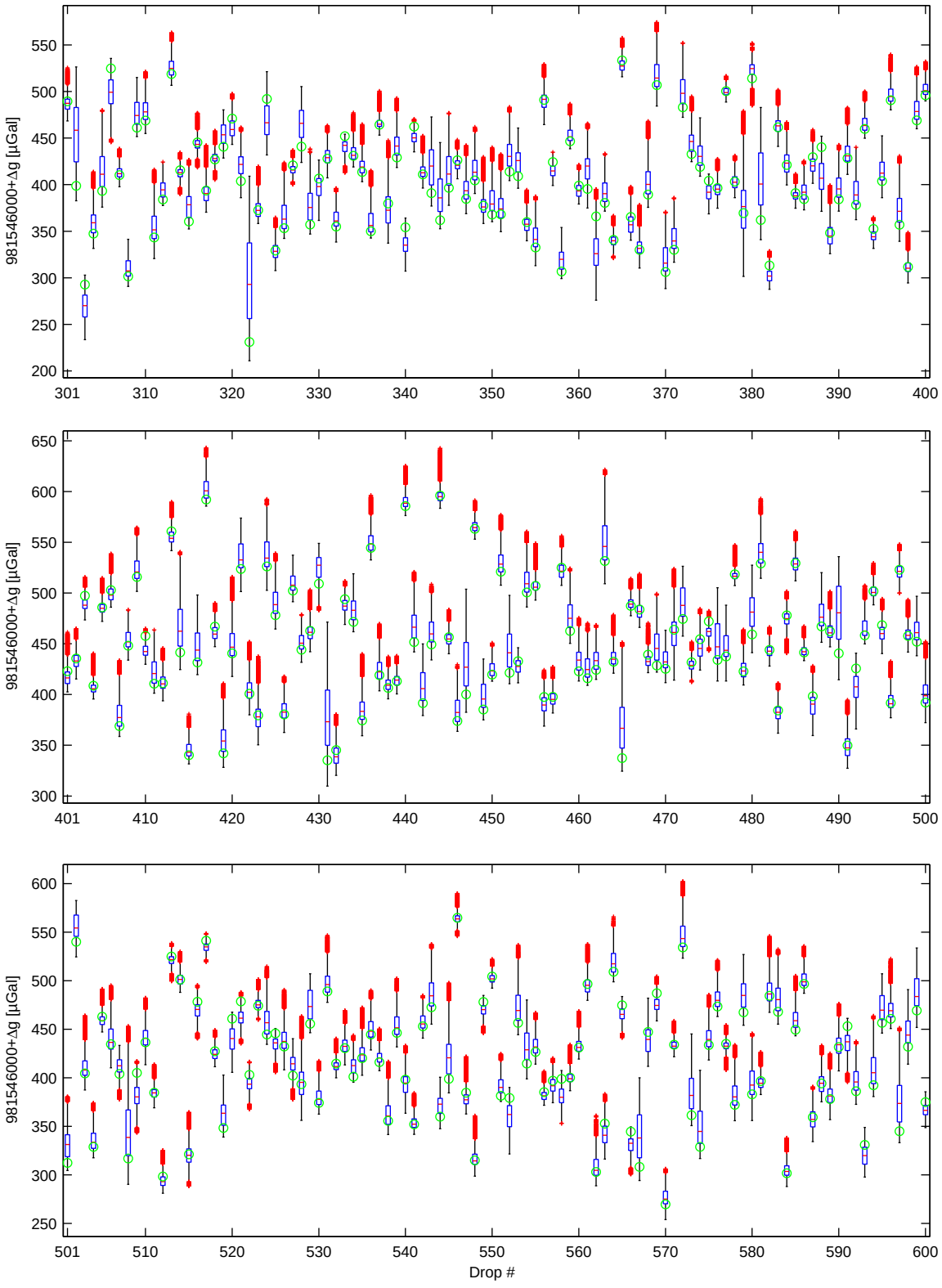
981546000+Δg [µGal]
Drop #

G Synthetic data

The synthetic data used for different investigations is produced by adding a number of harmonic terms to data of a free fall trajectory. The free fall data is produced with Equation (3.4) and the harmonics added are calculated with Equation (3.13).
In the example given here 20 harmonics are added a free fall. The data consists of 750 fringes. The Δg are relative to the input gravity value that has been used to produce the free fall. The residual after processing the synthetic data containing 20 harmonics is displayed in Figure G.1.

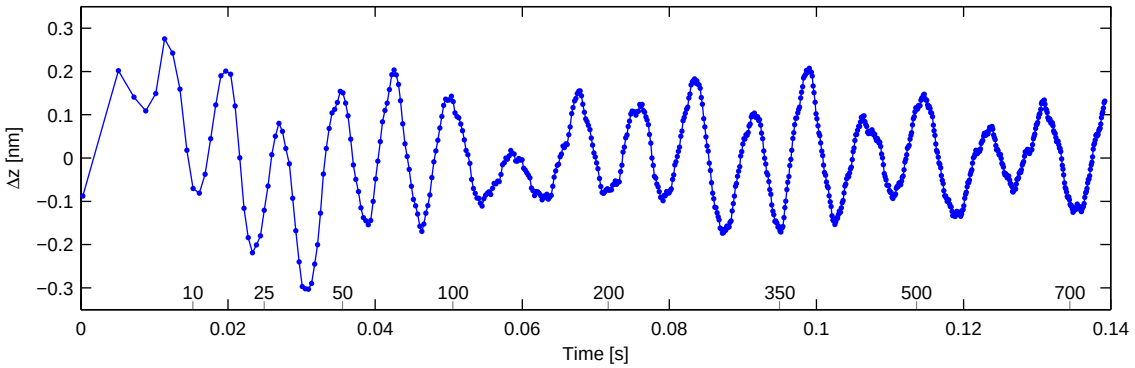

Figure G.1: Synthetic residual containing 20 harmonics.

Investigating the processing of the synthetic data with different truncations is presented in Figure G.2.

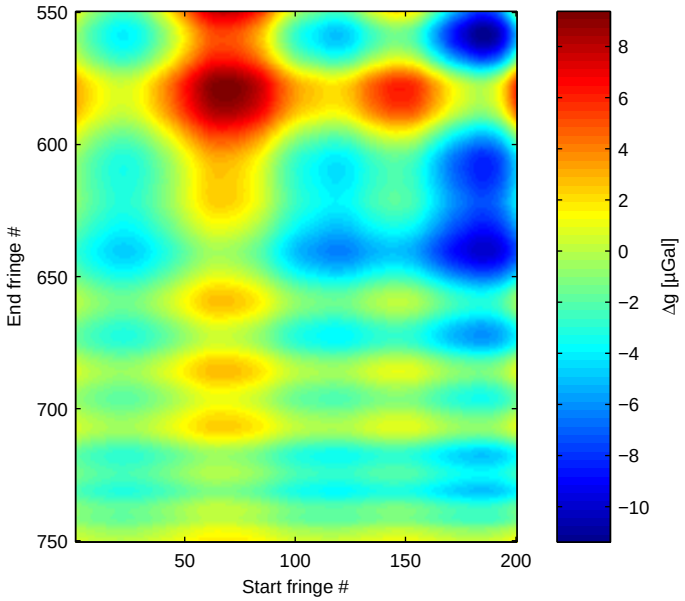

Figure G.2: The start fringe is varied within fringe number 1 to 200, and the end fringe is varied within fringe number 550 and 750.

The start fringe varies from 1 to 200 while the end fringe varies from fringe number 550 to 750 giving a total of 40200 combinations. The color bar indicates the difference of the indi-

vidual solutions with the input g-value. In Figure G.3 a) is the distribution of the differences found in Figure G.2.

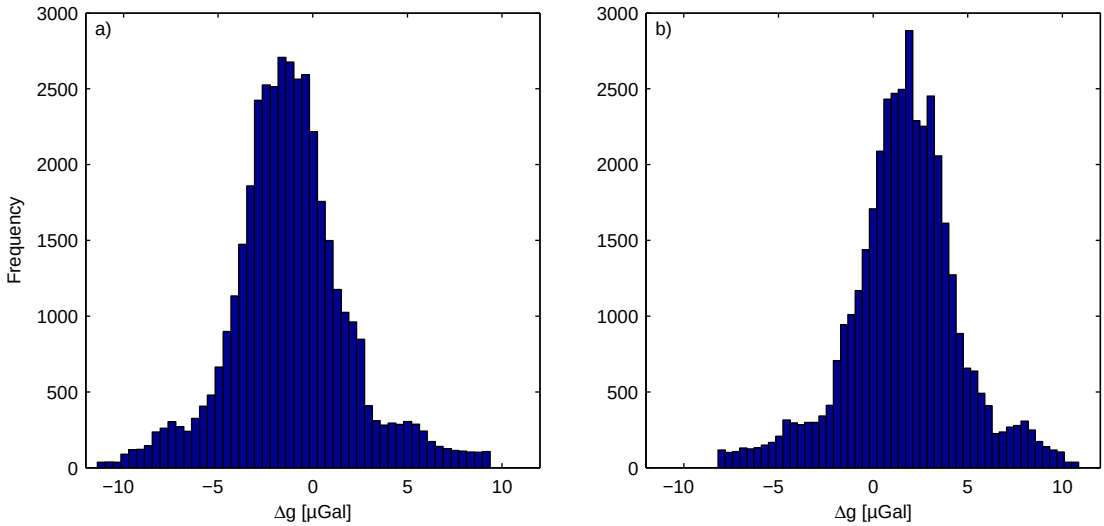

Figure G.3: All solutions of the different truncations tested a) for the data presented in Figure G.1 and G.2. In b) is the system response signal flipped around the time axis.

The distribution in Figure G.3 a) has the mean -1.2, the median -1.3 and the mode at $-1.6\mu Gal$. If using the same system response as in Figure G.1, however flipped around the time axis, and performing the same calculations as in the previous case the distribution becomes as Figure G.3 b). This distribution has the mean 1.6, the median 1.7 and the mode at $1.9\mu Gal$

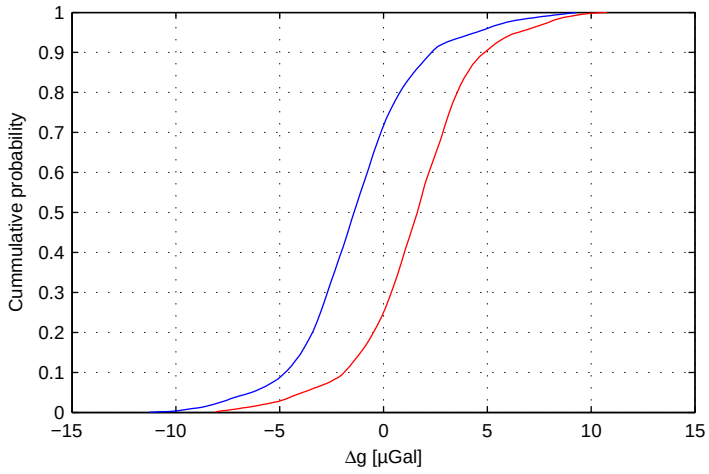

Figure G.4: Cumulative probability function. Blue is distribution a) and red is distribution b) in Figure G.3

The cumulative probability function of the two distributions in Figure G.3 is plotted in Figure G.4. The correct g-value is in the 0.25 and 0.75 probability interval for these two distributions.

DTU Space
National Space Institute
Technical University of Denmark

Elektrovej, building 328
DK-2800 Kgs. Lyngby

Tel +45 4525 9500
Fax +45 4525 9575

http://www.space.dtu.dk

ISBN-10: 87-92477-19-4
ISBN: 978-87-92477-19-4